# Analytical Applications of Modified Electrodes

by

**Margaret Stanley**

**A thesis submitted for the Degree of**

**Doctor of Philosophy**

**Dublin City University**

**School of Chemical Sciences**

**Supervisor: Prof. J. G. Vos**

October 1998

## Declaration

I hereby certify that this material, which I now submit for assessment on the programme of study leading to the award of Doctor of Philosophy is entirely my own work and has not been taken from the work of others save and to the extent that such work has been cited and acknowledged within the text of my work.

Signed:  I.D. No.: 91700299

Dublin,
31 October, 1998.

**For my dear parents.**

# Acknowledgements

This thesis would not be complete without recognising the help and support from many people.

Thanks to the kind patience, support and encouragement of Prof. Han Vos who waited a long time for this thesis.

Thanks to Dr. Andrew Doherty who was there to help with good advice.

Thanks to Dr. Margaret Hartnett, Dr. Dave Kelly, Dr. Tia Keyes and Dr. Patxi Sáez de Viteri who were always ready to put up with my many enquiries.

Thanks to all the technical staff in the School of Chemical Sciences at Dublin City University.

Thanks to my parents to whom this thesis is dedicated and to my brothers and sister.

The financial support from Forbairt (formerly EOLAS) is also gratefully acknowledged.

## Abstract

The redox polymers $[Os(bpy)_2(PVP)_{10}Cl]Cl$ and $[Ru(bpy)_2(PVP)_{10}Cl]Cl$ uncross-linked and cross-linked 10% with 1,10-dibromodecane were used to modify glassy carbon electrodes. Their amperometric surface characteristics in conventional three electrode assemblies were compared with those found in thin layer flow cells of flow injection systems with the working electrode in each case modified with the osmium and ruthenium polymers. The peak-to-peak separation for the osmium polymer increased to 50 mV in the thin layer flow cell compared with 0 mV in the conventional cell. For the ruthenium polymer separation of 60 mV was found compared to 0 mV. Other amperometric surface characteristics were similarly affected. Examination of the Nernst behaviour was also affected by the changeover from the conventional to the thin layer cell and it was shown that the slope of the Nernst plot decreased from 57 decade$^{-1}$ to 48 decade$^{-1}$ for the osmium polymer and from 58 decade$^{-1}$ to 50 decade$^{-1}$ for the ruthenium polymer. Analysis of the effect of cross-linking on the stability of these metallo-polymers showed that the time taken for the response to reach half of its initial value, increased from 45 hours, for the uncross-linked osmium polymer to 100 hours for the cross-linked version. For the ruthenium polymer, cross-linking did not affect stability as the time taken for the response to reach half of its initial value was in each case measured at 8 hours.

The cross-linked $[Os(bpy)_2(PVP)_{10}Cl]Cl$ was shown to mediate the reduction of nitrite in a through layer reaction. The use of this modified electrode in a thin layer flow cell at 0.12 V vs. SCE in a flow injection manifold, which incorporated a cadmium reduction column, allowed the formation of a nitrate sensor. The sensitivity of this sensor was 0.05 μA mg$^{-1}$ cm$^3$ and its linear range was 0.1 to 190 mg l$^{-1}$ $NO_3$-N with correlation coefficients > 0.999. The limit of detection was found to be 50 μg l$^{-1}$ $NO_3$-N (S/N=2). It was successfully used for measurement of nitrate in well and river water samples. This sensor was then applied to the determination of $NO_x$ by adapting an off-line sampling technique for this gas. A sampling time of 2 hours in a stirred solution of dilute $H_2SO_4$ containing $H_2O_2$ was found to be sufficient to collect the gas sample. Good correlation was obtained between the measurements of the absorbed gas samples made using this sensor and that obtained with an ion chromatographic sensor.

Reduction of free chlorine at the cross-linked $[Os(bpy)_2(PVP)_{10}Cl]Cl$ modified electrode was found to be mediated by a surface reaction at the polymer-solution interface. A thin layer flow cell modified with this polymer was used in a flow injection manifold to develop a free chlorine sensor at 0.1 V vs. SCE. The linear range was calibrated between 0.1 and 50 ppm free chlorine and a limit of detection of 0.05 ppm was found. This modified electrode remained stable for 24 hours. The oxidation of ascorbic acid was also found to be mediated by $[Os(bpy)_2(PVP)_{10}Cl]Cl$ by a surface reaction. A thin layer flow cell modified with this polymer was used in a flow injection manifold to develop an ascorbic acid sensor. The working potential was 0.25 V vs. SCE. The sensitivity of this sensor was found to be 7.3 μA dm$^{-3}$ mM$^{-1}$ and the limit of detection was 1 x 10$^{-6}$ mol dm$^{-3}$. The sensor was applied to the analysis of ascorbic acid in real samples and the results obtained compared well with a standard titrimetric method.

# TABLE OF CONTENTS

# Chapter One

## Theory and Application of Modified Electrodes

## 1.1 Introduction

Electrochemical sensors can be based on a number of electrochemical phenomena and can be amperometric or potentiometric in nature. The sensing surface can include membranes, solid electrolytes, electrodes and redox mediators. These materials provide the unique surfaces which allow these sensors to function [1,2].

Poly(4-vinylpyridyl) complexes of Ruthenium and Osmium will receive close scrutiny in further chapters of this thesis. Their utility as redox mediators of electrode surfaces is due to a number of intrinsic qualities [3]. They can undergo oxidation state changes without losing integrity and they are catalysts for a wide number of reactions. They can also be photochemically reactive and have been shown to absorb visible light. These properties are not lost when absorbed onto a solid support [4]. Consequently, these supported complexes can have many useful applications in fields as diverse as electrocatalysis, solar energy conversion, screen-printed microelectrodes, optical sensors and biosensors [5].

In the first part of this chapter, an overview will be presented of analytical voltammetry, mediated electrocatalysis and the preparation of modified electrodes. In the second part, a literature review will be presented of the applications of modified electrodes as electrochemical sensors.

For more than a century the electrode/electrolyte interface has been studied. The current of interest must be distinguished from processes such as double-layer charging and adsorption. The double-layer charging current results from the change in structure of the interfacial region of the electrode with applied potential [6-8].

## 1.2 Voltammetry

Voltammetry measures a number of points of the current-voltage profile, whilst

amperometry involves the measurement of a current at a fixed applied potential, i.e. at one point on the current-voltage curve. These techniques are used to obtain a response, the current, which can be related to the concentration of analyte in the bulk solution. These faradaic currents can be masked by processes such as adsorption and desorption at the electrode surface which cause a change in the structure of the electrode/solution interface, thereby causing a change in the potential or in the solution composition. These are called non-faradaic processes and they must be considered when investigating electrochemical processes. Operation at a fixed potential reduces charging currents significantly [9-11].

Cyclic Voltammetry

This technique of cyclic voltammetry involves the application of a continuously time-varying potential to the working electrode. The sweep direction is inverted at a certain, chosen potential as illustrated in Figure 1.1.

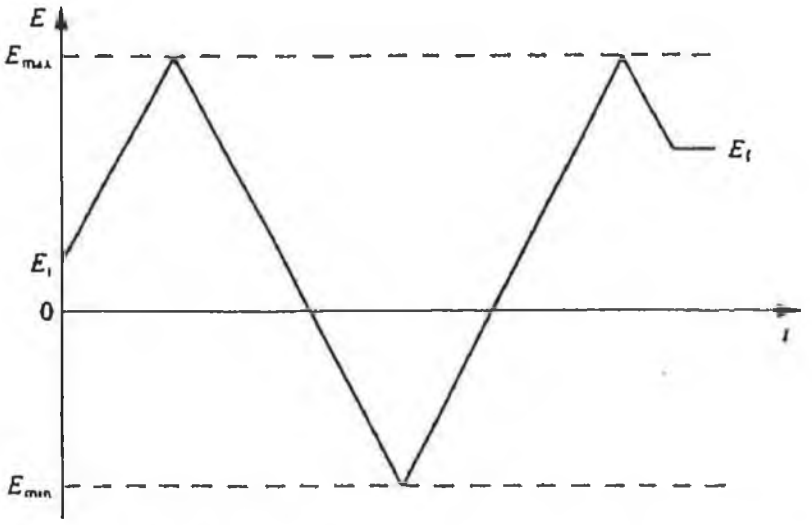


Figure 1.1 Variation of time with applied potential in cyclic voltammetry [5].

This prompts the oxidation or reduction of electroactive species in solution and a capacitive current due to double layer charging as well as the possible adsorption of species. That is, both faradaic and non-faradaic reactions occur. The total current is:

$$I = I_f + I_C \qquad \text{(Eq. 1.1)}$$

The important parameters are the initial potential, $E_i$, the initial sweep direction, the sweep rate, $\nu$, the maximum potential, $E_{max}$, the minimum potential, $E_{min}$, and the final potential, $E_f$ as illustrated in Figure 1.2.

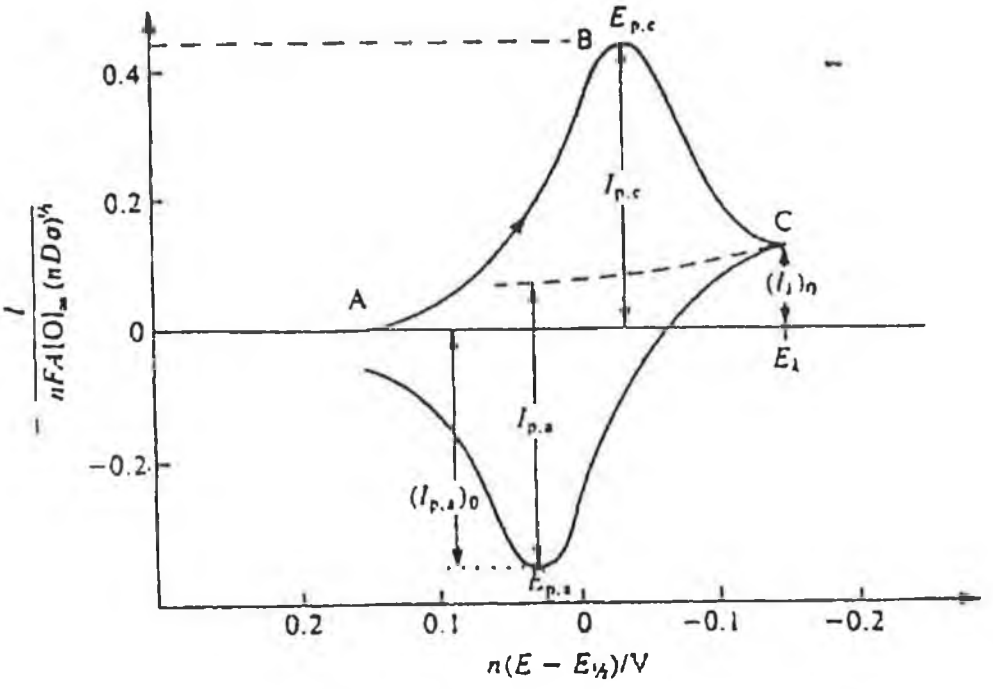


Figure 1.2 Cyclic voltammogram for a reversible system [5].

A simple electron transfer for the redox couple O/R with only O present in solution can be expressed as follows:

$$O + ne^- \Leftrightarrow R \qquad \text{(Eq. 1.2)}$$

Assuming that the initial sweep direction is negative, then the observed faradaic current depends on the kinetics and transport by diffusion of the electroactive species, O. If the species present in bulk solution is R and the initial sweep direction is positive then such a reversible system could be described by the Nernst equation:

$$E = E^{o} + \frac{RT}{nF}\left( In\frac{[C_O]}{[C_R]} \right) \qquad \text{(Eq. 1.3)}$$

where E is the electrode potential, $E^{o'}$ is the formal potential of the couple [O/R], R is the gas constant, T is the absolute temperature, F is the Faraday constant, $C_O^*$ is the bulk concentration of [O] and $C_R^*$ is the concentration of [R].

The shape of the experimental curve obtained can be explained as follows. At a potential where the electrode reaction starts, the current begins to rises and as the potential continues to vary, the trace obtained mimics a steady-state voltammogram. But as more electroactive species are consumed by the reaction, a concentration gradient forms before the electrode surface. Therefore, the supply of electroactive species decreases after reaching a maximum (the peak) and though the potential is further increased, there is no longer a corresponding rise in the current. Instead, the current decreases or decays. By inverting the scan direction after passing the peak for a reduction reaction a cyclic voltammogram is obtained

For the process, $O + ne^- \Leftrightarrow R$ the current is given by:

$$i = nFAk^{o}\{C_O(0,t)\exp[-\alpha nf(E - E^{o'})] - C_R(0,t)\exp[(1-\alpha)nf(E - E^{o'})]\} \qquad \text{(Eq. 1.4)}$$

where $f = (F/RT)$, $\alpha$ is the transfer coefficient, A is the electrode area and the current is the difference between the currents due to the forward and backward reactions in equation 1.2.

It is necessary to determine the concentration of the species O and R at the electrode surface. In an unstirred solution where there is a large amount of supporting electrolyte and the electrode area is large, the diffusion process for O is described by Fick's second law, which in one dimension is:

$$\frac{\partial C_o}{\partial t} = D_o \frac{\partial^2 C_o}{\partial x^2} \qquad \text{(Eq. 1.5)}$$

where $D_o$ is the diffusion coefficient of the species O. Under conditions were the current is diffusion controlled, the current is given by:

$$i = nFAD_o \frac{\partial C_o}{\partial x}\Big|_{x=0} \qquad \text{(Eq. 1.6)}$$

In cyclic voltammetry the two distinctive parameters are the peak potential and the peak current, which for a reversible system at 298 K, the peak current is given by:

$$i_p = 2.69 \cdot 10^5 n^{\frac{3}{2}} A\sqrt{D_o}\sqrt{v}C_o^* \qquad \text{(Eq. 1.7)}$$

where $i_p$ is the current and $v$ is the scan rate.

The position of the peak potential occurs after the formal potential:

$$E_p = E^{0'}_{O/R} \pm \frac{0.0285}{n} \qquad \text{(Eq. 1.8)}$$

The difference in potential between the potential at half peak height and the maximum is given by:

$$|E_{p,c} - E_{p/2,c}| = 2.2(RT/nF) = 56.6/n \text{ mV} \qquad \text{(Eq. 1.9)}$$

For reversible systems, cyclic voltammetric behaviour can be summed up by the following qualities.

(1) $i_p \propto v^{1/2}$

(2) $E_p$ independent of $v$

(3) $|E_p - E_{p/2}| = 57/n$ mV

(4) $E_{p,a} - E_{p,c} = 57/n$ mV

(5) $|I_{p,a}/I_{p,c}| = 1$

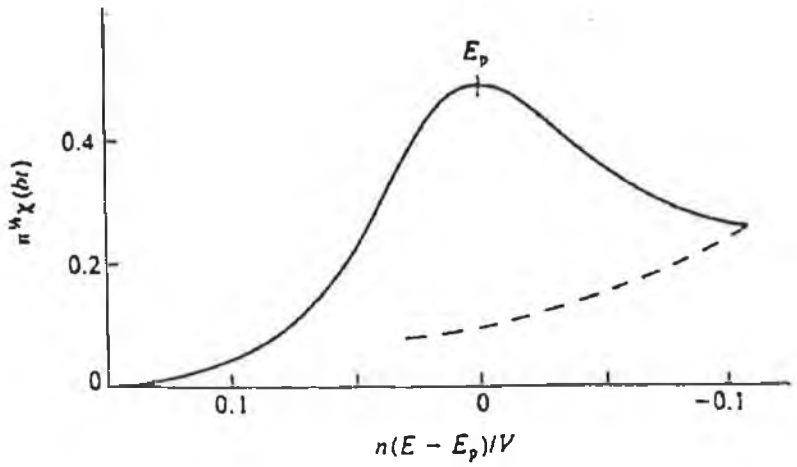


Figure 1.3 Voltammogram for an irreversible system [5].

When an irreversible system (Figure 1.3) of the type O + ne → R is considered, the irreversible process will not yield a peak on the reverse scan so there is no peak separation to consider. The current function is independent of $v^{1/2}$ but the peak potential is a function of the scan rate unlike the reversible case.

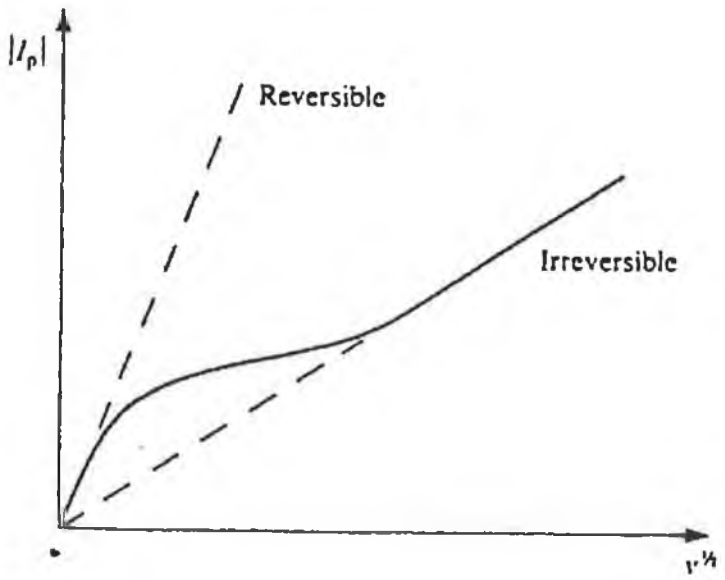


Figure 1.4 Transition from a reversible to an irreversible system on increasing sweep rate [5].

In some cases it has been found that an electrode reaction is reversible at low scan rates but upon increasing the scan rate, the reaction is observed to be irreversible (See Figure 1.4).

In the interval between these two mechanisms, the reaction is quasi-reversible [12] (see Figure 1.5). The extent of irreversibility generally increases with an increase in the scan rate. This is often accompanied by a decrease in the peak current relative to the reversible case and an increase in the separation between the anodic and cathodic peaks.

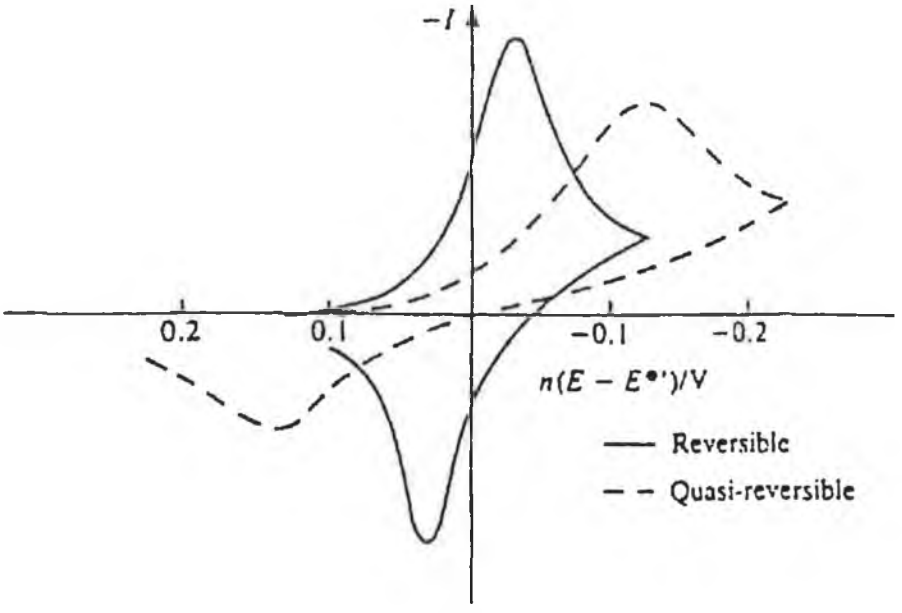


Figure 1.5 The effect of increasing irreversibility on the shape of cyclic voltammograms [5].

The preceding paragraphs all describe cases where the electrode reaction is occurring in solution. If the redox active material is adsorbed onto the electrode, then the resulting voltammetric wave is modified [13].

The current-potential curve for the reduction of O to R is given by:

$$I_c = (-nF\sigma A\Gamma_{O,i}(b_O/b_R)\theta)/([1+(b_O/b_R)\,\theta]^2) \qquad \text{(Eq. 1.11)}$$

where $\Gamma_{O,i}$ represents the surface concentration of adsorbed O on an electrode area A and $\sigma$ equals (nF/RT)v. The terms $b_O$ and $b_R$ represent the concentration of O and R respectively and is given by:

$$\theta = \exp[(nF/RT)\,(E - E')] \qquad \text{(Eq. 1.12)}$$

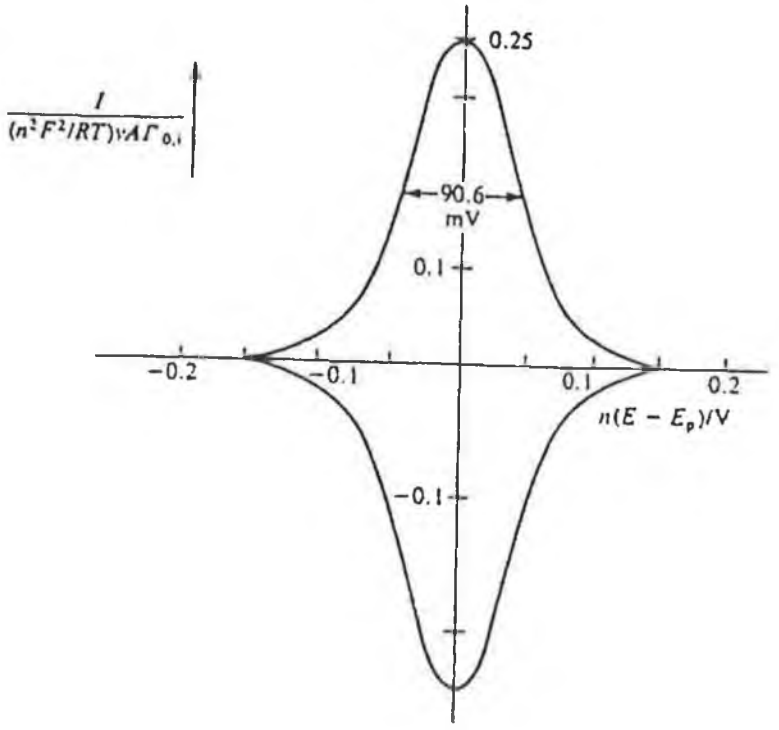


Figure 1.6 Cyclic voltammogram for a reversible system of species adsorbed on the electrode [5].

The reduction peak current, $i_{p,c}$, is obtained when $(b_O/b_R) = 1$, which can be expressed as:

$$I_{p,c} = (-n^2F^2vA\Gamma_{O,i})/(4RT) \qquad \text{(Eq. 1.13)}$$

Figure 1.6 illustrates an idealised example of such a case. The peak potential is given

by:

$$E_p = E' - RT/nF(\ln(b_O/b_R)) \qquad \text{(Eq. 1.14)}$$

The value for $E_p$ is the same for oxidation as for reduction. When $(b_O/b_R) = 1$, then the peak width at half peak height can be shown to be 90.6/n mV.

Cyclic voltammetry is an excellent tool for investigating the mechanism of electrode reactions but as this technique's limit of detection is quite poor generally $10^{-3}$ to $10^{-4}$M level) [14], it is not used in conjunction with chemical sensors. This limit of detection is due to the relative contributions to the total cell current of the faradaic and non-faradaic, or capacitative, currents. The contribution of the non-faradaic current is a linear function of scan rate, whereas the faradaic current is a function of the square root of the scan rate for a reversible process. Therefore, when a scan rate is increased in order to produce a larger faradaic current, there is a deterioration in the signal to noise ratio. Assuming typical values for the diffusion coefficient ($10^{-5}cm^2s^{-1}$) and the double layer capacitance (20 $\mu F\ cm^{-2}$), an approximate relationship between the relative contribution of the capacitative current, $i_C$, and the peak faradaic current, $i_p$, can be expressed as:

$$\left|\frac{i_c}{i_p}\right| \approx \frac{2.4 \cdot 10^{-8}\sqrt{v}}{n^{\frac{3}{2}} C_o^*} \qquad \text{(Eq. 1.15)}$$

where the units for $v$ are $vs^{-1}$ and for C are mol $cm^{-3}$.

Some of these disadvantages can be overcome by using hydrodynamic electrodes. They have little dependence on the electrolyte's properties and natural convection in the detection cell is suppressed. A disadvantage is that the fraction of species electrolysed at the electrode is small due to the high speed that transports the electroactive species to its surface. This fraction can be increased by using a thin-layer cell, this will be further discussed in a later section.

The most commonly used electrode in hydrodynamic voltammetry experiments is the rotating disc electrode. This electrode rotates around its axis in a solution with the disc centered on the axis. The limiting current obtained at a rotating disk electrode is given by the Levich equation which will be described later in the chapter. The streamlines at such an electrode are shown in Figure 1.7. The rotating disc sucks solution from below and spreads it out sideways making this electrode uniformly accessible.

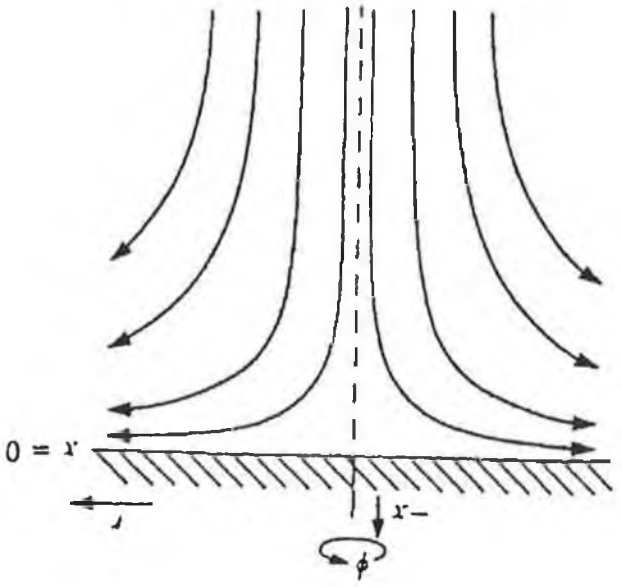


Figure 1.7 Streamlines for a rotating disc [5]

## 1.3 Amperometry

Amperometric techniques are commonly used in conjunction with chemical sensors. This is because the faradaic currents are measured at fixed potentials. Because no potential scan is being applied, capacitative currents no longer contribute to the overall cell current and far lower detection limits can be obtained compared to voltammetric techniques.

### 1.3.1 Hydrodynamic Amperometry

Convective diffusion can be obtained by moving the solution with respect to the electrode or vice versa. For the latter case, a rotating disc electrode is the most common technique used, though this electrode is more commonly associated with voltammetric methods.

For the rotating disc electrode, there is a continuous quantity of solution coming into contact with the electrode surface outside of which convection is the primary form of mass transport. The thickness of this layer is proportional to the square root of the rotation rate and the limiting current and is given by:

$$i_L = nFAD_o^{2/3} v_k^{-1/6} \omega^{1/2} (v_m)^{1/2} C_O^* \qquad \text{(Eq. 1.16)}$$

where $v_k$ is the kinematic viscosity, $v_m$ is the main stream fluid velocity and $\omega$ is the rotation rate.

This equation does not hold for all cases as at higher rotation rates the current becomes limited by kinetics at the surface. In such a case the substrate can't react quickly enough at the electrode and so the following equation describes the condition where the system is irreversible:

$$\frac{1}{i_{Lim}} = \frac{1}{i_F} + \frac{1}{i_{Lev}} \qquad \text{(Eq. 1.17)}$$

In the other case of hydrodynamic voltammetry, the electrode is held stationary in a flowing stream. And such a detection cell is commonly used in flow injection analysis techniques (FIA) and chromatographic techniques. The flowing stream is pumped through the cell where electroactive compounds elicit a response from the electrode. The current obtained is equivalent to the amount of these species present. The response is dependent on the number of electrons involved in the electrode reaction, the electrode kinetics, and the thickness of the diffusion layer [15].

The solution above the electrode in these techniques can be characterised as

belonging to two types of zones. In the first, at some distance from the electrode surface, convection is important and the concentration/distance profile is essentially flat. In the second, at the electrode surface, there is a sharp concentration gradient and the mass transport process of most importance is diffusion [14]. The mass transport limited current, $i_L$, for a reversible electrode couple in this case can be characterised by:

$$i_L = nFAD_o^{2/3} v_k^{-1/6} x^{1/2} (\nu_m)^{1/2} C_O^* \qquad \text{(Eq. 1.18)}$$

where x is the distance along the electrode.

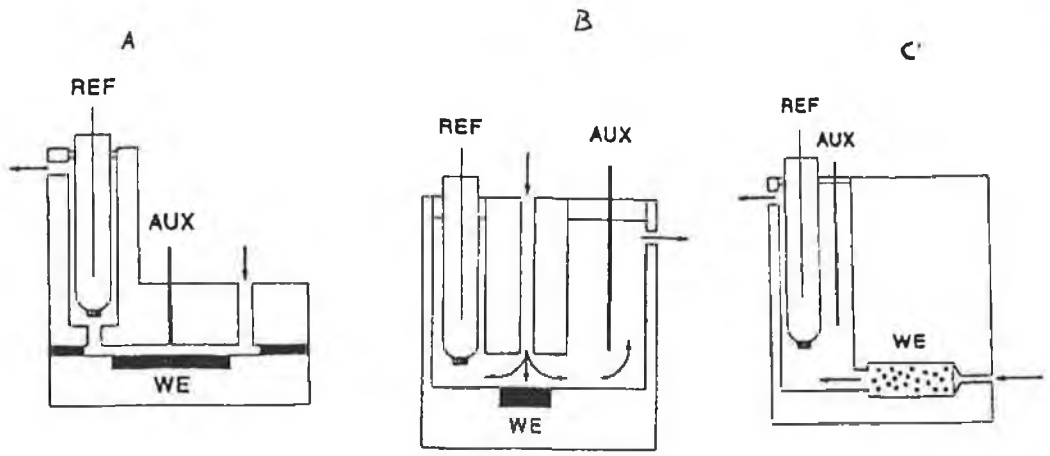


Figure 1.8 (a) Thin-layer cell, (b) Wall-jet cell, (c) Packed-bed cell Note: Ref = Reference Electrode, Aux = Auxiliary Electrode, WE = Working Electrode [17].

This current rapidly reached a plateau value, how rapidly is controlled by the thickness, d, of the steady-state diffusion layer which forms at the electrode/solution interface. This layer thickness can be approximated by calculating:

$$d = D^{1/3} v_k^{1/6} (x/v_m)^{1/2} \qquad \text{(Eq. 1.19)}$$

The relationship between the limiting current and the diffusion layer thickness is:

$$i_L = nFADC/d \qquad \text{(Eq. 1.20)}$$

Therefore, at a uniformly accessible electrode, the limiting current is directly proportional to the electrode area. Also, the limiting current increases when the diffusion layer, d, is smaller. Since d decreases with an increasing flow rate, it is important to construct a flow cell so that the diffusion layer is as thin as possible.

The most popular flow cell designs [16,17] are illustrated in Figure 1.8. The thin-layer cell design is based on reducing the diffusion path length so that the flowing stream is directed along the electrode as a thin film of liquid. The wall-jet design is based on flow-rate acceleration perpendicular to the working electrode in order to create strong convective motion of the electroactive species towards the electrode. The flow-through, or porous, electrode can be regarded as a combination of thin-layer and wall-jet designs. It has a short diffusion path length and strong convective motion due to high liquid velocities in narrow pores.

Peak current increases at a decreasing rate as a function of the electrode surface area. Background current increases proportionally to the electrode surface area. Therefore, the signal-to-noise ratio decreases with increasing electrode surface area. Electrolytic efficiency should be less than 20 per cent for an optimum signal-to-noise ratio. Thin-layer and wall-jet cells usually have electrolytic efficiencies within this optimum range. Porous flow-through cells have typical electrolytic efficiencies of 100 per cent.

In a flow injection system with amperometric detection, the detector response is equivalent to the current measured at the working electrode and this current is directly affected by potential differences between the electrode and the carrier solution. Therefore, to produce a stable and reproducible response, a constant and known voltage between the working electrode and the carrier is required.

A working electrochemical cell possessing only a reference and a working electrode is possible but, due to practical considerations, this type of cell assembly is not often used. This is because the potential of the reference electrode depends on the current flowing through it in such a setup. Adding a counter electrode compensates for the current flowing through the working electrode and the reference electrode is only used as a reference to which the potential of the working electrode is set.

As a consequence, the most common type of detector cell arrangement in flow systems is the three electrode detection cell, with a working, reference and auxillary, or counter, electrode. This allows the working electrode to be kept at zero potential. The counter electrode allows the potential difference between the working and reference electrode's to be regulated.

The reference electrode is used because its potential versus the carrier is constant and known and does not vary, thereby allowing a stable and predictable potential difference between the carrier and the working electrode. This is vitally important because of the effect of polarisation processes in the boundary layer between the working electrode's surface and the carrier solution and, sometimes, the potential drop caused by electrical resistance of the carrier when the carrier used is a poor conductor.

By allowing the counter electrode to control the potential of the working electrode versus the reference electrode by adapting its potential, any difference between these electrodes can be removed.

Since the working electrode always remains at virtual zero potential, a positive potential difference of the working electrode versus the reference electrode is obtained by applying a negative potential versus the working electrode on the carrier solution with the counter electrode. For reductive potentials at the working electrode, a positive potential is applied on the carrier.

Therefore, this three-electrode set-up is used most commonly in amperometric sensor

design. Once the flow cell has been designed, a number of criteria are used to evaluate any particular flow cell detector [15].

(1) Sensitivity, the ratio of the change in detector signal to the change in analyte concentration and it can be measured from the slope of the calibration plot and it should be as high as possible.

(2) The amount of noise obscuring the signal. This can be caused by impurities in the flowing stream, unwanted reactions, bias currents of the signal amplifiers, random pulses, drifts in the detector response, bubbles in the flowing stream and many other such disturbances. The signal-to-noise ratio should be as high as possible.

(3) The limit of detection is related to the sensitivity and the noise and is often expressed as a ratio of signal to noise.

(4) The reliability of the measurement is assessed using statistical measures of precision and accuracy as well as long-term stability and reproducibility.

(5) The linear dynamic range is that interval in which a change in the substrate concentration causes a proportional change in the signal.

(6) The selectivity of the method is a measure of how the sensor responds to substances other than the one being measured. If it is specific to one analyte, it will produce no response on the introduction of any other species.

(7) The dynamic properties of a sensor relate to its ability to accurately follow any changes in concentration of the analyte. These properties can depend on factors such as the measuring technique, the sensor design and the experimental conditions.

Having discussed the general theory underlying voltammetric and amperometric processes and the resulting techniques that are commonly used, there follows a general discussion on the theory of modified electrodes in particular and the

preparation of these modified sensors.

## 1.4 The Theory of Mediated Electrocatalysis at Modified Electrodes

The theory of mediated charge transfer has been widely studied by many authors and, as a result, their work allows mechanistic elucidation and kinetic parameters to be evaluated [18-26]. These established theories can then be used to optimise the design and performance of electrodes modified with electrocatalysts used in the development of analytical sensors.

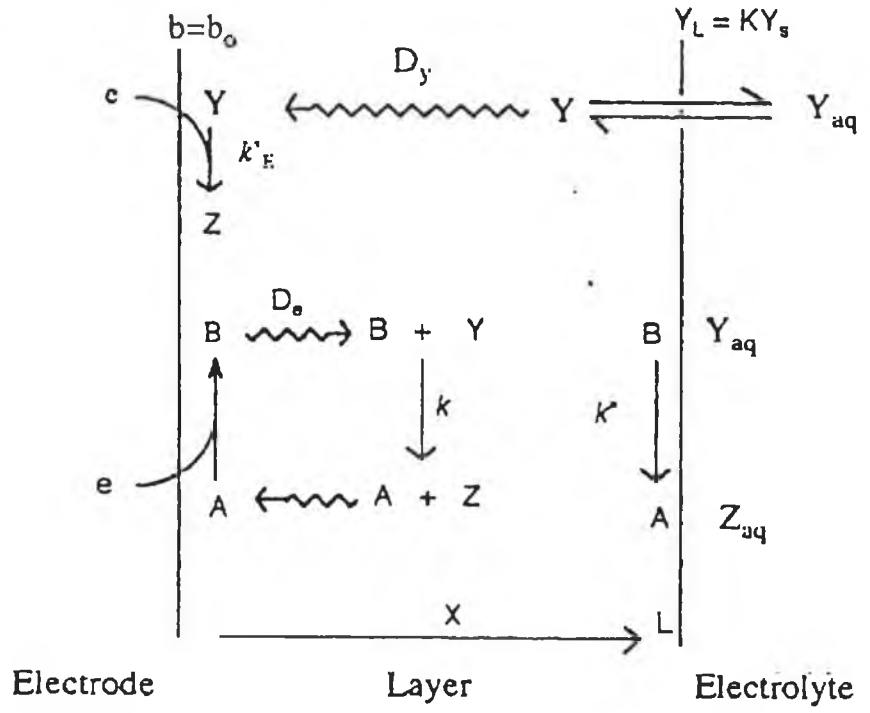


Figure 1.9 Schematic representation of the processes possible at redox polymer modified electrodes [5].

The fundamental redox reactions which occur between a solution species Y and a mediating layer containing the redox couple A/B are shown in Figure 1.9. These mediating processes can be described by the following reactions:

$$A + e^- \rightarrow B \qquad \text{(Eq. 1.21)}$$

$$B + Y \rightarrow A + Z \qquad \text{(Eq. 1.22)}$$

In this particular example, the mediating process involves the reduction of the surface-bound species A, but the same reasoning can be used for a mediating process based on the oxidation of the surface-bound species. More complex mediating processes involving reversible mediating reactions, self-exchange reactions, additional chemical steps and charge exchange have been considered by Saveant and co-workers [27-32].

Depending on factors such as film morphology, film thickness, the diffusion rate of the electroactive species through the film and electron transfer rates, four types of limiting cases can be isolated[33]. These are described by the Saveant approach as follows.

(1) Electron and substrate diffusion ($D_E$ and $D_Y$) are so fast that the rate-controlling step is the rate, k, of the catalytic reaction.

(2) The catalytic reaction is so fast that the rate is controlled by the two diffusion processes ($D_E$ and $D_Y$).

(3) When diffusion of electrons is faster than diffusion of substrate, a pure kinetic situation may arise by mutual compensation of the latter process and the catalytic reaction.

(4) In the opposite case a pure kinetic situation may again arise resulting in the mutual compensation of electron diffusion and catalytic reaction.

The fundamental processes involved in this mediating process are identified as charge introduction at the modifying layer/electrode interface, charge introduction at the layer/solution interface and reaction of the substrate, Y, with the modifying layer

containing the redox couple, A/B. Linked to these reactions is the diffusion of the substrate into the film which is controlled by the partition coefficient, K. If the substrate can penetrate the film, then the diffusion rate of the substrate within the layer, $D_Y$, will most likely be considerably less than the solution value $D_S$.

An alternative theory is that developed by Albery and co-workers [19,33-35]. The two theories are similar except that Albery uses the concept of 'reaction layers' to describe two different reaction zones within the same film; firstly a region where permeating Y is converted to product Z, and secondly a region of consumption of an electron or B. These reaction layers are generally located in the vicinity of the film/electrolyte and electrode/film interfaces respectively. In contrast, in Saveant's work, no reaction layers are identified but the mediating process is described in terms of characteristic currents. Alternative models have also been developed [36-38].

In the Albery model the following equations must be solved, given certain boundary conditions, if the mediating processes for electrocatalytic modified electrodes are to be studied:

$$D_E \frac{\delta^2 b}{\delta x^2} - kby = 0 \qquad \text{(Eq. 1.23)}$$

$$D_E \frac{\delta^2 y}{\delta x^2} - kby = 0 \qquad \text{(Eq. 1.24)}$$

The former equation deals with charge transport within the film, and the latter with substrate diffusion within the film. By solving them, the concentration profiles within the layer of both the fixed redox couples and the substrate can be described. In these equations b and y are the concentration in the layer of B and Y respectively. The boundary conditions used are:

(1) Assuming Marcusian A/B self-exchange behaviour, it is assumed that charge introduction at the electrode/layer interface will be more rapid than charge

propagation [39]. Thus charge transfer at the electrode/layer interface is not expected to be rate limiting.

(2) At x = 0 the concentration of B is $b_0$, and is controlled by the electrode potential.

(3) The modifying layer acts in a catalytic manner, such that any substrate which permeates the layer and reaches the underlying electrode will not react there, therefore $(dy/dx)_0 = 0$. This boundary condition is in agreement with the perception of a modified electrode where the substrate is not reacting directly with the underlying electrode surface, but where the electrochemical process is controlled by the mediating layer. It should be noted here that in the work developed by Saveant, the case where the substrate reacts directly at the electrode surface has been considered [28-32].

(4) The partitioning of the substrate, Y, between the solution and the modifying layer is given by:

$$Y_L = Ky_s \qquad \text{(Eq. 1.25)}$$

(5) The electron flux at the layer/solution interface is related to the kinetics by the equation:

$$-D_E \frac{\delta b}{\delta x} = k'' b_L y_s \qquad \text{(Eq. 1.26)}$$

where $b_L$ is the concentration of B at the interface (X = L) and k" is the rate constant for the cross-exchange reaction.

Using these boundary conditions and equations (1.21) and (1.22), the electron flux at the electrode, $j_0$, which is proportional to the current, i, can be obtained:

$$j_0 = \frac{i}{FA} = -D_E\left(\frac{\delta b}{\delta x}\right)_0 \qquad \text{(Eq. 1.27)}$$

At this point an electrochemical rate constant, $k'_{ME}$, can be introduced. This relates the concentration of Y at the layer/solution interface to the electron flux, as follows:

$$j_0 = k'_{ME} y_s \qquad \text{(Eq. 1.28)}$$

The rate constant, $k'_{ME}$, can be evaluated from the intercept of Koutecky-Levich plots using rotating disk voltammetry [19]. The observed current, $i_F$, is thus related to the sum of the fluxes of direct ($j_Y$) and mediated ($j_B$) charge transfer and the concentration gradients at the electrode/film interface by:

$$(i_F/nFA) = j_0 = j_B + j_y = -D_E\,(\delta b/\delta x)_0 + D_Y\,(\delta y/\delta x)_0 = k'_{ME} y_s \qquad \text{(Eq. 1.29)}$$

As described previously, reaction layers are an essential component in the development of this theory. The first reaction layer, $X_L$, defines the distance which Y can travel within the film before it reacts with B and is represented in the following equation:

$$X_L = (D_Y/kb_L)^{1/2} \qquad \text{(Eq. 1.30)}$$

The second reaction layer, $X_0$, defines the average distance an electron can diffuse before reacting with Y, as follows:

$$X_0 = (D_E/ky_0)^{1/2} \qquad \text{(Eq. 1.31)}$$

With the concepts of, first, the electrochemical rate constant, and secondly, the reaction layer introduced, equations (1.23) and (1.24) can be considered more closely. Depending on the relative importance of electron and substrate diffusion, different approximations for $k'_{ME}$ can be obtained. If $D_e b_0 >> D_y k y_S$, i.e. fast electron

transport or slow permeation or ineffective partitioning of the substrate then the following equation is obtained:

$$\frac{1}{k'_{ME}} = \frac{y_s L}{D_e b_o} + \frac{1}{k'' b_o + k b_o K X_L \tanh(L / X_L)} \qquad \text{(Eq. 1.32)}$$

If permeation is very fast and/or electron transport within the film is relatively slower then $D_e b_0 << D_y k y_S$ and the equation becomes:

$$\frac{1}{k'_{ME}} = \frac{L}{k D_Y} + \frac{k'' \tanh(L / X_0) + k K X_0}{k K X_0 b_0 [k'' + k K X_0 \tanh(L / X_0)]} \qquad \text{(Eq. 1.33)}$$

From these two equations it can be deduced that the slower contributions to the mediating reaction, which can be kinetic or diffusional in nature, will determine the magnitude of $k'_{ME}$. In the limiting case, as represented by equation (1.32), the last term on the right hand side represents the competition between the surface reaction, $k''$, and the layer reaction, k. However, the flux may alternatively be limited to a value of $D_e b_0/L$ by electron transport through the film. The position of the reaction layer is reflected in the equation obtained for $k'_{ME}$ in these limiting cases and will depend on the ratio between the reaction layer, $X_L$, and the layer thickness, L. For cases where $X_L >> L$, the whole layer participates in the reaction, this is called the layer or L case. In the reverse case the reaction layer occurs in a thin layer at the layer/electrolyte interface, which is known as the surface or S case.

The position of the reaction layer in the second limiting case, as represented by equation (1.33), can be obtained by applying a similar approach. If the layer thickness is far greater than the reaction layer, $L >> X_L$, then the kinetic term can be presented as $kKX_0b_0$ and the reaction takes place in a layer adjacent to the electrode. This is called the layer/electrode or LE case. In the reverse situation, when $L >> X_0$, the reaction takes place at the layer/electrolyte interface. This is termed the layer/surface or LS case. For intermediate ratios of L and $X_0$, the reaction takes place throughout the entire layer.

Another situation arises when neither equations (1.28) or (1.29) are valid. This would be the case if the electron and substrate diffusion contribution are of an equivalent magnitude, and it can be described as:

$$\frac{D_e b_0}{K D_Y y_s} \approx \frac{X_0^2}{X_L^2} \approx 1 \qquad \text{(Eq. 1.34)}$$

Under such conditions, and if $X_0$ or $X_L$ is less than L, then the reaction will take place somewhere in the middle of the layer and is controlled by the diffusion rates of both electrons and substrate. This is called the layer/reaction zone or LRZ case. For this situation the solution for $k'_{ME}$ is given by:

$$\frac{1}{k'_{ME}} = \frac{L}{D_Y K + D_e b_0 / y_s} \qquad \text{(Eq. 1.35)}$$

Table 1.1 The kinetic cases possible at redox polymer modified electrodes along

| Case | A | $k'_{ME}$ | Location |
|---|---|---|---|
| Sk'' | - | $k'' b_0$ | Surface reaction at electrolyte |
| $St_e$ | E | $D_e b_0 / L y_s$ | layer interface |
| LSk | SR | $K(k b_0 D_Y)^{1/2}$ | Reaction layer close to electro- |
| $LSt_e$ | E | $D_e b_0 / L y_s$ | lyte layer interface |
| Lk | R | $K k L b_0$ | Throughout the layer |
| $LRZt_e t_Y$ | S + E | $\frac{D_e b_0}{L y_s} + \frac{K D_Y}{L}$ | Narrow reaction zone in layer |
| LEk | ER | $K b_0 (D_e k / y_s)^{1/2}$ | Reaction layer close to |
| $LEt_Y$ | S | $K D_Y / L$ | electrode |
| $Ek'_E$ | - | $k'_E$ | Direct reaction |
| $Et_Y$ | S | $K D_Y / L$ | on electrode |

From these equations it can be seen that the LE, LS and S cases can be controlled either by the transport or by the kinetic term. So, depending on the relative importance of these two terms, these cases can be subdivided into two subclasses. These subclasses are controlled either by transport processes, in which case they are labelled $t_e$ or $t_y$, depending on whether electron or substrate transport is rate limiting, or by kinetic factors, in which case the label is k or $k^{''}$. So LEk denotes a mediated reaction that takes place at a layer close to the underlying electrode surface and is controlled kinetically. In the $LEt_y$ case the reaction takes place in the same part of the layer but is controlled by substrate transport.

Table 1.1 lists the various limiting cases along with their corresponding rate constants. Figure 1.10 gives a diagrammatic representation of the various different positions and notations for the reaction layer.

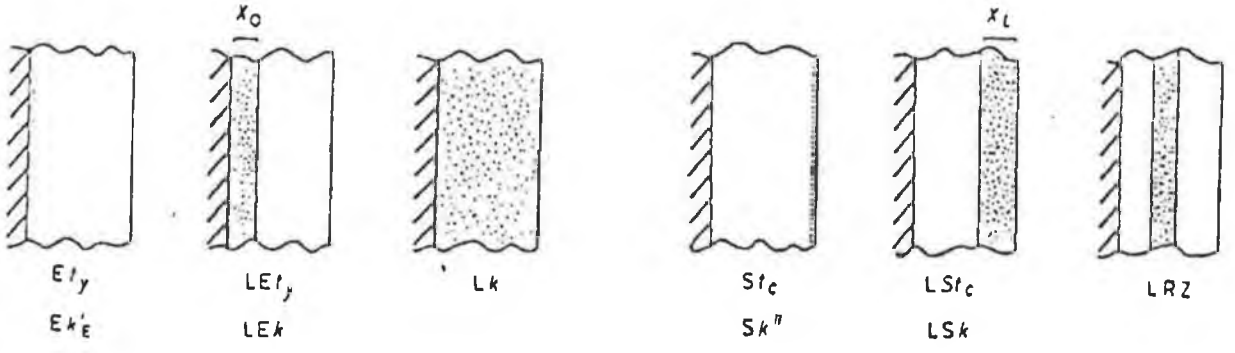


Figure 1.10 Locations of the possible reaction zones at redox polymer modified electrodes and the notation used to describe them [34].

Albery and co-workers have used these equations to construct a kinetic zone diagram[39]. An example of such a diagram showing the layer cases is given in Figure 1.11. Some of the parameters described above such as $b_0$, $y_S$ and L can be easily changed, while others such as $D_E$, $D_Y$ and k are not so easily variable. All these parameters are, though, subject to changes in the nature of the electrolyte and its concentration, and to temperature.

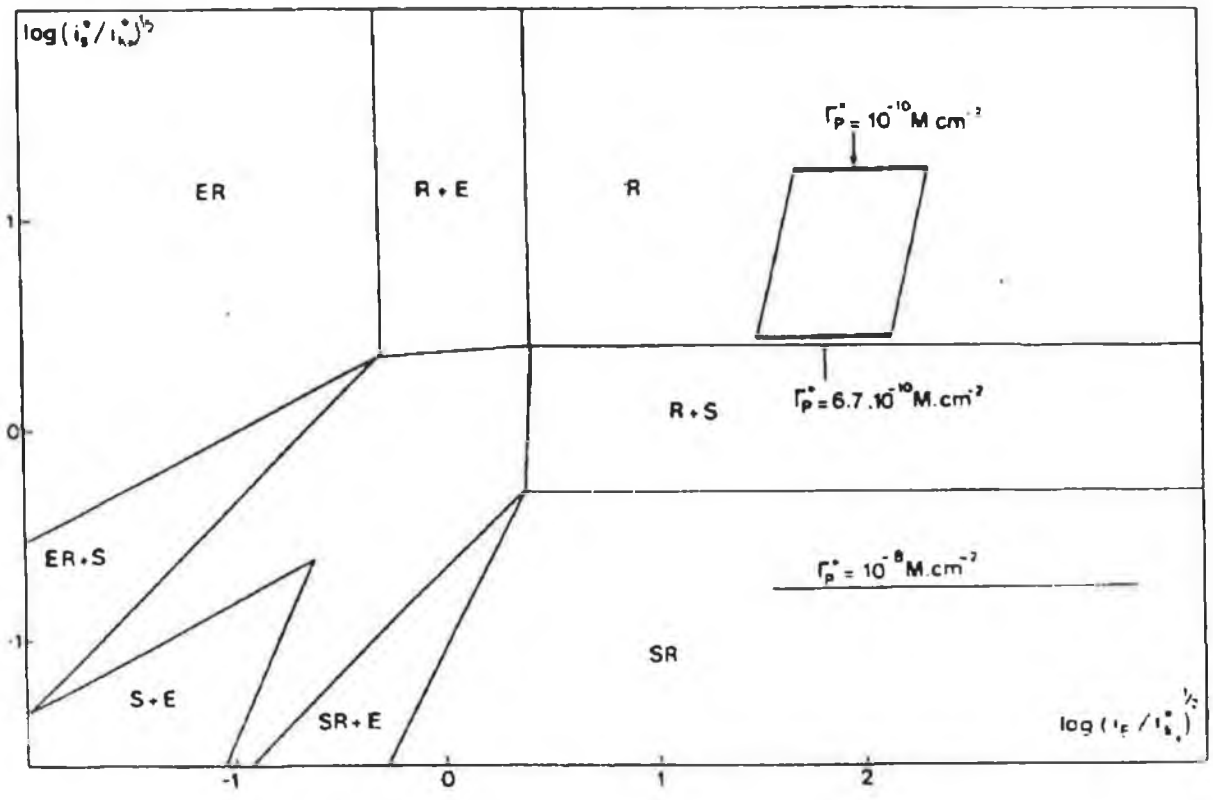


Figure 1.11 Kinetic zone diagram showing the kinetic control of the processes taking place in the redox polymer ilm as a function of surface coverage, Γ. [30]

The Saveant approach leads to the same conclusions as the Albery model, without recourse to reaction layers. Instead the mediating processes are described by the characteristic current, $i_A$, $i_S$, $i_E$ and $i_K$. These currents represent the contribution to the observed currents by substrate diffusion from the solution to the electrode surface, substrate diffusion within the film, electron diffusion within the film by the rate of the cross-exchange reaction between the redox centre and the substrate. The equations described for these characteristic currents and the processes they describe are given in the following equations:

The substrate diffusion from the solution to the film.

$$i_A = FAC_A^0 D / d \qquad \text{(Eq. 1.36)}$$

Substrate diffusion in the film.

$$i_S = FAC_A^0 D_S K / L \qquad \text{(Eq. 1.37)}$$

Electron transfer between redox sites in the film, the electron self-exchange process.

$$i_E = FAC_P^0 D_E / L \qquad \text{(Eq. 1.38)}$$

The cross-exchange reaction between the redox centre and the substrate in the film.

$$i_K = FAC_A^0 kKC_0 L \qquad \text{(Eq. 1.39)}$$

In these equations, F is the Faraday constant, $C_A$ is the bulk concentration of the redox substrate, $C_P$ is the concentration of the redox site within the film, A is the electrode area, D is the diffusion coefficient of the substrate in solution, $D_E$ is the charge transport parameter describing electron movement through the film, $D_S$ is the substrate diffusion within the film, K is the partition coefficient of the substrate between the film and the solution, k is the second order rate constant describing the mediated reaction between the film and substrate, d is the diffusion layer thickness and L is the film thickness.

The conditions for optimum efficiency of modified electrodes have been considered by Albery and Hillman and by Andrieux et al. They are a high value for $k'_{ME} / k'_E$, the ratio between the electrochemical rate constant for the modified and bare electrode. In their studies, factors such as the thickness of the modifying layer and limits for the kinetic parameters were considered. Where the electrode response has been optimised with respect to electron transport and morphology, it is usually found that electron diffusion is faster than substrate diffusion and that the concentration of the surface-bound redox couple is larger than that of the substrate.

The optimum efficiency cases are LSk and LEk. LSk corresponds to rapid electron transfer compared to substrate diffusion through the film, with the reaction occurring

near the layer/electrolyte interface with the exact position depending on the mediated rate constant, k. In the LEk case, the mediated reaction occurs close to the underlying electrode surface. For the layer cases, the magnitude of $k'_{ME}$ will initially increase with the layer thickness, since all the redox couple sites mediate electron transfer under kinetic control, and will then reach a maximum before decreasing due to transport limitations of the substrate. Therefore, these ideal cases correspond to sufficient mediation sites for substrate consumption combined with efficient charge diffusion through the layer, resulting in an ideal three-dimensional modified electrode. For the LSk case the catalytic advantage becomes:

$$k'_{ME}/k'_E = KX_L/l \qquad \text{(Eq. 1.40)}$$

This can be very large as the thickness of the reaction layer can be much greater than the distance, *l*, over which electron transfer can take place. Therefore, for reactions whose homogeneous kinetics are slow, a layer reaction is required where Y permeates the film rapidly. This requires an open porous structure for the film so that B can easily permeate through it. This must be coupled with rapid electron transport so that charge transfer isn't limiting.

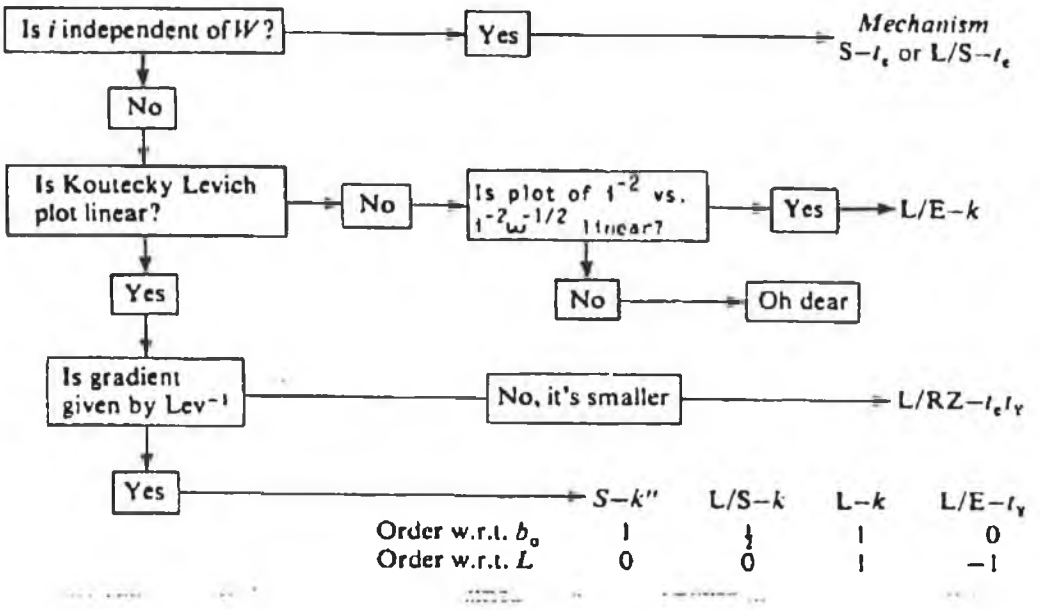


Figure 1.12 Diagnosis of mechanism for redox polymer modified electrodes [46].

Last for consideration are the optimum surface and electrode cases, notated as $Sk^{'}$ and $E\ k^{'}_{E}$. In these cases mediation is no longer through-layer, instead the reaction is limited to the layer/solution and the electrode/layer interface respectively. In other words, the reaction is restricted to a monolayer.

The experimental determination of the parameters involved in the theoretical approach described above relies on recognition of the appropriate limiting processes. It is the use of the rotating disk and of the rotating ring-disc electrode which provides the means of analysing the kinetics of catalysis at the modified electrode surface. These techniques allow control of the substrate diffusion in solution and thereby the elucidation of the kinetics and mechanism of the electrocatalytic reaction. By controlling the electrode potential, the concentration of the species in solution at the modified electrode surface can be reduced to zero and the current response becomes limited by mass transport and can be described by the Levich equation [40]:

$$i_{Lev} = 1.554nAFD^{2/3}\nu^{-1/6}y\omega^{1.2} \qquad \text{(Eq. 1.41)}$$

Since the rate of mass transport of the substrate can thus be calculated, rotating disc measurements are an ideal technique for the investigation of mediated reactions at electrode surfaces and literature shows it has been widely exploited [41-44]. However, the modified electrode behaviour is not always described by the Levich equation as mass transport may not represent the rate-limiting process in all cases. A model for such cases can be constructed using a variation of the Levich equation as follows:

$$1/i_{\mathrm{Lim}} = i/i_{\mathrm{F}} + 1/i_{\mathrm{Lev}} \qquad \text{(Eq. 1.42)}$$

or for a redox polymer [19]

$$1/i_{\mathrm{Lim}} = (nFAk^{'}_{ME}y)^{-1} + (1.554nAFD^{2/3}\nu^{-1/6}y\omega^{1/2})^{-1} \qquad \text{(Eq. 1.43)}$$

This is known as the Koutecky-Levich equation [45] and a plot of $i^{-1}$ versus $w^{-1/2}$ gives a straight line, whose slope is the reciprocal of the Levich slope and whose intercept is equivalent to the modified electrode rate constant, $k'_{ME}$. Albery and Hillman have published a useful flowchart for the diagnosis of reaction type based on this mode of analysis [46] as shown in Figure 1.12. In this flowchart the functional dependence of $k'_{ME}$ on $b_0$, $y_S$ and L allows classification of the mechanism for modified electrodes.

## 1.5 Preparation of Modified Electrodes

A modified electrode has its electrode surface deliberately altered in such a way that its ability to measure particular species in solution is enhanced. Modification can be by processes such as adsorption or covalent attachment. The modified electrode thus produced may demonstrate greater selectivity due to the inhibition of some electrode processes and the promotion of others. Often the modifying layer is electroactive and acts by mediating the electron transfer between an electroactive substance in solution and the electrode itself. Some of the techniques used in the modification and recent examples in the literature will now be discussed.

There is a wide choice of materials [5] to use for the underlying electrode to which the modifying layer is attached. Which material is used depends on factors such as the potential range in which the experiments are to take place, the electrolytic solvent that will bathe the electrode and the particular qualities of the electrode material.

The most common types of electrode materials used for this purpose are metal and carbon. Metal electrodes have high conductivity, ease of construction and of polishing. However they can also undergo corrosion and passivation. Carbon electrodes can exist in a number of different conducting forms. Generally electrochemical reactions are slower at carbon electrodes in comparison with metal electrodes. However, the kinetics are highly dependent on the surface preparation of the electrode. Probably the most widely used material for the underlying electrode is

glassy carbon. It is formed by heating a mixture of phenol and formaldehyde polymers or polyacrylonitrile between 1000°C and 3000°C under pressure. The structure of glassy carbon is showed in Figure 1.13.

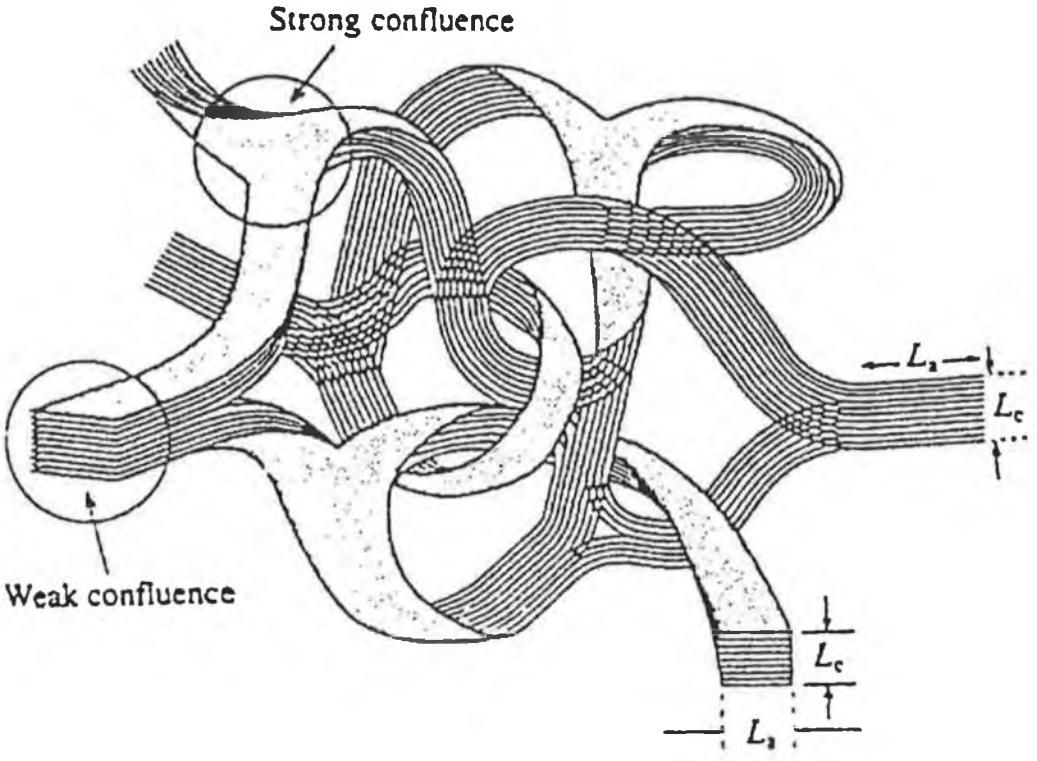


Figure 1.13 Representation of the structure of glassy carbon. La and Lc refer to the length and thickness of the microcrystallines respectively [5].

## 1.6 Covalent Attachment

In this technique an electroactive species is immobilised on the electrode surface by a chemical reaction. A common method is the silanization process. Silane groups are reacted with naturally occurring hydroxyl groups on the electrode surface. These in turn react with the species of interest.

Reflux and vacuum distillation techniques have been used to silanize glass to indium tin oxide coated surfaces. Further modification could be undertaken by covalently attaching species to the aminosilanized surfaces [47].

The covalent attachment of toluidine blue as a monolayer on a gold electrode which had previously been modified by chemisorption of sulphur-containing compounds has been described [48]. This modified electrode was found to possess an amperometric response dependent on the concentration of the substrate, in this case NADH oxidation. The availability of functionalised ultra-thin-layer systems to which different species can be immobilised may prove useful by improving the reproducibility and acquisition time of the amperometric response.

A modified electrode useful in the determination of phenolic compounds was formed by the covalent attachment of the enzyme phenol oxidase to carbon [49]. With the aim of developing electrochemical sensors for iron (III), a method was described in the literature which used covalent attachment of hydroxamic acid groups to carbon paste electrodes [50]. The direct covalent attachment of glucose oxidase to an activated platinum surface was used to form a glucose-sensitive electrode [51]. Glucose oxidase has also been successfully immobilised onto electrode surfaces using carbodiimide to facilitate direct covalent attachment [52]. Carbon paste electrodes modified by the inclusion of octadecylamine or stearic acid further modified by the covalent binding of DNA. Such modified electrodes have been applied to the selective detection of the cystic fibrosis sequence in an 18 base nucleotide sample [53].

## 1.7 Adsorption

This method has found widespread use in the modification of many types of species to electrode surfaces. Particularly in the preparation of polymer modified electrodes. Electroadsorption is a similar technique except that an applied electrode potential is used.

Direct adsorption on a graphite electrode was found to be a satisfactory technique for the immobilisation of enzymes on such surfaces. In complex media such as blood, interference was found to be greatly reduced [54].

A prussian blue-modified vitreous-carbon electrode prepared by simple adsorption of hydrazine in cyclic voltammetry showed excellent stability and electrocatalytic activity in the oxidation of hydrazine but when placed in a flowing stream, the modifying layer quickly destabilised [55]. Further modification using Nafion helped to redress this effect.

Electrodeposition has been used to prepare a polypyrrole modified platinum electrode whose stability was demonstrated when it was utilised in a microelectrochemical flow cell [56]. A carbon electrode modified by the electrodeposition of a film of mixed valent cobalt oxide/cyanocobaltate was found to be suitable for the catalytic oxidation of hydrazine compounds [57]. A vitreous-carbon electrode modified by the electrodeposition of palladium was found to have useful qualities in the development of a cholesterol biosensor [58]. The modified electrode provided a stable surface for the immobilising of cholesterol oxidase to produce a stable and reproducible sensor. Chemisorption was also used to immobilise DNA onto a gold electrode [59].

To produce biosensors based on conducting polymers, films of polymers such as polypyrrole are formed on electrode surfaces and by covalent attachment of the enzyme to functional groups in the conducting polymer film [60]. The active centres in redox enzymes are often submerged in the protein structure. An N-substituted pyrrole derivative was modified with an osmium complex and a co-polymer of this compound, pyrrole and pyrrole-modified glucose oxidase were coated onto an electrode surface. In the presence of glucose a direct electron transfer was observed between the redox centre of the enzyme and the electrode surface by electron hopping across the osmium redox centres present in the polymer.

## 1.8 Applications of Modified Electrodes

Having discussed the theory and preparation of modified electrodes, part two of this introduction will illustrate the many electroanalytical applications which have been arisen as a result of exploitation of this flexible approach to producing a sensing surface. These applications utilise the unique characteristics of modified electrodes.

The modification of electrode surfaces can be used for improving the analyte response compared with that obtained at an unmodified surface, to create a novel response to an analyte, to increase the stability and reproducibility of the electrode's response to an analyte, to enhance the selectivity of the electrode's response, or to reduce the effect of interferences on the electrode's response.

Therefore, for electroanalytical applications it is necessary to consider how such properties can be incorporated into sensors constructed from modified electrodes. The ideal sensor should be sensitive, selective, free from interferences and be stable and reproducible. It should also have a low limit of detection, work over a large concentration range and be capable of a high analytical through-put.

Modification of electrodes to achieve these goals can be undertaken in a number of ways. Preconcentration, permselectivity and electroanalysis methods are the most typical. By applying or combining these techniques to modified electrode design, sensors can be produced which achieve some or all of these attributes to varying degrees. Preconcentration and permselectivity applications will be discussed initially followed by an examination of electroanalytical applications. This review will mostly consider recent developments in the application of modified electrodes as a number of reviews have been published recently which comprehensively cover past developments. [61-66]

## 1.8 Preconcentration and Permselectivity

Preconcentration is often achieved by utilising ion-exchange, complexation and precipitation methods. Preconcentration can also be a selective technique when

combined with selective concentration of a particular analyte by selecting for molecular properties such as size, charge, shape and polarity [67,68].

Preconcentration essentially involves accumulating the target analyte at the electrode surface before its determination. This process generally involves adsorption of the species onto the electrode for a fixed period of time under potential control followed by reduction or oxidation of the accumulated analyte at the electrode [69]. By manipulating the modifying surface on the electrode, the limits of this technique can be extended from the best known electrode surface used for this technique – mercury. Mercury has a low background current because of its large hydrogen overpotential but the choice of analyte is limited. Ion-exchange [70-73], complexation [74-76] and precipitation [77] have been used in the development of preconcentration type modified electrodes.

Permselective films added to electrode surfaces confer selectivity onto the modified electrode by separating the response of the substrate from interfering species and improving the electrode's response by selectively partitioning the analyte within the modifying layer. Permselectivity provides a refinement of the preconcentration technique. It allows separation of the analyte from interfering species at the electrode surface thereby selecting for the analyte whilst simultaneously protecting the underlying electrode surface.

Preconcentration and permselective techniques when used in unison can help stabilise the modified electrode's response and extend its lifetime by discouraging passivation of the electrode. In polymer modified electrodes once the analyte has passed the permselective barrier, if a preconcentration layer is present, the electrode's response will be increased and its sensitivity will also be increased compared to a non-active diffusion of the analyte to the underlying electrode surface. Such a preconcentration step is often necessary because permselective films can cause a diminution in the electrode's sensitivity due to the effect of the film on mass transport.

Electroanalyses of a number of analytes using poly(vinylferrocennium) perchlorate

coated platinum electrodes has been described which utilises a preconcentration step. This chemically modified surface contains ferrocenium/ferrocene sites and electrooxidation and electroreduction can take place at these sites. An anion exchange process can incorporate anions such as iodide, thiocyanate and cyanide into the modifying layer. After preconcentration of the target substrate, anodic stripping of the anions from the polymer modified electrode can be carried out. Further modification of the electrode can be achieved by incorporating enzymes into the polymer structure to achieve a more selective response and it has been demonstrated that immobilisation of glucose oxidase and invertase into the poly(vinylferrocenium) allows development of an amperometric sucrose sensor [77].

Polypyrrole (PP) has been used both for its preconcentration and permselective properties. The ability of N-carbodithioate PP to concentrate copper has been demonstrated [78]. Its utility as a permselective layer has been exploited to form an interference free glucose sensor [79].

Not just PP but other polymer films such as polyaniline and polyphenol have been shown to be permselective towards analytes such as hydrogen peroxide, catechol and acetaminophen [80]. These conducting polymers can be switched between an oxidised conducting state and a reduced insulating state. This property was exploited for developing a sensor of electroinactive anions. This involved the electropolymerisation of a PP layer onto a platinum electrode. When held at an oxidising potential, the addition of carbonate, phosphate and acetate caused an anionic current peak to form. Applying a reducing potential allowed the regeneration of the polymer layer [81].

Permselectivity has been utilised in the production of a sensor for the electrochemical detection of alcohols and carbohydrates. Electrochemical polymerisation of 4-(3-hydroxyphenylacetyamino)-2,2,6,6-tetramethylpiperidinyl-1-oxyl onto a glassy carbon (GC) electrode was used to produce a modified electrode for use in FIA. This modifying surface facilitated the detection of a number of alcohols due to their interaction with the hydrophobic modifying film [82].

The application of a permselective layer to the development of an amperometric sensor for choline has been shown. A carbon fibre electrode modified by immobilising horseradish peroxidase and choline oxidase within a redox polymer was found to be selective towards choline but ascorbate interfered by acting as a reducing agent within the polymer. By adding a Nafion layer to the modified surface the ascorbate could be selectively excluded from the underlying polymer matrix [83].

An electrochemical nitrate biosensor has recently been described based on an ultrathin film composite membrane. The composite membrane is prepared by electropolymerisation of a thin anion-permselective coating of 1-methyl-3-(pyrrol-1-methyl)pyridinium onto a microporous support membrane. This film separates the analyte solution from a solution containing the enzyme nitrate reductase and a methylviologen catalyst which is in contact with a GC electrode. The permselective film allows the selective movement of the nitrate substrate into the sensing solution where it can be reduced enzymatically. The resulting oxidised form of the enzyme can then be reduced by the electrocatalyst. The GC electrode's response to the methylviologen reduction can then be related to the initial nitrate concentration [84].

## 1.10 Electroanalysis

The application of polymer modified electrodes to mediated electrocatalysis can result in the reduction or elimination of overpotentials or to reduce the redox potential of the analyte in order to reduce interferences. The redox reaction can also occur at a higher rate compared to the unmodified electrode. Modified electrodes which demonstrate electrocatalytic properties include deposited metallo-polymers, polymer immobilised micro-particles and inorganic films on electrodes.

Inorganic film modified electrodes can be categorised as a number of types, namely metal phthalocyanines [85-87], metal porphyrins [88-90], polynuclear transition metal cyanides [91-93], metal oxides [94,95] or zeolites/clays [96-98]. But their selectivity is limited because of their broad catalytic response to substrates and they are

generally used in combination with selective methods such as ion chromatography. A dispersed Pt modified electrode was found to detect nitrite at an applied potential of 1.1 V vs. SCE. To prevent interferences from affecting its response, it was used as a sensor within an exclusion chromatography manifold [99,100]. Colloidal gold supported onto a GC electrode has been used to detect carbohydrates in flow injection and ion chromatography systems.

Polymer immobilised micro-particles have also been reported for use in electrocatalytic detection. Voltammetric determination of uric acid by electrooxidation at a Nafion-Ruthenium oxide pyrochlore modified electrode [101] has been reported as has a Nafion modified electrode which incorporated ytterbium and uranyl particles used for nitrate detection [102]. A modified electrode prepared by electropolymerisation of 4-vinylpyridine onto a glassy carbon (GC) electrode formed a polyvinylpyridine (PVP) surface onto which palladium was electrodeposited. The ion-exchange ability of the PVP aided this electrodeposition and this PVP/Pd film electrode was found to retain mechanical stability in a flowing stream whilst displaying a sensitive response to the analyte, hydrazine [103]. The mediator osmium phenanthrolinedione was mixed with glucose dehydrogenase, $NAD^+$ and carbon paste to form a modified electrode. It's redox potential was at 0.15 V vs. Ag/AgCl and it was found to respond well to its substrate, glucose [104].

Electrodes modified with metallo-polymers are widely described in the literature. They contain a metal-containing mediator site covalently bound within a three dimensional polymer network. The theory describing their kinetic and transport characteristics has been discussed earlier in this chapter [33-35]. Analysis of this theory can be used in the design and optimisation of metallo-polymer modified electrodes. Such redox polymers have been found to be mechanically robust, producing a more stable and long-lived response – a particular advantage when used under hydrodynamic conditions such as found in FIA systems.

The use of ruthenium and osmium species as mediator sites within redox polymers has found extensive application [105-110]. Electrodes modified by drop coating

preformed redox polymers with the general formula $[M(bpy)_2(pol)_nCl]Cl$, where M is a ruthenium or osmium metal centre co-ordinated to 2,2'-bipyridine ligands (bpy) and attached to a pyridine or imidazole nitrogen of a PVP or poly(N-vinylimidazole) polymer (pol), have been prepared and characterised with respect to charge transport rates and mechanisms. The complexes of these metal centres have displayed facile reversible kinetics at various electrode surfaces, their complexes are stable in a number of oxidation states, the $E_{1/2}$ of the metal centre can be regulated by controlling its coordination sphere and their electrochemistry is well documented.

Neutron reflectivity has been used to observe the behaviour of $[Os(bpy)_2(PVP)_{10}Cl]Cl$ polymer films with respect to pH and counterion [111]. The polymer film structure was found to be dependent upon factors such as film hydration, the nature and effect of the counterion and pH. PTSA was found to allow electrolyte to enter the film causing it to swell and affecting its permselectivity properties whilst perchlorate left the film relatively unaffected. In general it was found that film swelling occurred to a greater extent near the polymer/solution interface compared to the inner part of the film.

The use of the electrochemical quartz crystal microbalance technique to examine the interaction of osmium redox polymer films with $HClO_4$ electrolyte has been used to examine the solvent and ion content of polymer coatings and to measure the $pK^{app}_a$ of the polymer units [112]. For the polymers investigated in this study, there was found to be good correlation between the mass change observed in the electrolyte and the mass change anticipated.

The examination of the effect of the nature of the polymer backbone on the stability and analytical response to a slightly different type of osmium redox polymer - $[Os(bpy)_2(PS)_{7.5}(DMAP)_{2.5}Cl]Cl$, where PS is polystyrene and DMAP is poly[4-(N-methyl-N-p-vinylbenzylamino)pyridine, has shown that this general model for designing modified electrodes is highly flexible [113]. Using well documented synthetic routes, tailor-made electrode surfaces can be prepared. The polymer material used in this study showed improved physical stability. The redox potential

of the osmium centre did not change, however, charge transport and permeability of the polymer film were affected compared with the PVP based film.

The electrochemical behaviour of the Os(II)/Os(III) couple immobilised with the cross-linked $[Os(bpy)_2(PVP)_{10}Cl]Cl$ redox polymer has been examined [114]. The redox couple demonstrated Nernstian behaviour with a slope of 0.058 V decade$^{-1}$ over the range $-2 \geq \log [Os(III)/Os(II)] \leq +2$. The potential at which this modified electrode was examined was varied and so too was the polymer layer thickness. The resulting amperometric responses to Fe(III) and $NO_2^-$ reduction were examined and presented as three dimensional plots. These plots demonstrated the ability of the modified electrode to distinguish between these two reductions since the two reactions took place at different areas of the modifying layer. The Fe(III) reduction is a surface reaction and the $NO_2^-$ is a through film reaction.

The application of $[Os(bpy)_2(PVP)_{10}Cl]Cl$ polymers for use in biosensors is a growing area due to their low redox potentials and rapid charge transport characteristics [115]. An amperometric biosensor for in vivo glucose sensing has been developed based on glucose oxidase immobilised in a cross-linked poly(vinylpyridine) complex of $[Os(bis\text{-}bipyridine)_2Cl]^{+1/+2}$. The osmium redox centres mediated the electron transfer between the underlying electrode, which in this case was a platinum wire, and the flavin adenine dinucleotide redox centres contained in the glucose oxidase [116].

A hydrogel containing $[Os(2,2'\text{-}bipyridine)_2(N\text{-}methylimidazole)Cl]^+$ was immobilised onto a glassy carbon electrode along with the oxygenase enzymes, laccase and tyrosinase. The resulting modified electrodes were found to be useful in the detection of enzyme inhibitors with reproducible inhibition curves being obtained from the sensors' response [117].

Redox polymer electrodes prepared using electrochemical deposition techniques were also detailed. In one type, $[Os(bpy)_2(PVP)_{10}Cl]Cl$ and glucose oxidase were electrochemically deposited onto a platinum surface simultaneously with a polyphenol film. In a second type, the osmium polymer was adsorbed onto the

platinum electrode first followed by a glucose oxidase/polyphenol film. The bilayer electrode was found to exhibit greater sensitivity to glucose and to suffer less interference from other electroactive compounds [118].

## 1.11 Conclusion

This thesis will examine the electrochemical behaviour of ruthenium and osmium redox polymer modified electrodes. The performance of these modified electrodes will be examined in conventional three electrode assemblies and will then be compared with the response in flow injection assemblies. The results will be used in the development of sensors for use on "real" samples.

## 1.12 References


1 J. D. Wright, Chemistry in Britain, 31 (1995) 374

2 S. Gould, R. M. Leasure, T. J. Meyer, Chem. Britain, 31 (1995) 891

3 E. A. Seddon, K. R. Seddon, The Chemistry of Ruthenium, Amsterdam, Elsevier, 1984

4 R. W. Murray, A. G. Ewing, R. A. Durst, Anal. Chem., 59 (1987) 379A

5 C. M. A. Brett, A. M. O. Brett, Electrochemistry, Oxford, Oxford University Press, 1993

6 G. Gouy, Compt. Rend., 149 (1910) 654; D. L. Chapman, Phil. Mag., 25 (1913) 475

7 J. O'M. Bockris, M. A. Devananthan, K. Muller, Proc. R. Soc., A274 (1963) 55

8 S. Trasatti in A. F. Silva ed., Trends in Interfacial Electrochemisry, Reidel, Dordrecht, 1985, 25-48

9 P. T. Kissinger, W. R. Heineman, J. Chem. Educ., 60 (1983) 702

10 A. J. Bard, L. R. Faulkner, Electrochemical Methods, New York, John Wiley and Sons, 1980

11 J. F. Cassidy in M. R. Smyth, J. G. Vos, eds., Analytical Voltammetry, Amsterdam, Elsevier, 1992

12 H. Matsuda, Y. Ayabe, Z. Elektrochem., 59 (1955) 494

13 E. Laviron in A. J. Bard, ed., Electroanalytical Chemistry, New York, Dekker, 1982

14 T. Edmonds (ed.), Chemical Sensors, New York, Blackie: Chapman and Hall, 1988

15 K. Stulik, V. Pacakova, Electroanalytical Measurements in Flowing Streams, Chichester, Ellis Horwood

16 B. Karlberg, G. E. Pacey, Flow Injection Analysis, Amsterdam, Elsevier

17 Electrochemical Detection in HPLC, Germany, Hewlett-Packard, 1989

18 D.C.S. Tse, T. Kuwana, Anal. Chem., 50 (1978) 1315

19 W. J. Albery, A.R. Hillman, Ann. Rep. Prog. Chem., C, 78 (1981) 377

20 G. Inzelt, G. Horanyi, J. Q. Chambers, J. Electroanal. Chem., 218 (1987) 297

21 K. Shigehara, N. Oyama, F. C. Anson, J. Am. Chem. Soc., 103 (1981) 2552

22 F. C. Anson, J. M. Saveant, K. Shigehara, J. Phys. Chem., 87 "(1983) 214

23 J. Leddy, A. J. Bard, J. T. Maloy, J. M. Saveant, J. Electroanal. Chem., 187 (1985) 205

24 R. D. Rocklin, R. W. Murray, J. Phys. Chem., 85 (1981) 2104

25 D. A. Buttry, F. C. Anson, J. Electroanal. Chem., 130 (1981) 333

26 J. M. Saveant, K. B. Su, J. Electroanal. Chem., 171 (1984) 431

27 C. P. Andrieux, J. M. Dumas-Bouchiat, F. M'Halla, J. M. Saveant, J. Electroanal. Chem., 113 (1980) 19

28 C. P. Andrieux, J. M. Dumas-Bouchiat, J. M. Saveant, J. Electroanal. Chem., 131 (1982) 1

29 C. P. Andrieux, J. M. Dumas-Bouchiat, J. M. Saveant, J. Electroanal. Chem., 169 (1984) 9

30 C. P. Andrieux, J. M. Saveant, J. Electroanal. Chem., 171 (1984) 65

31 C. P. Andrieux, J. M. Saveant, J. Electroanal. Chem., 142 (1982) 1

32 C. P. Andrieux, J. M. Saveant, J. Electroanal. Chem., 134 (1982) 163

33 W. J. Albery, A. W. Foulds, K. J. Hall, A. R. Hillman, J. Electrochem. Soc., 127 (1980) 654

34 W. J. Albery, A. R. Hillman, J. Electroanal. Chem., 170 (1984) 27

35 W. J. Albery, W. R. Bowen, F. S. Fisher, A. W. Foulds, K. J. Hall, A. R. Hillman, G. G. Edgell, A. F. Orchard, J. Electroanal. Chem., 107 (1980) 37

36 K. Aoki, K. Tokuda, H. Matsuda, J. Electroanal. Chem., 199 (1986) 69

37 S. Komorsky-Lovric, M. Lovric, Anal. Chim. Acta, 305 (1995) 248

38 M. Delamar, M. C. Pham, P. C. Lacaze, J. E. Dubois, J. Electroanal. Chem., 108 (1980) 1

39 F. C. Anson, J. Phys. Chem., 84 (1980) 3336

40 V. G. Levich, Physicochemical Hydrodynamics, Prentice Hall, Englewood Cliff, N. Y., 1962

41 T. Ikeda, C. R. Leidner, R. W. Murray, J. Electroanal. Chem., 138 (1982) 343

42 T. Ikeda, R. Schmehl, P. Denisevich, K. Willman, R. W. Murray, J. Am. Chem. Soc., 104 (1982) 2683

43 Y. Ohnuki, H. Matsuda, T. Osaka, N. Oyama, J. Electroanal. Chem., 158 (1983) 55

44 F. C. Anson, J. M. Saveant, K. Shigehara, J. Electroanal. Chem., 145 (1983) 423

45 J. Koutecky, J. G. Levich, Zh. Fiz. Khim., 32 (1958) 1565

46 W. J. Albery, M. G. Boutelle, A. R. Hillman, J. Electroanal. Chem., 182 (1985) 99

47 R. Wilson, D. J. Schiffrin, Analyst, 120 (1995) 175

48 D. D. Schlereth, E. Katz, H. L. Schmidt, Electroanalysis, 6 (1994) 725

49 L. Ortega, E. Dominguexz, E. Burestedt, J. Emneus, L. Gorton, G. Marko-Varga, J. Chromatogr., 675 (1994) 65

50 D. W. M. Arrigan, J. D. Glennon, G. Svehla, Anal. Proc., 30 (1993) 141

51 G.J. Moody, G. S. Sanghera, JDR Thomas, Anal. Proc., 23 (1986) 446

52 E. R. Reynolds, A. M. Yacynych, Electroanalysis, 5 (1993) 405

53 M. K. Millan, A. Saraullo, R. S. Mikkelsen, Anal. Chem., 66 (1994) 2943

54 G. Palleschi, H. S. Rathore, M. Mascini, Anal. Chim. Acta, 209 (1988) 223

55 W. Hou, E. Wang, Anal. Chim. Acta, 257 (1992) 275

56 P. Ward, M. R. Smyth, Talanta, 40 (1993) 1131

57 J. X. Zhou, E. K. Wang, Talanta, 40 (1993) 943

58 S. J. Dong, Q. Deng, G. G. Cheng, Anal. Chim. Acta, 279 ( 1993) 235

59 K. Hashimoto, K. Ito, I. Yoshio, Anal. Chem., 66 (1994) 3830

60 W. Schuhmann, GIT-Fachz..-Lab., 39 (1995) 563

61 R.W. Murray in Electroanalytical Chemistry, V. 13, (A.J. Bard, ed.), Marcel Dekker, New York, 1984, p. 191

62 A.R. Hillman in Electrochemical Science and Technology of Polymers, V. 1, (R.G. Linford, ed.) Elsevier, Amsterdam, 1987, pp. 102, 241

63 J. Wang, Electroanalysis, 3 (1991) 255

64 R.J. Forster, J. G. Vos in Comprehensive Analytical Chemistry, V. 27, (G. Svehla, ed., M.R. Smyth, J.G. Vos, volume eds.), Elsevier, Amsterdam, 1992, p. 465

65 J. Janata, M. Josowicz, D.M. DeVaney, Anal. Chem., 66 (1994) 207R

66 D.P. Leech in Electroactive Polymer Electrochemistry, Part 2, (M.E.G. Lyons, ed.), Plenum, New York, 1996, p.269

67 M. D. Baker, C. Senartne, Anal. Chem., 64 (1992) 697

68 J. Wang, L.D. Hutchins, Anal. Chem., 58 (1986) 402

69 Z. Gao, M. Zi, B. Chem, Anal. Chim. Acta, 286 (1994) 213

70 N. Oyama, T. Ohsaka, T. Okajima, Anal. Chem., 58 (1986) 979

71 J.F. Cassidy, K. Tokuda, J. Elec. Chem., 285 (1990) 287

72 W. Diewald, K. Kalcher, X. Cai, R.J. Magee, Anal. Chem. Acta, 273 (1993) 237

73 D.W.M. Arrigan, G. Svehla, S.J. Harris, M.A. McKorvey, Electroanalysis, 6 (1994 97

74 E. Lorenzo, J. Fernandez, F. Pariente, K. Trible, B. Pendley, H.D. Abruna, J. Elec. Chem., 356 (1993) 43

75 S.K. Cha, B.K. Ahn, J-U. Hwang, H.D. Abruna, Anal. Chem., 65 (1993) 1564

76 G.G. Wallace, Y.P. Lin, J. Electroanal. Chem., 247 (1988) 145

77 H. Gulse, S.S. Celebi, H. Ozyoruk, A. Yildiz, Pure App. Chem., 69 (1997)173

78 (a) D.M.T. O'Riordan, G.G. Wallace, Anal. Proc., 22 (1985) 199; (b) D.M.T.

O'Riordan, G.G. Wallace, Anal. Proc., 23 (1986) 14

79 Q.S. Li, B.X. Liu, J.T. Jin, Z.K. Zhang, J.J. Zhong, Anal. Lett, 31 (1998) 937

80 J. Wang, S.P. Chen, M.S. Lin, J. Electroanal. Chem., 273 (1989) 231

81 Y. Ikariyama, W.R. Heineman, Anal. Chem., 58 (1986) 1803

82 Y. Yamauchi, H. Maeda, H. Ohmuri, Chem. Pharm. Bull., 45 (1997) 2024

83 M.G. Garguilo, A.C. Michael, Anal. Chem., 66 (1994) 2621

84 L.M. Moretto, P. Ugo, M. Zanata, P. Guerrira, C.R. Martin, Anal. Chem., 70 (1998) 2163

85 E.F. Perez, G.D. Neto, A.A. Tanaka, L.T. Kubota, Electroanalysis, 10 (1998) 111

86 M.A. Carsol, I. Pouliquen-Sonaglia, G. Lesgards, M. Mascini, Food Tech. Biotech., 34 (1996) 147

87 C.Q. Sun, X.Y. Zhang, D. Jiang, Q.A. Gao, H.D. Xu, Y.P. Sun, X. Zhang, J.C. Shen, J. Electroanal. Chem., 411 (1996)73

88 X.Y. Wu, Y.J. Li, B. Grundig, N.T. Yu, R. Renneberg, Electroanalysis, 9 (1997) 1288

89 Q. Deng, S.J. Dong, Analyst, 121 (1996) 1123

90 F. Bedioui , S. Trevin, V. Albin, M.G.G. Villega, J. Devynck, Anal. Chim. Acta, 341 (1997) 177

91 Q.J. Chi, S.J. Dong, Anal. Chim. Acta, 310 (1995) 429

92 T.R.I. Cataldi, D. Centonze, A. Guerrieri, Anal. Chem., 67 (1995) 101

93 M.S. Lin, B.I. Jan, Electroanalysis, 9 (1997) 340

94 K. Shachl, H. Alemu, K. Kalcher, J. Jezkova, I. Svancara, K. Vytras, Anal. Lett., 30 (1997) 2653

95 T.R.I. Cataldi, D. Centonze, I.G. Casella, E. Desimoni, J. Chromatogr., 773 (1997) 115

96 J. Walcurius, L. Lamberts, Anal. Lett., 31 (1998) 585

97 J.M. Zen, C.W. Lo, P.J. Chen, Anal. Chem., 69 (1997) 1669

98 Chen, N.K. Goh, L.S. Chia, Electrochim. Acta, 42 (1997) 595

99 I.G. Casella, A.M. Salvi, Electroanalysis, 9 (1997) 596

100 I.G. Casella, A. Destradis, E. Desimoni, Analyst, 121 (1996) 249

101 J.M. Zen, J.S. Tang, Anal. Chem., 67 (1995) 1892

102 P. Ugo, L.M. Moretto, B. Ballarin, Electroanalysis, 7 (1995) 129

103 T. Li, E. Wang, Electroanalysis, 9 (1997) 1205

104 M. Hedenmo, A. Narvaez, E. Dominguez, I. Katakis, Analyst, 121 (1996) 1891

105 C.P. Andrieux, O. Haas, J.M. Saveant, J. Am. Chem. Soc., 108 (1986) 8175

106 M.E.G. Lyons, H.G. Fay, J.G. Vos, A.J. Kelly, J. Electroanal. Chem., 250 (1988) 207

107 R.J. Forster, J.G. Vos, Macromol., 21 (1988) 2432

108 A.J. Kelly, T. Ohsaka, N. Oyama, R.J. Forster, J.G. Vos, J. Electroanal. Chem., 287 (1990) 185

109 D. Leech, R.J. Forster, M.R. Smyth, J.G. Vos, J. Mater. Chem., 1 (1991) 629

110 R.J. Forster, J.G. Vos, M.E.G. Lyons, J. Chem. Soc. Faraday Trans., 87 (1991) 3761

111 R.W. Wilson, R. Cubitt, A. Glidle, A.R. Hillman, P.M. Saville, J.G. Vos, J. Electrochem. Soc., 145 (1998) 1454

112 D.M. Kelly, J.G. Vos, A.R. Hillman, J. Mater. Chem., 7 (1997) 913

113 A.P. Doherty, M.A. Stanley, G. Arana, C.E. Koning, R.H.G. Brinkhuis, J.G. Vos, Electroanalysis, 7 (1995) 333

114 A.P. Doherty, J.G. Vos, Anal. Chim. Acta, 344 (1997) 159

115 A.P. Doherty, M.A. Stanley, J.G. Vos, Analyst, 120 (1995) 2371

116 B. Linke, W. Kerner, M. Kiwit, M. Pishko, A. Heller, Biosensors & Bioelectronics, 9 (1994) 151

117 F. Daigle, F. Trudeau, G. Robinson, M.R. Smyth, D. Leech, Biosensors & Bioelectronics, 13 (1998) 417

118 M. Pravda, C.M. Jungar, E.I. Iwouha, M.R. Smyth, K. Vytras, A. Ivaska, Anal. Chim. Acta, 304 (1995) 127

# Chapter 2

# Stability and Charge Transport of Electrodes Modified with Cross-Linked Redox Polymers in Thin Layer Flow Cells

## 2.1 Introduction

The development of polymer-coated modified electrodes has led to new areas of research in electrochemistry and has produced a wide range of promising applications in fields as diverse as electroanalysis, electrocatalysis, photoelectrochemistry, energy storage, electronic devices and electrochromic displays [1-5].

These polymer based materials are generally prepared by deposition of thin layers of the material onto an underlying electrode which is usually composed of carbon or metal. Deposition can be achieved using drop or spin coating methods or by in-situ electropolymerisation. The redox sites immobilised within this thin film act as electrochemically reactive sites and can catalyse the reaction of particular analytes. The underlying electrode does not play a part in this catalytic reaction but instead acts as a conducting agent and a support surface for the modifying layer. The immobilised redox sites allow the mediated catalysis of the substrate to proceed by electron transfer from the substrate to the redox sites and on to the underlying electrode. This electron transfer at the polymer film/electrode interface completes the cyclic mediation process by allowing the redox sites within the polymer matrix to return to their original redox state.

There are three general types of electroactive polymer films. These are redox polymers, electronically conducting polymers and ion exchange polymers. The redox polymers consist of polymer films containing localised immobilised redox sites. The film conducts electricity via a process known as electron hopping by electron self-exchange between oxidised and reduced sites. Electronically conducting polymers conduct electricity via delocalised metal-like band structures. Charge transport along the polymer chain is very rapid and interchain transfer is rate limiting and is largely dependent on chain alignment. Ion exchange polymer films become electroactive by exchange of their charge compensating counterions for electroactive ones. Charge transport can be caused by physical diffusion of these electroactive ions or by self-exchange between neighbouring groups. In general, these polymer films are stable

compared to other modifying surfaces which allows such modified electrodes to have more widespread use in sensor applications.

Electrodes modified with ion-exchange polymers have been used for the determination of ionic electroactive analytes preconcentrated at the modifying layer. With these electrodes the formal half-wave potentials for the redox couples incorporated within the ion-exchange polymer film were different to the values obtained for the same redox couples in solution. The half-wave potential differences were found to be dependent on the charge and concentration of the counter-ion and on the ratio of the ion-exchange equilibrium constants for the redox partners [6]. Modified electrodes formed by the electrodeposition of polypyrrole on Nafion coated platinum electrodes have been examined. Voltammograms were obtained in various electrolyte solutions including sodium chloride, sodium butylsulphonate and trimethylammonium chloride. It was found that transport of cations was responsible for the charge transport process and the efficiency of the ion transport in the film decreased as the radius of the cation increased [7]. A redox polymer modified electrode incorporating covalently bound electrocatalytic osmium sites was developed and its ability to mediate the reduction of iron (III) was examined. The mediated reaction was found to occur throughout the immobilised film for layers containing ca. $10^{-8}$ mol $cm^{-2}$ of redox active material in a supporting electrolyte containing $H_2SO_4$. The site of this mediated reaction could be altered to a surface reaction by changing the supporting electrolyte to $HClO_4$. It was suggested that the latter electrolyte retarded ion permeation of the polymer layer due to the dehydrating effect on the layer of the perchloric acid [8].

Ideally, a chemically modified electrode should be mechanically stable and remain unaffected by the conditions found in flow through systems or under specialised conditions such as in vivo work. An ideal polymer modified electrode would be stable with no dissolution of the modifying layer occurring would also be highly permeable to ions whilst allowing fast electron transfer through the polymer layer to the underlying electrode. These phenomena are, however, generally mutually exclusive. Therefore it is necessary to attempt to alter the structure of the modifying

polymer layer by varying the experimental conditions so as to arrive at an optimally behaved polymer modified electrode which can be used in the development of applications such as analytical sensors.

A number of methods have been developed to try and enhance the stability of these polymer modified electrodes. The redox polymer $[Ru(bpy)_2(PVP)_5Cl]Cl$ was found to have a half-life of eight hours in a flow injection system [9]. By covering this polymer with a layer of electropolymerised poly(3-methylthiophenol) or poly(N-ethyltyramine) the half-life was increased to greater than forty-eight hours. This enhanced stability was, however, at the expense of sensitivity. It was found that there was a reduction in these electrodes' responses due to restrictions in mass transport across the overlying layers. The formation of styrene copolymers of poly(4-vinylpyridine) imparted improved stability on the ruthenium polymer without affecting its electrocatalytic response [10]. An osmium redox polymer comprising poly[styrene-co-4-(N-methyl-N-p-vinylbenzylamino)pyridine] has been described as demonstrating excellent physical stability [11]. It showed itself to be stable for at least seven days under severe hydrodynamic conditions. A limited substrate linear range and restricted charge transport properties were the trade off required for this enhanced stability.

An electrodeposited polymer film of the $[Ru(bpy)_2(vpy)_2]^{2+}$ complex was used to modify an electrode. The catalysed detection of nitrite was found to proceed at a lower overpotential and it produced larger currents than the unmodified surface whilst preventing passivation of the electrode surface. The electrodeposited film demonstrated higher mechanical stability and reproducibility under hydrodynamic conditions when compared with similar preformed chemisorbed coatings [8]. A bulk-modified electrode comprised of polymeric mixed valence ruthenium oxide with cyano cross-links was prepared by immobilising the ruthenium oxide onto graphite particles by electroplating the catalytic film onto the graphite and then adding epoxy to form a conducting composite. The long-term stability of this bulk-modified electrode was advantageous compared to the traditional surface-modified electrode with the ruthenium coated powder stable for up to three months. In a thin layer flow

cell these electrodes required highly positive potentials to operate and so lacked selectivity. It was postulated that the higher overpotential required for the bulk-modified electrode compared to the surface-modified electrode was due to a thin film of the binder substance remaining on the redox sites which caused locally high resistance values at the catalytic sites [12]. A surface-modified electrode using a similar coating of mixed-oxidation state ruthenium oxide sites cross-linked with ruthenium cyanide was examined for use in a thin-layer electrochemical flow cell. This modified electrode showed a decrease in amperometric response of approximately 40 % over an eight hour period due to leaching of the catalytic sites under the vigorous hydrodynamic conditions existing in the flow cell. By using a carrier solution to which had been added equimolar concentrations of the ruthenium salts, the modifying surface was continuously replenished [13].

Cobalt-porphyrin-clay complexes used to modify electrodes were stabilised by adding polymers such as poly(vinylalcohol) and poly(vinylpyridine). This enhanced stability was achieved at the price of decreased conductivity of the modifying layer. The polymers were found to insulate the other modifying compounds. To improve this situation, silver colloid was added to the mix of modifying materials and the resulting cobalt-porphyrin-clay/AgCol/polymer modified electrode system was found to act as an effective oxygen sensor [14]. Modifying an electrode surface by incorporating oxometallic compounds in an electronically conducting and non-conducting polymer matrix has also been examined. This PPy-$PMo_{12}O_{40}$ film modified glassy carbon electrode demonstrated good electrochemical properties and generated a stable response over two days of continuous use when used for liquid chromatographic detection [15]. A bis(4-pyridyl) disulfide modified gold electrode was used for the electrooxidation of ascorbic acid. This oxidation process was found to be pH dependent. By controlling the pH, the electrode currents showed a good linear relationship with the ascorbic acid concentration. This modified electrode demonstrated sufficient stability to be used in a flow injection system [16].

Amperometric enzyme electrodes have also been stabilised by using a bilayer encagement technique. Lactate dehydrogenase was encaged on an electrode surface

and was used as the working electrode in a flow system and its response was compared with a non-chemically stabilised enzyme modified electrode. The native enzyme exhibited a 90 per cent loss of activity whilst the encaged enzyme maintained a stable response [17]. A carbon fibre micro-electrode modified with a chemisorbed osmium polymer was demonstrated to have a stable response when used for the determination of nitrite in food samples. Long-term stability with no surface fouling was found for this modified electrode when used as a detector in a flow injection analysis system. A horseradish peroxidase modified electrode demonstrated an ability to detect a wide range of analytes including peroxides, thiourea and ethylenethiourea. Different organic solvents were found to affect the sensitivity of the electrode's response and also the modified electrode's stability [18].

Prussian blue adsorbed as a film on a vitreous carbon electrode showed reasonable stability when applied to the detection of hydrazine. But this stability did not remain when the film-modified electrode was used in flowing streams at potentials greater than 0.9 V. Stability was regained by further modifying the electrode with a coating of Nafion [19]. The use of Nafion to further improve the mechanical stability of modified electrodes has also been demonstrated for mercury film electrodes [20] and copper/copper oxide modified electrodes [21].

A particular technique which can be used to enhance the stability of polymer layers is cross-linking of the polymer's chains whether covalent or ionic. Cross-linking of redox polymers has been used with good results in the development of biosensors. Since the ultimate aim of such sensors is for their use in vivo, an important consideration in their design and operation is their stability. Using osmium polymers as mediators, electrostatic complexes have been formed which incorporate glucose oxidase [22]. By further modifying these polycationic redox polymers with cross-linking agents such as glutaraldehyde [23-25], triethylenetetraamine [26] and a diepoxide [27], reproducible and physically stable redox films have been produced which have proved useful in the development of glucose biosensors [28]. The use of a similar osmium-containing polymer, $[Os(bpy)_2(PVP)_{20}Cl]Cl$, and glucose oxidase cross-linked with glutaraldehyde has been shown to remain stable even in organic

media [29]. A poly(vinylimidazole)-based osmium redox polymer incorporating glucose oxidase and cross-linked with a diepoxide was also found to selectively measure glucose in the presence of oxidising inteferents [30]. Other in vivo sensors have been developed using this technique whereby the glucose oxidase has been replaced with other enzymes such as cellbiose oxidase [31] and horseradish peroxidase [32]. Such biosensors are useful because the in-situ cross-linking of the polymer has been shown to not affect the sensitivity of the biosensor's response, that is, the osmium mediator's reversible electrochemical characteristics remain unchanged.

Other methods of enhancing the stability of such modified electrodes have not had such benign effects on the mediated response of the electropolymer. For example, a ruthenium redox polymer modified electrode was coated with electropolymerised conducting poly(3-methylthiophene) and nonconducting poly(N-ethyltyramine) polymers [9]. This process enhanced the stability of the sensor's response but caused a diminution in its sensitivity. An electrode modified using a similar ruthenium-containing polymer but cross-linked using UV radiation was also found to result in enhanced stability at the expense of decreased sensitivity [33].

A closer look at charge transfer processes may aid in the development of polymer modified electrodes which retain characteristics of their stabilising ability and their sensitivity. Charge transfer processes in electroactive polymer films can be characterised as self-exchange between fixed redox sites, ion diffusion within the polymer matrix or migration of counter ions on application of an applied potential. The rate of the charge transport process is determined by processes which include the intrinsic barrier to self-exchange, counter-ion movement to maintain electroneutrality and physical displacement of the polymer chains to allow sufficient separation between the fixed redox sites so that electron transfer can take place [34].

Other factors which may influence the charge transport process include substrate diffusion in the Nernst diffusion layer adjacent to the film/solution interface, substrate partitioning and diffusion within the polymer matrix, electron percolation through the

film, and chemical reaction between the immobilised redox species and substrate within the film [35].

Experimentally adjustable factors as diverse as electrolyte composition, pH, redox site loading, polymer backbone composition and temperature can all significantly affect the charge transport rate [11,36,37]. Charge transport, as characterised by the charge transport diffusion coefficient, $D_{ct,,}$ can also be affected by the technique used in its estimation. Methods which can be employed include cyclic voltammetry, potential step chronoamperometry and chronocoulometry. The $D_{ct}$ values derived by these different techniques have been found to produce different values for the same modified electrode. It appears that the rate of charge transport through these redox polymer films depends on the experimental time scale used. Potential step techniques have been found to give consistently larger charge transport values than cyclic voltammetry. The longer time scale cyclic voltammetry experiments appear to affect a greater portion of the modifying layer, thus requiring counter-ion diffusion to occur over a greater portion of the layer than the potential step methods.

Research carried out on the electroanalysis of La (III) by electrodes modified with alizarin derivatives and quaternized polyvinylpyridine has shown that low film cation permeability results in low La (III) mass transport rates despite the presence of a co-ordinating ligand within the film [38]. This work also demonstrated that the mechanism of electron hopping between electron sites arising from electron self-exchange was the dominant form of charge transport in the film. An increase in $D_{ct}$ was observed for this film as the concentration of La (III) increased due to an increase in the mobility of the complex in the modifying layer. Data from Auger depth profiling suggested that this was due to the decreased charge of the complex relative to the free ligand which led to enhanced site-site exchange or more frequent collisions resulting in increased rates of self-exchange [39]. A polypyrrole-Nafion composite electrode was examined using cyclic voltammetry and impedance data. The efficiency of ion transport in the layer was found to decrease as their radius increased [7]. It was found that the transport of cations was responsible for the charge transport process accompanying the redox reactions within the composite film whereas at an

electrode modified only with polypyrrole, the transport of anions dominated the charge transport process. By adjusting the weight ratio of polypyrrole to Nafion a film in which the transport of cations and anions could occur simultaneously may be created. Therefore, the relationship between charge transport efficiency and the ratio of the electronic insulator and conductor layers could be designed with specific applications in mind. The electrochemical quartz crystal microbalance technique has been used to probe a poly(tetracyanoquinodimethane) electrode in contact with LiCl solutions. This work showed that the film swelling dynamics and equilibrium affected the response of the polymer modified electrode. As the bulk electrolyte's concentration was increased, the polymer layer's structure compacted, whilst an increase in temperature resulted in solvent swelling. At higher temperatures (>50°C), the diffusion of counter-ions and the movement of the polymer chains increased with an accompanying increase in the rate of charge transport [39].

Electrodes modified with films of plasma-polymerised vinylferrocene were examined with respect to temperature. At room temperature the ferrocene sites underwent rapid exchange of electrons with the underlying platinum electrode. At low temperatures, <-50°C, the transport of electrochemical charge through the polymer film was found to be controlled by diffusion according to Fick's law. The diffusion of the charge through the film was considered to be limited by the motion of the polymer chains required for site-site collisions and counter-ion transport. This demonstrates the importance of the polymer framework in controlling electron hopping between the redox sites within the polymer film [40].

In this chapter glassy carbon electrodes will be modified with cross-linked layers of the redox polymers $[Os(bpy)_2(PVP)_{10}Cl]Cl$ and $[Ru(bpy)_2(PVP)_{10}Cl]Cl$. These layers will then be examined with regard to their stability and sensitivity when in conventional and flow cells. The harsh hydrodynamic conditions present in thin layer flow cells will provide a stringent test of their useful lifetimes. In the past redox polymer modified sensors were restricted in their use due to the flow of electrolyte destabilising the layer and causing it to strip off into the flowing electrolyte. Flow cells are now commonly used in many working sensors and if redox polymer

modified electrodes are to become more widespread in their use, then this problem of attaining better stability will have to be addressed. This improved stability must not be achieved at the expense of the electrodes' stability and for this reason the surface behaviour and charge transport characteristics of these modified electrodes will also be examined in this chapter. Also under examination will be the effect of the thin layer flow cell itself on the response of the $[Os(bpy)_2(PVP)_{10}Cl]Cl$ and $[Ru(bpy)_2(PVP)_{10}Cl]Cl$ modified electrodes in comparison with the response measured in conventional three electrode cells.

## 2.2 Experimental

### 2.2.1 Preparation of High Molecular Weight Poly(4-Vinylpyridine)

The 4-vinylpyridine monomer was purified by vacuum distillation at 70°C. 12 $cm^3$ of this solution was then degassed using nitrogen which had been purged of oxygen. A free radical initiator, 2,2'-azobisisobutyronitrile was added at a mole ratio of 500:1, monomer to initiator. The monomer then polymerised at 80°C whilst under nitrogen for 4 hours. The product was dissolved in methanol to allow molecular weight fractionation. This was achieved by firstly evaporating the methanol until a concentrated solution of the polymer solution was produced. Toluene was then added dropwise whilst the solution was being stirred. When the solution became cloudy no more toluene was added and the solution was heated to 40°C. That part of the polymer remaining undissolved was retained, this being the high molecular weight fraction, and was subsequently dissolved in methanol and then precipitated in diethylether. The collected polymer was dried in vacuo at 80°C. A determination was then made of the molecular weight of the poly(4-vinylpyridine) using viscometry. This was carried out by preparing polymer solutions in dry ethanol over the concentration range 0.2 to 1.0 g/100$cm^3$. The efflux time for each solution and solvent between the graduations of an Ubbelohde suspended level viscometer were determined at 25°C. A viscosity average molecular weight of 600,000 g $mol^{-1}$ was found for the high molecular weight fraction of the poly(4-vinylpyridine).

### 2.2.2 Preparation of $[Os(bpy)_2Cl_2]$

3 mmol of $OsCl_3.3H_2O$ and 6 mmol of 2,2-bipyridyl were heated under reflux in dimethylformamide for 30 minutes whilst being stirred continuously. After cooling, the solution was added to a solution containing 2g $Na_2SO_4$ in 200 $cm^3$ water and was stirred for approximately one hour and was then stored at 0°C overnight. The product was then filtered and washed with distilled water and dried in vacuo at 80°C.

### 2.2.3 Preparation of $[Os(bpy)_2(PVP)_{10}Cl]Cl$

This electropolymer was synthesised using the procedure described by Forster et al [41] except that the solvent 2-methoxyethanol was substituted for ethanol. A metal loading of one osmium centre per ten poly(4-vinylpyridine) units was chosen as this loading exhibits optimum charge transfer characteristics [34]. 54 mg of $[Os(bpy)_2Cl_2]$ was dissolved in 40 $cm^3$ 2-methoxyethanol and 100 mg of the PVP was dissolved in a similar amount. When both solutions had thoroughly dissolved, the two solutions were added to a 150 $cm^3$ round bottomed flask which was refluxed at 125°C. This reaction was monitored by cyclic voltammetry. The reaction was completed after 72 hours when the appearance of a redox wave at 0.250 V vs. SCE due to the formation of the osmium-polymer complex and the disappearance of the redox wave at 0.0 V vs. SCE due to the $[Os(bpy)_2Cl_2]$ was observed. The polymer was then precipitated in diethylether before being dried in vacuo at 80°C. 105 mg of product was recovered which corresponds to a 68 % yield. A 1 % w/v solution of this electropolymer was prepared in methanol for use in modifying electrodes. Using UV/Visible spectrometry, $\lambda_{max}$ values for this electro-polymer were found to be at 730 nm, 490 nm, 430 nm and 360 nm. These results indicate that the redox polymer has the co-ordination sphere $[Os(N)_5Cl]$ and that the metal loading is 1:10 [42].

### 2.2.4 Preparation of $[Ru(bpy)_2Cl_2].2H_2O$

30 mmol of $RuCl_3.2H_2O$ and 60 mmol of 2,2'-bipyridyl were heated under reflux in dimethylformamide along with 0.8 g LiCl for 8 hours whilst being stirred continuously. After cooling, 250 $cm^3$ acetone was added and was stored at 0°C overnight. The precipitated product was then filtered and washed with distilled water followed by diethylether. This product was then examined by UV/Visible spectroscopy was found to have maxima at 365 nm and 525 nm which corresponds with previously reported values for this product [42].

### 2.2.5 Preparation of $[Ru(bpy)_2(PVP)_{10}Cl]Cl$

This electropolymer was synthesised using the procedure described by Forster et al [34] except that the solvent 2-methoxyethanol was substituted for ethanol. A metal loading of one ruthenium centre per ten poly(4-vinylpyridine) units was chosen as this loading exhibits optimum charge transfer characteristics. 49 mg of $[Ru(bpy)_2Cl_2]$ was dissolved in 50 $cm^3$ 2-methoxyethanol and 100 mg of the PVP was dissolved in a similar amount. When both solutions had thoroughly dissolved, the two solutions were added to a 150 $cm^3$ round bottomed flask. This solution was then refluxed at 125°C whilst being kept free from any traces of light. This reaction was monitored by cyclic voltammetry and UV/Visible spectroscopy. The reaction was completed after 48 hours when the appearance of a redox wave at approximately 700 mV vs. SCE due to the formation of the ruthenium-polymer complex. The polymer was then precipitated in diethylether before being dried in vacuo at 80°C. 78 mg of product was recovered which gives a 52 % yield. A 1 % w/v solution of this electropolymer was prepared in methanol for use in modifying electrodes. Light was excluded to prevent the photo-substitution of the chlorine ligand of this ruthenium polymer [43]. Using UV/Visible spectrometry, $\lambda$ max values for this electro-polymer were found to be at 495 nm, 350 nm. These results indicate that the redox polymer has the co-ordination sphere $[Ru(N)_5Cl]$ and that the metal loading is 1:10 [44].

### 2.2.6 Electrolytes and Solutions

The electrolyte used throughout was 0.1 mol $dm^{-3}$ $H_2SO_4$ and $NH_4[Fe(SO_4)_2].12H_2O$ was used to prepare solutions of Fe(III). Deionised water obtained by passing distilled water through a Milli-Q water purification system was used to prepare all electrolytes and solutions.

### 2.2.7 Preparation of Modified Electrodes

Modified electrodes were prepared by polishing the 3 mm diameter glassy carbon electrodes with 5 μm alumina as an aqueous slurry on a felt cloth. The electrodes were rinsed thoroughly with distilled water and methanol and dried in vacuo at room temperature. The electrodes were modified by drop coating 1μl of the 1 % w/v solution of the polymer. This modifying layer was then cross-linked in situ by reaction with a 1μl methanolic solution of 1,10-dibromodecane to give a 10 mol % quaternisation of the vinyl pyridine residues. The electrodes were allowed to dry slowly in air before being placed overnight in a methanolic atmosphere before use.

### 2.2.8 Cyclic Voltammetry

Cyclic voltammetry was carried out in situ in a flow injection cell using an EG&G Princeton Applied Research Model 400 electrochemical detector and a Linseis X-Y recorder. The rest of the flow injection apparatus consisted of a Gilson Minipuls 3 peristaltic pump, a six port Rheodyne injector valve fitted with a 20 μl fixed volume sample loop. All connected with Teflon HPLC tubing. In the flow cell an Ag/AgCl electrode acted as the reference. The stainless steel body acted as the counter electrode. The working electrodes were 3 mm diameter glassy carbon shrouded in Teflon. All potentials are quoted after conversion to the SCE scale. Sample

injections were made using a 2 $cm^3$ glass syringe fitted with a Rheodyne injection needle. The carrier electrolyte used was 0.1 mol $dm^{-3}$ $H_2SO_4$ at a flow rate of 1.0 $cm^3$ $min^{-1}$. During amperometric measurement, the Linseis recorder was replaced by a Philips PM 8252 X-t chart recorder.

Cyclic Voltammetry was also carried out using a conventional three-electrode electrochemical cell. The potentiostat was the EG&G Princeton Applied Research Model 362 potentiostat. Voltammograms were recorded on the Linseis Model 17100 X-Y recorder. The reference electrode was the saturated calomel electrode (SCE). All potentials are quoted with regard to the liquid junction potential. The counter electrode was 1.0 $cm^2$ platinum gauze placed parallel to the working electrode at a distance of approximately 1 cm.

Coulometry was carried out using the EG&G Princeton Applied Research model 379 digital coulometer placed in series between the working electrode and the potentiostat return. The charge owing to the oxidation of Os(II) to Os(III) within the polymer film was measured during slow sweep rate cyclic voltammetry at 1.0 mV $s^{-1}$ from 0.0 to 0.6 V versus SCE. For the ruthenium containing films, measurements were extended to 1.0 V vs. SCE. Results were corrected for background charging currents.

### 2.2.9 UV/Visible Spectroscopy

UV/Visible spectroscopy was carried out using a Shimadzu UV 240 spectrophotometer. 2 x 1 cm matched quartz cells were used. UV/Visible spectra were recorded in the region 900 nm to 190 nm. A scan speed of 10 nm $s^{-1}$ and a slit width of 2 nm was used. Methanol was placed in the reference beam.

## 2.3 Results and Discussion

### 2.3.1 Electrochemical Behaviour of the Cross-linked Redox Polymers

In the introductory chapter the behaviour of an ideal immobilised surface or thin layer species was discussed. The criteria to examine include the parameters of peak-to-peak separation ( $\Delta_{Ep}$), peak width at half the maximum height (FWHM), the ratio of anodic to cathodic peak currents ($i_{pa}/i_{pc}$) and the sweep rate at which semi-infinite diffusion behaviour is altered to a mixture of finite and semi-infinite diffusion behaviour. Figure 2.1 shows the structure of the osmium and ruthenium metallo-polymers. Figure 2.2 shows the typical cyclic voltammograms for the osmium and ruthenium redox modified electrodes obtained in the thin-layer flow cell environment. The electrochemical parameters found for the 1,10-dibromodecane cross-linked ruthenium and osmium redox polymer modified electrodes in the thin layer cell are shown in Table 2.1 where they are compared with the behaviour observed in these polymers when cross-linked or uncross-linked in a conventional three electrode cell. The values shown in the Table represent averages of at least three experiments each.

| Type of Modified Layer | Cross-linked | Type of Cell* | $E_{1/2}$ mV vs. SCE | $d_{Ep}$ mV | $i_{pa}/i_{pc}$ | FWHM mV | DC+ mV $s^{-1}$ |
|---|---|---|---|---|---|---|---|
| $[Ru(bpy)_2(PVP)_{10}Cl]Cl$ | x | c | 750 ± 5 | 0 ± 5 | 1 ± 0.1 | 90 ± 5 | 100 |
| $[Ru(bpy)_2(PVP)_{10}Cl]Cl$ | ✓ | c | 750 ± 5 | 0 ± 5 | 1 ± 0.1 | 90 ± 5 | 100 |
| $[Ru(bpy)_2(PVP)_{10}Cl]Cl$ | ✓ | f | 714 ± 5 | 60 ± 5 | 0.7 ± 0.1 | 82 ± 5 | 100 |
| $[Os(bpy)_2(PVP)_{10}Cl]Cl$ | x | c | 250 ± 5 | 0 ± 5 | 1 ± 0.1 | 90 ± 5 | 100 |
| $[Os(bpy)_2(PVP)_{10}Cl]Cl$ | ✓ | c | 250 ± 5 | 0 ± 5 | 1 ± 0.1 | 90 ± 5 | 100 |
| $[Os(bpy)_2(PVP)_{10}Cl]Cl$ | ✓ | f | 249 ± 5 | 50 ± 5 | 0.9 ± 0.1 | 84 ± 5 | 100 |

* c = conventional cell, f = flow cell

+ Scan rate at which change-over to semi-infinite diffusional control occurs

Table 2.1 Parameters indicative of surface behaviour at crosslinked and un-crosslinked $[Os(bpy)_2(PVP)_{10}Cl]Cl$ and $[Ru(bpy)_2(PVP)_{10}Cl]Cl$ modified electrodes in conventional and thin layer electrode cells. Experimental conditions as before.

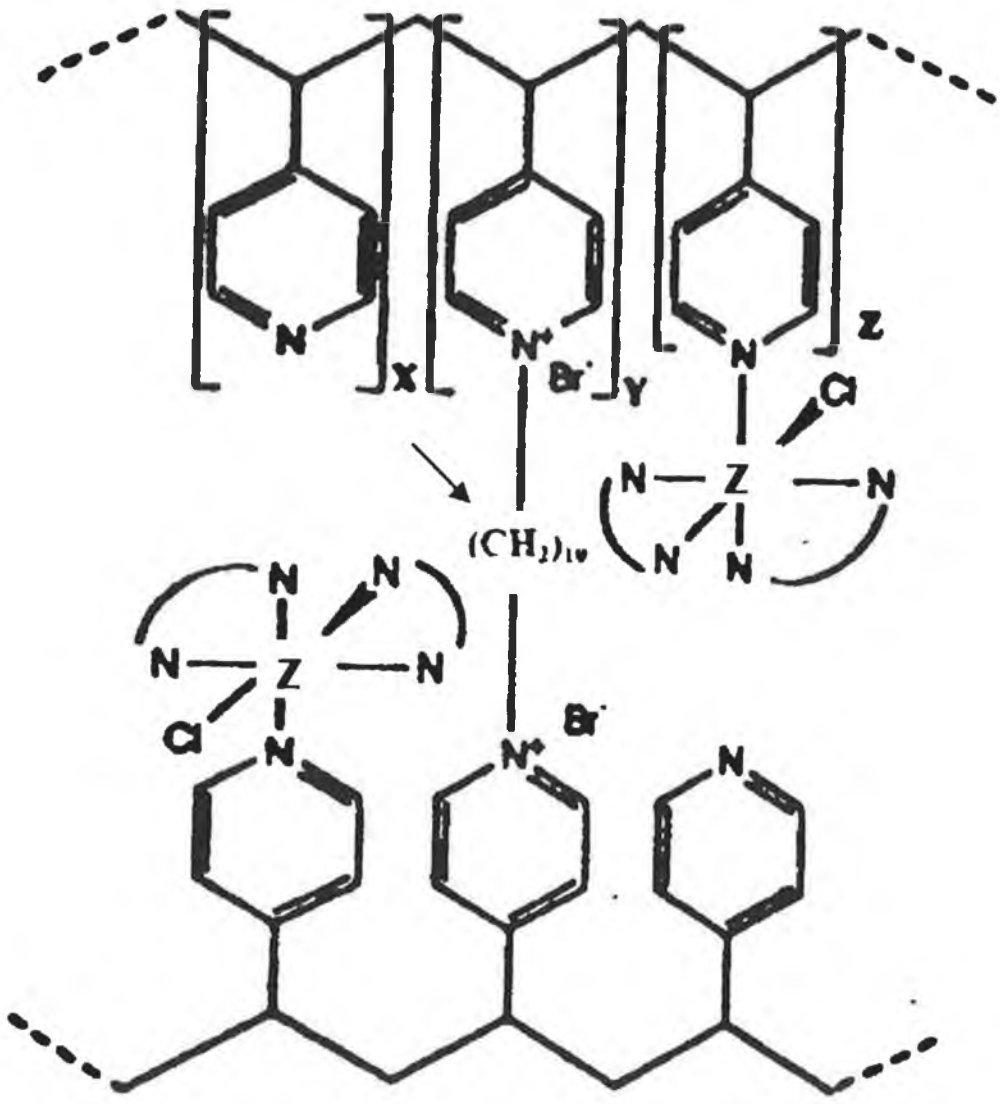


Figure 2.1 Structure of the metallo-polymer $[Z(bpy)_2PVP_{10}Cl]Cl$ where Z can be Os or Ru. Indicated by an arrow is the crosslinking agent 1,10-dibromodecane with which the polymer is 10% crosslinked.

For the cross-linked and uncross-linked polymers in the conventional cell the value for peak-to-peak separation was found to be 0 mV, the ratio of anodic to cathodic peak currents was 1.0 +/- 0.05 and peak widths at half maximum height were 90 mV. These values are consistent with rapid reversible surface behaviour for the redox

couples. Finite diffusional surface behaviour was also observed up to potential sweep rates of 100 mV $s^{-1}$ in all cases.

These observations suggest ideal surface behaviour on the part of the modifying surfaces and are close to the theoretically expected ideal for such surface immobilised redox couples. For the cross-linked modified layer in the thin layer flow cell, the observed results were somewhat different from these aforementioned results. The peak-to-peak separation for the osmium polymer layer was 50 ± 2 mV and that for the Ruthenium polymer was 60 ± 2 mV. The ratio of anodic to cathodic peak currents for the osmium polymer was 0.9 ± 0.1 and for the ruthenium polymer was 0.7 ± 0.1.

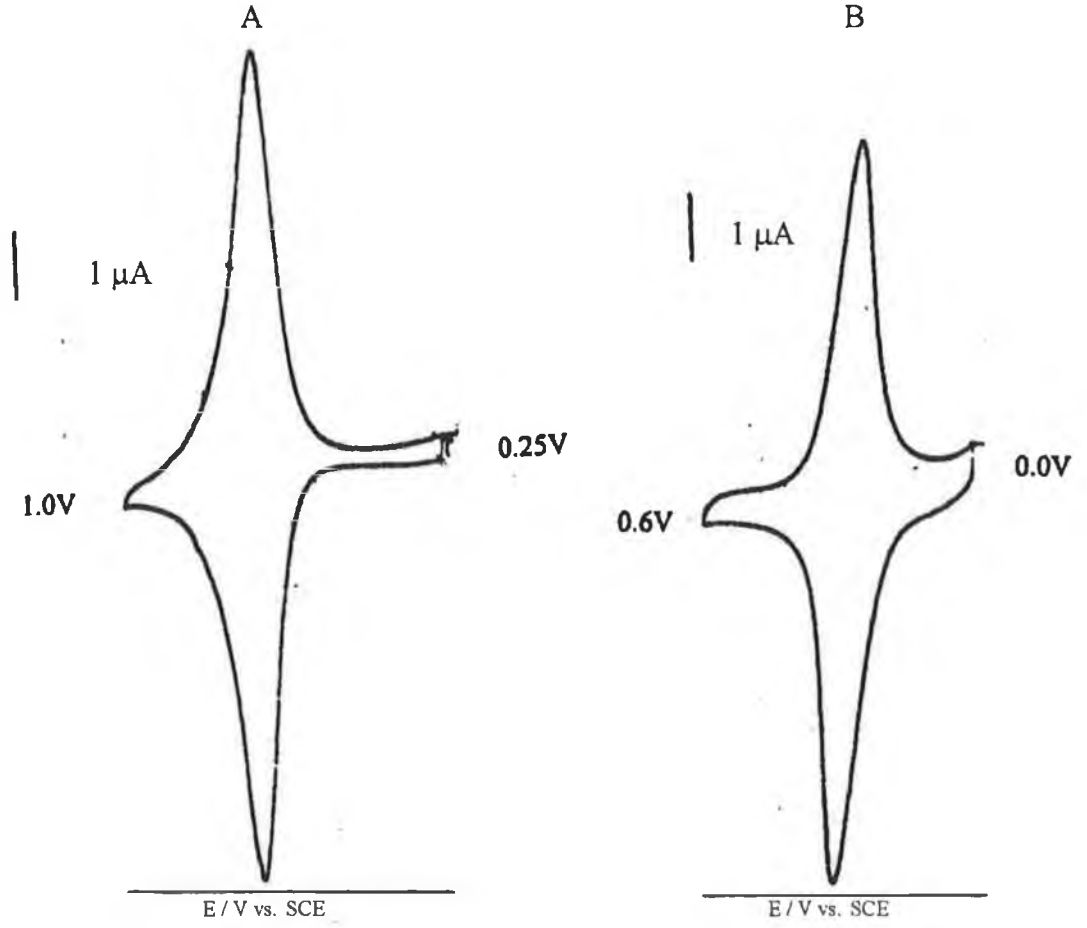


Figure 2.2 A cyclic voltammogram of (A) $[Ru(bpy)_2(PVP)_{10}Cl]Cl$ and (B) $[Os(bpy)_2(PVP)_{10}Cl]Cl$ coated on a glassy carbon electrode in a thin layer flow cell. Polymer surface coverage is 1 x $10^{-8}$ mol $cm^{-2}$, electrolyte is 0.1 mol $dm^{-3}$ $H_2SO_4$, potential sweep rate is 2 mV $s^{-1}$, electrolyte flow rate is 1 $cm^3$ $min^{-1}$.

The osmium polymer layer's peak width at half height was observed to be 84 mV and a value of 82 mV was found for the ruthenium polymer layer.

The onset of semi-infinite linear diffusion appeared as expected at the potential sweep rate of 100 mV $s^{-1}$. It can be seen that the cross-linked polymers' surface behaviour in the thin layer cell does not match that found at the cross-linked and homopolymers in the conventional cell. The experimentally obtained values in the conventional cell indicate that the surface behaviour of these electropolymer films are unaffected by the cross-linking process. So it appears that it is the nature of the modified electrode's environment which causes the alteration in the expected surface behaviour results.

### 2.3.2 Stability of Uncrosslinked $[Os(bpy)_2(PVP)_{10}Cl]Cl$

The stability of the uncrosslinked homopolymer in a flow injection cell was first considered to allow future comparison with the crosslinked polymer. After being placed in the flow injection cell, the carrier electrolyte commenced to flow and a cyclic voltammogram was taken of the modified electrode in situ.

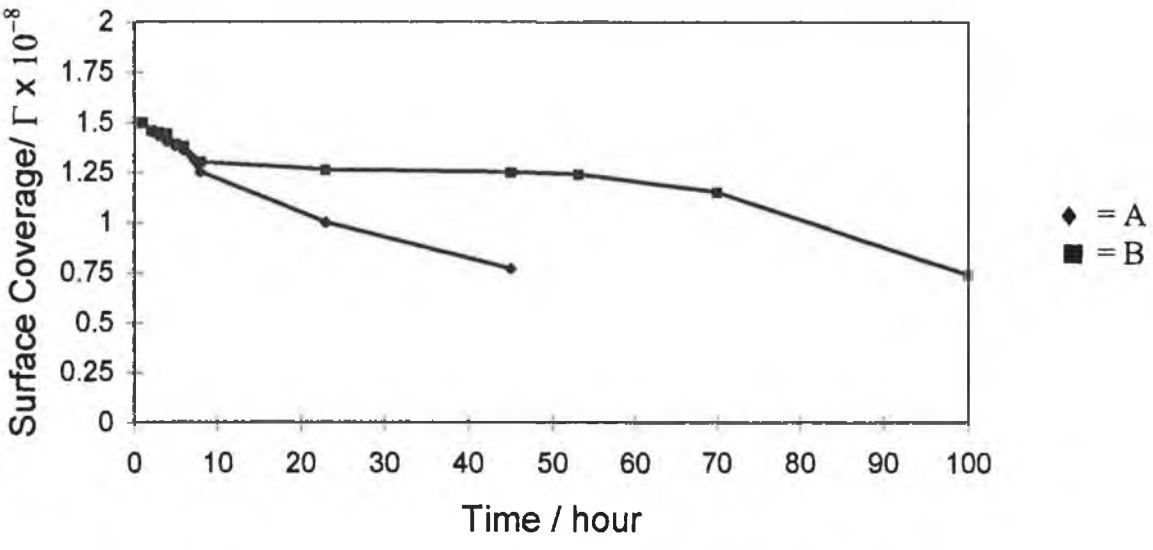


Figure 2.3 A plot of surface coverage versus time of $[Os(bpy)_2(PVP)_{10}Cl]Cl$ in a thin layer flow cell. Initial surface coverage is 1.5 x $10^{-8}$ mol $cm^{-2}$. The electrolyte was 0.1 mol $dm^{-3}$ $H_2SO_4$. A = un-crosslinked modified layer, B = crosslinked with 10 mol % of 1,10-dibromodecane. Carrier flow rate was 0.7 $cm^3$ $min^{-1}$.

Therefore the effect of a cross-linking agent on the polymer should be observable without such a complicating factor.

In Figure 2.3a a plot of surface coverage versus time can be seen for the modified electrode. From an initial surface coverage of 1.5 x $10^{-8}$ mol $cm^{-2}$, the surface coverage had reduced to 1.0 x $10^{-8}$ mol $cm^{-2}$ after a period of 20 hours. After 45 hours, approximately 50% of the osmium polymer remained on the electrode surface. This gives a measure of the half-life of the polymer, $t_{1/2}$ = 45 hours.

Examination of the cyclic voltammograms taken of this modified electrode show a gradual decease in the redox wave at 250 mV with no accompanying increase at any other potential.

### 2.3.3 Stability of Crosslinked $[Os(bpy)_2(PVP)_{10}Cl]Cl$

The osmium polymer was 10% cross-linked with a solution of 1,10-dibromodecane and was then placed in the flow injection cell as before. Figure 2.3b shows a plot of surface coverage versus time for this modified electrode.

A dramatic increase in the lifetime of this crosslinked layer compared with the uncrosslinked layer can be observed for similar layer thicknesses. A decrease in the surface coverage of the electrode to 50% of its starting size occurs after 100 hours. This represents an increase of more than 100% of the half-life of this polymer from $t_{1/2}$ = 45 hrs to $t_{1/2}$ = 100 hrs. The limiting factor for the stability of this polymer is its ability to remain adsorbed to the underlying electrode in a hydrodynamic environment rather than, as will be seen in the case of the ruthenium polymer, the labile nature of one the compound's ligands.

The crosslinking of the polymer has an observably powerful impact on the stability of the modified layer. The crosslinking reaction causes a polymer network to form on the electrode which allows a firmer anchoring of the entire layer onto the electrode's

surface. This polymer structure exhibits a greater ability to resist the effect of the flowing stream of electrolyte and thus desorption of the layer due to wear and tear is lessened.

When the cyclic voltammograms of this experiment were examined, it was observed that, initially, very little of the crosslinked layer was lost. A cyclic voltammogram of a modified electrode covered with $1.0 \times 10^{-8}$ mol $dm^{-3}$ after 1 hour in the flow injection system compared with the same layer after 24 hours can be seen in Figures 2.4a and 2.4b. There is very little difference in the surface coverage of these two layers. A gradual decline in the surface coverage then appears to begin after 24 hours, as observed in Figure 2.4c. The rate of decline is approximately $2 \times 10^{-10}$ mol $dm^{-3}$ $hr^{-1}$.

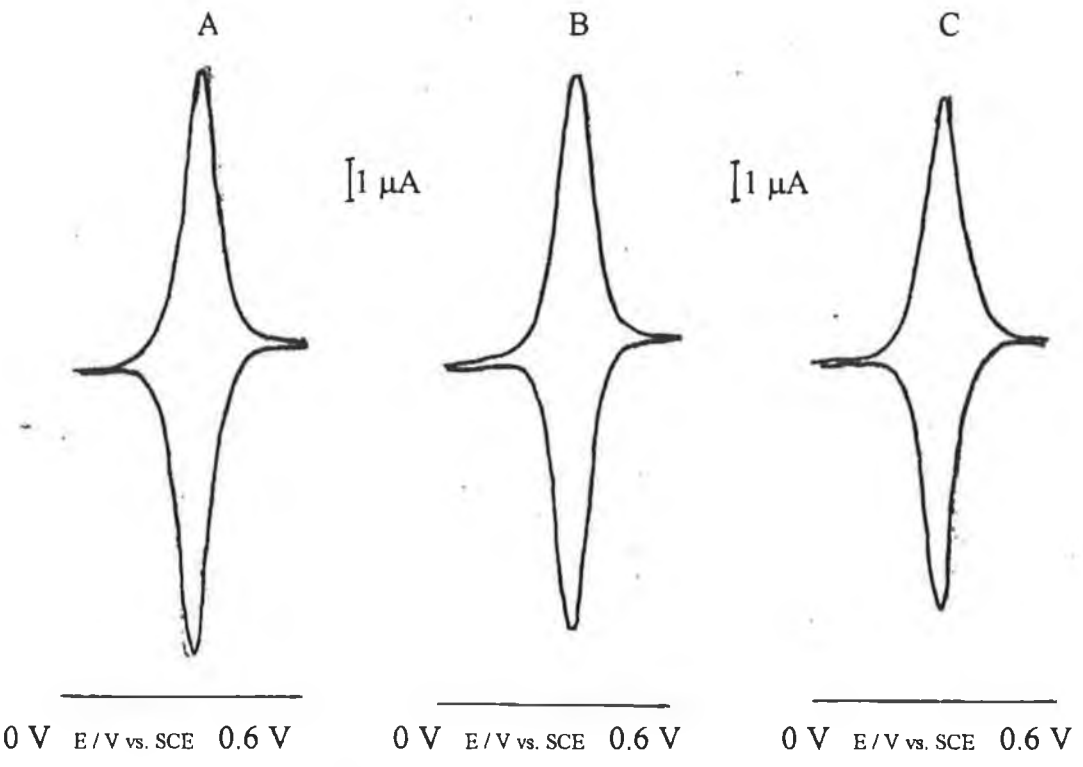


Figure 2.4 Cyclic voltammograms of $[Os(bpy)_2(PVP)_{10}Cl]Cl$ crosslinked with 10 mol % of 1,10-dibromodecane in a thin layer flow cell. The electrolyte was 0.1 mol $dm^{-3}$ $H_2SO_4$ and the surface coverage was $1 \times 10^{-8}$ mol $dm^{-3}$.. Carrier flow rate was 0.7 $cm^3$ $min^{-1}$. A = initial cyclic voltammogram, B = cyclic voltammogram after 24 hours, C = cyclic voltammogram after 48 hours.

### 2.3.4a Stability of Uncrosslinked vs. Crosslinked $[Ru(bpy)_2(PVP)_{10}Cl]Cl$

*Observation of Sensor's Response*

The stability of the uncrosslinked ruthenium polymer was studied by placing an electrode modified with 1 x $10^{-8}$ mol $cm^{-2}$ $[Ru(bpy)_2(PVP)_{10}Cl]Cl$ in a flow injection cell at a fixed potential of 0.85 V vs. SCE and monitoring the response of the modified electrode with respect to a potential analyte. Initially, injections of 50 ppm Fe(II) were made onto the flow injection system and the peak height was measured as the iron was oxidised at 0.85 V vs. SCE. This iron solution was then reinjected every hour. Figure 2.5a shows how the peak height thus measured decreased over time.

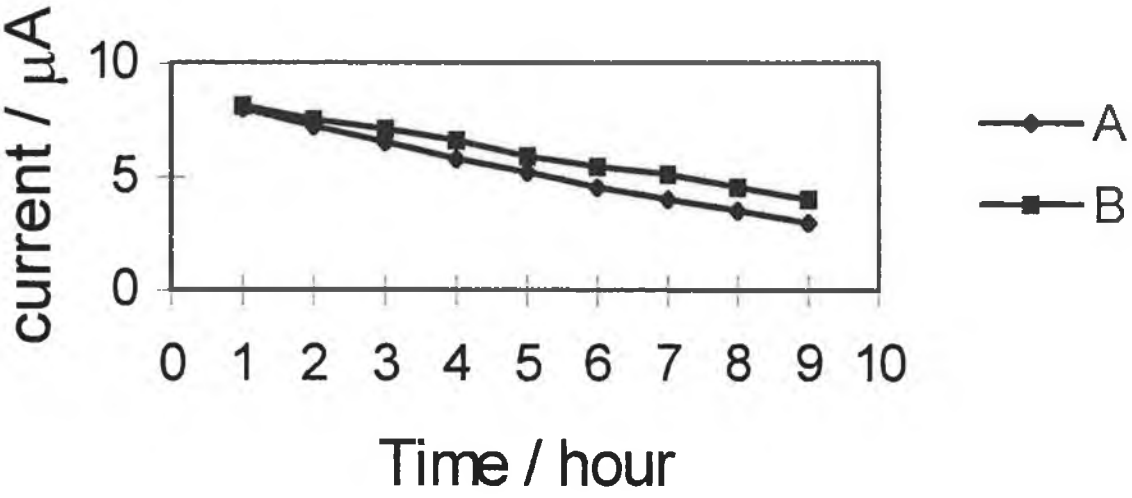


Figure 2.5 Response of $[Ru(bpy)_2(PVP)_{10}Cl]Cl$ modified electrodes in a thin layer flow cell to injections of 50 ppm Fe(II). The electrolyte was 0.1 mol $dm^{-3}$ $H_2SO_4$ and the surface coverage was 1 x $10^{-8}$ mol $dm^{-3}$.. Applied potential is 0.85 V vs. SCE. A = un-crosslinked modified layer, B = crosslinked with 10 mol % of 1,10-dibromodecane. Carrier flow rate was 0.7 $cm^3$ $min^{-1}$.

It can be seen that it took nine hours for the sensor response to drop by a factor of 50% to the iron substrate. This experiment was repeated using a cross-linked

ruthenium modified electrode. The resulting effect of the cross-linking by 1,10-dibromodecane can be seen in Figure 2.5b. The sensor's response to the substrate over time is essentially the same as the uncross-linked sensor, with a 50% decrease in response observed after approximately nine hours.

Since this result mirrors the response found at the uncross-linked modified electrode, it appears that cross-linking with the dibromomdecane has no effect. This is an apparently unexpected result when the effect of the cross-linking agent on the analogous osmium electropolymer is considered. In that previously described experiment the cross-linker was found to retard the physical removal of the polymer film from the underlying glassy carbon electrode. The in-situ cross-linking of the poly(4-vinylpyridine) would be expected to hold the electropolymer in place to allow its use over a longer period of time than with the uncross-linked polymer. To investigate why this does not in fact happen, it was decided to observe more closely the processes occurring at the modified electrode in situ.

Plots of $i_{pa}$, peak current, versus scan rate, were examined to ascertain the surface behaviour of these modified electrodes. These plots (Figure 2.6) were found to be linear up to 100 mV $s^{-1}$ indicating the finite diffusion behaviour of charge transport at this modifying layer.

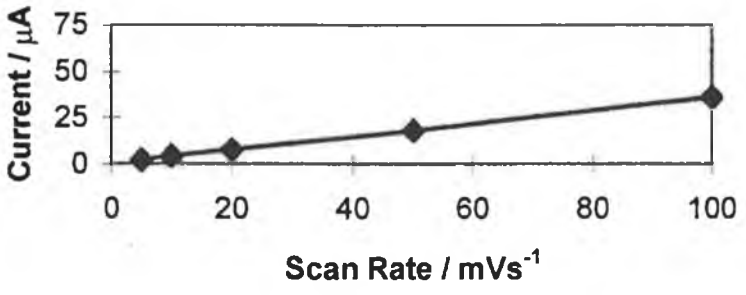


Figure 2.6 Plot of peak current versus potential scan rate over the range 1 - 50 mV $s^{-1}$. The electrolyte was 0.1 mol $dm^{-3}$ $H_2SO_4$ and the surface coverage was 1 x $10^{-8}$ mol $dm^{-3}$ $[Ru(bpy)_2(PVP)_{10}Cl]Cl$.

At higher sweep rates the changeover to semi-infinite diffusional behaviour is observed. This can be seen in Figure 2.7 which plots $i_{pa}$ vs. $v^{1/2}$ which is also linear. This indicates that the polymer exhibits good surface behaviour. and that the current is limited by semi-infinite diffusional processes and possibly by migration effects as well.

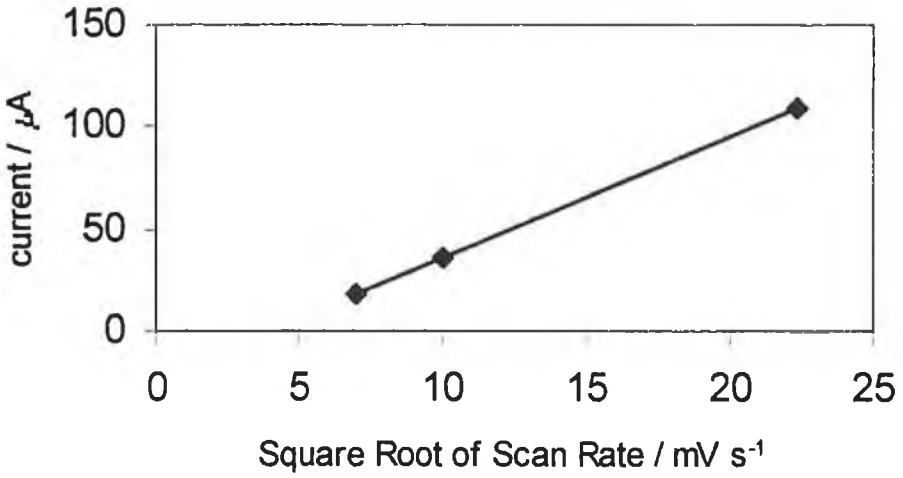


Figure 2.7 Plot of peak current versus the square root of the scan rate from 50-500 $mVs^{-1}$. The electrolyte was 0.1 mol $dm^{-3}$ $H_2SO_4$ and the surface coverage was 1 x $10^{-8}$ mol $dm^{-3}$ $[Ru(bpy)_2(PVP)_{10}Cl]Cl$.

### 2.3.4b Stability of Uncrosslinked vs. Crosslinked $[Ru(bpy)_2(PVP)_{10}Cl]Cl$

***Observation of Cyclic Voltammograms***

Cyclic voltammograms were then taken of the in situ electrode whilst the flow of carrier solution around the flow injection system was maintained at 0.7 $cm^3$ $min^{-1}$. A plot of surface coverage versus time is shown in Figure a.

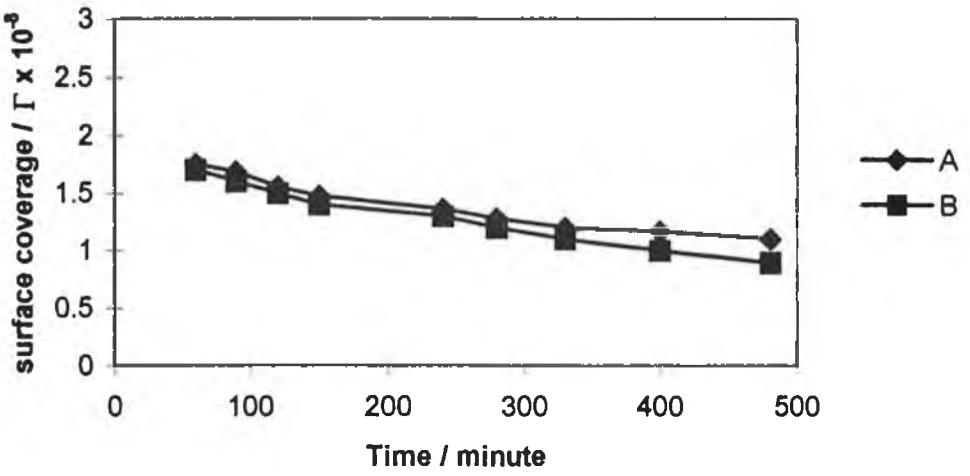


Figure 2.8 Plot of surface coverage versus time for the $[Ru(bpy)_2(PVP)_{10}Cl]Cl$ modified electrode. The electrolyte was 0.1 mol $dm^{-3}$ $H_2SO_4$ and the surface coverage was 1 x $10^{-8}$ mol $dm^{-3}$ and flow rate was 0.7 $cm^3$ $min^{-1}$. A = un-crosslinked modified layer, B = crosslinked with 10 mol % of 1,10-dibromodecane.

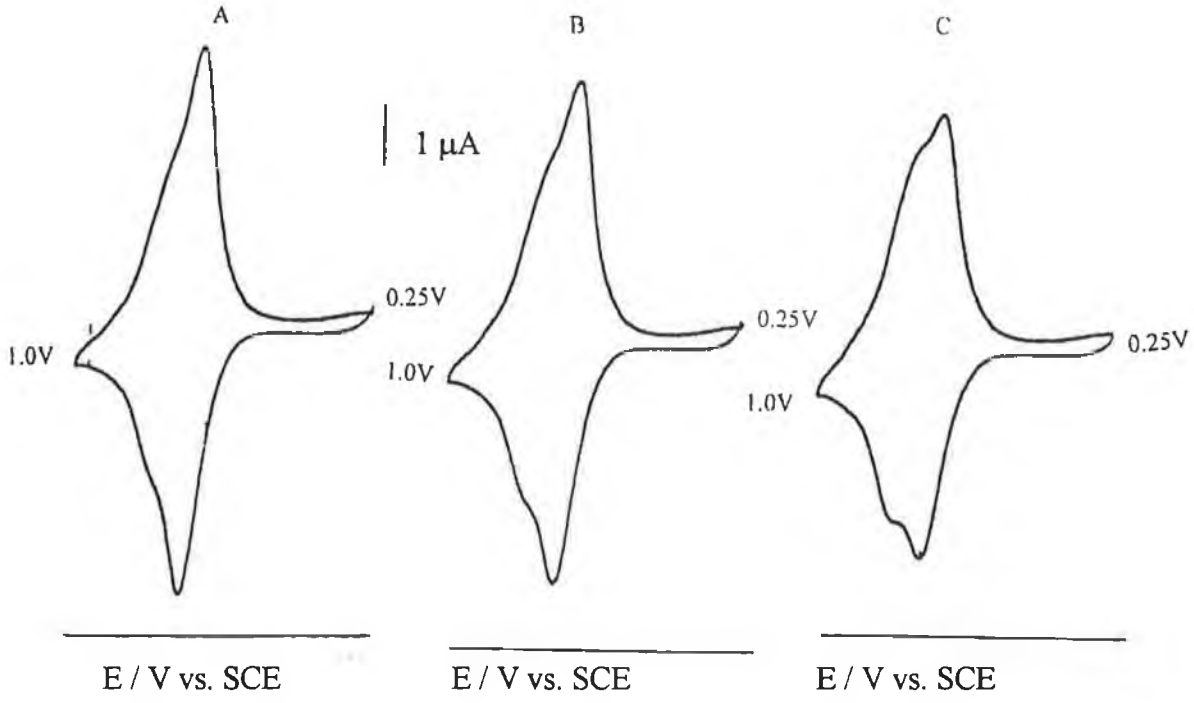


Figure 2.9 Cyclic voltammograms of $[Ru(bpy)_2(PVP)_{10}Cl]Cl$ crosslinked with 10 mol % of 1,10-dibromodecane in a thin layer flow cell. The electrolyte was 0.1 mol $dm^{-3}$ $H_2SO_4$ and the surface coverage was 1 x $10^{-8}$ mol $dm^{-3}$.. A = after 150 min B = after 250 min, C = after 350 min. Carrier flow rate was 0.7 $cm^3$ $min^{-1}$.

Surface coverage dropped from an initial value of 1 x $10^{-8}$ mol $cm^{-2}$ to 4.5 x $10^{-9}$ mol $cm^{-2}$ within 9 hours. Which gives a half life, $t_{1/2}$, for this uncrosslinked ruthenium polymer layer of 9 hours. This mirrors the result obtained in the sensor response experiment. Figure 2.9 shows some of the cyclic voltammograms taken of this uncross-linked layer during this experiment. It can be seen that as time passes the redox peak at 720 mV is joined by a second peak at approximately 800 mV which appears after approximately 4 hours. This ruthenium-containing polymer has previously been shown to undergo photosubstituion with the photo product typically displaying a redox potential of approximately 800 mV vs. SCE. This second peak is characteristic of the substitution of the chlorine ligand with a molecule of water [45]. After nine hours the second peak at 800 mV vs. SCE has grown larger than the initial peak at 720 mV and the $t_{1/2}$ of the polymer has been reached.

A ruthenium polymer cross-linked 10% with 1,10-dibromodecane was then observed to see if the cross-linking process had any effect on the stability of the polymer in a flow injection cell. Figure 2.8b shows a plot of surface coverage versus time and it can be seen that a decrease of approximately 50% in the polymer coverage is reached within 9 hours. In other words, the half-life of the polymer remained unchanged after cross-linking with no observable increase in stability which again mirrors the observed response of the modified electrode to the iron substrate. The cyclic voltammograms of this cross-linked polymer showed a similar pattern to that already observed in the uncrosslinked polymer. After 4 hours a second peak began to form at 800 mV. This peak increased in time whilst the first peak at 720 mV correspondingly decreased.

After 9 hours this second peak was larger than the first. Therefore, the crosslinking of the vinylpyridine groups of this polymer had no effect on the stability of the ruthenium-chlorine bond. The chlorine ligand of the ruthenium polymer is the limiting factor in the stability of this material [46].

### 2.3.5 Charge Transport Characteristics of Crosslinked $[Os(bpy)_2(PVP)_{10}Cl]Cl$

The rate of charge transport through such films has been characterised as being limited by a number of factors. These are the intrinsic barrier to electron self-exchange, $k_{ex}$, the transport of charge-compensating counter-ions through the polymer and polymer segment motion required for redox site juxtapositioning. A compromise between these opposing limiting factors must be reached to allow optimisation of charge transport diffusion, $D_{ct}$. The effect of cross-linking on the electrochemical behaviour of the osmium polymer was examined using cyclic voltammetry and the Randles-Sevčik equation. Under these conditions the peak current for the redox reaction is governed by the Randles Sevčik equation:

$$i_p = \frac{0.4463 n^{\frac{3}{2}} F^{\frac{3}{2}} A (D_{ct} v)^{\frac{1}{2}}}{(RT)^{\frac{1}{2}}} \qquad \text{(Eq. 2.1)}$$

A high rate for self-exchange will be found in compact films where the redox sites are close together. The compactness of the film also results in an effective concentration of redox sites which also leads to enhanced self-exchange. The transport of counter-ions into and out of the polymer film will be enhanced if the film is swollen as there will be a larger volume available within the layer within which the ions can travel, thus allowing faster ion transport.

The cross-linking of the polymer film results in both inter and intra molecular bonding and in the quaternisation of the pyridine groups on the polymer backbone. This results in a stable polymer film which may have the effect of decreasing the volume of the layer and thus restrict counter-ion movement and thus cause a decline in the layers charge transport characteristics. However, it is also possible that by cross-linking the film, the self-exchange reaction may increase due to effectively linking the osmium moieties more closely together which would result in enhanced charge transport characteristics.

| Level of Cross-linking<br>mol % 1,10-dibromodecane | $D_{ct}$<br>$cm^2\ s^{-1}$ |
|---|---|
| 0 | $2 \pm 0.2 \times 10^{-10}$ |
| 5 | $4.9 \pm 0.2 \times 10^{-9}$ |
| 10 | $4.9 \pm 0.2 \times 10^{-9}$ |
| 20 | $4.9 \pm 0.2 \times 10^{-9}$ |

Table 2.2 Charge transport diffusion coefficient at various levels of cross-linking. The $[Os(bpy)_2(PVP)_{10}Cl]Cl$ modified electrode has a surface coverage of $1 \times 10^{-8}$ mol $cm^{-2}$, electrolyte is 0.1 mol $dm^{-3}$ $H_2SO_4$, potential sweep rate used from 100 - 500 mV $s^{-1}$, electrolyte flow rate is 1 $cm^3\ min^{-1}$.

The $D_{ct}$ values for a number of osmium polymer layers modified with differing amounts of 1,10-dibromodecane are shown in Table 2. It can be seen that for all levels of cross-linker in 0.1 mol $dm^{-3}$ $H_2SO_4$, the $D_{ct}$ value remains constant at $4.9 \pm 0.2 \times 10^{-9}$ $cm^2\ s^{-1}$. This compares with the $D_{ct}$ value found for the uncrosslinked polymer which was calculated to be $2 \pm 0.2 \times 10^{-10}$ $cm^2\ s^{-1}$. This $D_{ct}$ value is higher than that found for the uncrosslinked polymer which indicates that the cross-linking process enhances the charge transport characteristics of these electropolymers. It is clear from the $D_{ct}$ values that the energy barrier to self-exchange between the redox species is not the controlling process. It appears that the cross-linking reaction brings the polymer chains closer together thus allowing an improvement in the rate of electron transfer. This compacting of the polymer chains does not appear to result in the limiting of charge transport due to restricted counter-ion movement in the 0.1 mol $dm^{-3}$ $H_2SO_4$ electrolyte. From the results it seems that the cross-linking process leaves enough internal volume in the polymer film within which the counter-ions have enough room to manoeuvre. 1,10-dibromodecane itself is a relatively large molecule and may not cause much retardation of ion transport. The compacting of the film due to cross-linking may be balanced with the tendency of the acidic electrolyte to cause a swelling of the polymer due to protonation of the pyridine moieties.

| Electrolyte Molarity<br>x mol $dm^{-3}$ | $D_{ct}$<br>$cm^2\ s^{-1}$ |
|---|---|
| 0.1 | $4.9 \pm 0.2 \times 10^{-9}$ |
| 0.5 | $0.9 \pm 0.2 \times 10^{-8}$ |
| 0.75 | $1.2 \pm 0.2 \times 10^{-8}$ |
| 1.0 | $1.6 \pm 0.2 \times 10^{-8}$ |

Table 2.3 Charge transport diffusion coefficient at various levels of molarity of the electrolyte $H_2SO_4$. The $[Os(bpy)_2(PVP)_{10}Cl]Cl$ modified electrode has a surface coverage of $1 \times 10^{-8}$ mol $cm^{-2}$, potential sweep rate used from 100 - 500 mV $s^{-1}$, electrolyte flow rate is 1 $cm^3$ $min^{-1}$.

The effect of increasing the molarity of the electrolyte on the rate of charge transfer was investigated. Table 3 characterises the $D_{ct}$ values found at a cross-linked osmium polymer as the electrolyte was adjusted from 0.1 mol $dm^{-3}$ to 1.0 mol $dm^{-3}$. It appears that as the molarity of the $H_2SO_4$ electrolyte is increased, the rate of charge transport increases. This indicates that the charge transport characteristics of this cross-linked polymer improve with increasing molarity of the electrolyte. This is most likely due to the slight swelling effect of the acidic electrolyte contributing to freer counter-ion movement within the layer even while cross-linked. The cross-linking agent has a long, flexible structure that does not repress the characteristics of the electropolymer entirely. This mirrors what was found when the surface behaviour of this redox polymer was examined and where it appeared that the cross-linker had no effect.

### 2.3.6 Nernstian Behaviour

The chemical and mechanical properties of redox polymer modified electrodes have been examined and a model has been developed based on the observed behaviour of a polyvinylferrocene modified electrode [46-48]. This model was used to describe the coupling of the mechanical and electrochemical thermodynamics of redox polymer films for systems in which there was a net change in the charge per redox site

associated with this redox conversion. It appeared that mechanical work can be coupled to the electrode potential in this and other polymer modified electrode systems. This mechanical work was associated with the elastic expansion and contraction of covalently and ionically cross-linked redox polymers due to charge compensating counter-ion incorporation and expulsion. This forced swelling of the cross-linked polymer film required energy input in excess of what was needed to carry out electron transfer to and from the redox sites and resulted in non-Nernstian thermodynamics. In other words, the electrostatically forced intrusion of the ions of the supporting electrolyte into the polymer layer resulted in this non-Nernstian behaviour because of the finite void volume within the polymer film and the finite molar value of the charge compensating ions. By altering the electrolyte, the mechanical state of cross-linked polymers can be changed. This elastic deformation of the cross-linked polymer matrix was related to the electrode potential by the equation:

$$E = E^{o} + \frac{RT}{nF} In \frac{f}{(1-f)} + nvA^{2} cK_{m} \frac{F - 0.5}{10^{4} Fz^{2}} \qquad \text{(Eq. 2.2)}$$

where E is the electrode potential, $E_o'$ is the formal electrode potential, f is the fraction of redox sites in the polymer film which are oxidised, $v$ is the molar volume of the electrolyte anion, c is the total concentration of redox sites in the polymer film, K is the bulk modulus of elasticity and z is the charge of the counter-ion species. R, T, n and F retain their usual meanings.

Covalently cross-linked plasma polymerised vinylferrocene modified electrodes were found to have super-Nernstian slopes in a number of different electrolytes including perchlorate and acetonitrile [48]. Research suggested that this behaviour was related to stress induced by the forced incorporation of the anions of the supporting electrolyte in order to maintain electroneutrality within the film. Quantitative analysis of the super-Nernstian slope showed it to be consistent with the postulated model. This was not unexpected given that the film consisted of a highly cross-linked polymer and the solvent had to compete with the counter-ions for the available free

volume as the film was oxidised. The osmium redox polymer, $[Os(bpy)_2(PVP)_{10}Cl]Cl$, has also displayed super-Nernstian behaviour in perchlorate electrolyte [36], an electrolyte which causes extensive cross-linking of the polyvinylpyridine matrix.

In sulphuric acid electrolyte, this same osmium redox polymer was found to display a Nernstian response [36]. This latter electrolyte allows the immobilised polymer film to swell resulting in a polymer matrix that is more elastic which does not provide a mechanical barrier to the influx of charge compensating counter-ions.

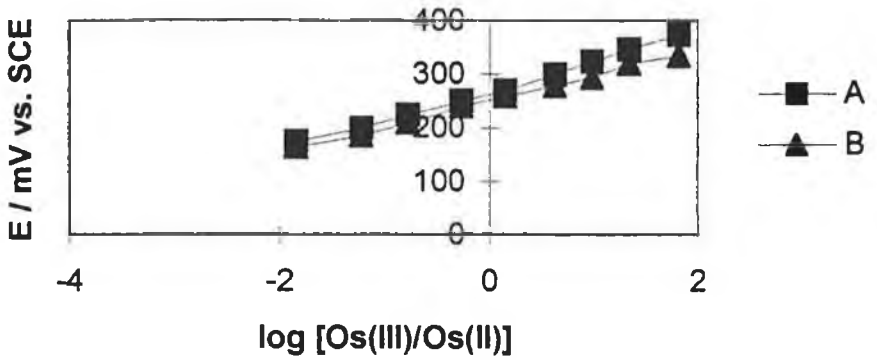


Figure 2.10 Nernstian plot for the $[Os(bpy)_2(PVP)_{10}Cl]Cl$ modified electrode crosslinked with 10 mol % of 1,10-dibromodecane. A = in a conventional electrode cell, B = in a thin layer flow cell. The electrolyte was 0.1 mol $dm^{-3}$ $H_2SO_4$ and the surface coverage was 1 x $10^{-8}$ mol $dm^{-3}$. Carrier flow rate in B was 1.0 $cm^3$ $min^{-1}$.

However, when this osmium redox polymer was partially cross-linked with 1,5-dibromopentane, super-Nernstian behaviour was observed in the modified film, suggesting that insufficient void volume was available to incorporate incoming counterions and therefore additional over potential was necessary to enforce the incorporation of the counterions [37].

This osmium redox polymer modified electrode, when partially covalently cross-linked with 1,10-dibromodecane, instead of the 1,5-dibromopentane, has been shown to give a Nernstian response in sulphuric acid electrolyte in a conventional electrochemical cell [37]. This suggested that the void volume of the partially cross-linked polymer layer was sufficient to ensure that electroneutraility was maintained without the forced expansion of the polymer for inclusion of counter-ions.

The Nernstian behaviour of the partially cross-linked osmium and ruthenium redox polymers was examined in the thin layer flow cell to see whether the modified electrode behaved similarly in two such different environments. The Nernstian plots for these cross-linked modified electrodes are shown in Figures 2.10 and 2.11.

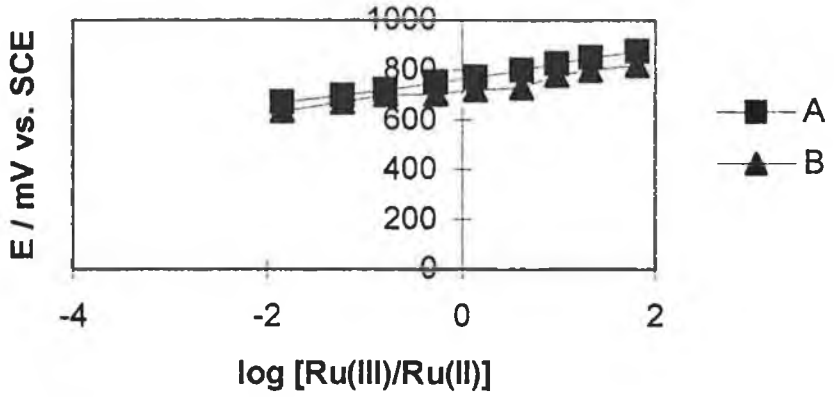


Figure 2.11 Nernstian plot for the $[Ru(bpy)_2(PVP)_{10}Cl]Cl$ modified electrode crosslinked with 10 mol % of 1,10-dibromodecane. A = in a conventional electrode cell, B = in a thin layer flow cell. The electrolyte was 0.1 mol $dm^{-3}$ $H_2SO_4$ and the surface coverage was 1 x $10^{-8}$ mol $dm^{-3}$. Carrier flow rate in B was 1.0 $cm^3$ $min^{-1}$.

Each plot is compared with the behaviour of the cross-linked layer in the conventional cell. For the osmium-containing polymer, the operational potential where [Os(II)] = [Os(III)] was found to occur at 0.250 + 0.005 V vs. SCE. Over the region -2 << log [Os(II)/Os(III)] << +2, the slope of the Nernst plot in the conventional cell was found

to be 57 ± 2mV decade-1 and in the thin layer cell was found to be 48 ± 2mV decade-1. That is, the redox polymer exhibited ideal Nernstian behaviour in the conventional cell as expected but sub-Nernstian behaviour was found for the same film in the thin layer cell.

The Nernstian plot for the cross-linked ruthenium polymer in the thin layer flow cell can be compared with the plot for the equivalent cross-linked modified electrode in a conventional three electrode cell. The operational potential where [Ru(II)] = [Ru(III)] was found to occur at 0.715 ± 0.005 V vs. SCE. A similar result as was found for the osmium redox polymer was found for the ruthenium redox polymer with the plot for the cross-linked electrode in the conventional cell yielding a slope of 58 ± 2 mV decade-1 over the region -2 << log[Ru(III)]/[Ru(II)] << +2 and a slope of 50 ± 2 mV decade$^{-1}$ over the same region for the thin layer flow cell. The cross-linked redox polymer in the conventional cell demonstrated ideal Nernstian behaviour whilst a sub-Nernstian response was found for the modified electrode in the flow injection analysis system.

This observation is akin to the behaviour found in non-covalently cross-linked polyvinylferrocene modified electrodes. That electrode demonstrated complex electrochemical behaviour including a thermodynamic region characterised by sub-Nernstian behaviour which was interpreted in terms of an increasing association of ferrocenium/perchlorate ion pairs in dimers or higher order aggregates.

### 2.3.7 Flow Injection Analysis

The electropolymer modified electrodes described in this chapter can be used as the working electrode in a conventional electrode cell for batch analysis or in a flow injection analysis system. These cross-linked polymer modified electrodes, though prepared in an identical fashion, can demonstrate different responses depending on whether the measurement is made using the thin-layer or conventional electrode cell.

For an ideal sensing system, the response should accurately mirror the change in the sample analyte's concentration no matter what the setting. A real detector will, of course, deviate from this ideal due to limited response characteristics. However, in batch analysis the time available for the working electrode to respond is generally sufficient for a constant steady state signal corresponding to the analyte concentration to be measured.

In flow injection systems, the sample is dynamically carried to the active surface of the electrode through narrow-bore tubing. Within the carrier liquid stream the sample containing the analyte occupies only a small volume. The flow rate used in the experiments described here was typically 1.0 $cm^3$ $min^{-1}$. With a sample volume of only 20 microlitres, this means that the sample plug remains in contact with the modified electrode surface for only 1.2 seconds. The modified electrode is in contact with this sample for a very short period of time and so is unlikely to generate a steady state response. Instead a sub-Nernstian response is to be expected. As the condition of steady state equilibrium is not reached, the electrode response is smaller than expected.

In Figure 2.12 an experiment is shown which illustrates this effect. The flow injection peak was obtained due to the amperometric response of a cross-linked osmium polymer modified electrode to an injection of 20 microlitres of an 1 x $10^{-3}$ mol $dm^{-3}$ Fe(III) solution. The carrier stream was 0.1 mol $dm^{-3}$ $H_2SO_4$ and the surface coverage of the modified electrode was 1 x $10^{-8}$ mol $dm^{-3}$. The plateau corresponds to the same electrode's response when the carrier electrolyte was 'spiked' with Fe (III) at a concentration of 1 x $10^{-3}$ mol $dm^{-3}$. It can be seen that the analyte peak does not reach the steady state equilibrium response. The dispersing effect of the column was measured. Dispersion is the amount that the chemical signal is reduced by injecting a sample plug onto the FIA system. This is represented mathematically by

$$D = \frac{C^{o}}{C^{max}} \qquad \text{(Eq. 2.3)}$$

where D is the dispersion coefficient. $C^o$ is the measured concentration when only the analyte is in the system and $C^{max}$ is the measured concentration when the analyte is injected onto the system [49]. Experimentally, a value of 1.02 was measured for the diffusion in this flow injection system by comparing the response at the steady state versus the response at an FIA peak. This value though approaching the ideal of 1, does not and cannot reach this value. Instead a pseudo equilibrium is reached at the sample response peak.

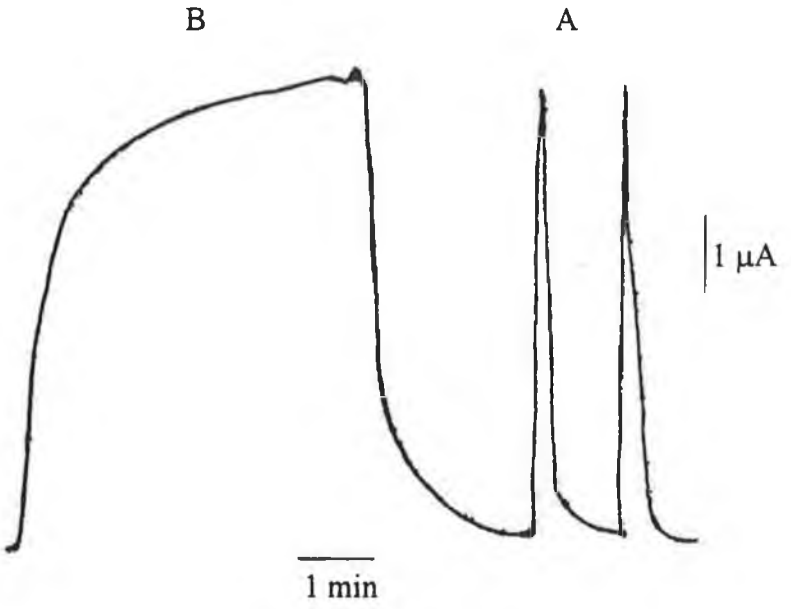


Figure 2.12 Response of the $[Os(bpy)_2(PVP)_{10}Cl]Cl$ modified electrode crosslinked with 10 mol % of 1,10-dibromodecane to (A) injections of a 1 x $10^{-3}$ mol $dm^{-3}$ Fe(III) solution and (B) to an electrolyte containing 0.1 mol $dm^{-3}$ $H_2SO_4$ and 1 x $10^{-3}$ mol $dm^{-3}$ Fe(III). The electrolyte was 0.1 mol $dm^{-3}$ $H_2SO_4$ and the surface coverage was 1 x $10^{-8}$ mol $dm^{-3}$. Carrier flow rate was 1.0 $cm^3$ $min^{-1}$.

This experimental result indicates the reason why the cyclic voltammetric characteristics of the modified electrode in the flow injection system are more removed from the ideal than the equivalent modified electrodes in conventional three electrode cells. It appears that it is the nature of the FIA system, wherein there are fast flowing and turbulent streams, that is the cause of the modifying film displaying

narrower than expected reduction and oxidation peaks, a shift in the difference between the anodic and cathodic peak potentials and, in addition, a sub-Nernstian response.

Because a steady state response is not reached under the flow system's experimental conditions, it is especially important that the hydrodynamic characteristics of the flow injection system are reproducible in order to obtain reliable measurements. Some typical flow injection peaks for repeat injections of 1 x $10^{-3}$ mol $dm^{-3}$ Fe(III) are shown in Figure 2.12. The concentration gradient equivalent to the FIA peak is very reproducible as the injected analyte sample always travels the same distance from the injection port to the working electrode which results in high experimental reproducibility. The reproducibility of a series of peaks was measured and a standard deviation of 0.04 was found. This demonstrates that the electropolymer modified electrode is responding to the analyte in a predictable way at least in the short term. Using a basewidth calculation, these repeat injections show that an analytical throughput of 75 samples per hour is experimentally possible.

Since the modified electrode is in contact with the analyte for only short periods of time in comparison with the time it is in contact with the carrier stream, it is likely that most of the erosion of the modifying layer will be due to mechanical abrasion rather than chemical interaction. Therefore the modifying layer must be resistant to the deteriorating qualities of the flowing stream with which it is constantly in contact as well as preventing passivation of the sensing surface. As previously demonstrated, the cross-linked osmium modified layers are more resistant to this type of deterioration and so enjoy longer life spans than are typical for such modified electrodes. This suggests that the predictable nature of the electrode's response can be expected to extend over the long-term of its lifetime.

As discussed, the sample volume used in these experiments was 20 microlitres. This volume is far less than is generally required when an equivalent analysis is performed on a batch scale. The smaller volume required in the flow system means that less analyte is needed and generally more repeat analyses can be performed leading to

greater precision. Also, because of the small sample size, complex sample matrices such as blood, milk and fruit juices can be injected directly onto the flow system without prior sample preparation. Solid samples such as meat [50], tablets [11] or fertilisers [51] generally require only as much sample preparation as is necessary to get them into a liquid state for injection into the carrier electrolyte.

The response of this modified electrode to a number of different analytes was examined. Certain species such as $Na^{+}$, $Mg^{2+}$ and $Ca^{2+}$ produced no amperometric response. Others such as $Fe^{3+}$, $NO_2^{-}$ and ascorbic acid generated good responses which could be maximised by altering the applied potential. The selectivity of the modifying layer comes from trying to balance the maximised response of the electrode at a particular applied potential with using as low a potential as possible in order to screen out interfering species.

## 2.4 Conclusion

Initial examination of the surface characteristics of the $[Os(bpy)_2(PVP)_{10}Cl]Cl$ and $[Ru(bpy)_2(PVP)_{10}Cl]Cl$ cross-linked modified electrodes indicated that the close to ideal behaviour expected of these redox electrodes in conventional cells does not necessarily translate to the thin layer flow cell environment (Note. The thin layer flow cell figuration used in this experiment is illustrated in Figure 1.8a of Chapter 1.). The peak-to peak separation between the oxidation and reduction waves in the flow cell was found to shift by 50 mV from the expected value found in conventional cells. The ratio of the anodic to the cathodic currents was also found to diverge from the expected result and the full width of the peaks at half maximum height no longer approached the theoretical ideal of 1 for these types of polymer layers. These anomalous results were repeated in the examination of the Nernst plots of these modified electrodes. Nernst plots with slopes of approximately 57 mV $decade^{-1}$ were found when the experiments were carried out in conventional cells but the slopes of these redox modified layers were found to be reduced to approximately 49 mV $decade^{-1}$ when measured in-situ in the flow cell.

Sub-Nernstian responses have also been observed in the operation of a number of other modified electrodes including glass electrodes [52], polyvinylchlorine-based ion selective electrodes [53], and ion-sensitive field effect transistors [54]. However, a common theory for the non-ideal nature of these latter electrodes' responses was not suggested. The non-ideality of the PVC based electrode appeared to be based on diffusion but no particular reason for the sub-Nernstian response could be isolated. Zirconia sensors used for measuring oxidisable gases such as carbon monoxide and hydrogen gas were found to have potential values which deviated from those predicted by the Nernst equation depending on the levels of carbon monoxide and hydrogen present. For microelectrodes, it has been found that electroneutrality cannot be assumed to be present regardless of the electrolyte concentration. It was found that this assumption was invalid when the ratio of the concentration of the supporting electrolyte to that of the electroactive species was ten. This invalid assumption was found to lead to systematic errors in measuring heterogeneous electron-transfer rate constants. For the glass electrode and the ISFETs, it appears that the electrode functioning was found to be the result of a phase boundary equilibrium between located functional groups at the electrode surface and ions in the solution so that the concentration of the charged forms of the groups determines the electrode potential. Such an effect would not be expected for redox electrodes.

From the results of the examination of the flow injection analysis of the $[Os(bpy)_2(PVP)_{10}Cl]Cl$ cross-linked modified electrodes, it appears that it is the nature of the thin layer flow cell environment itself which is generating the sub-Nernstian response. Because only a pseudo-equilibrium is reached at the thin-layer modified electrode in the flow cell compared with the equilibrium available to the thin layer modified electrode in a conventional cell, the deviations from the expected characteristics of this $[Os(bpy)_2(PVP)_{10}Cl]Cl$ modified electrode is observed.

Examination of the effect of cross-linking on the stability of the redox polymer modified electrodes showed mixed results depending on whether the osmium or the ruthenium metallo-polymers were used. The time taken for the surface coverage of the osmium modified electrode to decrease to half its initial value when uncross-

linked was 45 hours but after cross-linking 10% with 1,10-dibromodecane this time increased to 100 hours. Whereas the cross-linking agent had no effect on the stability of the ruthenium polymer modified surface with an observable lifetime of only 9 hours whether cross-linked or not. The osmium polymer was found to be not susceptible to substitution of its chlorine ligand as unlike the ruthenium polymer, so the effect observed in the ruthenium polymer of the appearance of a second wave is not seen in the osmium polymer.

In general, polymer layers are more stable than the equivalent monolayer films, although in recent times advances have been made in prolonging the working lifetime of monolayer modified electrodes [55-58]. Often this is as a result of chemisorption or simply because the polymer film is insoluble in the electrolyte. The use of polymer-based materials with their enhanced stability has resulted in an expanded range of new materials for modification of modified surfaces[1]. However, under hydrodynamic conditions, the contacting electrolyte will cause stability problems due to mechanical abrasion. Therefore, it is necessary to enhance the physical stability of such polymer layers in order to develop modified electrodes with reasonably long lifetimes.

The osmium polymer's useful lifetime, even when uncross-linked is 5 times that of its ruthenium analogue, and when cross-linked this value increases to more than 10 times that of the ruthenium polymer. This result demonstrates that the osmium polymer is more suitable to use in the development of modified electrode sensors compared to the ruthenium polymer. Its extended lifetime will allow more flexibility in the analysis and investigation of the modified electode's suitability for measuring analytes.

## 2.5 References

1. R. W. Murray, A. G. Ewing, R. A. Durst, Anal. Chem., 59 (1987) 379A

2. A. R. Hillman, Electrochemical Science and Technology of Polymers, ed. R. G. Linford, Elsevier, Amsterdam, 1987

3. S. Dong, Y. Wang, Electroanalysis, 1 (1989) 99

4. S. A. Wring, J. P. Hart, Analyst, 117 (1992) 1215

5. G. Inzelt, Electroanalytical Chemistry, Vol. 18, ed. A. J. Bard, Marcel Dekker, New York, 1993

6. R. Toniolo, N. Comisso, G. Bontempelli, G. Schiavon, Talanta, 41 (1994) 473

7. C. M. Chang, H. J. Huang, Anal. Chim. Acta, 300 (1995) 15

8. J. N. Barisci, G. G. Wallace, Anal. Lett., 24 (1991) 2059

9. G. G. Wallace, M. Meaney, M. R. Smyth, J. G. Vos, Electroanalysis, 1, (1989), 357

10. D. P. Lynch, Ph.D. Thesis, Dublin City University, 1991

11. A. P. Doherty, M. A. Stanley, G. Arana, C. E. Koning, R. H. G. Brinkhuis, J. G. Vos, Electroanalysis, 7 (1995) 333

12. J. A. Cox, K. Lewinski, Electroanalysis, 6 (1994) 976

13. T. R. I. Cataldi, D. Centonze, E. Desimoni, V. Forastiero, Anal. Chim. Acta, 310 (1995) 257

14. M. Yuasa, T. Nagaiwa, M. Kato, I. Sekine, S. Hayashi, J. Electrochem. Soc., 142 (1995) 2612

15. A. Liu, E. Wang, Anal. Chim. Acta, 296 (1994) 171

16. Y. Xie, S. Dong, Electroanalysis, 6 (1994) 119

17. W. Schuhmann, C. Lehn, H. L. Schmidt, B. Gruendig, B., Sens-Actuators-B, B7 (1992) 393

18. O. Adeyoju, E. I. Iwuoha, M. R. Smyth, Electroanalysis, 7 (1995) 924

19. W. Hou, E. Wang, Anal. Chim. Acta, 257 (1992) 275

20. B. Hoyer, T. M. Florence, G. E. Batley, Anal. Chem., 59 (1987) 1608

21. J. M. Zadeii, J. Marioli, T. Kuwana, Anal. Chem., 63 (1991) 649

22. Y. Degani, A. Heller, J. Amer. Chem. Soc., 111 (1989) 2357

23. Q. Deng, S. Dong, Analyst, 121 (1996) 1123

24. S. J. Dong, Q. Deng, G. G. Cheng, Anal. Chim. Acta, 279 (1993) 235

25. S. K. Jung, G. S. Wilson, Anal. Chem., 68 (1996) 591

26. B. A. Gregg, A. Heller, Anal. Chem., 62 (1990) 258

27. B. A. Gregg, A. Heller, J. Phys. Chem., 95 (1991) 5970 & 5976

28. M. V. Pishko, A. C. Michael, A. Heller, Anal. Chem., 63 (1991) 2268

29. E. I. Iwuoha, M. R. Smyth, J. G. Vos, Electroanalysis, 6 (94) 932

30. T. J. Ohara, R. Rajagopalan, A. Heller, Anal. Chem., 65 (1993) 3512

31. M. Elmgren, S.-E., Lindquist, G. Henriksson, J. Electroanal. Chem., 341 (1992) 257

32. M. Vreeke, R. Maidan, A. Heller, Anal. Chem., 64 (1992) 3084

33. J. N. Barisci, G. G. Wallace, Anal. Lett., 24 (1991) 2059

34. R. J. Forster, A. J. Kelly, J. G. Vos, M. E. G. Lyons, J. Electroanal. Chem., 270 (1989) 365

35. M. E. G. Lyons, Analyst, 119 (1994) 805

36. R. J. Forster, J. G. Vos, J. Chem. Soc. Faraday Trans., 87 (1991) 1863

37. A. P. Doherty, T. Buckley, D. M. Kelly, J. G. Vos, Electroanalysis, 6 (1994) 553

38. K. K. Shiu, D. J. Harrison, J. Electroanal. Chem. Interfac. Electrochem., 262 (1989) 145

39. G. Inzelt, J. Bacskai, J. Electroanal. Chem., 308 (1991) 255

40. P. Daum, J. R. Lenhard, D. Rolison, R. W. Murray, J. Am. Chem. Soc., 102 (1980) 4649

41. R. J. Forster, J. G. Vos, Macromolecules, 23 (1990) 4372

42. F. E. Little, D. M. Hercules, J. Am. Chem. Soc., 91 (1969) 253

43. J. M. Clear, J. M. Kelly, J. G. Vos, Macromol. Chem., 184 (1983) 613

44. S. M. Gerarty, J. G. Vos, J. Chem. Soc. Dalton Trans., (1987) 3073

45. O. Haas, M. Kriens, J. G. Vos, J. Am. Chem. Soc., 103 (1981) 1318

46. E. F. Bowden, M. F. Dautartas, J. Electroanal. Chem., 219 (1987) 49

47. M. F. Dautartas, E. F. Bowden, J. Electroanal. Chem., 219 (1987) 71

48. E. F. Bowden, M. F. Dautartas, J. F. Evans, J. Electroanal. Chem., 219 (1987) 91

49. B. Karlberg, G. E. Pacey, Flow Injection Analysis, Elsevier, Amsterdam, 1989

50. M. M. Malone, A. P. Doherty, M. R. Smyth, J. G. Vos, Analyst, 117 (1992) 1259

51. A. P. Doherty, M. A. Stanley, D. Leech, J. G. Vos, Anal. Chim. Acta, 319 ` (1996) 111

52. F. G. K. Baucke, Anal. Chem., 66 (1994) 4519

53. U. Oesch, Z. Brzozkz, A. Xu, B. Rusterholz, G. Suter, H. V. Pham, D. H. Welti, D. Ammann, E. Pretsch, W. Simon, 58 (1986) 2285

54. L. Bousse, P. Bergfeld, Sens. Actuators, 6 (1984) 65

55. W. Hou, E. Wang, Talanta, 38 (1991) 557

56. P. Luo, S. V. Prabhu, R. P. Baldwin, Anal. Chem., 62 (1990) 752

57. J. A. Cox, R. K. Jaworski, Anal. Chem., 61 (1989) 2176

58. M. S. Tunuli, Talanta, 35 (1988) 697

# Chapter 3

## Detection of Nitrate with a Cross-linked Osmium Modified Electrode

## 3.1 Introduction

Nitrate plays an important role in the Nitrogen Cycle, in unfertilised soil it can be derived from the rain and from microbial degradation of nitrogen containing compounds and it enters natural waters from many such sources. However, over the past few decades, its concentration has increased progressively in the environment [1]. It is believed that the dominant factor in this trend has been the increased usage of nitrate based fertilisers in agriculture and the consequential leaching of nitrate into freshwater supplies [2-4]. Nitrates are frequently hydrated [5] so that the nitrate anion is quite mobile due to its solubility in water and the predominantly negative charge on soil particles. So it is readily leaches if not utilised by plants. The solubility aspect has the consequence that agriculture is a major contributor to nitrate loading in freshwater supplies and therefore in drinking water [3].

Nitrate represents a potential hazard because of its participation in reactions similar to those found in the human stomach which give rise to N-nitroso compounds, some of which are carcinogenic [6,7,8]. It has been suggested that gastric cancer is associated with nitrate intake through this mechanism [9]. Furthermore, certain species of bacteria in humans can enzymatically reduce nitrate to nitrite [10]. Nitrite can react with secondary and tertiary amines forming carcinogenic nitrosamines [8]. Nitrite can also induce methaemoglobinaemea and other toxic effects include vasodilation, hypertension and lowering of blood pressure [11].

The European Community Directive on the quality of water intended for human consumption came into effect in August 1985 with a limit of 11 mg $l^{-1}$ $NO_3$-N (nitrate as nitrogen) as the maximum admissible level for nitrate and a guide level of 6 mg $l^{-1}$ $NO_3$-N [12].

The standard method for nitrate measurement involves reduction of nitrate to nitrite using a copper activated cadmium catalyst and determination of the nitrite concentration by reaction with sulphanilamide and N-1-naphthylethylenediamine in HCl to produce a purple/red azo dye. The absorbance of this dye at 543 nm is

measured using a spectrophotometer and this is related to the sample nitrate concentration by means of a calibration curve derived from reference nitrate standards [13]. This batch technique takes about 30 min to perform and it is subject to interference by some reducing compounds [14] and metal ions or colour [13].

In view of the increase in interest in the quality of drinking water, sensitive, selective and simple methods for the determination of nitrate are desirable. Attempts have been made to automate this standard procedure. One approach was pretreatment of the sample prior to the sampling valve and injection of the sample in its final form into a carrier stream where it was detected colorimetrically [15]. On-line reduction columns have also been developed to allow automated colorimetric determination of nitrate [16-19]. Strong interferences in this colorimetric determination were found to include sulphate [20,21], sulphide [22], metal ions [20,23,24] and chlorine [13]. Overcoming these interferences using chromatographic techniques have run into problems due to the complexity of the instrumentation required [25,26].

To pre-empt these interference effects from such commonly occurring species, an alternative approach to take is that of electrochemical detection. The direct amperometric detection of nitrate, based on its cathodic reduction, occurs at very negative potentials at most electrode materials. The wave of nitrate reduction is then obscured by the wave of hydrogen evolution. Reductive detection is mostly performed on liquid mercury of amalgam electrodes. Mercury represents a health hazard; it is an inconvenient electrode in flow through cells and amalgam electrodes require frequent reconditioning. Converting nitrate into another nitrogen containing compound with more facile electrochemical behaviour would allow such difficulties to be circumvented.

A flow through amperometric detector has been developed based on the electrochemical reduction of nitrates at a silver cathode. The nitric oxide formed is detected by a gold-plated porous membrane electrode placed downstream of the cathode [27]. The presence of chloride was found to lead to a decrease in the response and metals also caused interference. Very sensitive detection was required

as the flow through tubular reactor converted only a very small, though reproducible, portion of each nitrate sample into a detectable species.

Nitrate, after its reduction by concentrated sulphuric acid in the presence of sodium bromide, has been detected as nitric oxide followed by nitration of an organic reagent using differential pulse polarography [28]. A similar procedure was developed into an on-line technique for nitrate determination. The nitrogen-containing derivative was detected at a glassy carbon electrode. Contamination of the electrode was found to occur very quickly and flow through the system posed problems due to the viscous nature of the sulphuric acid. This made the technique unsuitable and dangerous for on-line analysis [29].

The application of strongly reducing agents such as chromium (II) and vanadium(II) in the flow injection analysis of nitrate followed by polarographic analysis has also been investigated [30,31]. Nitrate was detected in the form of ammonia in this system. The amalgamated zinc in this application converted no more than 26 % of the nitrate to ammonia. Electrocatalytic reduction of nitrate to ammonia using metal cyclams has been described [32]. This technique proved useful for mechanistic studies but it would be unsuitable for use as an analytical technique. Detection occurred at a hanging mercury drop electrode under a nitrogen atmosphere to prevent oxygen interference.

As already described in the standard spectrophotometric method [13] nitrite can be easily formed by reducing nitrate at a copper cadmium catalyst. The electrochemical behaviour of nitrite is well documented and can be carried out at more convenient working potentials. Therefore, the determination of nitrate as nitrite remains the method of choice owing to the accuracy with which low concentrations of nitrite can be detected.

Chromatography techniques allied to electrochemical detection have utilised this approach [33]. A detector with a platinum electrode set at an oxidative potential of 1.0 V vs. Ag/AgCl reference electrode has been applied to nitrate detection that had

previously been reduced to nitrite. Drawbacks of this technique included the requirement of filtration of all samples to avoid damage to the chromatography column [33]; the very narrow linear range of detection (0-1.5 ppm nitrite), which meant that additional off-line dilution steps had be taken, and interferences from any electrochemically active species present in the water sample due to the non-selective nature of the detecting surface.

Studies have been carried out on the possibility of flow-injection determination of nitrate with two platinum electrodes polarised with a small potential difference [34,35]. Nitrate was first reduced to nitrite in a reduction column and measurement was then based on the iodine concentration formed in the reaction between iodide and nitrite. This was found to be a sensitive measurement system with a detection limit of 6 $\mu g\ l^{-1}$ $NO_3$-N.

More facile FIA (flow injection analysis) manifolds have been described which use anodic amperometric detection of nitrate after on-line reduction on a cadmium reductor column [36,37]. The working electrode was, in one case, carbon paste [36] and in another glassy carbon [37]. A serious drawback with using such electrodes is the complete dependence of the rate of the redox reaction on the surface state of the electrode. They are also subject to interference by many cations and anions [38]. Sequential injections of nitrate onto the FIA system with a bare glassy carbon working electrode resulted in a steady decrease in the measured signal [37]. This decrease was the result of adsorption of the oxidation product of nitrite at the electrode surface.

Development of a modified electrode sensor in which the underlying electrode is covered by a modifying film which can alleviate surface poisoning and also diminish the effect of inteferents is one approach to overcoming this problem. A platinum electrode modified by the adsorption of an iodine film was found to eliminate the passivation caused by the accumulation of nitrite side products [39]. A glassy carbon electrode was also reported to have been modified by coating it with quaternised poly(4-vinyl pyridine) and impregnating the film with $[IrCl_6]^{4-3-}$. This anion-exchange polymer film did not suffer from surface poisoning but it was found to be

less sensitive than the bare glassy carbon electrode. A lower effective diffusion coefficient caused the lower sensitivity obtained due to the incursion of nitrite into the polymer and the charge transport required to regenerate the $Ir^{IV}$. A further drawback of this modified electrode was that it required frequent reconditioning and recalibrating.

The nitrate sensor described in this chapter utilises the facile electrochemical behaviour of nitrite by first reducing nitrate on a copperised cadmium column and then measuring the nitrite at a modified electrode, which as well as preventing surface contamination also is sensitive, selective and can be easily incorporated into a bench-top flow injection analysis system. The modified electrode described is further modified by partial cross-linking of its polymer modifying layer in an effort to bestow enhanced stability onto the sensor.

## 3.2 EXPERIMENTAL

### 3.2.1 *Electrolytes and Solutions*

The electrolyte used was 0.1 mol $dm^{-3}$ $H_2SO_4$. Nitrite solutions were prepared freshly each day from $NaNO_2$. $NaNO_3$ was used to prepare the nitrate solutions. The carrier solution used with the cadmium column was composed of 0.1 mol $dm^{-3}$ NaCl and 2.5 g $l^{-1}$ EDTA. A 2% w/v solution of $CuSO_4.5H_2O$ was used to copperise the cadmium. All chemicals described in the text were of A.R. grade and were prepared with Milli-Q water.

### 3.2.2 *Preparation of $[Os(bpy)_2(PVP)_{10}Cl]Cl$*

This material was synthesised according to the procedure described by Forster et al [40] except that 2-methoxyethanol was used as the solvent instead of ethanol. A metal loading of one osmium centre per ten vinyl pyridine units was chosen as this

loading has been shown to display optimum charge transfer characteristics [41]. PVP (poly-4-vinyl pyridine) of molecular weight 600,000 a.m.u., as determined by viscometry, was used, and bpy = bipyridine.

### 3.2.3 *Preparation of Modified Electrode*

Modified electrodes were prepared by polishing glassy carbon electrodes with 5 μM alumina as an aqueous slurry on a felt cloth followed by a thorough rinsing with distilled water and methanol. The freshly prepared electrode surfaces were modified by drop coating using a 1% w/v methanolic solution of the polymer. Cross-linking of this polymer was achieved by adding an appropriate volume of 1,10-dibromodecane dissolved in methanol to the polymer deposited on the electrode [42]. These two solutions were then mixed gently and allowed to dry slowly overnight in a methanolic atmosphere. Surface coverage was measured by controlled potential coulometry using an EG&G digital coulometer, model no. 379.

### 3.2.4 *Cyclic Voltammetry and RDE Voltammetry*

Cyclic voltammetry (CV) and rotating disc electrode voltammetry (RDE) were carried out using a conventional three electrode assembly. The potentiostat used was an EG&G Princeton Applied Research Model 362. The rotating disc assembly was the Metrohm Model 629-10. Voltammograms were recorded on a Linseis X-Y recorder. The working electrodes, manufactured by Metrohm, were 3 mm diameter glassy carbon discs shrouded in Teflon. The counter electrode was 1 $cm^2$ platinum gauze placed parallel to the working electrode. The reference electrode was a saturated KCl calomel electrode. All potentials are quoted with respect to the SCE. All measurements were carried out at room temperature. Modified electrodes were prepared and allowed to dry as before.

### 3.2.5 *Flow Injection Apparatus*

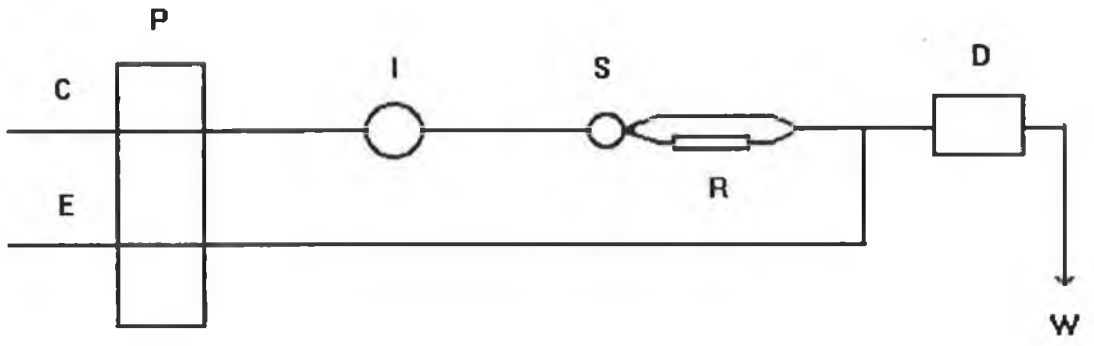


Figure 3.1 FIA Manifold: P=pump; I=injection port; S=switching valve; R= Cu/Cd reduction column; D=detector; W=waste; C=carrier flow of 0.1 mol $dm^{-3}$ NaCl with 2.5 g $l^{-1}$ EDTA; E=electrolyte =0.1 mol $dm^{-3}$ $H_2SO_4$

The flow injection apparatus consisted of a Gilson Minipuls 3 peristaltic pump, a six port Rheodyne injector valve (no. 9125) fitted with a 20 μL fixed volume sample loop, a Rheodyne switching valve (no. 0792), an EG&G Princeton Applied Research Model 400 electrochemical detector and a Kipp & Zonen X-t recorder. Silicone rubber tubing was used at the peristaltic pump and Teflon 1/16" Outer Diameter x 1/32" Inner Diameter tubing for the rest of the system. A Teflon T-piece connected the merging tubing to the detector. For the reduction column a 3 mm bore, 50 mm length glass column was used. This was filled with cadmium granules (40-60 mesh) or 100 mesh cadmium powder which had been washed in a 2 % solution of copper sulphate. The column thus obtained was found to give a stable response over a two week period.

A schematic diagram of the FIA apparatus can be seen in Figure 3.1. Sample injections were made using a 2 $cm^3$ glass syringe fitted with a Rheodyne injection needle. In the standard EG&G flow cell, an Ag/AgCl electrode acted as the reference and the auxiliary electrode was the stainless steel cell body.

### 3.2.5 Ion Chromatography

The system consisted of a Dionex gradient pump module model 4500 and Dionex eluent gas module. Column elient was monitored by a Dionex conductivity sensor, CDM2, and detection output was monitored and processed by Dionex AI450 computer software, version 2.1, linked by a Dionex advanced interface to a 286-PC.

The separator column was an IonPac AS4A column. This 4x250mm column is composed of 15mm polystyrene/divinylbenzene substrate agglomerated with anion exchange latex that has been completely aminated. The latex particles have a diameter of approximately 0.05mm and carry anion exchange sites. The suppressor was an Anion Micromembrane suppressor. Ultrapure water from a Millipore Milli-Q system was used for preparing all solutions. All reagents used were of AnalR grade.

The method used was based on the Dionex Application Update AU131. Although this method was primarily developed for nitrate and nitrite determinations , other anions that commonly occur in water can also be separated by this method. Using similar conditions to those provided in AU131, separations were obtained for the following ions: Fluoride, Chloride, Nitrite, Bromide, Nitrate, Phosphate, Sulphate, using isocratic conditions, in less than 10 minutes.

General Operating Conditions used were:

| | |
|---|---|
| Guard Column: | IonPac AG4A |
| Separator Column: | IonPac AS4A |
| Eluent: | 1.8 mM $Na_2CO_3$ |
| | 1.7 mM $NaHCO_3$ |
| Eluent Flow Rate: | 2.0 $cm^3$/min |
| Suppressor: | Anion MicroMembrane |
| Regenerant: | 12.5mM $H_2SO_4$ |
| Regenerant Flow Rate: | 5 $cm^3$/min |
| Sample Loop Volume: | 50 μL |
| Background Conductivity: | 10-20 μs |

## 3.3 RESULTS

### 3.3.1 General Electrochemistry

A cyclic voltammogram of the electrocatalytic polymer $[Os(bpy)_2(PVP)_{10}Cl]Cl$, cross-linked 10% with 1,10-dibromodecane on a glassy carbon electrode can be seen in Figure 3.2. The $E_{\frac{1}{2}}$ of the osmium redox centre in the 0.1 mol $dm^{-3}$ sulphuric acid electrolyte is 0.250 V vs. SCE. This value indicates that the co-ordination sphere of the metal centre is $[Os(N)_5Cl]$ as expected from the synthetic strategy [43]. This value is identical with that found for the uncross-linked polymer [44] which shows that cross-linking does not affect the osmium redox centre.

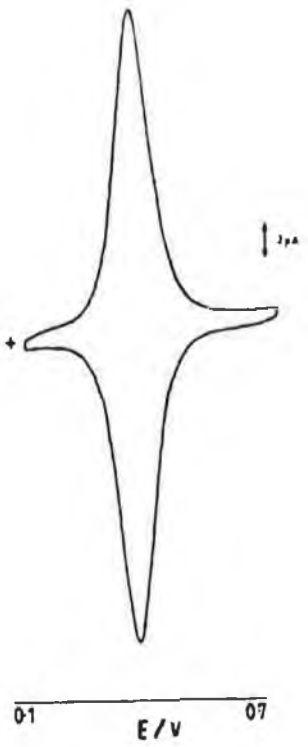


Figure 3.2 Cyclic voltammogram of the 10% crosslinked $[Os(bpy)_2PVP_{10}Cl]Cl$ polymer coated on a glassy carbon electrode. Polymer surface coverage is 1 x $10^{-8}$ mol $cm^{-2}$. Electrolyte is 0.1 mol $dm^{-3}$ $H_2SO_4$. Potential sweep rate is 2 mV $s^{-1}$

Examining the CV of this cross-linked electropolymer gives rise to a number of observations regarding the surface attachment characteristics of the polymer. The ratio of $i_{pa}/i_{pc}$ is close to one. This indicates that the kinetics of the forward and reverse waves are similar [45]. The peak to peak separation between the oxidation and reduction peaks is almost zero at low sweep rates with no diffusional tailing. A plot of peak current versus potential sweep rate is linear up to about 50 mV $s^{-1}$ indicating that at low sweep rates the polymer film exhibits surface behaviour [46].

These results demonstrate the close to ideal features of the cyclic voltammetric behaviour of the modifying film, i.e. zero peak separation and linearity of oxidation and reduction waves. These features are not observed if the kinetics cannot maintain equilibrium [45]. These values are consistent with rapid reversible surface behaviour of the redox couple.

From a plot of the square root of the scan rate versus peak current it is demonstrated that at low scan rates the plot is curved whereas linearity is observed at higher scan rates (see Figure 3.3). This demonstrates the cross-over to semi-infinite diffusion behaviour of the electropolymer at higher scan rates and the consequent transformation from surface to solution type behaviour of the electropolymer.

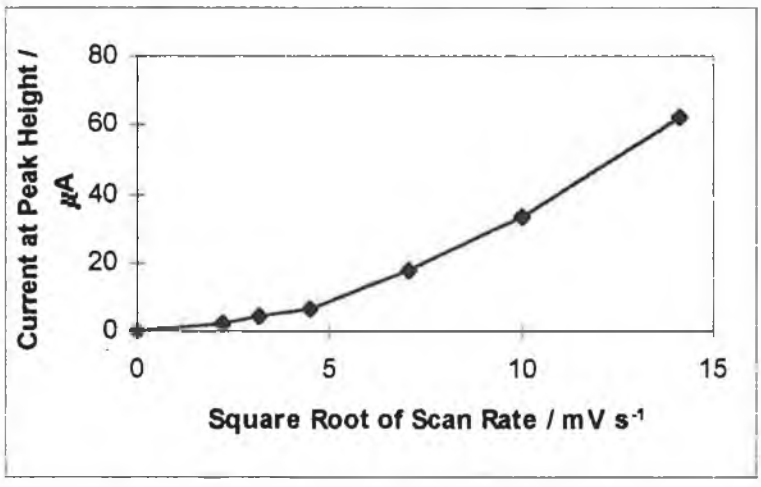


Figure 3.3 Plot of the square root of scan rate versus peak current in 0.1 mol $dm^{-3}$ $H_2SO_4$. Polymer surface coverage is 1 x $10^{-8}$ mol $cm^{-2}$ $[Os(bpy)_2(PVP)_{10}Cl]Cl$. Electrolyte is 0.1 mol $dm^{-3}$ $H_2SO_4$.

Under semi-infinite diffusional conditions the cyclic voltammograms can be analysed using the Randles-Sevčik equation [47].

$$i_p = 0.4463\ (nF)^{\frac{3}{2}}\ AD_{ct}^{\frac{1}{2}}\ Cv^{\frac{1}{2}}/(RT)^{\frac{1}{2}} \qquad \text{(Eq. 3.1)}$$

where $i_p$ is the anodic peak current, n is the number of electrons transferred, F is Faraday's constant, A is the geometric electrode area, $D_{ct}$ is the charge transport diffusion coefficient, C is the concentration of redox sites within the film, v is the scan rate, R is the gas constant and T is the absolute temperature. From this equation the charge transport diffusion coefficient, $D_{ct}$, was evaluated for the mediating layer in 0.1 mol $dm^{-3}$ sulphuric acid. Its value was measured as $2.39 \times 10^{-10}$ $cm^2$ $s^{-1}$ which can be considered fast on the CV timescale.

This indicates a substantial increase in the charge transport properties of the modifying layer upon cross-linking with 1,10-dibromodecane. The charge transport properties of the uncross-linked osmium homopolymer have been studied extensively and these studies have lead to the conclusion that the overall rate of charge transport is probably controlled by counter-ion motion [41,49,50].

Studies of completely cross-linked polymer films indicates that compaction of the polymer film occurs which in turn hinders short-range ion motion and so reduces the current capacity of these films [51,52]. Since the polymer in this study was only lightly cross-linked it is unlikely that such radical changes in the polymer's morphology occurred.

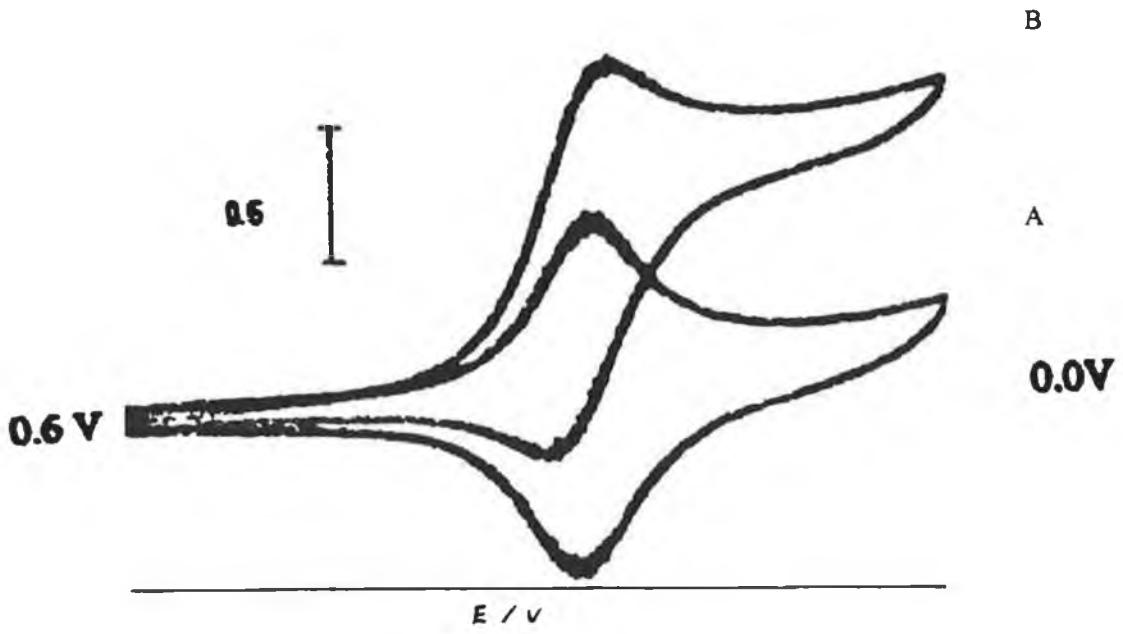


Figure 3.4 Cyclic voltammogram showing the metallo-polymer before (A) and after (B) the addition of 1.0 x $10^{-3}$ mol $dm^{-3}$ nitrite. Sweep rate is 2 mV $s^{-1}$ and the electrolyte is 0.1 mol $dm^{-3}$ $H_2SO_4$. Polymer surface coverage is 1 x $10^{-8}$ mol $cm^{-2}$ [Os(bpy)2(PVP)10Cl]Cl

Typical cyclic voltammograms obtained in 0.1 mol $dm^{-3}$ sulphuric acid electrolyte at the modified glassy carbon electrodes in the presence and absence of nitrite are depicted in Figure 3.4. The wave representing the cyclic voltammogram of the reduction of nitrite at the cross-linked polymer modified electrode demonstrates the electrocatalytic nature of this reaction. The shape of the wave is indicative of an electrocatalytic reaction occurring at the electrode. Also, unlike the case with the bare electrode no surface passivation is found to occur. The mediating effect begins as the applied potential approaches the redox potential of the Os(II)/Os(III) couple. As soon as Os(II) is generated in the modified film by scanning in the negative direction, mediation begins. In the reverse wave, as the concentration of Os(II) centres becomes depleted, so too does the mediation stop. The reduction of the nitrite is superimposed on the reduction and re-oxidation of the osmium centres. These results are characteristic of mediated charge transfer by redox cycling of the Os(III)/Os(II) couple fixed on the electrode of a species present in solution [62].

Similarly, voltammograms obtained using RDE, (a rotating disc electrode), also show this mediation process occurring. Figure 3.5 shows current potential curves for the mediated reduction of nitrite at the modified electrode. Once more when Os(II) is generated in the modified film by scanning in the negative direction, mediation begins. Mediation limits when the switching potential is reached and Os(III) is regenerated. A limiting current is reached which is well-defined and so easily measured. This limiting current is a function of the nitrite concentration as demonstrated by Figure 3.5.

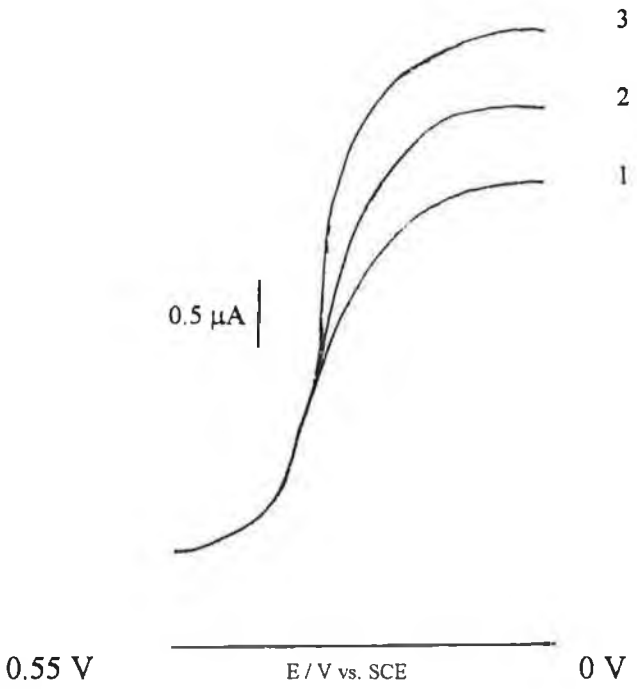


Figure 3.5 Current potential curves for nitrite reduction at the cross-linked modified electrode. Curves 1-3 show the reduction of 1, 2, and 4 x $10^{-3}$ mol $dm^{-3}$ nitrite. Rotation speed is 500 rpm. Sweep rate is 2 mV $s^{-1}$ and the electrolyte is 0.1 mol $dm^{-3}$ $H_2SO_4$. Polymer surface coverage is 1 x $10^{-8}$ mol $cm^{-2}$ $[Os(bpy)_2(PVP)_{10}Cl]Cl$.

### 3.3.2 Kinetics of the Mediated Reduction

A number of theoretical models have been described for the analysis of the kinetic and transport properties of mediation at polymer modified electrodes [53-56]. These models can be used for the investigation of the modified electrode process. According to these models, the reaction of the substrate at the modified electrode can occur at any one of six possible reaction zones under ten different transport or kinetically limiting processes. The reaction site can be at the electrolyte/layer interface, at a reaction zone close to this interface, throughout the layer, at a narrow reaction zone somewhere in the layer, close to the electrode/layer interface, or at the underlying electrode surface.

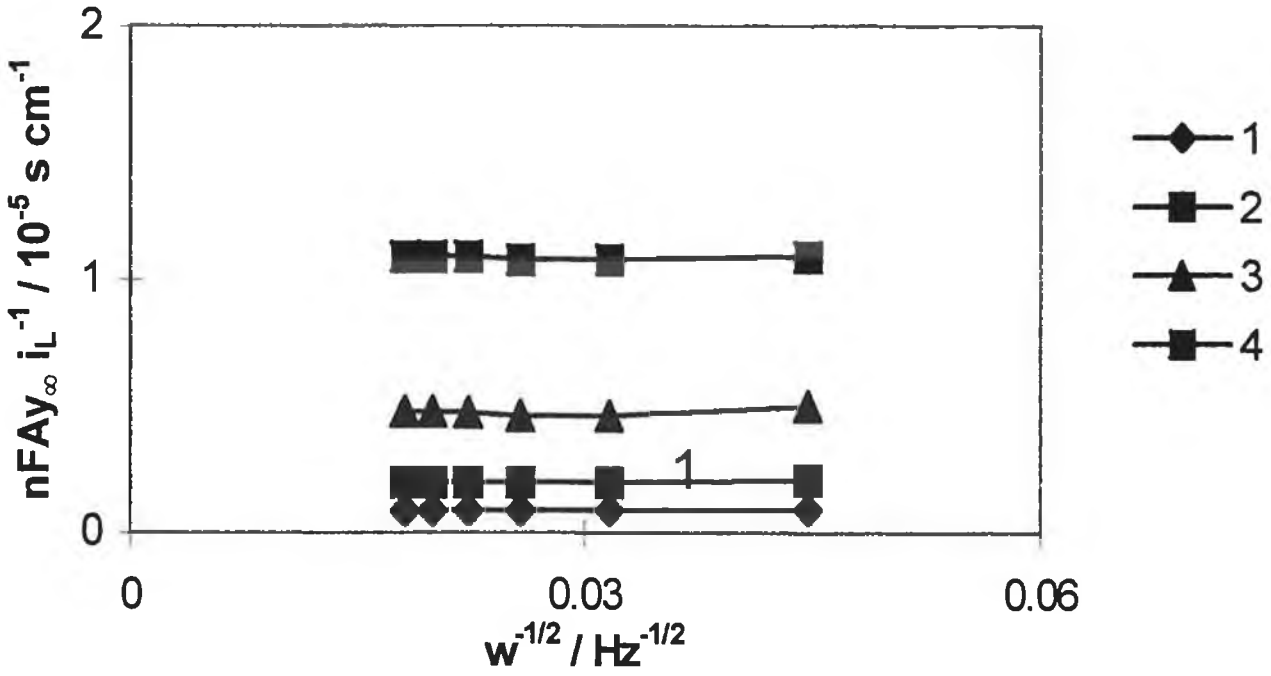


Figure 3.6 Levich plots for the reduction of 2 x $10^{-3}$ mol $dm^{-3}$ nitrite at a cross-linked modified electrode. Curves 1 - 4 represent surface coverages of 32, 14.6, 6.30, 2.37 x $10^{-9}$ mol $cm^{-3}$ respectively. Sweep rate was 2 mV $s^{-1}$ and the electrolyte was 0.1 mol $dm^{-3}$ $H_2SO_4$.

An illustration of these possible reaction sites is shown in Figure 1.10 of Chapter 1. These studies have been based on the theoretical work of Koutecky and Levich. Analysis is carried out by examining the effect of the rotation rate of the electrode, ω,

the reciprocal slope of the Koutecky-Levich plot, the polymer layer thickness, L, and the concentration of electroactive species within the film, $b_O$. Since the rotating disc voltammograms show that a mediated reduction of nitrite occurs in the potential region of the Os(II)/(III) redox couple and also that $i_{lim}$, the limiting current, is dependent on the rotation rate, $\omega$, of the rotating disc, they can be used to investigate the mediated electrocatalysis at the cross-linked $[Os(bpy)_2(PVP)_{10}Cl]Cl$ electrode.

Levich plots obtained for the reduction of nitrite at cross-linked modified electrodes with various polymer surface coverages can be seen in Figure 3.6. These plots show that the currents generated at these modified electrodes are independent of the electrode's rotation speed and therefore they are independent of the rate of substrate diffusion.

Koutecky-Levich plots obtained for the reduction of nitrite at cross-linked modified electrodes with various polymer surface coverages are illustrated in Figure 3.7.

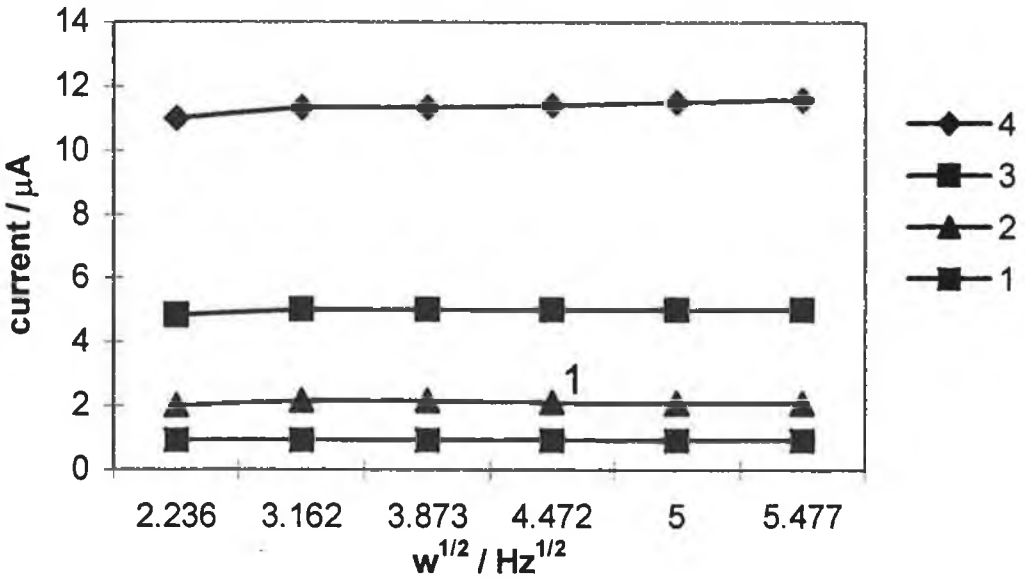


Figure 3.7 Koutecky-Levich plots for the reduction of 2 x $10^{-3}$ mol $dm^{-3}$ nitrite at a crosslinked $[Os(bpy)_2(PVP_{10}Cl]Cl$ modified electrode. Curves 1-4 represent surface coverages of 32, 14.6, 6.30, 2.37 x $10^{-9}$ mol $cm^{-3}$ respectively. Sweep rate was 2 mV $s^{-1}$ and the electrolyte was 0.1 mol $dm^{-3}$ $H_2SO_4$

These plots are linear with slopes equal to zero as would be expected from the Levich plots. The intercepts of these plots are inversely proportional to the polymer surface coverage. This suggests that an increase in the number of electrocatalytic sites at the electrode was achieved by increasing the electrode's surface coverage and that this in turn provides an increased number of sites at the electrode at which electrocatalytic mediation could occur. The reciprocals of these Koutecky-Levich plots yield the modified rate constant, $k'_{ME}$, for the mediated reaction. In Table 3.1 a number of values for $k'_{ME}$ are shown for a number of different surface coverages. A plot of ln $k'_{ME}$ vs. ln L, layer thickness, yields a slope of 1 ± 0.01 which illustrates the first order relationship between layer thickness and the rate constant of the modifying layer [57].

| $k'_{ME}$ / $10^{-6}$ cm$^2$ s$^{-1}$ | L / nm | K / dm$^3$ mol$^{-1}$s$^{-1}$ |
|---|---|---|
| 9 ± 0.7 | 32 ± 5 | 0.402 |
| 21 ± 1 | 85 ± 10 | 0.353 |
| 49 ± 2 | 197 ± 20 | 0.357 |
| 119 ± 5 | 436 ± 40 | 0.332 |

Table 3.1. Dependence of $k'_{ME}$ on $[Os(bpy)_2(PVP_{10}Cl]Cl$ polymer layer thickness

These results indicate that the mediated reaction occurs throughout the entire polymer film. This is the $L_k$ case described by Albery and Hillman, or, alternatively, the R case in Saveant's notation. This corresponds to a situation where there is rapid electron transport compared with cross-reaction kinetics. Consequently, mediation occurs throughout the film without significant reactant depletion. First order behaviour in $b_o$ and L can be used to diagnose this case [58,59]. The analytical expression which describes this relationship is:

$$k'_{ME} = kKb_oL \qquad \text{(Eq. 3.2)}$$

This equation relates $k'_{ME}$ to the rate of the cross-exchange reaction, k, and the partition coefficient, K. The value of $b_o$ has been estimated from the dry density of the material determined by flotation in non-swelling solvents [40] to be $0.7 \times 10^{-3}$ mol cm$^{-3}$. The layer thickness, L, was calculated from the dry density of the polymer.

Using the values from Table 1, a value of $4.0 \pm 1 \times 10^{-2}$ $dm^3$ $mol^{-1}$ $s^{-1}$ for the apparent rate constant kK is estimated. Assuming that the rate constant for the cross-exchange reaction is similar for the cross-linked polymer compared to the homopolymer (where $k = 9.4 \times 10^{-2}$ $dm^3$ $mol^{-1}$ $s^{-1}$ [48]) then the partition coefficient can be estimated to be ~0.4. In the uncross-linked $[Os(bpy)_2(PVP)_{10}Cl]Cl$ film it was found that nitrite was rapidly incorporated into the polymer film with K~1 [60]. So in comparison cross-linked films have a reduced partition coefficient which indicates hindered mass transport. This indicates that though the site of the mediated reaction remains unaltered, cross-linking the polymer chains affects the rate of the reaction. The kinetic condition found for a specific system is controlled by parameters such as the rate of charge transport through the polymer, $D_{ct}$, the extent of substrate diffusion within the film, $D_S$, the partition coefficient, K, and the rate of the cross-exchange reaction, k.

However, the partition coefficient is still large enough to allow incorporation of the analyte into the layer. This results in through-film catalysis, the $L_k$ case, which is the same kinetic situation found for the homopolymer [61]. This penetration of the polymer film by the nitrite species even though the film is partially cross-linked may be as a result of the highly swollen nature of the polymer which allows diffusion of the species [62] when in the sulphuric acid electrolyte. It is possible that since the film is subjected only to a limited amount of cross-linking therefore when the redox polymer modified electrode is immersed in the electrolyte, the polymer does not swell completely.

Since the $D_{ct}$ value for the cross-linked film was found to be larger than for the uncross-linked film, it appears that the cross-linked film is sufficiently swollen to incorporate charge compensation counter-ions. This indicates that cross-linking can act to separate the polymer chains. The reduced rate of substrate permeation, however, indicates that some film compression does occur.

## 3.4 Amperometry And Sensor Characterisation

### 3.4.1 Effect of Applied Potential

A hydrodynamic voltammogram of the modified electrode response to nitrate reduction in a thin layer flow cell over the range of 0 to 0.4 V vs. SCE can be seen in Figure 3.8. At a potential of 0.4 V vs. SCE no response to nitrite reduction is observed. At this potential the electrocatalytic sites are in the Os(III) state and therefore cannot mediate the reduction of nitrite. Decreasing the applied potential results in the generation of catalytic Os(II) sites within the polymer film and the onset of mediated reduction of nitrite is evident. As the potential is decreased below the redox potential of the electropolymer, the number of Os(II) sites reaches a maximum and a limiting plateau is reached beyond which the response of the sensor does not increase. From these results the optimum potential for the detection of nitrite was found to be 0.12 V vs. SCE.

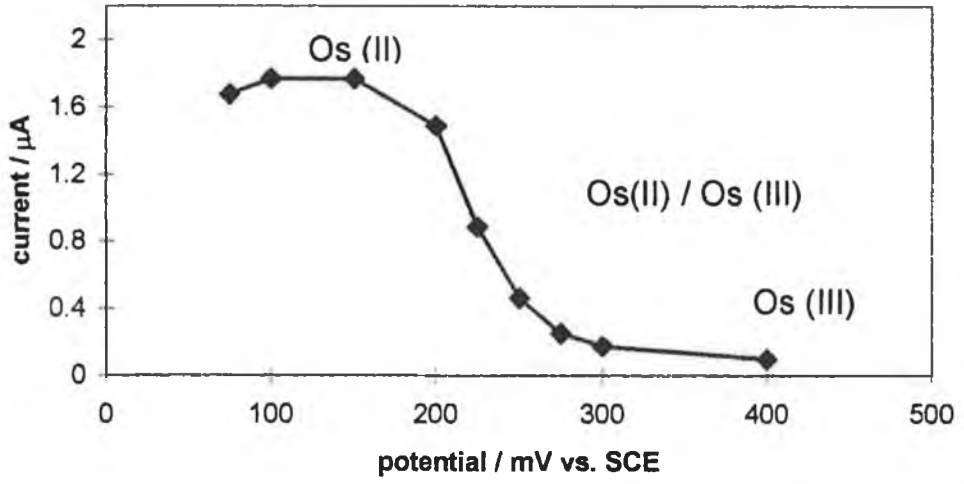


Figure 3.8 Hydrodynamic voltammogram for the reduction of 1.0 x $10^{-3}$ mol $dm^{-3}$ nitrate at the modified, crosslinked $[Os(bpy)_2(PVP_{10}Cl]Cl$ electrode in a thin layer flow cell with a surface coverage of 1 x $10^{-9}$ mol $cm^{-2}$. Flow rate is 1.0 $cm^3$ $min^{-1}$ and the electrolyte is 0.1 mol $dm^{-3}$ $H_2SO_4$

### 3.4.2 Optimisation of Carrier Electrolyte

The carrier solution flowing through the Cu/Cd column must be compatible with the reduction step occurring there. This reduction takes place according to the mechanism:

$$NO_3^- + 2H^+ + Cd^o \rightarrow NO_2^- + 2H_2O + Cd^{2+} \qquad \text{(Eq. 3.3)}$$

Copper deposited at the cadmium surface has been found to catalyse this reaction. Accordingly, copperised cadmium is used in the reducing column. An alkaline pH encourages the equilibrium of this reaction to proceed to the right. A carrier solution of 0.1 mol $dm^{-3}$ NaCl adjusted to pH 9 with NaOH was used.

However, when using this carrier solution, a white precipitate was found to form within the reductor column. This precipitate was believed to be cadmium hydroxide and its appearance co-incided with a loss in the reducing capability of the column. The conversion efficiency did not return to normal until after the column was reconditioned and reactivated by alternatively washing the column with solutions of dilute acid and copper sulphate. To prevent the precipitate being formed it is necessary to remove the cadmium ions generated in the reduction. Addition of EDTA to the carrier allowed chelation of the $Cd^{2+}$ ions to occur:

$$NO_3^- + H_2O + EDTA^{4-} + Cd^o \rightarrow NO_2^- + 2OH^- + Cd(EDTA)^{2-} \qquad \text{(Eq. 3.4)}$$

For this chelation to be successful, a pH of 9 is required. The presence of EDTA in the carrier has the added advantage of driving this reaction from left to right.

Addition of 2.5 g $dm^{-3}$ EDTA was made to the carrier solution. Upon this addition being made, the white precipitate was no longer found in the column. The lifetime for this column with this optimised carrier solution was two weeks before deterioration in the analytical signal became evident.

### 3.4.3 Effect of Carrier Electrolyte pH

The electrocatalytic response of the modified electrode was found to have a first order relationship with respect to hydrogen ion concentration in previous studies [61]. Which indicates that a low pH is required for optimum detector sensitivity. It was found that at pH 4 the response to an injection of a sample solution containing 14 mg $dm^{-3}$ $NO_3$-N onto the manifold was 0.07 μA while at pH 1, the response to the same solution was 2 μA. This demonstrates how the pH of the electrolyte can significantly affect the sensor's response. However, as previously described, a high pH is required for reduction of nitrate to nitrite at the copperised cadmium column. The carrier solution flowing through the column must be at a pH of 9. Consequently, the flow of carrier from the column was merged with the sulphuric acid electrolyte before reaching the detector to maintain maximum sensitivity.

| Tubing Type | Length / cm | Analytical Peak Height / cm |
|---|---|---|
| Straight | 8 | 8.31 |
| Straight | 13 | 10.16 |
| Straight | 19 | 8.52 |
| Looped | 13 | 8.68 |
| Mixing Chamber | 13 | 8.52 |

Table 3.2 Effect of tubing type and length on response of the modified electrode to injections of 10 ppm nitrate.

Detection of the all the nitrite present in the sample plug would not occur at the sensor if the carrier stream from the reduction column did not thoroughly mix with the acidic electrolyte. To ensure sufficient mixing of the two streams before reaching the detector, the tubing which connected the T-piece with the detector was varied and

the resulting analytical peak height was observed. The effect of the different tubing types is detailed in Table 3.2.

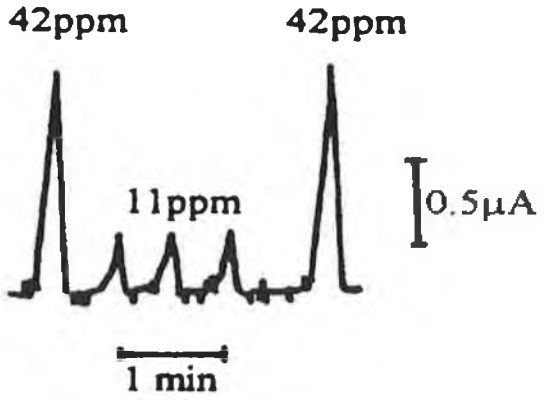


Figure 3.9 Flow injection peaks found using the FIA manifold as described in the text. Flow rate is 0.5 $cm^3$ $min^{-1}$ and the electrolyte is 0.1 mol $dm^{-3}$ $H_2SO_4$. The cross-linked osmium polymer's surface coverage was 1 x $10^{-9}$ mol $cm^{-2}$

The maximum signal was obtained when using a tubing of length 13 cm. Shorter lengths of tubing did not provide sufficient time for the nitrite to become completely acidified. Longer lengths of tubing, as well as the looped tubing and the tubing with the mixing chamber, completely acidified the nitrite but at the same time caused the signal to broaden. As a result the analytical peaks were less symmetrical with more tailing effects. The optimum tubing length of 13 cm was therefore chosen as regards sensitivity and ease of measurement.

### 3.4.4 Effect of Flow Rate

A graph of the modified electrode's response with respect to flow rate in the FIA system is shown in Figure 3.10. Increasing the flow rate is shown to cause a non-

linear decrease in the sensor's response. When nitrite was reduced at the rotating disc electrode, hydrodynamic conditions were found not to affect the modifying layer's response. As can be seen from Figure 3.10, this is not the case in the thin layer flow

cell. This is because at lower flow rates the nitrate injected onto the FIA system is reduced to nitrite in a reproducible way. At higher flow rates a reduced percentage of the nitrate is converted producing a lesser amount of nitrite which can be detected since the injected sample is in the reduction column for a shorter length of time. To maximise the current being observed at the sensor it is necessary to use low flow rates. However, at low flow rates peak broadening occurs which limits analytical throughput and makes the signal more difficult to measure. Figure 3.9 showed typical FIA peaks found when the flow rate was 0.5 $cm^3$ $min^{-1}$. This flow rate was picked as the optimum as it allowed a high sampling rate to be used along with an acceptable level of sensitivity.

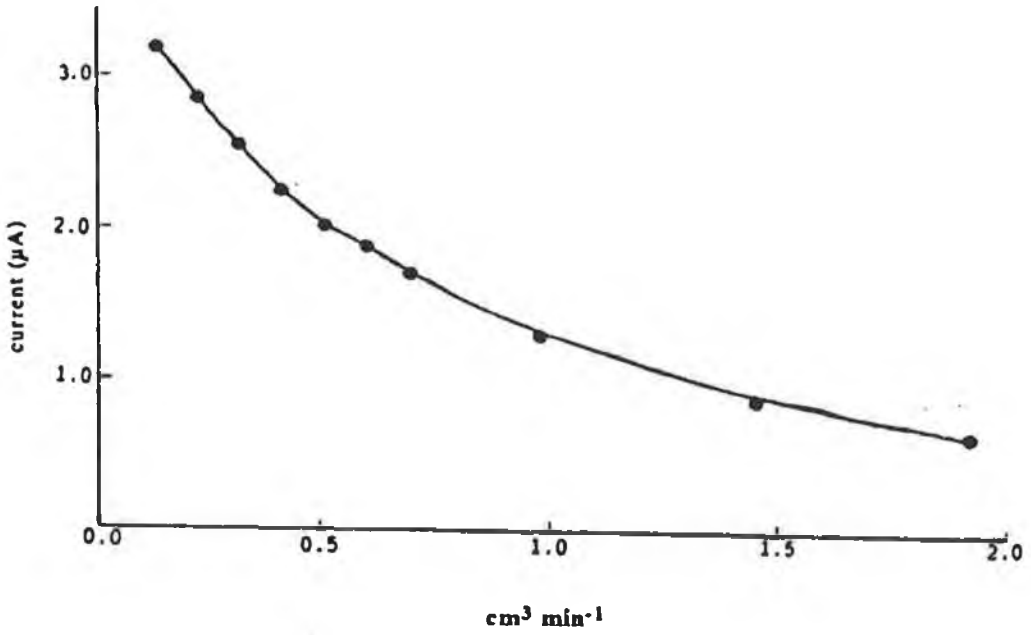


Figure 3.10 The effect of flow rate on the sensor's response. The nitrate concentration is 1.0 x $10^{-3}$ mol $dm^{-3}$. Electrolyte is 0.1 mol $dm^{-3}$ $H_2SO_4$. Polymer surface coverage is 1 x $10^{-9}$ mol $cm^{-2}$ $[Os(bpy)_2(PVP)_{10}Cl]Cl$.

### 3.4.5 Cadmium Reduction Column

Two types of cadmium were examined to see which had the optimum characteristics for use in the reduction column of the FIA. First to be examined was the copperised 100 mesh cadmium. The efficiency of this column's reduction of nitrate to nitrite was considered. Equimolar concentrations of $1.0 \times 10^{-3}$ mol $dm^{-3}$ nitrate and nitrite were injected via the column alternatively. 100% conversion of the nitrate to nitrite was found to occur upon comparison of the peak areas of the resulting analytical signals. This 100 mesh cadmium is finely powdered and hence has a very high surface area which allows the nitrate samples to be closely and comprehensively mixed with the catalytic surface. The result being a highly efficient reduction capability due to the closely packed column providing a long pathway for the sample to traverse.

The effect this reduction column had on the analytical signal itself was also studied. Injections of nitrite via the column were examined. These peaks, obtained after elution from the column, were found to be dispersed and difficult to use analytically. Without the column in place, the nitrite peaks were high and narrow, yielding a higher sensitivity of measurement and a higher sampling frequency. Whereas the inclusion of the column resulted in a decrease in peak height and thus a low sampling frequency. The width at half peak height of these peaks was measured to be 45 s. A value which is common in spectrophotometric systems but which is less than desirable in this electrochemical system [66]. So this column, due to its closely packed nature and hence long pathway, provided close contact with the catalytic particles but also caused the injected sample to mix to a great extent with the carrier flow with consequent broadening of the sample plug.

Next to be considered was the reductor column filled with copperised 40-60 mesh cadmium. With this column, 100 % conversion of nitrate to nitrite was observed only at very low flow rates (0.1 $cm^3$ $min^{-1}$) where broadening of the signal resulted in peaks which were difficult to measure with accuracy. At flow rates > 0.5 $cm^3$ $min^{-1}$ the conversion efficiency of this column was found to decrease to *ca.* 80-90 %. At a flow rate of 0.5 $cm^3$ $min^{-1}$, the conversion efficiency was found to be 92.5 %. A

conversion rate less than 100 % is acceptable only if it reduces nitrate in a reproducible manner. Successive injections of 1.0 x $10^{-3}$ mol $dm^{-3}$ nitrate onto the column were found to have a coefficient of variation of 2.25 % (n=7). Two other columns made in an identical manner were also tested for their conversion efficiency. At a flow rate of 0.5 $cm^{3}$ $min^{-1}$ their percentage conversion efficiencies were found to be 92.5 and 92.3 % respectively. This shows that such columns can be made reproducibly and that the level of variance of reducing capability between the columns is low.

The response of the sensor to injections of nitrite via this column was next measured. The width at half peak height of these peaks was 15 s. So these peaks were found to be narrow and well-shaped and more useful analytically than those peaks which were eluted from the reductor column packed with 100 mesh cadmium. Successive injections of the 1.0 x $10^{-3}$ mol $dm^{-3}$ nitrite standard had a coefficient of variation among the peaks of 2.21 % (n=10). This value is close to the variation in signal of 2.25% found when successive injections of 1.0 x $10^{-3}$ mol $dm^{-3}$ nitrate were made via this column packed with the 40-60 mesh copperised cadmium. This cadmium is in a granular form, unlike the powdered 100 mesh cadmium, and so they are less closely packed than powder. Also they have a smaller surface area. The injected sample therefore has a shorter pathway to travel before being detected by the sensor. Broadening of the sample plug is less but this also results in less than 100 % efficiency of reduction of the nitrate to nitrite as has been demonstrated.

Considering both columns and the analytical nature of the sensor being developed, it was decided to use the 40-60 mesh cadmium in the reduction column. This cadmium, when copperised, displayed a reproducible reduction efficiency combined with high sample throughput and the nitrite sample plugs eluting from this column were usable analytically.

### 3.4.6 Sensor Response Characteristics

Typical modified electrode responses to nitrite generated by the reduction of nitrate at the copperised cadmium reduction column in the optimised electrolyte can be seen in Figure 3.9. These responses are due solely to nitrite reduction at the sensor.

Pure electrolyte did not cause a response at the sensing surface. It was also determined that nitrate solutions in the absence of the column did not produce responses at the modified electrode. Injections of increasing nitrate concentration via the column resulted in corresponding increases in the sensor's response. As can be seen from Figure 3.9, the sensor's responses are well-defined and can be considered useful for analytical purposes. At a flow rate of 0.5 $cm^3$ $min^{-1}$, the peak width at the peak base is approximately 30s. The broad nature of this peak is due to the broadening effect of the reduction column, whose bore is 3 mm. The internal diameter of the tubing used in the rest of the system is 1/32". Which clearly illustrates the considerable broadening a sample plug must endure when moving from the tubing to the column and back again.

The precision of the sensor's response was found to be excellent with a relative standard deviation of 0.91% (n=10). The maximum sample throughput was calculated to be 100 samples/hour from basewidth measurements. At bare electrodes this reaction has been found to cause surface passivation [63]. This passivation was not observed at the modified electrode. No deterioration in the electrode's response was found even after hundreds of determinations. This stability was obtained by the 10% cross-linking of the metallopolymer with 1,10-dibromodecane. Crosslinking the polymer bestowed greater stability on the electrode without compromising its sensitivity or selectivity. The effect of two weeks of constant electrolyte flow on the sensor's performance was monitored. The peak current of a standard solution of nitrate containing 1.0 mg $dm^{-3}$ $NO_3$-N was found to have decreased from 0.135 μA to 0.117 μA over this period, a reduction in signal of only 13%. The precision of this signal slightly decreased to a relative standard deviation of 0.75% for n=10. This

showed a remarkable improvement in stability compared with the uncrosslinked polymer which was found to have a half-life of only 46 hours [61].

At a surface coverage of 1 x $10^{-9}$ mol $cm^{-2}$ the sensitivity of the modified electrode in this flow cell was found to be 0.05 μA $mg^{-1}$ $cm^{3}$. The linear range extends from 0.1 to 190 mg $dm^{-3}$ $NO_3$-N with correlation coefficients typically > 0.999. The linear range encompassed both the normal nitrate levels and the occasionally excessive levels found in environmental water samples without the need for dilution. This linear range is large compared to existing spectrophotometric and electrochemical procedures [64,65]. This large linear range is a function of the kinetic control of the sensor's response. The limit of detection, defined as twice the height of the noise (S/N=2), was found to be 50 μg $dm^{-3}$ $NO_3$-N.

### 3.4.7 Interferences in Water Analysis

Millimolar concentrations of the cationic species K(I), Na(I), Li(I), Mg(II), Al(III) produced no interfering response at the sensor. The anions $Cl^-$, $SO_4^{2-}$, $PO_4^{3-}$ similarly did not interfere. These anions and cations were examined due to their presence in well and river samples which were analysed by the modified electrode sensor. Analysis of these samples is described in section 3.4.9. Ascorbic acid, though it is a common interferent in colorimetric procedures, was found to have no interfering effect at the osmium polymer. A possible interferent is Fe(III) which has previously been shown to be capable of mediation by the osmium polymer [61]. The formal potential of the Fe(II)/Fe(III) couple is 0.46 V vs. SCE therefore the reduction of Fe(III) can be mediated by the osmium couple (whose $E_{\frac{1}{2}}$ = 0.25 V vs. SCE). However, formation of the EDTA complex of iron results in a shift in the formal potential to a region negative of the formal potential of the osmium electrocatalyst. The $[Fe(EDTA)]^+$ formal potential being -0.13 V vs. SCE, which eliminates the interference. Nitrite will of course interfere in the analysis. This can be overcome by comparing the sample's response directly at the sensor and then via the column. Any difference being due to the presence of nitrite.

### 3.4.8 Validation of Method

The modified electrode sensor was then compared with an ion chromatographic procedure based on the Dionex Method AU131. A regression graph (See Figure 3.11) was plotted using the data obtained for both the experimental method and the standard method. Each point on the graphs represents a single sample analysed by the FIA in comparison with the ion chromatographic system. The graph shows only a small deviation from the ideal with a correlation coefficient of 0.994. This shows that minimum systematic errors occur in the modified electrode sensor.

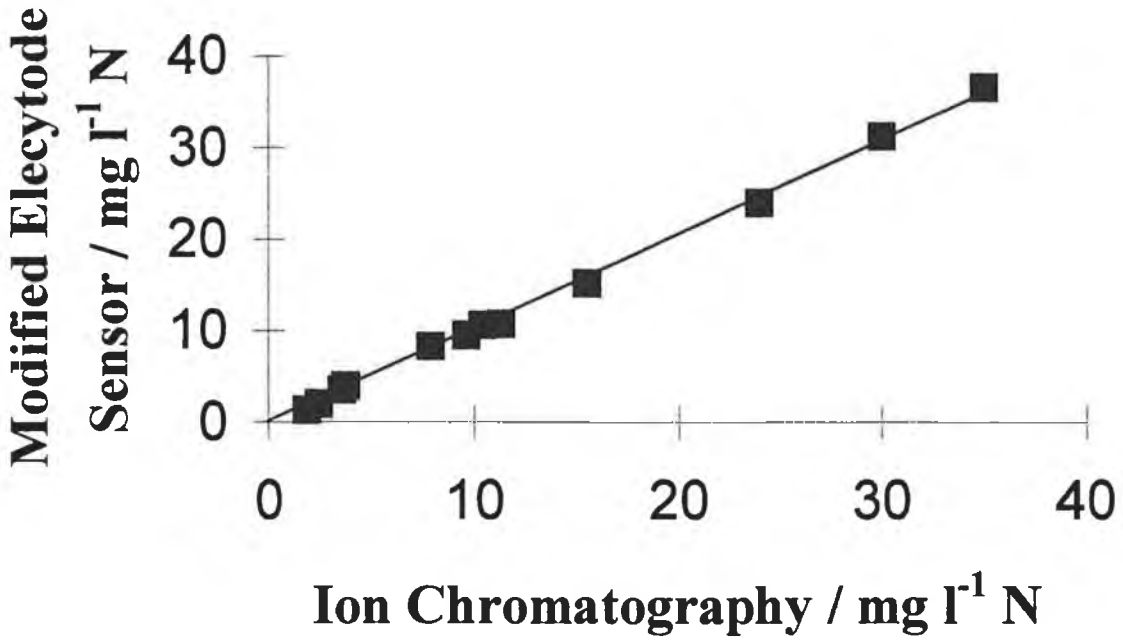


Figure 3.11 Regression chart comparing the values obtained for nitrate standards run on the ion chromatographic system compared with the FIA system.

### 3.4.9 Analysis of Water Samples

This system was applied to the analysis of real environmental samples to test its usefulness. Water samples from rivers and wells were obtained and analysed for nitrate using the FIA. Injection of these samples onto the FIA bypassing the column

confirmed that these samples contained less than LOD nitrite. No sample preparation was performed on these samples before injecting into the system. The results of this measurement are shown in Table 3.3. These water samples were analysed by the ion chromatographic procedure as well as by the FIA system and by another nitrate analysing system using an optical sensor developed in the University [67]. Good correlation was observed between these methods. Use of the ion chromatographic procedure allowed the analysis of the water samples for the presence of other anions apart from nitrate. In the ion chromatographic method, due to the chromatographic process, nitrate is separated from any other anions present thus removing any interferences.

| **Samples from rivers and wells in Co. Meath** | **Concentration / ppm $NO_3$-N** | | |
|---|---|---|---|
| | **Ion Chromatographic Method** | **Fibre Optic Sensor Method [67]** | **Modified Electrode Method** |
| **Arvagh** | 2.32 | 2.45 | NA |
| **Boyne** | 0.84 | 0.73 | 0.89 |
| **Hillcrest** | 2.43 | 2.37 | 2.48 |
| **Kells** | 18.47 | 17.34 | 19.83 |
| **Kill (1)** | < 0.1 | < 0.5 | < 0.05 |
| **Kill (2)** | < 0.1 | < 0.5 | < 0.05 |
| **Knockmoylan** | 2.52 | 2.71 | 2.61 |
| **Mattock** | 2.1 | 2.02 | 2.41 |
| **Monasterevin** | 3.45 | 3.29 | NA |
| **Stradbally** | 3.67 | NA | 3.61 |
| **Tinnock** | 13.12 | 13.99 | 13.74 |
| **Ward** | 1.97 | 2.24 | 1.99 |

Table 3 Concentration of $NO_3^-$ (as ppm N) in samples collected from rivers and wells.

Once separation has occurred results depend only on the performance of the conductivity detector and calibration procedures. The modified electrode sensor, however, measures the nitrate in the presence of these ions whose concentrations vary from sample to sample. Despite this the sensor showed good selectivity for nitrate.

## 3.5 CONCLUSION

It has been shown that the redox polymer $[Os(bpy)_2(PVP)_{10}Cl]Cl$ cross-linked 10% with 1,10-dibromodecane can electrocatalyse the reduction of nitrite at a low pH. The theoretical model describing this mediated electrocatalysis at the redox polymer modified electrode was found to be $L_k$. This regime described a situation where electrocatalysis occurs throughout the modified layer. This kinetic model was found to be the case both at the rotating disc electrode and in the thin layer flow cell. The $L_k$ case describes the ideal case in mediated catalysis as the electrocatalytic reaction occurs throughout the entire metallo-polymer layer. The polymer film therefore has high permeability to the substrate and charge transfer through the layer must be rapid.

The $L_k$ case was also found to describe the mechanism occurring in an uncross-linked $[Ru(bpy)_2(PVP)_{10}Cl]Cl$ polymer modified electrode when applied to nitrite oxidation [70]. The charge transport diffusion coefficient for the ruthenium polymer was found in that paper to be $3.7 \times 10^{-5}$ $cm^2$ $s^{-1}$ which is significantly higher than the diffusion coefficient found for the cross-linked osmium polymer found here of $2.39 \times 10^{-10}$ $cm^2$ $s^{-1}$. This indicates that the effect of the cross-linking of the polymer was to retard the diffusion of the substrate through the polymer film. However, this suppressing effect did not prevent the through layer mechanism occurring in the cross-linked osmium polymer.

The cross-linked electrocatalytic polymer $[Os(bpy)_2(PVP)_{10}Cl]Cl$, when used to modify a glassy carbon electrode, was found to display an analytical response to the nitrite anion. When combined with a copperised cadmium column used for nitrate reduction suitable for in situ catalytic generation of nitrite in a flow injection manifold, it was found to produce an analytical response to samples of nitrate injected onto the FIA. Thus a modified electrode sensor for the detection of nitrate was produced. This sensor can also be adapted to nitrite analysis by bypassing the catalytic column.

When this sensor was used as the detector in the FIA manifold described in this chapter, it allowed development of an on-line sensor for nitrate detection. The sensor itself had a large linear range from 0.1 to 190 mg $dm^{-3}$ $NO_3$-N and with a low L.O.D of 50 μg $dm^{-3}$ $NO_3$-N. These compare favourably with nitrate and nitrite sensors described in the literature such as found using a biosensor [68], an inorganic film modified electrode [69] and a ruthenium metallo-polymer modified electrode [70].

Its enhanced stability compared with uncross-linked modifying layers proved to be mechanically robust and allowed it to be used for long periods of time under the hydrodynamic conditions present in the FIA. The determination of actual water samples using this sensor indicated that this amperometric FIA procedure was both accurate and precise even when applied to the analysis of samples that contained other cationic and anionic species. The response of the sensor to nitrate was fast and did not require expensive reagents and would therefore be cost effective compared to standard methods of analysis.

## 3.6 REFERENCES


1 P. Brimblecombe and D. H. Stedman, Nature, 298 (1982) 460

2 D. Forman, S. Al-Dabbagh and R. Doll, Nature, 313 (1985) 620

3 H. Moller J. Landt, E. Pedersen, P. Jensen, H. Autrup and O. Moller Jensen, Cancer Research, 49 (1989) 3117

4 P. J. Flanagan, Parameters of Water Quality: Interpretation and Standards, Environmental Research Unit, Dublin, 1990,

5 H.A. Laitinen, W.E. Harris, Chemical Analysis, McGraw-Hill, New York, 1975

6 R. Armijo, A. Gonzalez, M. Orellana, A. H, Coulson, J. W. Sayre and R. Detels, Int. J. Epidemiol., 10 (1981) 57

7 C. Cuello, P. Correa, W. Haenszel, G. Gordillo, C. Brown, M. Archer and S. Tannenbaum, J. Natl. Cancer Inst., 57 (1976) 43

8 L. C. Green, D. Ralt, S. R. Tannenbaum, in Human Nutrition, Eds. A. Neuberger, T. H. Jukes; J. K. Burgess: Englewood, New Jersey, 1982

9 P. Correa, Cancer Surv., 2 (1983) 437

10 Assembly of Life Sciences (U.S.). Committee on Diet, Nutrition, and Cancer, Diet, Nutrition, and Cancer", National Academy Press, Washington, D.C, 1982

11 W. Lijinsky and S. Epstein, Nature, 225 (1970) 21

12 D. J. Briggs, The State of the Environment in the European Community 1986, Office for Official Publications of the European Communities, Luxembourg, 1987

13 A. E. Greenberg, R. R. Trussel and L. S. Clesceri, Standard Methods for the Examination of Water and Waste Water, American Public Health Association, 1985

14 C. D. Usher, G. M. Telling, J. Sci. Food Agric., 2 (1975) 1793

15 J.J. Pauer, H.R. Van Vliet, J. F. van Staden, Water-SA, 16 (1990) 105

16 M. P. Stainton, Anal. Chem., 46 (1974) 1616

17 J. Hilton, E. Rigg, Analyst, 108 (1983) 1026

18 K. Nagashima, X.-X. Qian, S. Suzuki, Analyst, 111 (1986) 771

19 J. R. Clinch, P. J. Worsfold, H. Casey, Anal. Chim. Acta, 200 (1987) 523

20 J. I. Skicko, A. Tawfik, Analyst, 113 (1988) 297

21 J. H. Margeson, J. C. Suggs, M. R. Midgett, Anal. Chem., 52 (1980) 1955

22 E. D. Wood, F. A. J. Armstrong, F. A. Richards, J. Mar. Biol. Assoc. U.K., 47 (1967) 23

23 A. T. Faizullah, A. Townshend, Anal. Chim. Acta, 179 (1986) 233

24 S. Devi, A. Townshend, Anal. Chim. Acta, 225 (1989) 331

25 L. J. Galante, G. M. Hieftje, Anal. Chem., 60 (1988) 995

26 R. Nakata, M. Terashita, A. Nitta, K. Ishikawa, Analyst, 115 (1990) 425

27 A. Trojanek, F. Opekar, J. Electroanal. Chem., 214 (1986) 125

28 W. Holak, J. J. Specchio, Anal. Chem., 64 (1992) 1313

29 A. G. Fogg, S. P. Scullion, T. E. Edmonds, Analyst, 114 (1989) 579

30 R. C. Schothorst, G. den Boef, Anal. Chim. Acta, 153 (1983) 133

31 R. C. Schothorst, J. J. F. van Veen, G. den Boef, Anal. Chim. Acta, 161 (1984) 27

32 I. Taniguchi, N. Nakashima, K. Matsushita, K. Yasukouchi, J. Electroanal. Chem., 224 (1987) 199

33 H.-J. Kim, Y.-K. Kim, Anal. Chem., 61 (1989) 1485

34 R. Karlsson, L. G. Torstensson, Talanta, 21 (1974) 705

35 A. Hulanicki, W. Matuszewski, M. Trojanowicz, Anal. Chim. Acta, 194 (1987) 119

36 J. Halasz, G. Horvai, Electroanalysis, 4 (1992) 469

37 A. Y. Chamsi, A. G. Fogg, Analyst, 113 (1988) 1723

38 J. A. Cox, K. R. Kulkarni, Analyst, 111 (1986) 1219

39 J. A. Cox, P. J. Kulesza, Anal. Chim. Acta, 158 (1984) 335

40 R. J. Forster, J. G. Vos, Macromolecules, 23 (1990) 4372

41 R. J. Forster, J. G. Vos and M. E. G. Lyons, J. Chem. Soc., Faraday Trans., 87 (1991) 3761

42 A. P. Doherty and J. G. Vos, Anal. Chim. Acta, 344 (1997) 159

43 R. J. Forster, A. J. Kelly, J. G. Vos, M. E. G. Lyons, J. Electroanal. Chem., 270 (1989) 365

44 A. P. Doherty, R. J. Forster, M. R. Smyth, J. G. Vos, Anal. Chem., 64 (1992) 572

45 A. R. Hillman, "Electrochemical Science and Technology of Polymers", R. G. Linford, Ed., Elsevier, Amsterdam, 1987

46 R.J. Forster, J. G. Vos in Comprehensive Analytical Chemistry, V. 27, (G. Svehla, ed., M.R. Smyth, J.G. Vos, volume eds.), Elsevier, Amsterdam, 1992, p. 465

47 A. Sevčik, Collect. Czech. Chem. Commun., 44 (1948) 327

48 A. P. Doherty, Ph.D. Thesis, Dublin City University, 1992

49 R. J. Forster, A. J. Kelly, J. G. Vos, M. E. G. Lyons, J. Electroanal. Chem., 270 (1989) 365

50 R. J. Forster, M. E. G. Lyons, J. G. Vos, J. Chem. Soc. Faraday Trans., 87 (1991) 3761

51 S. M. Oh, L. R. Faulkner, J. Electroanal. Chem., 269 (1989) 77

52 A. P. Doherty, J. G. Vos, Anal. Chem., 65 (1993) 3424

53 W. J. Albery, A. R. Hillman, Ann. Rep. Prog. Chem. C, 78 (1986) 371

54 W. J. Albery, A. R. Hillman, J. Electroanal. Soc., 170 (1984) 27

55 C. P. Andrieux, J. M. Saveant, J. Electroanal. Chem., 171 (1984) 6527

56 C. P. Andrieux, J. M. Saveant, J. Am. Chem. Soc., 108 (1986) 8175

57 W. J. Albery, M. G. Boutelle, A. R. Hillman, J. Electroanal. Chem., 182 (1985) 99

58 F. C. Anson, J. M. Saveant, K. Shigehara, J. Electroanal. Chem., 145 (1983) 423

59 N. Oyama, N. Oki, H. Ohno., Y. Ohnuki, H. Matsuda, F. Tsuchids, J. Phys. Chem., 87 (1983) 3642

60 A. P. Doherty, J. G. Vos, J. Chem. Soc. Faraday Trans., 88 (1992) 2903

61 A. P. Doherty, R. J. Forster, M. R. Smyth, J. G. Vos, Anal. Chim. Acta, 255 (1991) 45

62 R. J. Forster, J. G. Vos, J. Chem. Soc. Faraday Trans., 87 (1991) 1863

63 G. Mengoli and M. M. Musiani, J. Electroanal. Chem., 199 (1989) 99

64 D. Chen, M. D. Luque de Castro, M. Valcarel, Analyst, 116 (1991) 1095

65 F. Canete, A. Rios, M. D. Luque de Castro, M. Valcarel, Analyst, 113 (1988) 739

66 R. B. Willis, Anal. Chem., 52 (1980) 1377

67 M. Stanley, J. Maxwell, M. Forrestal, A.P. Doherty, B.D. MacCraith ,D. Diamond, J. G. Vos, Anal. Chim. Acta, 299 (1994) 81

68 L.M. Moretto, P. Ugo, M. Zanata, P. Guerriro, C.R. Martin, Anal. Chem., 70 (1998) 2163

69 I.G. Casella, A.M. Salvi, Electroanalysis, 9 (1997) 596

70 A.P. Doherty, M.A. Stanley, D. Leech, J.G. Vos, Anal. Chim. Acta, 319 (1996) 111

## Chapter 4

# Development of a NOx Sensor

## 4.1 Introduction

The effect of industrial processes on the environment is giving rise to much disquiet. Emissions of noxious fumes from stationary sources is a particular source of widespread concern. Estimates from industrialised countries suggest that the total damage caused by air pollution at the beginning of the seventies amounted to roughly 2% of the gross national product of these countries at this time and since then this figure has increased [1]. Old ice in Greenland has a measured pH of 6-7, new ice is pH 4-5 [2]. This drop in pH has been linked to the increasing prevalence of acid rain, one of whose precursors is $NO_x$. $NO_x$ consists of a mixture of NO and $NO_2$. These gases are generated from the combustion of fossil fuels, the exhaust gas from automobiles, and waste gas from electric power plants, steelworks, metal smelters and nitric acid plants. Coal has a high nitrogen content compared to other fuels so coal burning plants add greatly to the $NO_x$ content in the atmosphere. Cities where households burn coal are also subjected to increased $NO_x$ pollution and motor vehicles produce both $NO_x$ and hydrocarbons in amounts that could lead to photochemical smog. Coal burning is the source of about 24% of the $NO_x$ made by man. Most emissions (95%) are in the form of NO but this gas reacts almost immediately in the atmosphere to form $NO_2$.

When illuminated by sunlight, atmospheric nitrogen monoxide reacts with gaseous hydrocarbons and oxygen to form photochemical oxidants such as peroxyacetal nitrate (PAN) and ozone. Nitrogen dioxide is also an important air pollutant, is a participant in photochemical reactions that produce smog and is a precursor of acid rain [3]. Experiments with animals have shown that $NO_x$ can affect the respiratory organs and has been implicated in cases of bronchial asthma and other diseases [4]. Concentrations greater than 100 ppm (parts per million) are lethal to most species and they also assist in the corrosion of metals and the deterioration of textiles. Some of the $NO_x$ may rain out as dilute nitric acid which can damage vegetation or fresh water sources. In 1974 in Scotland rain with pH 2.4 was measured [5] and in the Adirondack mountains of New York state some 51% of the lakes have been reported to have a pH of less than 5.0 [6]. Its has also been linked to Antarctic ozone depletion

[7-9]. Consequently there has been considerable pressure to monitor and control these gases issuing from fossil fuel burning combustion plants where emissions of $NO_x$ can range from several hundred to several thousand parts per million [refs 10-14]. A typical emission rate for a 660 MW coal fired station in Britain is 550 ppm $NO_x$ [15]. Nitric acid synthesis plants in the U.K. are allowed maximum emission levels of 2,700 ppm v/v $NO_x$ [16].

Different kinds and arrangements of measurement techniques are used at stacks to measure combustion products. On-line measuring procedures which utilise light absorption can be installed at the exhaust pipe and they analyse particular gas qualities without withdrawing a flow of gas [17,18]. Cross-duct analysers based on absorption of IR radiation have been applied to the measurement of $NO_x$. However, there is a strong overlap between the available absorption bands and those of water vapour which makes it less suitable for in-situ monitoring. On-line ultraviolet detection has also been considered but it is unsuitable for $NO_x$ measurement, as $NO_2$ is a very strong absorber of UV radiation which makes it difficult to achieve selective measurings without interferences using this technique [19]. Mass spectroscopy has size limitations and it uses expensive instrumentation which prevents it from replacing many analysers presently used [20,21]. Chemiluminescence is presently the most important in-situ measuring technique for the determination of $NO_x$ emissions [22-28]. When oxidising nitrogen monoxide with ozone at low pressure, light is emitted. In the presence of excess ozone the intensity of this emission is directly proportional to the nitrogen monoxide concentration. Nitrogen dioxide is determined indirectly after reduction to nitrogen monoxide with the subsequent measurement of the intensity of the chemiluminescent radiation emitted at the reaction of NO with ozone. The ozone required for this reaction is produced from the air by an electrical gas discharge. A photomultiplier detects the radiation released by the reaction of NO and $O_3$ in the reaction chamber. It is a very sensitive technique and its linear range extends to 1000 ppm which is suitable for many emission measurements.

However, there can be serious interferences with this method from organic nitrogen compounds. Chemiluminescence $NO_x$ analysers have been shown to respond nearly

quantitatively to other nitrogen containing compounds [28, 29]. More seriously, when measuring stack gas emissions, carbon dioxide and water vapour cause significant negative interferences [29, 30]. Using desiccants is not a useful option since as well as removing water vapour they also adsorb the $NO_2$ portion of the $NO_x$. $O_2$ enriched atmospheres also cause negative interference with this chemiluminescent technique, however in high combustion processes it would be unusual if the $O_2$ content was higher than 21 % [25].

Amperometric gas sensors [31-33] are used widely to qualify and quantify electroactive species in gas phases. These amperometric sensors produce a current when exposed to a vapour containing the analyte which reacts within the cell. The current is produced when the analyte is either reduced or oxidised at the sensors' electrocatalytic surface, which is in contact with an electrolyte. The energy of the electrons available at the electrode is set by a potentiostat which controls the potential of the working electrode with respect to a reference electrode by making current available via an auxiliary electrode. However, attempts to develop a $NO_x$ sensor have been hampered due to the poisonous effect of $NO_2$ on electrode surfaces.

An amperometric sensor based around a gold electrode has been described which was applied to the monitoring of low levels of $NO_2$ but this electrode suffers from reduction in sensitivity with use due to the cumulative poisoning effect of the $NO_2$ on the electrode's surface [32]. This problem was partially overcome by reactivation of the electrode by cyclic polarization.

A metallized-membrane electrode [31] has also been shown to be suitable for the measurement of NO in flue gases. The gases were allowed to diffuse through a non-porous but gas-permeable PTFE membrane to a layer of porous gold metal deposited directly on the membrane. The electrolyte used was phosphoric acid. The choice of gold rather than platinum as the sensing electrode is an example of kinetic selectivity. The rate of the anodic reaction of nitrogen monoxide on both gold and platinum is very fast. The rate of the reaction of carbon monoxide, whilst thermodynamically favoured (as is the nitrogen monoxide reaction), is in fact between 103 and 106 times

slower on the gold electrode. So nitrogen monoxide was selectively determined in the presence of carbon monoxide when a gold electrode was used. However, only NO could be determined by this sensor. $NO_2$ was found to poison the electrode surface and had to be excluded from entering the sensor. So this sensor was unsuitable for measuring the $NO_x$ content of the stack gas.

Attempts to overcome these drawbacks of on-line monitoring and to determine the true $NO_x$ concentration have led to the application of off-line techniques in the analysis of the flue gas concentrations of nitrogen oxides. This is achieved by sampling the exhaust gas by redirecting a partial flow of the gas out of the exhaust pipe. This sample is then freed from interfering factors and analysed by a process of absorption of the gas into an appropriate solution. Consequently, the standard method of analysis for measurement of stationary emissions of $NO_x$ uses this approach [34].

These wet chemistry measurement techniques all rely on the efficient absorption of $NO_x$ before its concentration can be measured. Consequently, absorption of nitrogen oxides from gaseous effluents into aqueous solutions has been extensively studied. This process may be summarised as containing three basic steps. The first is the conversion of the NO and $NO_2$ to products which are more easily absorbed. Second is the actual absorption and third is the analysis of the absorbed species.

The initial gas phase oxidation of NO and $NO_2$ is common to all the absorbing methods. NO itself is fairly insoluble in aqueous solutions but $NO_2$ is somewhat more soluble. Primarily, gas phase oxidation of the $NO_x$ occurs as follows:

$$2NO_{(g)} + O_2 \rightarrow 2NO_{2(g)} \qquad \text{(Eq. 4.1)}$$

Further variations may be observed such as:

$$NO_{2(g)} + NO_{(g)} \Leftrightarrow N_2O_{3(g)} \qquad \text{(Eq. 4.2)}$$

$$2NO_{2(g)} \Leftrightarrow N_2O_{4(g)} \qquad \text{(Eq. 4.3)}$$

This process involves the oxidation of nitrogen monoxide to the more soluble equilibrium mixture of nitrogen dioxide, nitrogen tetroxide and nitrogen trioxide. These species must then enter the aqueous phase of the absorption solution.

$$NO_{2(g)} \Leftrightarrow NO_{2(l)} \qquad \text{(Eq. 4.4)}$$

$$N_2O_{4(g)} \Leftrightarrow N_2O_{4(l)} \qquad \text{(Eq. 4.5)}$$

$$N_2O_{3(g)} \Leftrightarrow N_2O_{3(l)} \qquad \text{(Eq. 4.6)}$$

$$2NO_{2(l)} \Leftrightarrow N_2O_{4(l)} \qquad \text{(Eq. 4.7)}$$

During simultaneous absorption of NO and $NO_2$ mixtures into aqueous solutions, it is believed that the dissolution and hydrolysis of $N_2O_3$ and $N_2O_4$ are the controlling mechanisms of the absorption process [18, 24, 35, 36]. As production of an absorbable species controls the rate at which the nitrogen oxides can be absorbed. After absorption of the gas in aqueous solution the formation of nitrite and nitrate ions takes place;

$$N_2O_{4(aq)} + H_2O \rightarrow 2H^+ + NO_2^- + NO_3^- \qquad \text{(Eq. 4.8)}$$

$$N_2O_{3(aq)} + H_2O \Leftrightarrow 2H^+ + 2NO_2^- \qquad \text{(Eq. 4.9)}$$

Thus upon absorption of NO and $NO_2$, nitrite and nitrate ion formation occurs by two different pathways. To summarise all these processes, the absorption equilibria can be concisely described as;

$$2NO_{2(g)} + H_2O \rightarrow 2H^+ + NO_2^- + NO_3^- \qquad \text{(Eq. 4.10)}$$

$$NO_{(g)} + NO_{2(g)} + H_2O \rightarrow 2H^+ + 2NO_2^- \qquad \text{(Eq. 4.11)}$$

The nitrous acid thus produced is not stable due to its volatile nature [37]. So once these species are in solution, they may return to the gas phase unless the absorbing solution reacts with the solutes to produce stable products. In other words, the gaseous constituents must undergo an irreversible chemical reaction with the absorbent.

A number of strategies have been applied to this problem. Absorbing solutions have been introduced to try to maximize the degree of absorption of $NO_x$ in the liquid phase and once absorption has taken place, to maximise the stability of the absorbed species. The approaches taken include adjustment of the pH of the absorbing solution, manipulation of the ionic strength of this solution and inclusion of oxidising species in the absorbing solution.

Absorption of $NO_x$ into weak alkaline solutions has been studied by Komiyama and Inoue [18]. The alkaline conditions are used because in the presence of hydroxide ions, the hydrolysis products are believed to be rapidly ionised and neutralised i.e. by adjusting the solutes pH to alkaline, the presence of hydroxyl ions thus formed cause the reverse reactions to be negligible. However, experiments have shown that there is no evidence of a direct reaction between hydroxyl ions and $NO_x$ species, i.e. the absorption rate of $NO_x$ into NaOH solution is similar to that into water [36]. Other work has shown that though the solubility of $N_2O_3$ and $N_2O_4$ decreases with increasing NaOH concentration [18], the hydrolysis rate constants of the $N_2O_3$ and $N_2O_4$ increase more strongly with NaOH concentration. Therefore, since the hydration reactions of $N_2O_3$ and $N_2O_4$ dominate the process of absorption of $NO_x$, overall the absorption rate of $NO_x$ increases with increasing NaOH concentration [36].

The absorption of nitrogen dioxide into 0.09N sulphuric acid has also been investigated and it has been found that the absorption rate was not affected by the addition of the sulphuric acid within the experimental conditions used [38]. This is perhaps because the viscosity of dilute sulphuric acid is only about 1% larger than that of water. So that the presence of the acid causes only a small change in the absorbance of $NO_2$.

An alternative means for the absorption of nitric oxide through complexation is to use a solution of concentrated nitric acid in sulphuric acid [39]. This solution absorbs nitric oxide, forming nitrosylsulphuric acid in accordance with:

$$2NO + HNO_3 + 3H_2SO_4 \rightarrow 3NOHSO_4 + 2H_2O \qquad \text{(Eq. 4.12)}$$

An excess of nitric acid must be present to ensure complete absorption of the nitric oxide. Dilution of this solution with water releases nitrous acid from the nitrosylsulphuric acid.

$$NOHSO_4 + H_2O \rightarrow H_2SO_4 + HNO_2 \qquad \text{(Eq. 4.13)}$$

However due to the highly corrosive nature of this absorption scheme its application is very limited.

Preventing the loss of nitrite from the absorbing solution can also be achieved by adding a strongly oxidizing species to the absorbant. An alkaline permanganate solution has been shown to be capable of oxidizing $NO_x$ collected from electric utility plants and from factories that produce nitric acid [40, 41]. Sample collection involved the following additional reactions due to the presence of the permanganate;

$$2MnO_4^- + 4NO + 2OH^- \rightarrow NO_3^- + 3NO_2^- + 2MnO_2^- + H_2O \qquad \text{(Eq. 4.14)}$$

$$2MnO_4^- + 3NO_2^- + H_2O \rightarrow 3NO_3^- + 2OH^- + 2MnO_2 \qquad \text{(Eq. 4.15)}$$

So the overall reaction takes the form;

$$MnO_4^- + NO \rightarrow NO_3^- + MnO_2 \qquad \text{(Eq.4.16)}$$

A problem found with this method was that ammonia also reacts with the alkaline permanganate solution to form nitrate and the resultant concentration was found to increase as a function of the standing time of the collected sample.

Better success has been obtained with an absorbing solution containing hydrogen peroxide in dilute sulphuric acid [42]. This is because the hydrogen peroxide contained in the absorbent further reacts with the absorbed nitrite as described by the following reaction;

$$NO_2^- + H_2O_{2(aq)} \rightarrow NO_3^- + H_2O \qquad \text{(Eq. 4.17)}$$

Thus all the NO and $NO_2$ is collected exclusively in the form of the stable nitrate species. For this reason this absorbing solution is recommended as the standard absorbent when collecting $NO_x$ for further analysis.

Once the trapping of $NO_x$ in solution has been completed, the final stage of this analysis is the determination of the absorbed nitrogen oxides. This determination has attracted many different measurement techniques. Titrimetry requires very simple equipment but is time consuming and unsuitable when close monitoring of stack gases is required [36,38]. Ion chromatography has the advantage of being able to determine other species present in the emissions of stack gases as well as nitrogen oxides [43] but nitrogen compounds such as ammonia have been found to interfere with the measurement of $NO_x$ using this technique [40,41]. Other researchers have concentrated on exploiting the sensitivity of this technique for the environmental monitoring of $NO_x$ levels [44,45].

Spectroscopic methods have also been applied to the measurement of $NO_x$ once

absorbed into solution. Problems are encountered due to interference of other absorbed gaseous species, especially $SO_2$. This is because such methods involve the colorimetric determination of the absorbed $NO_x$ as the azo dye. The absorbed $SO_2$ has been shown to interfere with the colour intensity of this dye leading to negative interferences due to its decolourising effects [46-48]. This problem of $SO_2$ interference has been lessened by using a method recommended by the American Society for Testing and Materials. This method involves withdrawing a small sample of gas using a sampling probe which is then immediately trapped in an oxidising, absorbing solution consisting of hydrogen peroxide in dilute sulphuric acid [34]. The oxides of nitrogen are converted to nitric acid due to gas phase oxidation by oxygen in the sample and by the absorbent solution. The resulting nitrate ion is reacted with phenol disulphonic acid to produce a yellow compound (the tri-ammonium salt of6-nitro-phenol-2,4-disulphonic acid) which is subsequently measured colorimetrically. The hydrogen peroxide in the absorbing solution reduces the sulphur dioxide to sulphate which does not interfere with the diazotization reaction. Interference from $SO_2$ can still occur if it is present in very high concentrations and interference is also caused by the presence of organic nitrogen containing compounds and by halides [34]. As these also react with phenol disulphonic acid.

Electrochemical methods have also found application in the measurement of the absorbed $NO_x$. Surface acoustic wave devices have been investigated, though complex physical and chemical processes occurring at their chemical interfaces have so far made these chemosensors difficult to develop [49,50]. Chemically modified electrodes based on the immobilisation of $Fe^{(II)/(III)}$ centres have been demonstrated to be suitable for the determination of the low levels of $NO_x$ found in environmental samples [51-53]. The prospect of applying this technique to the determination of $NO_x$ from stack gas emissions will be deliberated. Similarly, the greater sensitivity of polarographic methods of analysis was taken advantage of for the determination of atmospheric nitrogen oxides [54,55].

The aim of this work is to produce an amperometric sensor capable of measuring the $NO_x$ content of stack gases. Chemically modified electrodes have attracted

considerable attention as they have the capacity to be useful sensing devices. This is because the chemical modification of the electrode surface offers a number of potential advantages, a change in the electrochemical reaction rate, protection of the electrode surface from fouling, and enhancement of selectivity and sensitivity.

It was previously demonstrated that the redox polymer $[Os(bpy)_2(PVP)_{10}Cl]Cl$ was a proficient electrocatalyst for the reduction of nitrite under acidic conditions. By adding a reducing capacity to the FIA, nitrate could also be determined by this sensor after its reduction to nitrite. This sensor was used to analyse for nitrite and nitrate species in aqueous environments. This sensor's linear range is large compared to existing spectrophotometric and electrochemical procedures [56,57] and is a function of the kinetic control of the sensor's response. This indicated that it could be successfully applied to the measurement of the high concentrations of $NO_x$ gases found in stack gas emissions after absorption of the gases in an aqueous solution. Modification of the polymer backbone allowed the development of a stable electrode which was found to be free from most common interferents due to the selective nature of the modifying layer.

A number of strategies to determine the $NO_x$ content of emissions from stationary sources will be examined in this chapter. Off-line sampling with subsequent determination as well as on-line direct measurement will be considered. Off-line techniques will be examined from the point of view of producing complete absorption of the $NO_x$ content of gas emissions. A number of solutions will be screened to determine the optimum properties necessary for both sampling and for the ensuing measurement with the sensor. Parameters such as stability, reproducibility, sensitivity and selectivity will be explored and finally a comparison with other techniques will be made.

## 4.2 Experimental

### 4.2.1 Electrolytes and Solutions

The cross-linked $[Os(bpy)_2(PVP)_{10}Cl]Cl$ polymer described in chapter 2 was used to modify a glassy carbon electrode. All conditions as before. All electrolytes and solutions were prepared from Milli-Q water. The electrolyte used was 0.1 mol $dm^{-3}$ $H_2SO_4$. $NaNO_3$ was used to prepare nitrate solutions and $NaNO_2$ was used in the preparation of nitrite solutions. The carrier electrolyte solution for the flow injection system was 0.1 mol $dm^{-3}$ $NH_4Cl$, and 0.01 mol $dm^{-3}$ EDTA. $CuSO_4$. $5H_2O$ was used to copperise the cadmium as described in chapter 3. All chemicals used were of reagent grade. The solutions used for absorbing $NO_x$ gas were 0.1, 0.5, 1.125, 2.5 and 5 mol $dm^{-3}$ NaOH, and an acidic peroxide solution containing various concentrations of $H_2O_2$ in 0.1 mol $dm^{-3}$ $H_2SO_4$.

### 4.2.2 Flow Injection Apparatus

The flow injection apparatus consisted of a Gilson Minipuls 3 peristaltic pump, a six port Rheodyne injector valve fitted with a 20 µL fixed volume sample loop, a Rheodyne switching valve, an EG&G Princeton Applied Research Model 400 electrochemical detector and a Kipp & Zonen X-t recorder. Silicone rubber tubing was used at the pump. Stainless steel tubing was used at the detector. Tubing used in the rest of the system was manufactured from Teflon. A copperised cadmium reductor column used in the flow system was constructed from a 4 x 50 mm polymeric column. The Cd was prepared from 100 mesh powder and from cadmium wire cut to form cadmium chips. The cadmium was cleaned with dilute HCl. After thorough rinsing with water, the cadmium was washed in a 2 % solution of copper sulphate. Sample injections were made using a 2 $cm^3$ glass syringe fitted with a Rheodyne injection needle or with a gas-tight syringe. In the flow cell, an Ag/AgCl electrode acted as the reference. All potentials are quoted after numerical conversion to the SCE scale. The working electrodes were 3 mm diameter glassy carbon shrouded in a Teflon block. The electrodes were then prepared as described in

chapter 3 to make a nitrate FIA sensor.

### 4.2.3 Ion Chromatography System

Measurements made using the electrochemical sensor were compared with a standard method of nitrate analysis based on an ion chromatography method. This system consisted of a Dionex gradient pump module model 4500 and Dionex eluent gas module. Column eluent was monitored by a Dionex conductivity sensor, CDM2, and detection output was monitored and processed by Dionex AI450 computer software, version 2.1, linked by a Dionex advanced interface to a 286-PC.

The separator column was an IonPac AS4A column. The suppressor was an Anion Micromembrane suppressor. The eluent contained 1.8 mol $dm^{-3}$ $Na_2CO_3$ and 1.7 mol $dm^{-3}$ $NaHCO_3$. Flow rate of the eluent was 2.0 $cm^3$/min. The regenerant was 12.5 mol $dm^{-3}$ $H_2SO_4$ and its flow rate was 5.0 $cm^3$/min. The sample loop volume was 50 μL and the background conductivity was between 10-20 μS.

### 4.2.4 Titration Method

Measurement of the nitrite and nitrate concentrations found when using the highly alkaline absorbing solutions was carried out by the following method. To the absorbed sample was added 5 g NaCl and a 15 $cm^3$ aliquot of 3 mol $dm^{-3}$ $FeSO_4$ in 5.6 x $10^{-1}$ $moldm^{-3}$ HCl and 20 $cm^3$ concentrated $H_2SO_4$. This was heated for 3 min and after cooling 50 $cm^3$ of water and 1 $cm^3$ of 2.5 x $10^{-3}$ mol $dm^{-3}$ 1,10-phenanthroline-ferrous sulphate indicator was added. The sample was then titrated with potassium dichromate. This method measures both nitrite and nitrate ions. To differentiate between the two species samples were analysed twice. First by the method as detailed above and then a second time after the initial addition of sulphamic acid which reacts with any nitrite present in the sample to form $NO_2$ which escapes into the atmosphere leaving behind only nitrate ions.

### 4.2.5 Gases

The $NO_2$ sampled was available as 10,000 ppm in air supplied by BOC. It was diluted where appropriate with nitrogen or air. The response of the instrument to $SO_2$, $CO_2$, nitromethane, aniline and ammonia was also investigated. The $SO_2$ was obtained from dilution of a lecture bottle of sulphur dioxide obtained from BDH. Samples of the organic compounds were prepared by collection of the vapour above the pure liquid placed in a flask. The ammonia sample was collected from above an aqueous ammonia solution and the $CO_2$ was collected from the reaction of HCl with calcium carbonate.

### 4.2.6 Sampling of $NO_2$

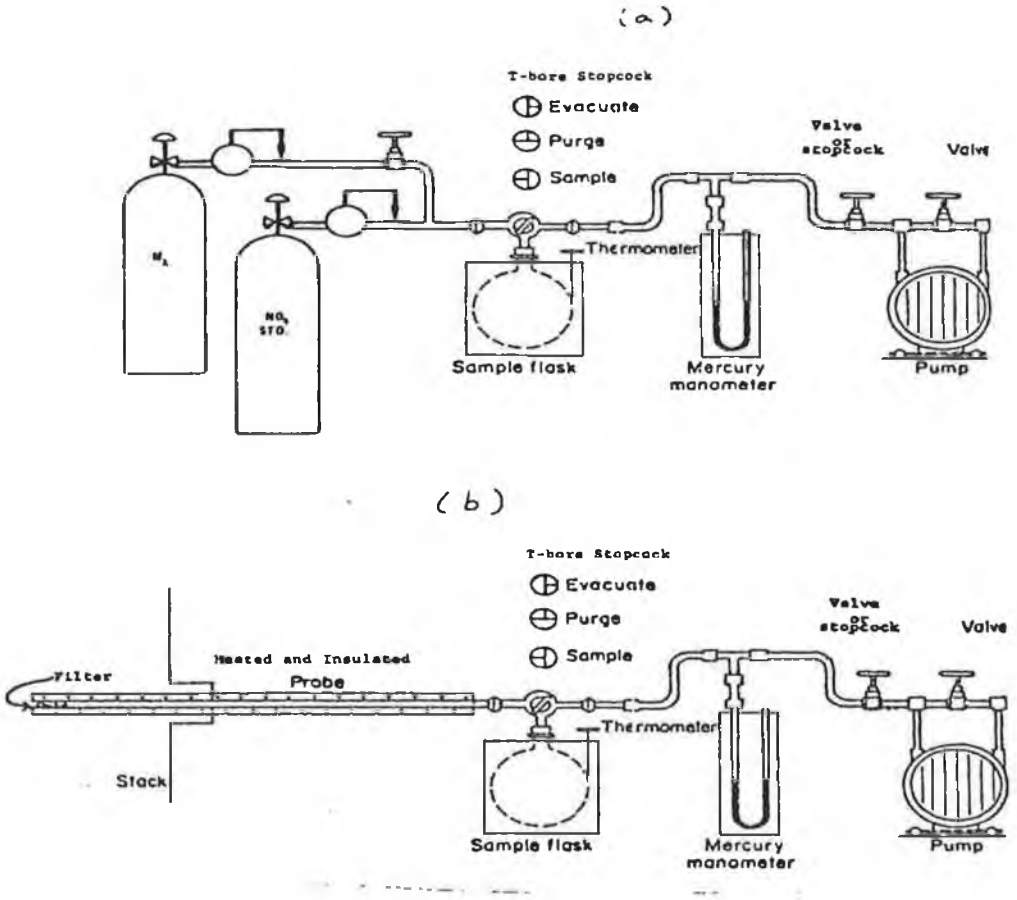


Figure 4.1 (a)Diagram of laboratory sampling system for nitrogen dioxide gas (b) Diagram of typical sampling apparatus used for determination of oxides of nitrogen by ASTM D 1608

The production of gas mixtures requires an accurate control of the volume and flow rate of the constituents if a high degree of accuracy is to be achieved. A capillary flow meter was used to measure the low flow rates of the gas. It was calibrated against a bubble flow meter. Constant pressure from the high pressure cylinder was achieved by use of a sensitive needle valve. Glass was the material of choice used throughout the gas sampling system due to its non-reactivity and its resistance to sorption. Stainless steel fittings were used due to the corrosive effects of the gas. Figure 4.1 shows a diagrammatic representation of this sampling system compared with typical sampling apparatus used for determination of Nitrogen Oxides.

#### 4.2.6.1 Dynamic generation of gas samples

The $NO_2$ gas samples generated to mimic $NO_x$ gas were prepared by this dynamic method. In the dynamic method, the gases are introduced at measured rates into a flowing diluent gas stream to give a continuous supply of the desired standard. The pressure transducer was type 122A from MKS Instruments Inc. and a two stage Edwards vacuum pump was used. Atmospheric pressure was measured using a barometer that was accurate to ±2 mm Hg. The barometric pressure and the room temperature was measured before and after sampling. A 1-liter round bottomed flask was used as a sample flask for most experiments. 2-liter and 5-liter flasks were also used to generate larger samples. Weighing in water was used to measure the exact volumes these flasks held. 25 $cm^3$ of the absorbing solution was placed in the sampling flask and this flask was evacuated to a pressure of 3 kPa where incipient boiling of the absorption solution was seen to occur. The gas to be absorbed was allowed to enter the flask which was then isolated from the vacuum line until absorption had been completed.

As all the experiments were conducted at varying room temperatures and atmospheric pressures, as should be the case when measuring real samples, it was necessary to correct the volume of the gas sample measured to a particular temperature and pressure so as to allow direct comparisons to be made.

The gas sample volume corrections were all standardized at 294 K and 101.33 kPa. Using this as a guide, the volume of the standardized gas sample was calculated using the formula:

$$V_c = \frac{\left(V_f - V_a\right)\left(\frac{P_f}{T_f} - \frac{P_i}{T_i}\right)294}{101.33} \qquad \text{(Eq. 4.18)}$$

$V_c$ = volume gas / $cm^3$

$V_f$ = volume flask / $cm^3$

$V_a$ = volume absorption solution / $cm^3$

$P_i$ = absorption pressure initially / kPa

$P_f$ = absorption pressure finally / kPa

$T_i$ = absorption pressure initially / K

$T_f$ = absorption temperature finally / K

294 = standardized temperature / K

101.33 = standardized pressure / kPa

Once the corrected volume of sample gas was measured, the concentration of $NO_2$ in parts per million by volume in the gas could be calculated using the formula:

$$NO_2 / ppm(v/v) = \frac{\left(24.1Wx10^3\right)}{46V_c} \qquad \text{(Eq. 4.19)}$$

W = weight of $NO_2$ found in the absorbed sample measured as mg

24.1 x $10^3$ = standard molar gas volume at 294 K and 101.33 kPa

46 = molecular weight of $NO_2$

The weight of $NO_2$ in the sample was calculated from the concentration measured on the FIA system, e.g. if 763 ppm nitrate was measured, this is equivalent to 763 mg/L w/v. It is required to convert this parts per million by weight to parts per million by volume in order to calculate the original gas concentration. Therefore in 25 $cm^3$ absorbing solution there was 19.1 mg. Therefore in the 1L absorbing flask there was 19.1 mg of the gas. With this value of milligrams of the gas per litre of air at 294 K and 101.33 kPa it is necessary to multiply by the molar gas volume and divide by the molecular weight (corrected to standard pressure and temperature) to obtain the concentration of the gas in parts per million by volume (ppm v/v):

$$\frac{19.1\ \text{mg/L air} \times 24.1 \times 10^3}{46} = 10,007\ \text{ppm v/v} \qquad \text{(Eq. 4.20)}$$

### 4.2.6.2 Static generation of gas samples

A static method of preparation was used in the generation of the interfering gas samples. This involved the introduction of a known volume of the interferent into a vessel of known volume containing the diluent gas (air). A heating mantle was used cautiously to ensure vaporisation of the interfering species. To prevent losses due to sorption, these gas mixtures were allowed to remain in the apparatus for some time before emptying the system and repeating the process.

When measuring the concentration of the interferent gases produced by the vaporisation of a known volume of the liquid contaminant, the following calculation was made:

$$\text{Concentation gas ppm v/v} = \frac{24.1\,\rho v \times 10^6}{VM} \bullet \frac{T}{294} \bullet \frac{101.33}{P} \qquad (2.21)$$

$\rho$ = density of interferent

M = molecular weight of interferent

v = volume of interferent / $dm^3$

T = temperature / K

V = volume of system / $dm^3$

P = pressure / kPa

## 4.3 Results and Discussion

### 4.3.1 Gas Absorption

Referral was made in the introduction to a chemically modified electrode which was used in the analysis of atmospheres containing low concentrations of nitrogen monoxide and nitrogen dioxide [51,52,53]. This work involved the injection of the gas containing $NO_x$ directly onto a continuous-flow FIA system. The working electrode had a chemically modified surface incorporating immobilised $Fe^{(II)/(III)}$ centres as redox mediators. The modified electrode's response to $NO_2$ in flow-through thin-layer cells showed a low limit of detection and good sensitivity and selectivity. The L.O.D. was found to be 2 ppb (1 part in $10^9$) with a linear dynamic range to 10 ppb [52]. NO could also be detected but demonstrated a less sensitive response.

This method of detection would greatly simplify the analysis of such gases. It would not be necessary to include an absorption step before measurements of gas concentrations and essentially instantaneous measurements of the gas could be made. To see if this direct on-line method of analysing $NO_x$ was feasible using the FIA sensor described in this chapter a number of experiments were carried out.

The gases analysed in Mottola's work contained very low levels of $NO_2$ and NO. The aim of this work is to produce a sensor capable of measuring far higher concentrations of $NO_x$. In order to obtain an electrolyte solution suitable for use with the FIA, the gas was bubbled through a flask containing the absorbing solution.

Figure 4.2 shows that the ratio of nitrite to nitrate present in the 5 mol $dm^{-3}$ NaOH solution after the absorption of $NO_2$, though somewhat scattered, is essentially 1. The slope of this graph is 0.976 with a correlation coefficient of 0.984. These measurements were made using the titration method described in the experimental section. This implies that with the alkaline conditions used, absorption proceeded

according to the reactions described in equations 4.10 and 4.11. When nitrogen dioxide is being absorbed into an aqueous, alkaline solution, the gas is absorbed as both nitrite and nitrate in equal proportions.

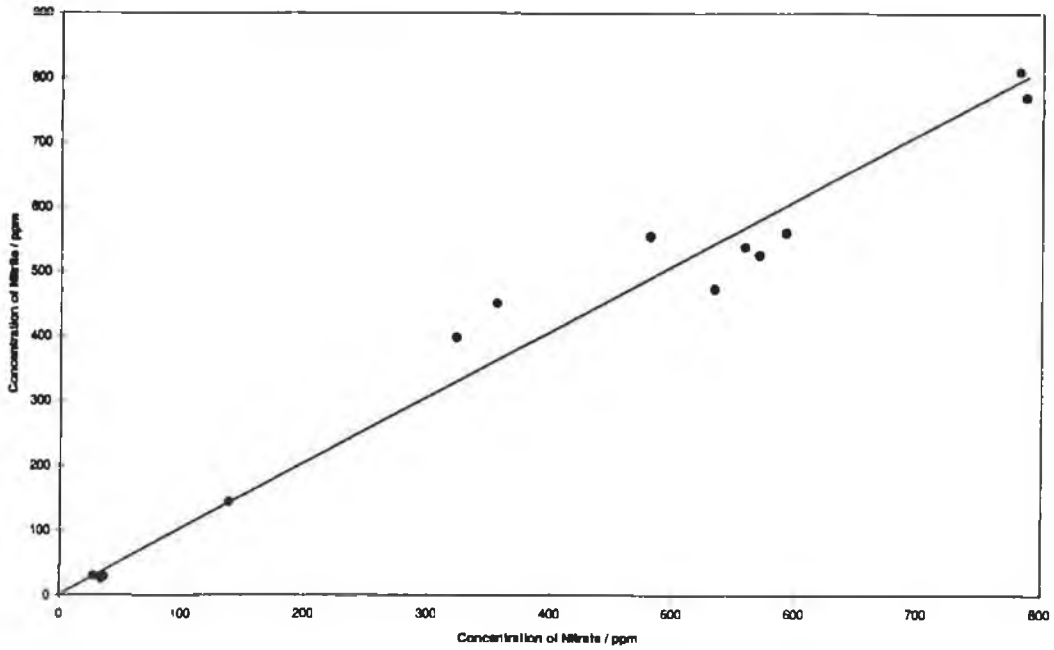


Figure 4.2 Comparison of nitrite and nitrate concentrations found absorbed in a 25 $cm^3$ aliquot of a solution of 5 mol $dm^{-3}$ NaOH after bubbling of a gas containing 10,000 ppm $NO_2$ for 15 min through the solution. r = 0.984. Found using titrimetric method.

This same behaviour has previously been observed when absorbing $NO_x$ into an alkaline solution [18]. In that study it was found that at different concentrations of NO and $NO_2$ the absorption rate changed i.e. the absorption of $NO_x$ changes depending on the ratio of NO to $NO_2$ in the $NO_x$ gas mixture. This provides a further complication for the analysis of nitrogen oxides.

| Absorbing Solution / mol $dm^{-3}$ NaOH | Percentage of $NO_2$ absorbed in solution / % |
|---|---|
| 0 | 2.30 |
| 0.1 | 3.54 |
| 1.125 | 70.80 |
| 2.5 | 76.60 |
| 5.0 | 98.82 |

Table 4.1 Percentage of 10,000 ppm $NO_2$ absorbed when the gas was allowed to pass for 15 minutes through a number of different solutions. Volume of absorbing solution in each case was 25 $cm^3$. Measured using the titrimetric method.

Table 4.1 shows the collection efficiency and the total concentration of nitrogen containing species found for absorbing $NO_2$ in absorbing solutions containing different concentrations of sodium hydroxide. The collection efficiency these values represent is shown by expressing the result as a percentage of the theoretical maximum amount which could be absorbed. The flow rate of the $NO_2$ gas through the solution was 10 $cm^3$ $min^{-1}$ for a period of 15 min. As can be seen only small amounts of nitrite and nitrate ions were found to have been absorbed when the absorbing solution was water or 0.1 mol $dm^{-3}$ NaOH. Improvement in the collection efficiency was found when more concentrated alkaline solutions were used. It had previously been shown that absorption does increase with increasing NaOH concentration [24].

It was most likely that the flow of gas through the solution was such that the absorbing solution, if dilute, did not have sufficient reaction time to collect the gas. The $NO_2$ gas flowing through this solution contained 10,000 ppm $NO_2$. Consequently with such a short reaction time it made it necessary to have a highly alkaline solution present so as to drive this oxidising reaction at as fast a rate as possible. At a low NaOH concentration this driving force was absent and thus not all the $NO_2$ gas that came into contact with it was reacted to form nitrite or nitrate.

These absorption experiments demonstrate a number of points. Firstly, incomplete absorption occurred so that only a percentage of the gas to be analysed was collected in aqueous form. Secondly, more concentrated alkaline solutions allowed for more complete absorption of the gas. Thirdly, the gas was speciated in the alkaline solution into nitrite and nitrate, whereas only nitrate was collected when peroxide or an acidic solution was used as the absorbent.

These points must be considered when applied to the FIA sensor. The absorbed gas behaved as expected from descriptions in the literature. FIA is not a chromatographic technique so species cannot be separated on it prior to analysis. However, the FIA sensor developed for this analysis can differentiate between nitrite and nitrate due to use of a copperised cadmium reduction column. However, this column could not be used if injections of gas were made directly onto the FIA as any oxygen present would react with the cadmium granules and cause passivation. Also, the concentrated alkaline solutions which demonstrated the best absorption characteristics cannot be used with the FIA sensor as the extreme conditions would immediately damage the sensing surface. Therefore, the less efficient solutions must be utilised. However, as long as the absorption of the gas within the solution is reproducible, this should compensate for the less than total absorption of the gas.

A slight modification was made to the FIA manifold before direct injections of gas were made onto the system. The straight tubing connecting the injection valve to the detector was replaced with looped tubing in order to ensure that the injected gas mixed well with the carrier solution before reaching the modified electrode.

Injections were made onto the system using a gas-tight syringe from a flask containing 10,000 ppm $NO_2$ in air. Injections of this sample were compared with injections of air. Air produced peaks on the system but the air containing $NO_2$ resulted in peaks approximately 10 times larger. This shows that the system does have a qualitative response to the test gas. Initially the response of the sensor was reproducible but the osmium polymer modified surface of the working electrode was found not to be stable. After approximately 10 injections of the test gas the sensor's

responses were found to become irreproducible. On examination, the working electrode was found to have been completely stripped of its sensing surface after approximately 15 injections of the gas.

To see if injections of air produced this same wearing effect on the modifying layer, a series of 10 repeat injections of air were made onto the FIA. Before and after this experiment injections of $1.0 \times 10^{-3}$ mol $dm^{-3}$ nitrite were made onto the FIA to see if its response changed. It was found that there was no deterioration in the sensor's response to the nitrite standard. From this it can be concluded that it is the species present in the gas, $NO_x$, which is causing the erosion of the osmium electropolymer from the underlying electrode's surface.

This lack of stability was not observed in other modified electrodes used for such analyses [51-53]. Most likely this was because of the low concentrations of NO and $NO_2$ examined by these researchers. In chapter 3, when examining the linear range of the osmium modified electrode for aqueous nitrite and nitrate species, it was found that at concentrations in excess of 1 mol $dm^{-3}$ the modifying layer became unstable. It was postulated that this was due to the formation of an excessive amount of NO in the carrier stream. By injecting the $NO_x$ containing gas straight onto the FIA, this highly reactive gas is being introduced into the carrier electrolyte and very high concentrations are reacting at the modified working electrode.

As stated earlier, because gas is being injected onto the FIA directly, the reduction column could not be included. This simplifies the manifold design. Without the copperised cadmium column the sensor does not respond to nitrate, only to nitrite. The carrier electrolyte absorbs the nitrite and nitrate in equal quantities but only the nitrite is measured so the stoichiometric factor used for the absorption calculations would be 0.5. The presumption being that 0.5 mole of nitrite would be equivalent to 1 mole of $NO_2$. If only $NO_2$ was being measured this would be correct as it has already been demonstrated in equation 4.10 in the introduction that the ratio of nitrite to nitrate produced in alkaline solutions is 1:1. However, it is the ultimate goal of this sensor to apply it to the measurement of $NO_x$. The stoichiometry of the absorption of

$NO_x$ as nitrite and nitrate is not so simple as when $NO_2$ is being absorbed alone. It has also been found that this stoichiometry does in fact change depending on the concentrations of NO and $NO_2$ and on their ratios in the $NO_x$ [18].

Therefore it is necessary when measuring $NO_x$ gases that all the absorbed nitrogen containing species are measured to gain an accurate measurement of the gas phase concentration of the $NO_x$. Thus use of an acidic oxidising solution which traps both $NO_2$ and NO in the same way and absorbs the total $NO_x$ as one species allows simplification of this measurement step. Only one species, nitrate, is now required to be measured which cuts down on the number of calibration solutions required to be run. This requires the reduction column to be retained to allow for the analysis of the nitrate.

The direct injection technique described in references 51-53 has shown itself suitable for the measurements of low, atmospheric levels, of $NO_2$ and to a lesser extent NO. When this technique was applied to the measurement of higher concentrations, a number of drawbacks were observed. Specifically, irreproducible results and unstable sensing surfaces. Also, due to the complex nature of $NO_x$ chemistry, exact determinations of its concentration levels could not be made without knowledge of the NO:$NO_2$ ratio. This could be achieved by including a reduction capability into the FIA manifold which would withstand direct gas injections and would not be irreversibly oxidised by gases such as oxygen which would also be present.

It is necessary to explore a different approach to this problem of measuring emissions containing high concentrations of $NO_x$ with the FIA sensor. Consequently, a technique for absorbing emissions into an aqueous solution before measurement on the FIA was considered, that is, an off-line rather than an on-line procedure was examined.

### 4.3.2 Optimisation of Absorbing Solution

### 4.3.2.1 Effect of pH

A number of solutions were examined in order to determine the optimum solution for the absorption of $NO_x$ gas. The first parameter considered was that of pH. A solution containing 100 $cm^3$ of 0.1 mol $dm^{-3}$ $Na_2SO_4$ was placed in the sampling apparatus after first having its pH adjusted to that of 1, 7 or 10. The solution was then introduced to a gas containing 10,000 ppm $NO_2$ and the absorbed concentration was subsequently measured. The percentage of measured gas absorption in the alkaline solution was found to be 73 %, that in the neutral solution was 66 % and the absorbed concentration contained in the acidic solution was 55 %. The first observation to make was that none of these solutions was found to have achieved complete absorption of the gas sample under investigation, in fact, the absorption capabilities of all three solutions were quite similar. This can be explained by examining the way in which each of these solutions absorbs the gas.

After absorption of the gas in a neutral aqueous solution the formation of nitrite and nitrate ions takes place as was described in equation 4.10. The nitrate species formed is stable but the nitrite is volatile and has a tendency to further react in solution to form $NO_2$. This may be explained by the fact that the absorption of the gas is an equilibrium reaction and if there is nothing present in the absorbing solution to help retain the $NO_2$ in solution, then the reverse reaction can occur and the $NO_2$ can return across the gas phase. Prevention of this loss can be accomplished by a number of means.

By adjusting the solutes pH to strongly alkaline more efficient absorption of $NO_x$ can be obtained as described in the introduction. The pH 10 solution used in the experiment described here was not strongly alkaline and it therefore could not prevent loss of nitrite from the liquid phase back into the gas phase in the form of $NO_2$. Previous work has shown that typical conditions required are solutions containing 5 mol $dm^{-3}$ NaOH at a pH of 14 do allow complete absorption of $NO_x$ under alkaline conditions. The reduction in the absorption capability of the $NO_x$ during absorption into the dilute NaOH solution is most likely due to the slow transportation of

hydroxide ions from the liquid bulk to the interface as a result of the reduced driving force available. This in turn leads to the accumulation and subsequent degeneration of the unstable nitrite species at the liquid surface [23]. In the presence of hydroxide ions the reverse reactions are negligible.

By adjusting the pH to a more acidic level insufficient absorption was also obtained. The absorption of nitrogen dioxide into 0.09N sulphuric acid described in the introduction found that the absorption rate was not affected by the addition of the sulphuric acid within the experimental conditions used [38].

Again, literature shows that by manipulating the concentration of the acidic solution, complete absorption can be obtained. For example through the mechanism of complexation a solution of concentrated nitric acid in sulphuric acid [39] absorbs NO forming nitrosylsulphuric acid, an excess of nitric acid must be present to ensure complete absorption of the gas. Dilution of this solution with water releases nitrous acid from the nitrosylsulphuric acid. NO also undergoes stepwise oxidation in concentrated sulphuric acid [58]. This behaviour has been employed for the continuous flow determination to determine NO [59].

This demonstrates that an optimum absorbing solution cannot be obtained simply by adjustment of pH. Using a strongly alkaline or a strongly acidic solution, which would accomplish this objective, on the FIA is not possible. Due to their highly corrosive nature, it was found that injections of samples containing these solutions caused immediate stripping away of the modified surface from the underlying glassy carbon electrode. Therefore, even though pH has an important effect on the way $NO_x$ is absorbed, the end result is the same- incomplete absorption unless drastic conditions prevail. Consequently it is necessary to add another substance to the absorbing solution which will effectuate complete absorption.

#### 4.3.2.2 Addition of Oxidising Agent

An alternative method of stabilising the absorption products was investigated. The

absorbed species which is leading to incomplete absorption is nitrite. In aqueous solution it exists in the form of nitrous acid which is unstable and can easily return through the liquid/gas interface to the gas phase [37]. As discussed in the introduction, the gas is not absorbed just in the form of nitrite. It is also absorbed as nitrate, a species which is extremely stable in aqueous solution. The incompletely absorbed $NO_2$ described in the initial experiments was detected in the form of nitrate. Therefore, if all the gas could be absorbed as nitrate it would be present in a stable form in solution and would thus allow a measurement of total absorbed concentration to be made.

An oxidizing species can be added to the absorbing solution which reacts with any absorbed nitrite to form the more stable nitrate species. Permanganate has been used in this way [40,41] however it would be unsuitable for use with this sensor as the modified electrode responds to permanganate and it would therefore cause an interfering signal. Similarly, iodine-containing species are electroactive at the osmium modified electrode.

However, hydrogen peroxide also reacts with the absorbed nitrite under acidic conditions but has no interfering effect at the modified electrode. The $NO_2$ is collected exclusively in the form of the stable nitrate species. To show that the presence of hydrogen peroxide in the absorbing solution results in more efficient absorption of the gas the following experiment was carried out. To a solution containing 100 $cm^3$ of 0.1 mol $dm^{-3}$ $H_2SO_4$, various concentrations of $H_2O_2$ were added and these solutions were then placed within the sampling apparatus and introduced to the presence of a gas containing 10,000 ppm $NO_2$. The results of this experiment are presented in Figure 4.3. These results show that when very low concentrations of peroxide were present, incomplete absorption was observed. Increasing the peroxide concentration to 0.03 mol $dm^{-3}$ resulted in complete absorption even at this extremely high $NO_2$ concentration. Therefore this concentration of hydrogen peroxide was chosen as the optimum due to its satisfactory oxidizing power and also because at this concentration it has no effect on the stability

of the FIA's sensing surface.

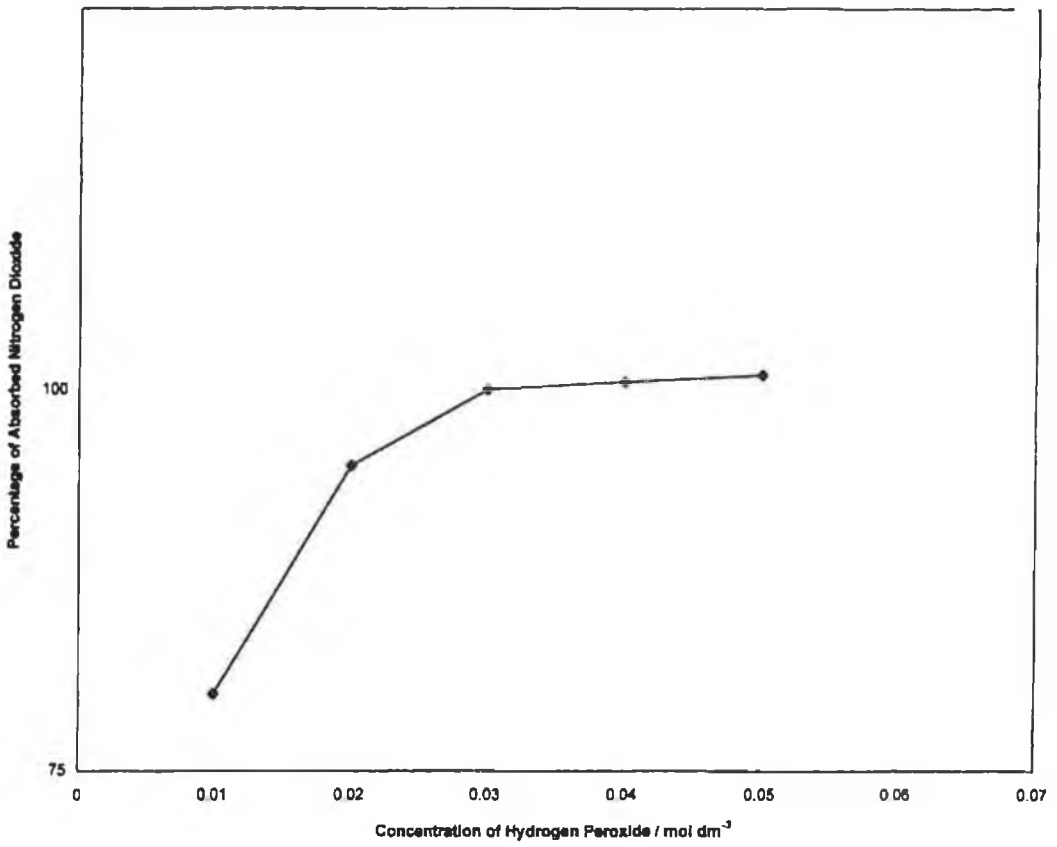


Figure 4.3 Effect of the concentration of hydrogen peroxide in a solution containing 0.1 mol $dm^{-3}$ $H_2SO_4$ on the solution's absorption capability. The gas absorbed contained 10,000 ppm $NO_2$ and the solution volume was 25 $cm^3$. The collection flask was 1L and absorption was measured after 24 hours. The sample flask was unstirred. Measured on a thin layer flow cell modified with $[Os(bpy)_2(PVP)_{10}Cl]Cl$ crosslinked 10 % with 1,10-dibromodecane with a surface coverage of 1 x $10^{-9}$ mol $cm^{-2}$. Flow rate is 1.0 cm3 min-1 and the electrolyte is 0.1 mol $dm^{-3}$ $H_2SO_4$.

The acidic absorption solution's collection efficiency was compared with that of non-buffered water's. After twenty four hours absorption time the acidic solution was found to have absorbed 100 % of the $NO_2$. Whereas water had absorbed only 66% of the $NO_2$ that was calculated to be present. The characteristic odour of $NO_2$ was also detected coming from the collecting flask which had pure water as the absorbing solution when it was removed from the gas sampling apparatus. This provided confirmation that water was less successful in absorbing the $NO_2$ in comparison to the acidic solution.

In alkaline solutions it has been found that these dissolved species were rapidly ionised and neutralised so that their reversibility was reduced or eliminated [18,60]. Similarly in the acidic absorbing solution used here the $NO_2$ undergoes oxidation by peroxide to form the nitrate, so these dissolution products are no longer available for the reverse reactions to occur.

#### 4.3.2.3 Effect of Absorption Volume and Collection Flask

The next experimental parameter to be considered was the volume of absorbing solution to be used for gas sampling. The absorbing solution contained 20, 50, 80 and 100 $cm^3$ aliquots of a solution containing 0.03 mol $dm^{-3}$ $H_2O_2$ in 0.1 mol $dm^{-3}$ $H_2SO_4$ in a 1-liter capacity round bottomed flask. A gas containing 10,000 ppm $NO_2$ was brought into contact with these solutions and was allowed to remain in contact for 24 hours. After this period of time, the flasks were unsealed and the volume of absorbed gas was calculated. The different volumes were found not to have an effect on the absorbing ability of the solution. Consequently, a volume of 25 $cm^3$ was chosen for the rest of the experimental work for reasons of convenience.

Using similar experimental conditions, different sizes of collecting flasks were used in which 25 $cm^3$ of the absorbing solution was placed for trapping of the $NO_2$ gas. It was found that the volume of the flask used had no bearing on the absorption of the gas into solution, i.e. the absorption was flask volume independent. Geometry also had no bearing on the flasks suitability using the sampling procedure described in this chapter. Both volumetric and round bottomed flasks were used as sampling flasks without affecting the subsequently measured $NO_2$ concentration.

#### 4.3.2.4 Optimisation of Absorption Time

The time taken to absorb a specific volume of the $NO_2$ gas was then considered. The major part of the absorption reactions has been found to occur not in the bulk phases, but instead takes place in the gas film and liquid film at the boundaries between the two phases [36]. Therefore, the effect of disturbing the quiescent sampling solution

and thereby increasing the area of this boundary between the phases was investigated. The spectroscopic reference method [34] recommends allowing the gas to be absorbed by the solution overnight. Alternatively it suggests that 2 hours is sufficient if the absorbing flask is periodically shaken. When measuring $NO_2$ alone [48], the standard phenol disulphonic acid procedure was found to produce systematically low results for known $NO_2$ gas concentrations when employing shorter sampling times. This work showed that absorption of the gas, especially when it was present at low concentrations, 40 ppm, into large sampling flasks, 2.5-liter capacity, was very slow. Previously, the sampling flask capacity was not found to affect the absorption of the gas when 24 hours was used as the sampling time and the test gas contained 10,000 ppm $NO_2$.

| **Length of Absorption Period / hours** | **Percentage of $NO_2$ Absorbed** | | |
|---|---|---|---|
| | No disturbance during absorption period | Solution shaken periodically during absorption period | Solution constantly stirred during absorption period |
| 3 | 0.84 | 0.87 | 1.01 |
| 24 | 1.02 | 0.99 | 0.99 |

Table 4.2 The effect on the absorption capability of a 25 $cm^3$ aliquot containing 0.03 mol $dm^{-3}$ $H_2O_2$ in 0.1 mol $dm^{-3}$ $H_2SO_4$ of mechanical disturbance when introduced to a gas sample containing 10,000 ppm $NO_2$. Absorption time was 24 hours and the collection flask was 1L. Measured on a thin layer flow cell modified with $[Os(bpy)_2(PVP)_{10}Cl]Cl$ crosslinked 10 % with 1,10-dibromodecane with a surface coverage of 1 x $10^{-9}$ mol $cm^{-2}$. Flow rate is 1.0 cm3 min-1 and the electrolyte is 0.1 mol $dm^{-3}$ $H_2SO_4$.

To investigate whether the period of time required for this sampling period could be improved it was decided to look more closely at the effect of stirring the absorbing solution. To do this a Teflon coated magnetic stirrer was placed in the flask. This allowed constant stirring of the absorbing solution.

Results obtained using various techniques are shown in Table 4.2. It can be seen that if the flask was neither stirred nor shaken complete absorption of the 10,000 ppm gas did not take place for 24 hr when using optimum conditions. Even shaking of the flask periodically did not produce satisfactory absorption. As can be seen, the experimental result did not match the expected value until 24 hr sampling time had elapsed. Also, shaking the vessel was found to result in the breaking of the vacuum seal a number of times. Consequently resulting in the abandoning of these experiments.

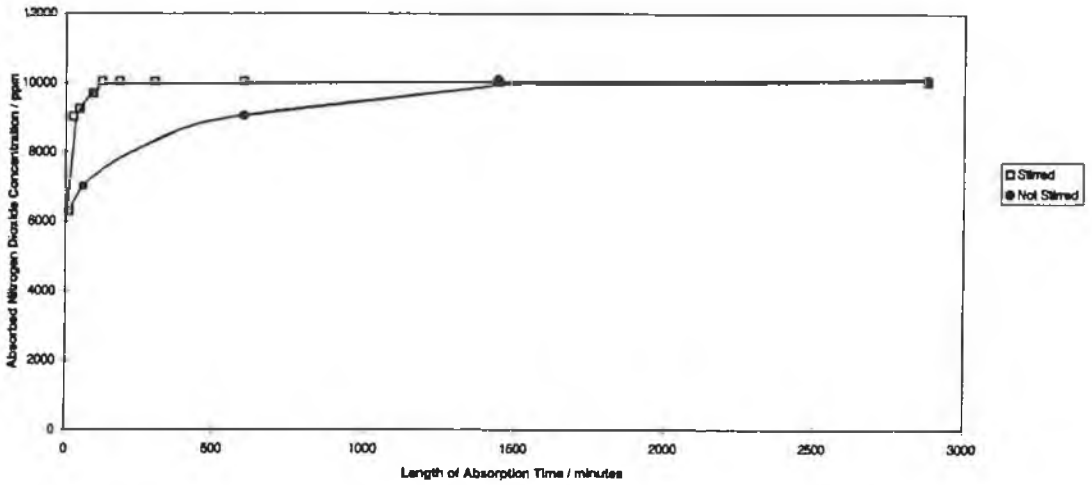


Figure 4.4 Comparison of the absorption profile of a gas containing 10,000 ppm $NO_2$ into stirred and unstirred absorption solutions. The boxes represent a 25 $cm^3$ aliquot solution containing 0.03 mol $dm^{-3}$ $H_2O_2$ in 0.1 mol $dm^{-3}$ $H_2SO_4$. A 1L flask was used as the sample flask. Measured on a thin layer flow cell modified with $[Os(bpy)_2(PVP)_{10}Cl]Cl$ crosslinked 10% with 1,10-dibromodecane with a surface coverage of 1 x $10^{-9}$ mol $cm^{-2}$. Flow rate is 1.0 $cm^3$ $min^{-1}$ and the electrolyte is 0.1 mol $dm^{-3}$ $H_2SO_4$

However, constant stirring of the solution was found to have a dramatic effect on the length of time required for the absorption period. Complete absorption of the gas was found to have occurred only 2 hr after coming into contact with the sample of gas. To further investigate this efficient absorption the $NO_2$ gas was introduced into the flask

for varying periods of time and samples of the absorbing solution were then analysed for nitrate content.

The rate at which the $NO_2$ was absorbed into solution was monitored by terminating the sampling at different times before complete absorption had taken place. Firstly, absorption taking place in a constantly stirred solution was examined. Figure 4.4 shows the course of this absorption. Within 10 minutes of the sample gas coming into contact with the solution, the test solution was found to have collected nitrate which was equivalent to a $NO_2$ gas concentration of 5,000 ppm. In other words, within ten minutes already 50 % of the $NO_2$ had been absorbed. Absorption continued to increase with time so that when ninety minutes had elapsed 83 % of the $NO_2$ gas had been absorbed and by two hours complete absorption was found to have taken place. This demonstrates how quickly equilibrium takes place between $NO_2$ in the gas and liquid phases and the subsequent reaction in solution to form nitrate. This also shows that after the initial dramatic uptake of $NO_{2(g)}$ by the solution, subsequent absorption takes place at a slower rate.

Since in the course of this experiment the absorbing solution was constantly stirred throughout, thorough mixing of the absorbing solution occurred allowing unreacted solution a greater probability of coming into contact with the $NO_{2(aq)}$ thus allowing complete absorption of the $NO_2$ gas within two hours.

To see if this was so, the absorption profile of the $NO_2$ into an unstirred solution was also examined and the results of this experiment are also represented in Figure 4.4. Within thirty minutes approximately 70 % of the gas had been absorbed as nitrate. After this initially fast absorption, the rate at which further nitrate was formed was again found to drop. But this time instead of complete absorption taking place within two hours, instead further absorption proceeded at far slower a pace. After ten hours 90 % of the expected nitrate concentration was measured as present in solution and 100 % was found only after twenty four hours had elapsed. This shows that initially the $NO_2$ quickly passed into solution and reacted there to form the stable nitrate species as was the case with the stirred solution. But since absorption was taking

place in a quiescent solution further nitrate formation could not take place until fresh peroxide had diffused to the gas/liquid interface.

When this absorption solution is being stirred, fresh absorbing solution is brought into contact with the interface constantly which promotes faster absorption. Literature recommends that when using this sampling technique, the solution is left undisturbed for twenty four hours to allow complete absorption to take place [42,61]. However, stirring produced far better results and allowed better mixing of the reaction mixture within the collection flask.

#### 4.3.2.5 Stability of Absorbing Solution

It is necessary to ensure that a freshly prepared absorbing solution is prepared before sampling of the gas. Hydrogen peroxide has only short term stability and its lifetime rapidly decreases if subjected to extreme conditions. Comparing the absorption efficiency of a freshly prepared solution with one that had been prepared two weeks previously showed that whereas the former solution had absorbed 100 % of the gas, the latter had absorbed 70 %.

During initial evacuating of the sampling flask to a pressure of between 2.5 and 3.0 kPa the solution can be seen to begin to boil. If the pressure was kept this low for a length of time or if the pressure was allowed to go below 2.0 kPa, subsequent analysis showed that absorption had been inefficient and not all the $NO_2$ had been trapped in the solution. This boiling was the release of oxygen and hydrogen peroxide from the solution, and since the peroxide plays such an important part in the absorption of the gas, its absence had a large effect on the collecting ability of the solution. Peroxide is an unstable species and is subject to decomposition with a resultant decrease in its concentration. The efficiency of the absorption solution in trapping the gas was found to decrease by up to 40 % when the absorbent was subjected to this low pressure for 30 min. This collection efficiency of ~60 % is similar to the collection efficiency of 66 % found when using pure water and is similar to the 70 % figure found for a two week old sample of the peroxide containing absorbing solution. The

absorbing solution should therefore be handled with care and not subjected to extremes of temperature or pressure and it should be protected from sunlight when not being used.

No observable effect of temperature on the sampling procedure was found over the range of temperatures 289-298 K. No trend in absorption efficiencies could be found over this range of temperatures. A wider range of temperatures would be required to be examined before a definite relationship could be said to exist or not between absorption and temperature. However, temperatures outside this range would be unlikely to occur during real time sampling as sampling probes used in stacks to extract the gas sample are heated or insulated or both to prevent condensation of moisture while purging and sampling. The calculations used in the determination of the $NO_2$ present takes into account the temperature and pressure at time of sampling so as long as these variables are measured accurately they should have no effect on the measurement of the $NO_2$ concentration.

In conclusion, the optimum conditions for the grab sampling procedure were found to be an absorption sample of 25 $cm^3$ of a solution containing 0.03 mol $dm^{-3}$ $H_2O_2$ in 0.1 mol $dm^{-3}$ $H_2SO_4$ and the collecting flask should be of 1-liter capacity. The absorption sample should have been freshly made and the vacuum that the absorbent is subjected to should be no less than 3 kPa. After this vacuum has been obtained the gas to be analysed should be introduced into the flask without delay to prevent loss of peroxide. A sampling time of no more than 2 hr is then required as long as the absorbing solution is constantly stirred during this time.

### 4.3.3 Analytical Development of Sensor

The response of the sensor to the measurement of the standard $NO_2$ gas, whose concentration of 10,000 ppm was known, was calculated for a number of samples obtained using the optimum sampling conditions. The $NO_2$ gas concentration was

measured to be 10,052 ppm ±1.5 % for n = 12.

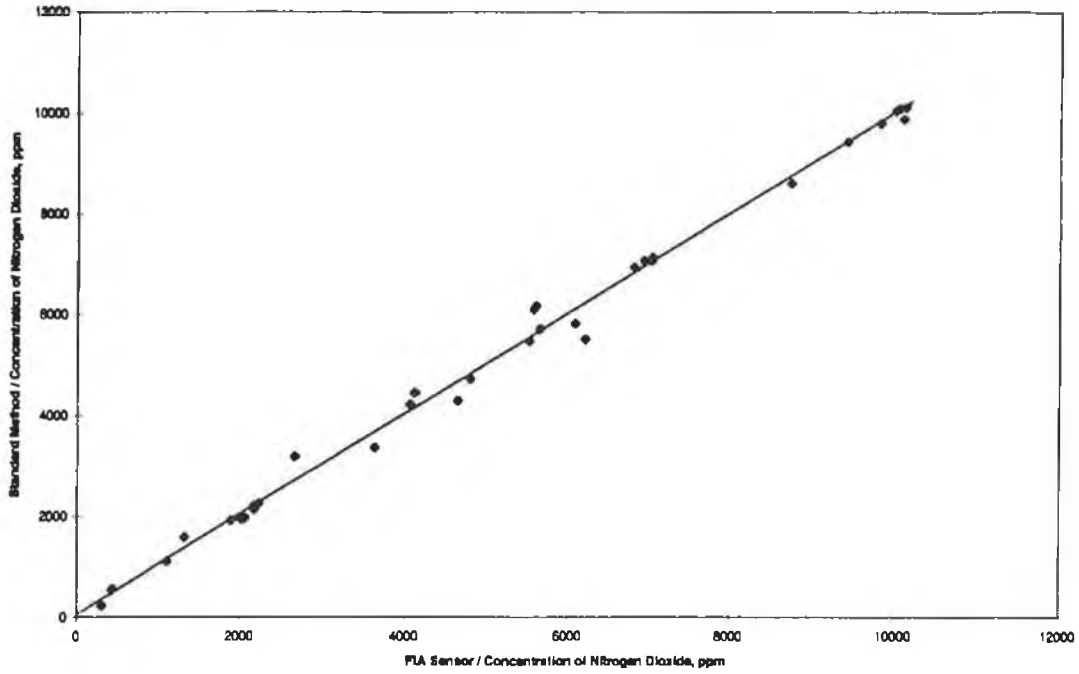


Figure 4.5 Regression plot comparing a number of gas samples containing various concentrations of $NO_2$ measured using the FIA sensor described in this chapter with the results obtained when measuring these samples with an ion chromatographic method.

It has been shown in chapter 3 that both nitrite and nitrate ions can be measured on this osmium modified electrode FIA sensor. Nitrite can be measured directly at the modified electrode. The nitrate must first be reduced to nitrite before being subsequently detected. This ability to measure nitrate was conferred on the sensor by the addition of a copperised cadmium column into the FIA manifold.

This method chosen to absorb the gas involved evacuating a sample flask which contained the oxidising absorbing solution [34]. The gas to be analysed was allowed to enter the flask which was then sealed. The $NO_2$ gas underwent gas phase oxidation and was converted to nitrate species by reaction with peroxide in the absorbing solution [62]. After absorption took place the flask was unsealed and the solution injected onto the FIA where it was detected in the form of nitrate. NO behaves similarly to $NO_2$ in the absorbing solution and is completely trapped as nitrate. So

this method of analysis allows the measurement of the total $NO_x$ concentration.

The response of the sensor to a wide range of $NO_2$ concentrations was observed by diluting the standard $NO_2$ gas with air using a standard dilution technique. These gas samples were subsequently absorbed into aqueous solution and analysed by the FIA sensor using the optimum conditions already described. Dilution of the sample prior to injection onto the FIA was performed when required in order to ensure that all samples were measured within the FIA's' linear range. Gas samples containing $NO_2$ concentrations in the range 200 - 10,000 ppm were produced by this method. Figure 4.5 compares the values obtained for the concentration of these gas samples by the FIA sensor with an ion chromatographic method of nitrate analysis (previously described in chapter 3). Good correlation is seen between these two methods at the different $NO_2$ concentrations. Each point on the graph represents a single sample analysed by both the FIA sensor and the ion chromatographic method for nitrate analysis described in the experimental section. The slope of this line is 0.996 and it has a correlation coefficient of 0.993. Which shows the suitability of the experimental method for the measurement of the absorbed $NO_2$ over a wide range of possible concentrations found in industrial gas emissions. Good correlation between the calculated and experimentally found concentrations was also found. This shows that minimum systematic errors occur in the modified electrode sensor.

The sample throughput based on peak width has been calculated as 60 samples per hour. This is significantly better than the standard method for nitrate analysis which requires the nitration of the sample with phenol disulphonic acid and subsequent colorimetric measurement. One of the steps in this standard method is the evaporating of the sample to dryness. Because of this evaporation step, each determination takes between 4 and 6 hours to complete.

The sampling method used with this analysis technique is known as grab sampling. Since the grab sample takes a relatively short sample over a very short period of time, the result obtained will be an instantaneous measure of the nitrogen oxides present. Therefore it will be representative of the emissions only if the gas stream is well

mixed and the concentration is constant with time. As this may not be the case, it is necessary that multiple samples are taken using this method [42]. The standard method presently requires 30 hours for complete analysis to take place. This consists of 24 hours absorption time to ensure complete absorption of the sample and then a further six hours for analysis of the sample, the major portion of this latter time being the evaporation step. $NO_2$ analysis using the method described in this chapter resulted in reduced times required for absorption and analysis of the gaseous species. In the time taken to obtain one measurement using the standard method, up to 15 samples could be obtained and measured using the FIA sensor.

### 4.3.4 Interferences in Gas Analysis

The interfering effects of a number of gaseous species which may be present in industrial emissions was measured. The effects of these common air pollutants is shown in Table 4.3. Interferent concentrations were generated far in excess of the levels expected to be found in flue gases.

| Interfering gas | Concentration of gas / ppm | Concentration of gas equivalent to 5 ppm nitrate / ppm |
|---|---|---|
| $SO_2$ | 5,000 | No Signal |
| $CO_2$ | 6,000 | $3 \times 10^4$ |
| $NH_3$ | 5,000 | $12 \times 10^3$ |
| Aniline | 17,000 | $6 \times 10^4$ |
| Nitromethane | 19,000 | $25 \times 10^5$ |

Table 4.3 The response of the FIA sensor to a number of interfering species.

This sensor was found to be essentially inert to ammonia, nitromethane and aniline even at levels far greater than would be expected to exist in stack gas emissions. Hazardous organic air pollutant emissions from combustion processes can be of the order $9.091 \times 10^9$ kg (107 t) per year [62]. Carbon dioxide and water vapour cause significant negative interferences in chemiluminescence detection [29] of $NO_x$ but

these cause no interfering effects with this sensor. Typically concentrations from 200 ppm to 12.7 % $CO_2$ would be expected under coal combustion conditions [62,63]. A high concentration of $SO_2$ was also found to cause no signal and it was not found to interfere in the absorption of the $NO_2$ gas sample into the recently made acidic peroxide absorbing solution. Chemiluminescence $NO_x$ analysers have been shown to respond nearly quantitatively to other nitrogen containing compounds [29]. The standard spectrophotometric method also suffers from interference by organic nitrogen compounds and by halides [34]. An ion chromatographic method suffered from ammonia interference [40]. $SO_2$ can also be a serious interferent when colorimetric detection is used due to its decolourising effects [47]. The amount of $SO_2$ present in flue gas depends on the industrial process, e.g. coal with a high sulphur content would produce an exhaust gas with a large component of $SO_2$. The selective nature of the modified electrode prevented such species from producing a similar interfering effect in the FIA sensor.

### 4.3.5 Conclusion

Direct injections of the $NO_x$ containing gas were found to be unsuitable for a number of reasons. Firstly, the cross-linked osmium modified electrode contained within the FIA was unstable when used to measure high concentrations of the gas and quickly developed irreproducible results. Secondly, only a small proportion of gas was absorbed due to the short residence time in the FIA manifold and the non-extreme conditions used. Thirdly, only nitrite was measured as the copperised cadmium reduction column and this column could not be used when direct injections of gas were made onto the FIA and without the reduction column the sensor does not respond to nitrate, only to nitrite. As was mentioned earlier in the chapter, it has been found that the ratio of absorption of $NO_x$ as nitrite and nitrate changes depending on the concentrations of NO and $NO_2$ and on their ratios in the $NO_x$ [18]. Therefore, it is necessary for the sensor to be able to measure both nitrate and nitrite species and this would not be possible with direct gas injections.

The use of an acidic oxidising solution which traps both $NO_2$ and NO in the same way

and absorbs the total $NO_x$ as one species, nitrate, allows simplification of this measurement step. Only one species, nitrate, is now required to be measured which cuts down on the number of calibration solutions required to be run. This requires the reduction column to be retained to allow for the analysis of the nitrate. Which in turn means that direct injections of gas cannot be made onto the FIA. Instead the gas must first be absorbed into solution and the aqueous absorption products can then be measured.

The present standard method of analysis for $NO_x$ is the grab sampling technique followed by colorimetric detection of the nitrate as an azo dye [34]. This analysis method is complicated and particularly time consuming and uses large quantities of reagents. The measurement method described in this chapter shows how the time taken for this analysis can be substantially reduced thus allowing more samples to be obtained over a shorter period of time. Up to 15 samples can be absorbed and measured in the time taken for one sample to be analysed by the standard method. The absorption efficiency of the recommended $NO_x$ sampling procedure [34] was also found to change depending on the concentration of the gas sample and on the size of the sampling flask [48]. Using the procedure outlined in this chapter allowed these factors to become insignificant. All samples of the $NO_2$ gas were found to be completely absorbed within 2 hrs. The interfering effects of both common and uncommon species found in stack gases were found to be negligible. The major drawback of the sensor is that it is not an on-line technique which would be the optimum solution to the measuring of $NO_x$ gases emitted from stacks and flues. Also, the absorption technique described in this chapter allowed complete absorption of $NO_x$ as nitrate. In other words total $NO_x$ was measured. Speciation into NO and $NO_2$ was not possible. This is a disadvantage if the technique was required for kinetic or mechanistic studies.

Teaming this mode of sampling with flow injection analysis allows a powerful sensing technique to emerge. The advantages of amperometry for electrocatalytic sensing are combined with the advantages of FIA, for example, ease of automation of the system, high analytical throughput and simplified analysis procedures. The flow

injection analysis system has been designed for the laboratory environment. It provides a stable detection method housed in an easy to construct manifold. It is a reliable method of detection which show good correlation between it and a standardised method. It doesn't use the costly reagents associated with typical nitrate analysis. It is simple to use with short analysis times.

In conclusion, the nitrate sensor based on a polymer modified electrode housed in an FIA manifold described in this chapter was found to be an accurate technique for measurement of the high concentrations of $NO_x$ emitted from industrial processes after absorption of the gas into aqueous solution. The construction of the instrument itself is very simple and the sensor was found to be free from many of the interfering gases which are present in emissions from stack gases. Even when these gases were present in far higher concentrations that would be expected in most industrial emissions [64].

### 4.3.6 References


1 W. K. Downey, G. Ni (eds)Uid, Proc. "Air Pollution- Impacts And Control", 1979

2 USGS NAWQA Fact Sheet 092-96

3 O. Hutzinger (ed), "The Handbook of Environmental Chemistry" V.4(A), Springer-Verlag, Berlin, 1986

4 J. R. Foster, R. C. Cottrell, I. A. Herod, H. A. C. Atkinson, K. Miller, Br. J. Exp. Pathol., 66 (1985) 193

5 G. E. Likens, R.W.Wright, J. N. Galloway, T. J. Butler, Scientific American, 241 (1979) 39

6 M.W. Holdgate in "Environmental Effects of Utilising More Coal", F.A. Robinson (ed), Royal Society of Chemistry, Cambridge, 1980

7 P. A. Mayewski, M. R. Legrand, Nature, 346 (1990) 258

8 M. A. Tolbert, M. J. Rossi, D. M. Golden, Science, 240 (1988) 1018

9 P. J. Crutzen, F. Arnold, Nature, 324 (1986) 651

10 A. Williams, Nature, 324 (1986) 612

11 S. M. Durrani, Environ. Sci. Technol., 28 (1994) 89A

12 D. K. Liu, D.-X. Shen, S.-G. Chang, Environ. Sci. Technol., 25 (1991) 55

13 D. K. Liu, L. P. Frick, S.-G. Chang, Environ. Sci. Technol., 22 (1988) 219

14 D. K. Liu, S.-G. Chang, Environ. Sci. Technol., 22 (1988) 1197

15 A. J. Clarke in "Environmental Effects of Utilising More Coal", F. A. Robinson (ed), Royal Society of Chemistry, Cambridge, 1980

16 Industrial Air Pollution Inspectorate, Chief Inspector's Annual Report, "Industrial Air Pollution - Health and Safety", HMSO, 1981

17 W. A. Glasson, C. S. Tuesday, J. Chem. Soc. Faraday Trans., 85 (1963) 2901

18 H. Komiyama, H. Inoue, Chem. Eng. Sci., 35 (1980) 154

19 G. Baumbach, NATO ASI Ser., vol. G31 (1992) 41

20 R. T. Talasek, K. E. Daugherty, J. Chrom. Sci., 30 (1992) 131

21 F. M. Benoit, Anal. Chem., 55 (1983) 2097

22 J. A. Hodgeson, W. A. McClenny, P. L. Hanst, Science, 182 (1973) 248

23 J. H. Y. Katima, A. Azapagic, D. Handley, TransIChemE, 70 (1992) 39

24 J. H. Y. Katima, D. Handley, Trans IChemE Part B, 69 (1991) 153

25 C. C. Miller, Lancet, 343 (1994) 300

26 J. G. Walega, D. H. Stedman, R. E. Shetter, Environ. Sci. Technol., 18 (1984) 823

27 K. Yoshizumi, K. Aoki, T. Matsuoka, S. Asakura, Anal. Chem., 57 (1985) 737

28 P. Mikuska, Z. Vecera, Anal. Chem., 64 (1992) 2187

29 J. M. Sedlak, K. F. Blurton, Talanta, 23 (1976) 811

30 R. M. Harrison, R. Perry (eds) "Handbook of Air Pollution Analysis", Chapman & Hall, London, 1977

31 I. Bergman, K. O. West, Proc. 2nd Int. Meeting on Chemical Sensors, 1986 p. 735

32 F. Opekar, Electroanalysis, 4 (1992) 133

33 Z. Cao, W. J. Buttner, J. R. Stetter, Electroanalysis, 4 (1992) 253

34 "ASTM method for sampling $NO_x$ from stack gases", Method D 1608-7735

M. 35 S. Peters, J. L. Holman, Ind. Eng. Chem., 47 (1955) 2536

36 M. S. Peters, C. P. Ross, J. E. Klein, Am. Inst. Chem. Engs. J., 1 (1955) 105

37 D. M. Stanbury, M. M. deMaine, G. Goodloe, J. Am. Chem. soc., 111 (1989) 5496

38 Y. Kameoka, R. L. Pigford, Ind. Eng. Chem. Fundam., 16 (1977) 163

39 (a)E. A. Burnsin in,"The Analytical Chemistry of Nitrogen and its Compounds", C. A. Streuli, P. R. Averill, (eds), Wiley-Interscience, New York, 197040

(b)J.H. Margeson, J.E. Knoll, M.R. Midgett, G.B. Oldaker, K.R. Loder, P.M. Grohse, W. F. Gutkecht, Anal. Chem., 56 (1984) 2610

41 J. H. Margeson, J. E. Knoll, M. R. Midgett, G. B. Oldaker, W. R. Reynolds, Anal. Chem., 57 (1985) 1586

42 H. F. Hamil, "Collaborative study of methods for the determination of nitrogen oxide emissions from stationary sources", Southwest Research Institute, San Antonio, Texas, EPA/650/4 74 025. EPA 68 02 0623. 102P, 5

Oct. 73

43 M. Geissler, R. van Eldik, Anal. Chem., 64 (1992) 3004

44 J. E. Sickles, P. M. Grohse, L. L. Hodson, C. A. Salmons, K. W. Cox, A. R. Turner, E. D. Estes, Anal. Chem., 62 (1990) 338

45 H.-J. Kim, J. Chromatogr., 503 (1990) 466

46 T. Nash, Atmos. Env., 4 (1970) 661

47 M. R. Jacobs, S. Hochheiser, Anal. Chem., 30 (1958) 426

48 B. E. Saltzman, Anal. Chem., 26 (1954) 1949

49 M. S. Nieuwenhuizen, S. Maarten, A. J. Nederlof, J. Arnold, A. W. Barendsz, Anal. Chem., 60 (1988) 230

50 M. S. Nieuwenhuizen, S. Maarten, A. J. Nederlof, Anal. Chem., 60 (1988) 236

51 F. W. Nyasulu, H. A. Mottola, J. Autom. Chem., 9 (1987) 46

52 M. Bonakdar, J. Yu, H. A. Mottola, Talanta, 36 (1989) 219

53 C. J. Hynes, M. Bonakdar, H. A. Mottola, Electroanalysis, 1 (1989) 155

54 W. Holak, J. J. Specchio, Anal. Chem., 64 (1992) 1313

55 L. Guanghan, H. Zhike, L. Yuling, Talanta, 39 (1992) 123

56 D. Chen, M. D. Luque de Castro, M. Valcarel, Analyst, 116 (1991) 1095

57 F. Canete, A. Rios, M. D. Luque de Castro, M. Valcarel, Analyst, 113 (1988) 739

58 D. Dutta, D. Landolt, J. Electrochem. Soc., 110 (1972) 1320

59 A. Trojanek, S. Bruckenstein, Anal. Chem., 58 (1986) 866

60 S. P. S. Andrews, D. Hanson, Chem. Eng. Sci., 14 (1961) 105

61 G. Margolis, J. N. Driscoll, Environ. Sci. Technol., 6 (1972) 727

62 C. A. Miller, R. K. Srivastava, J. V. Ryan, Environ. Sci. Technol., 28 (1994) 1150

63 I. Fangmark, B. Stromberg, N. Berge, Environ. Sci. Technol., 28 (1994) 624

64 D.D. Rostrup-Nielsen, P.F. Schubert, R.K. Sato, in Chenically Modified Surfaces, J.J. Pesek, M.T. Matyska, R.R. Abuelafiya eds., Royal Society of Chemistry, London, 1996

# CHAPTER 5

# DEVELOPMENT OF A FREE CHLORINE SENSOR

## 5.1 INTRODUCTION

Chlorine is widely distributed in the environment where it is present in many forms and it has a variety of uses in all its various oxidation states. Molecular chlorine and hypochlorite are used as bleaching agents [1,2] and as disinfectants of water where they prevent waterborne diseases from occurring. The most widespread form of a chlorine-containing species is the chloride ion. This is primarily due to the reactive nature of chlorine at higher oxidation states. The inorganic chloride ion is found in surface, ground and waste waters and is one of the major inorganic constituents of seawater. Photochemical oxidation of chloride to chlorine in sea water has been postulated but the hypochlorite thus formed is short lived [3]. Chloride levels are also used as an indicator of the condition of a body of water as elevated levels in drinking water are often associated with wastewater contamination [4]. Increased levels of chloride in water can also lead to deterioration of metallic pipes and holding tanks. A chemical etching technique for semiconductors has been reported using chlorine solution [5].

Chlorination occurs when chlorine is added to water in its elemental or hypochlorite form. An initial hydrolysis takes place in which free chlorine is formed. This consists of aqueous molecular chlorine, hypochlorous acid and hypochlorite ion. The relative proportion of these free chlorine forms is pH and temperature dependent. Typically hypochlorite ion and hypochlorous acid will predominate [6].

If ammonia and certain other nitrogen-containing substances are present, free chlorine will react to form compounds, known as combined chlorine, such as chloramines, monochloramine, dichloramine and nitrogen trichloride [7]. Again, whether these compounds are formed and their relative concentrations depends on a number of factors such as pH, temperature, ratios of reactants, absolute chlorine demand and reaction time. Chlorine demand is the quantity of chlorine that is reduced or converted to inert or less active forms of chlorine by substances in the water [6]. Trihalomethanes such as chloroform arise from reaction of chlorine with organic precursors such as humic or fulvic acid or some algae [4]. Concentrations of such

substances in untreated, uncontaminated water are usually low. It has been found that the level of chlorination of water is directly related to the concentration of trihalomethanes. In addition, recent epidemiological analyses of the correlation of human cancer with chlorinated water supplies has focused on singlet oxygen formation on decomposition of aqueous hypochlorite [8]. It is postulated that the singlet oxygen species is formed upon acidification of the chlorinated water and this species can attack DNA to form lesions which can in turn cause cancer. However, the risk assessment of whether to use chlorine in water must always consider the effect of discontinuing its use, i.e. increases in microbial contamination.

Species other than chlorine are used to disinfect water supplies. These include ozone, chlorine dioxide and chloramine. However, these compounds can also produce inorganic species such as organochloramines, aldehydes and ketones and they have lesser, or less prolonged, biocidal capabilities [9].

Consequently, chlorination of water supplies has become a common practice due to its disinfection abilities. The addition of free chlorine to water is effective for deactivation of most disease-bearing bacteria and viruses. The spread of chlorination is credited with dramatic reductions in the incidence of water-borne diseases such as typhoid and cholera. The process destroys algae, oxidizes organic compounds and removes some tastes and odours by its reaction with species such as ammonia, iron, manganese and sulfide. Residual levels of chlorine remain in the water to allow the disinfection process to continue until its final delivery into homes [4].

However, its disinfection ability can vary with different types of bacteria and it can react with phenolic compounds, and bluegreen algae to form objectionable odours. Nevertheless, chlorination is still the most widespread method of preventing microbial contamination of water supplies and its use guarantees safe drinking water for large numbers around the world. But chlorine can react with byproducts of organic decay to form trihalomethanes as previously described, which are suspected carcinogens. This has led to a question of how to balance the carcinogenicity of using chlorine against the risk of not using it. US regulations set a 100 ppb limit for

trihalomethanes which poses an estimated cancer risk of 1 in 10,000.

Studies by the US Environmental Protection Agency showing that chlorine compounds may create a slight cancer risk and may cause 700 extra cases of cancer each year in the United States have led, in some cases, to a disproportionate reaction. In 1991, a decision by Peruvian officials not to chlorinate much of the country's drinking water due to the perceived cancer risk was blamed for a cholera epidemic which affected more than 300,000 people and claimed nearly 4,000 lives [10].

An epidemiological study on this epidemic confirmed that the cholera outbreak was largely associated with drinking contaminated water from the municipal water system [11]. This reinforces the importance of balancing real and theoretical public health risks which translates into the balancing of chemical and microbial risks in water supplies.

In some cases it is important that chlorine be completely removed from water. For example oxidant damage occurs when red cells of hemodialyzed patients are given dialysis water which is incompletely dechlorinated. Measurements of chlorine-containing compounds are also important in certain experiments, e.g. estimating the activity of hypochlorite-producing reactions such as that mediated by the neutrophil enzyme myeloperoxidase [12].

Therefore, rapid and highly sensitive determinations of trace free chlorine levels in water are important so as to allow the monitoring of water quality for drinking and industrial use. Previously, official methods for the determination of residual chlorine in city water used a spectrophotonetric technique with o-tolidine as the dye but studies showed that most orthotolidine-bases procedures have poor accuracy and precision and high associated errors. This information and an associated study which showed the toxic nature of this dye caused this technique to be deleted from the list of approved standard methods [6]. Instead colorimetric and titrimetric methods are now used. Iodimetric techniques give the total residual chlorine content (free and combined chlorine), while Fe(II) with DPD (N,N-diethyl-1,4-phenylenediamine) can

distinguish between the free and combined chlorine. (Note. Free chlorine is composed of the species $Cl_2$/HOCl/$ClO^-$ and combined chlorine is the reaction products of chlorine with species present in the water)

These techniques provide reasonably good sensitivity (LOD = 0.1 ppm) but require several discrete steps and are generally time consuming. Also the possibility of these techniques recording false positive results due to the presence of other anions in solution has been suggested [13]. The time taken for a particular technique to work is a significant problem due to the instability of free chlorine in aqueous solutions and these techniques are particularly time-consuming. Exposure to sunlight or other strong light of agitation, such as stirring, will hasten its deterioration.

An approach towards obtaining more rapid analysis is the application of flow injection techniques. Spectrophotometric [14], chemiluminescent [15-19], amperometric [20-22], voltammetric [23] and potentiometric [24-28] procedures have all been used in flow injection analysis for trace chlorine in water. However, amperometric techniques for chlorine species at electrodes are often limited by electrode surface maintenance considerations and spectrophotometric molar absortivities of chlorine species are too low to allow sub parts per million measurements

A potentiometric titration method for determining chlorine species employing an osmium catalyst has been described [15]. The study showed that in a 70% v/v methanol solution, chlorite and chlorate can be reduced to form chloride ion by As(III) in the presence of $OsO_4^{n-}$. The reaction rate was found to increase as the osmium catalyst concentration increased. Another potentiometric determination was based on the reduction reaction with a buffer containing the Fe(II)/(III) couple [12]. Chlorine reacts with the iron couple to cause a potential change. The method is based on the transient potential changes which appear during the reduction of the chlorine species with the couple and the response was found to depend on the dispersion of the sample zone. A potentiometric stripping analysis technique which uses copper (I) deposited on a gold film electrode as a reagent for the determination

of chlorine species in flow systems has also been presented [25]. The stripping time was found to be proportional to the reciprocal of the concentration of chlorine species. A flow injection system has been described where the residual chlorine is detected by a potentiometric method with a coated-wire ion-selective electrode [26]. However, nitrite, ammonium and iodide all seriously interfere with its determination. The measurement of free chlorine by potentiometric titration with $SO_3^{2-}$ was shown to give good results at high concentrations [28].

The chemiluminescent reaction of Rhodamine 6G with free chlorine in aqueous solution has been demonstrated though the technique showed a limited linear range [15,19]. The chemiluminescence reaction between hypochlorite and luminol has been applied to the determination of inorganic chlorine species using pulse and flow techniques [16]. Deactivation of the excited species was observed with increases in temperature so it proved necessary to use a temperature of 15°C for experimentation. A chemiluminescence sensor using a xanthene dye immobilized on an ion-exchange resin has been described for the continuous monitoring of free chlorine in tap water [17].

A flow injection system with spectrophotometric detection based on the standard Iodimetric technique has been described [14]. Quite harsh conditions are required, however, such as the use of highly concentrated hydrochloric acid to enable the liberation of iodine which can then be measured spectrophotometrically.

A flow injection voltammetric determination of hypochlorite has been described whereby the chlorine species is introduced into an eluent containing 2.5 mol $dm^{-3}$ sulphuric acid and 1 % m/V potassium bromide. The reduced bromide was monitored at a glassy carbon electrode [23].

Amperometric detection at a gold electrode was reported and results indicate that by utilising flow injection many of the problems associated with measuring chlorine species at gold electrodes such as surface fouling can be overcome [20]. This was achieved by adding a pretreatment step to the analysis where the electrode was

subjected to a high voltage. This avoided surface activation but it did limit the sampling rate. Both platinum and glassy carbon electrodes were reported as working electrodes in the determination of chlorine species for the monitoring of pulp bleaching solution [22] and were found to be suitable for measurement of these species in the millimolar range.

Other techniques have also been reported such as an optoelectrochemical sensor based on an electrochromic thin-film sensing layer which was demonstrated to have a potential sensitivity below 1 ppm [29]. A coulometric technique using a thin layer electrochemical cell has been developed which used stopped-flow sampling to minimize interference from non-faradaic currents and achieved a limit of detection of approximately 0.02 ppm [30]. A novel sensing probe for measuring chlorine at levels of about 100 ppm in pulp bleaching based on reaction with acidified potassium iodide has been reported [31]. The reaction of silver sol with hypochlorite has been used to develop a spectrophotometric technique with an LOD of 0.04 ppm [32]. The reagents Acid Yellow 17 [33], Lissamine Green B [34] and chlorophenol red [35] have also proved useful as spectrophotometric reagents for free chlorine. Potentiometric [36] and chemiluminescent [37] determinations of chlorine have been reported which use a gas-diffusion separation of chlorine through a microporous poly(tetrafluroethylene) membrane. But these techniques tend to have unfavorable detection limits.

In this chapter a sensor will be described suitable for the measurement of free chlorine levels in potable water. A flow injection system will be utilised to allow rapid sample analysis and the modified electrode sensor will allow the free chlorine determination to be made free from interference. The linear range of this modified sensor will be demonstrated as suitable for the analysis of water and comparison will be made between this sensor and a standard titration technique using real samples. It will be shown that the sensitivity of the sensor is affected by, among other variables, pH. The kinetic reduction of free chlorine will be explored and the mediation process occurring at two different pH levels will be evaluated.

## 5.2 Experimental

### 5.2.1 Reagents

The synthesis of the $[Os(bpy)_2(PVP)_{10}Cl]Cl$ polymer is described elsewhere (Chapter 2). The source of free chlorine was sodium hypochlorite added to 0.1 mol $dm^{-3}$ sulphuric acid. Solutions of sodium hypochlorite were standardized by adding excess potassium iodide and titrating with sodium thiosulphate solution which had been previously standardized against potassium iodate [38]. Variation of pH was achieved by using dilute solutions of $H_2SO_4$ and NaOH where appropriate. The electrolyte was prepared from $K_2HPO_4$ and $KH_2PO_4$ to produce a 0.1 mol $dm^{-3}$ phosphate buffer. All solutions were freshly prepared and protected from light.

### 5.2.2 Apparatus

Cyclic voltammetry and RDE voltammetry were carried out using a conventional three electrode assembly. The potentiostat used was the EG&G Princeton Applied Research Model 362. The rotating disc assembly was the Metrohm Model 629-10 RDE. Voltammograms were recorded on a Linseis X-Y recorder. The working electrodes were 3mm diameter glassy carbon discs encased in Teflon and supplied by Metrohm. The electrodes were polished with 5 μm alumina prior to addition of the modifying layer. Modification was by a drop coating technique using a solution that was 1 % w/v of the redox polymer in methanol. This layer was then cross-linked by the addition of a 2 % solution of 1,10-dibromodecane in methanol. Surface coverages were determined by integration of the charge (Q) under a sweep rate cyclic voltammogram of 1 mV $s^{-1}$ where $Q = nF\Gamma$ and $\Gamma$ is the number of active sites, n = number of electrons and F is Faraday's constant. The counter electrode was 1 $cm^2$ platinum gauze placed in proximity to the working electrode. The reference electrode was saturated KCl calomel electrode (SCE). All potentials are quoted with respect to SCE. All measurements took place at room temperature.

### 5.2.3 Flow Injection Apparatus

The flow injection apparatus consisted of an EG&G Princeton Applied Research Model 400 electrochemical detector fitted with a thin-layer flow cell, a Gilson Minipuls 3 peristaltic pump, a six-port Rheodyne injection valve with a 20 µl fixed-volume sample loop and a Philips PM 8252 X-t recorder. The working electrodes were 3 mm glassy carbon shrouded in Teflon (EG&G) and were modified as described above. The Ag/AgCl electrode acted as the reference while the stainless-steel body cell body acted as the counter electrode. Potentials are quoted after conversion to the SCE scale. Silicone rubber tubing was used at the pump and Teflon 1/16 in od x 1/32 in id tubing for the rest of the system. Sample injections were made using a 2 $cm^3$ glass syringe fitted with a Rheodyne square-tipped injection needle.

## 5.3 Results and Discussion

### 5.3.1 General Chemistry

In Figure 5.1 a cyclic voltammogram of the redox polymer $[Os(bpy)_2(PVP)_{10}Cl]Cl$ with a surface coverage of $1.0 \times 10^{-9}$ mol $cm^{-2}$ in 0.1 mol $dm^{-3}$ $K_2HPO_4/KH_2PO_4$ can be seen. The CV shows a single, reversible redox process which corresponds to the oxidation/reduction of the Os(II/III) couple whose half-wave potential is 0.25 V vs. SCE. The peak-to-peak separation of this redox couple is close to zero and the peak width at half peak height corresponds to approximately 0.09 V. The anodic peak current was found to increase linearly as a function of potential sweep rate up to a scan rate of 0.1 V $s^{-1}$ which demonstrates finite diffusion behavior. These properties of the modified electrode indicate that the surface-immobilised redox species is in thermodynamic equilibrium with the electrode potential. Further information on the properties of such modified electrodes can be found in chapter 2.

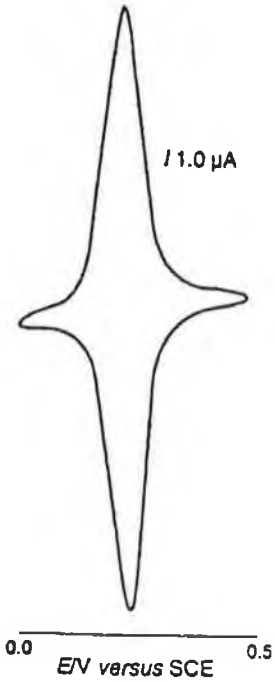


Figure 5.1 Cyclic voltammogram of a 1 x $10^{-9}$ mol $cm^{-2}$ $[Os(bpy)_2(PVP)_{10}Cl]Cl$ modified electrode in 0.1 mol $dm^{-3}$ $KH_2PO_4/K_2HPO_4$ electrolyte at 100 mV $s^{-1}$.

As already described in the introduction to this chapter, when free chlorine is present in an aqueous environment, it may take several different forms. These is aqueous molecular chlorine, hypochlorous acid and hypochlorite ion. These species are collectively known as free chlorine and the particular species present in solution will depend primarily on pH. At acidic pH (<3), free chlorine will be present in the form of molecular chlorine, $Cl_2$, Between pH 4 and 7, hypochlorous acid, HOCl is formed and at higher pH values the free chlorine exists as the hypochlorite ion, $OCl^-$. Indeed the $pK_a$ of the $HClO \rightarrow ClO^- + H^+$ reaction is approximately 7.3 [39].The standard potential of these reactions versus the standard calomel electrode are as follows:

$$Cl_2 + e^- \rightarrow 2Cl^- \qquad 1.14 \text{ V vs. SCE} \qquad \text{Eq. 5.1}$$

$$2HOCl + 2H^+ + 2e^- \rightarrow Cl_2 + H_2O \qquad 1.39 \text{ V vs. SCE} \qquad \text{Eq. 5.2}$$

$ClO^- + H_2O + 2e^- \rightarrow Cl^- + 2OH^-$ 0.62 V vs. SCE. Eq. 5.3

The formal potential of the Os(II/III) couple, 0.25V vs. SCE, is considerably less than the potentials of the free chlorine species and as such will have a strong driving force of -0.89V, -1.14V and -0.37 V respectively. As the standard potentials of their reduction reactions is anodic of the formal potential of the Os(II/III) couple, mediation of the reductions by the polymer-immobilised Os(II/III) redox centres should be thermodynamically possible. The Gibbs free energy associated with these electrocatalytic reactions can be calculated from:

$$\Delta G = nF\,\Delta E \qquad \text{Eq. 5.4}$$

where n is the number of electrons transferred, F is Faraday's constant and $\Delta E$ is the potential difference between the oxidant and the reductant. This gives in a free energy difference of -86 kJ mol-1 for reaction 5.1 and -110 kJ $mol^{-1}$ for reaction 5.2 and -36 kJ $mol^{-1}$ for the reaction described in Eq 5.3. As the Gibbs free energy for the reduction reactions is negative, they will be expected to occur spontaneously.

In Figure 5.2 an RDE voltammogram comparing the reduction of the free chlorine species at a bare glassy carbon electrode with that found at an osmium redox polymer modified glassy carbon electrode is shown at pH 1, 6 and 10. The elongation of the reduction wave at the unmodified electrode is indicative of poor kinetics and this is mirrored in the reduction wave found for the modified electrode at pH 10. The corresponding voltammograms for the modified electrode at pH 1 and 6 shows the onset of the mediated reduction at approximately 0.4 V vs. SCE and also show that this modified electrode is potentially an extremely effective and efficient electrocatalyst for the reduction of free chlorine in acidic and neutral pH environments where the free chlorine is present as $Cl_2$ and HClO respectively.

Considering that the modified electrode was able to mediate the reduction of the free chlorine only in acidic and neutral pH environments, this can be considered qualitatively by considering the following reactions:

$$HClO + Os(II) + H^+ \rightarrow \tfrac{1}{2}Cl_2 + Os(III) + H_2O \qquad \text{(neutral pH)} \quad \text{Eq. 5.5}$$

$$\tfrac{1}{2}Cl_2 + Os(II) \rightarrow Cl^- + Os(III) \qquad \text{(acidic pH)} \quad \text{Eq. 5.6}$$

In an acidic environment, it appears that the osmium mediator can reduce the molecular chlorine and similarly it can react with the hypochlorous acid in a more neutral environment. However the reduction of the hypochlorite ion in alkaline pH is not mediated by the Os(II/III) couple.

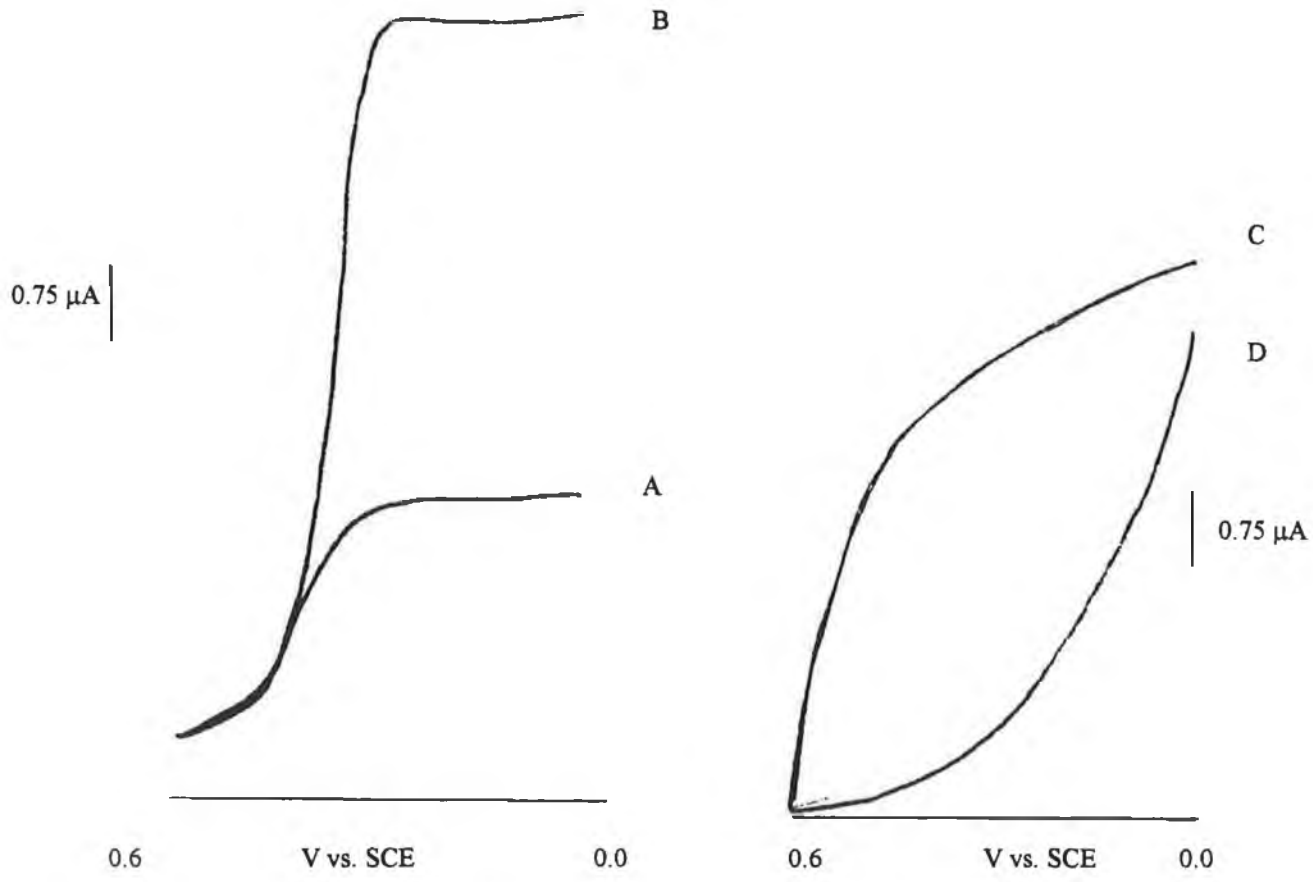


Figure 5.2 RDE voltammograms for the reduction of ppm HClO in 0.1 mol $dm^{-3}$ $KH_2PO_4/K_2HPO_4$ electrolyte at a potential sweep rate of 5 mV $s^{-1}$ and rotation rate of 500 rpm at a 1 x $10^{-9}$ mol $cm^{-2}$ $[Os(bpy)_2(PVP)_{10}Cl]Cl$ modified electrode where A = modified electrode response at pH 1, B = modified electrode response at pH 6, C = modified electrode

### 5.3.2 Modified Electrode Kinetics

The redox chemistry of free chlorine is poor at conventional electrodes [20] due to its deteriorating effect on the electrode's surface. Most electrochemical approaches to this species' detection rely on its prior reaction with other species such as iodine which may be more easily controlled and measured. The polymer-bound electrocatalyst described here has the potential of improving and simplifying this reaction. The electrocatalysis of this species was examined using the methods described by Albery et al as described in the introductory chapter.

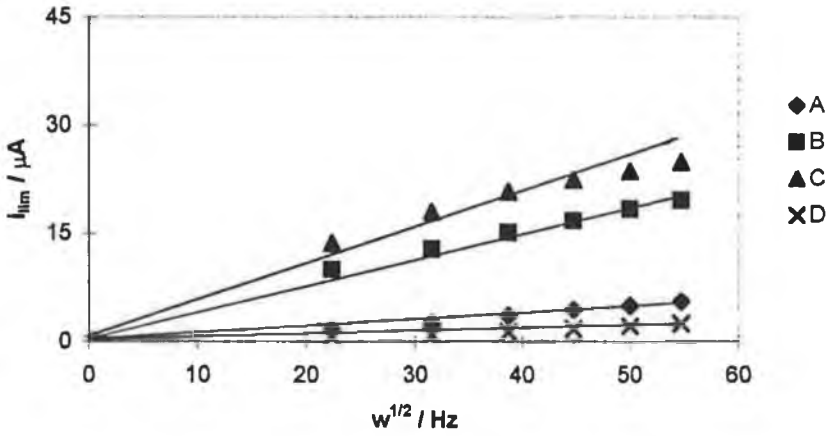


Figure 5.3 Levich plots for the reduction of 100 ppm HClO in 0.1 mol $dm^{-3}$ $KH_2PO_4/K_2HPO_4$ electrolyte at pH 1. A = 5 x $10^{-10}$ mol $cm^{-2}$ $[Os(bpy)_2(PVP)_{10}Cl]Cl$ modified electrode; B = 1 x $10^{-9}$mol $cm^{-2}$ $[Os(bpy)_2(PVP)_{10}Cl]Cl$ modified electrode; C = 2 x $10^{-9}$ mol $cm^{-2}$ $[Os(bpy)_2(PVP)_{10}Cl]Cl$ modified electrode and D = bare glassy carbon electrode.

The electrocatalytic reduction of the free chlorine was examined at pH 1 and pH 6 and the Levich plots thus obtained are illustrated in Figures 5.3 and 5.4. These plots are linear and the intercepts are seen to pass through the same point, the origin.

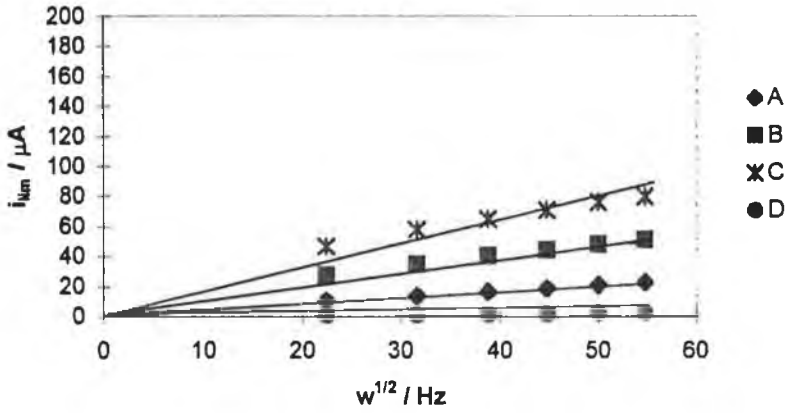


Figure 5.4 Levich plots for the reduction of 100 ppm HClO in 0.1 mol $dm^{-3}$ $KH_2PO_4/K_2HPO_4$ electrolyte at pH 6. A = 5 x $10^{-10}$ mol $cm^{-2}$ $[Os(bpy)_2(PVP)_{10}Cl]Cl$ modified electrode; B = 1 x $10^{-9}$mol $cm^{-2}$ $[Os(bpy)_2(PVP)_{10}Cl]Cl$ modified electrode; C = 2 x $10^{-9}$ mol $cm^{-2}$ $[Os(bpy)_2(PVP)_{10}Cl]Cl$ modified electrode and D = bare glassy carbon electrode.

It should be noted that the currents obtained at pH 6 are greater than those found at pH 1. The corresponding linear Koutecky-Levich plots shown in Figures 5.5, 5.6 and 5.7 also have essentially zero intercepts. This implies that the reduction current is not limited by any process within the film and its rate control is governed by diffusional mass transport in the solution. This would not occur if the chlorine species had to penetrate and permeate through the modifying layer before reacting. This suggests that the steady state current response is independent of layer thickness and the free chlorine is reduced at the polymer layer/solution interface. Which in turn indicates that a surface reaction is more likely than a reaction within the polymer layer.

The theory of Albery et al was used to examine these processes to investigate whether this diagnosis was correct. The inverse slope of the Koutecky-Levich plot for the

modified electrode was found to be $7 \pm 0.1 \times 10^{-4}$ cm $s^{-\frac{1}{2}}$ at pH 6. At the bare glassy carbon electrode the inverse Koutecky-Levich slope was calculated experimentally to be $5.9 \pm 0.15 \times 10^{-4}$ cm $s^{-\frac{1}{2}}$. This slope is slightly smaller and is most likely a product of the less facile electron transfer kinetics at the unmodified electrode. However, experimentally these values may be considered close enough to be the same and, therefore, the kinetic case of LRZtety can be eliminated. It can be observed from the Koutecky-Levich plots that increasing the polymer surface coverage was found not to affect the modified electrode rate constant, $k'_{ME}$, at either pH 1 or 6.

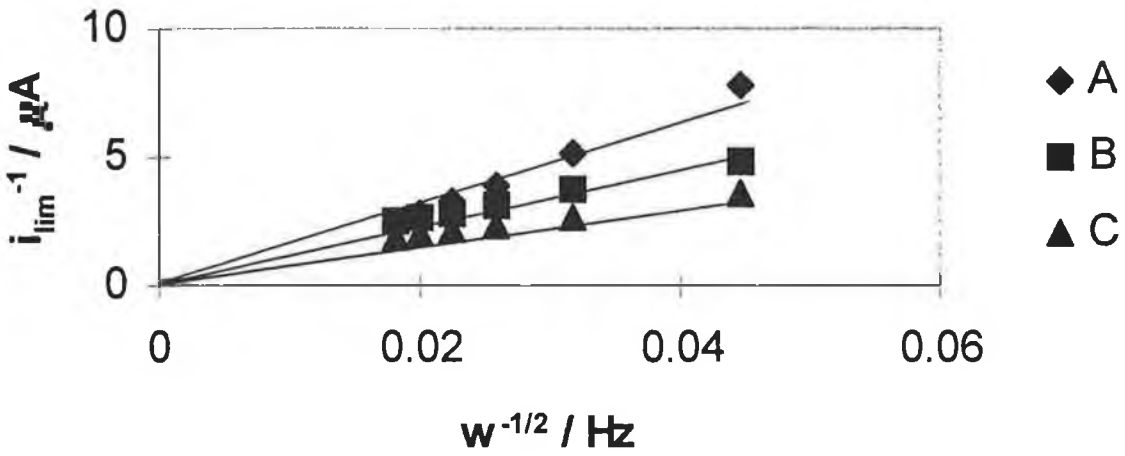


Figure 5.5 Koutecky-Levich plots for the reduction of 100 ppm HClO in 0.1 mol $dm^{-3}$ $KH_2PO_4/K_2HPO_4$ electrolyte at pH 1. A = $5 \times 10^{-10}$mol $cm^{-2}$ $Os(bpy)_2(PVP)_{10}Cl]Cl$ modified electrode; B = $1 \times 10^{-9}$ mol $cm^{-2}$ $[Os(bpy)_2(PVP)_{10}Cl]Cl$ modified electrode; and C = $2 \times 10^{-9}$ mol $cm^{-2}$ $[Os(bpy)_2(PVP)_{10}Cl]Cl$ modified electrode

Therefore, the reaction order with respect to the layer thickness was zero which allows the elimination of the Lk and LEty kinetic cases. The remaining possible kinetic cases are Sk" and LSk. To determine which is appropriate in this case it is necessary to examine the reaction order of the modified electrode rate constant with respect to the concentration of electrocatalytic sites within the polymer film. By varying the electrode potential, the concentration of the electroactive sites, $b_o$, can be

varied as the redox sites immobilised in the polymer film are in thermodynamic equilibrium with the electrode potential and are behaving in a Nernstian fashion. A plot of ln $k'_{ME}$ versus ln f where f is the fraction of the redox centres gives a slope of 1 which allows elimination of the LSk case and indicates that the kinetic regime at both pH 1 and pH 6 is Sk". This demonstrates that the free chlorine is undergoing a mediation reaction only at the surface of the polymer modified electrode. In this situation, the cross-exchange reaction occurs between the solution phase chlorine and the osmium sites at the polymer-solution interface. There is no penetration of the substrate into the polymer with the result that the currents are controlled by substrate diffusion in solution.

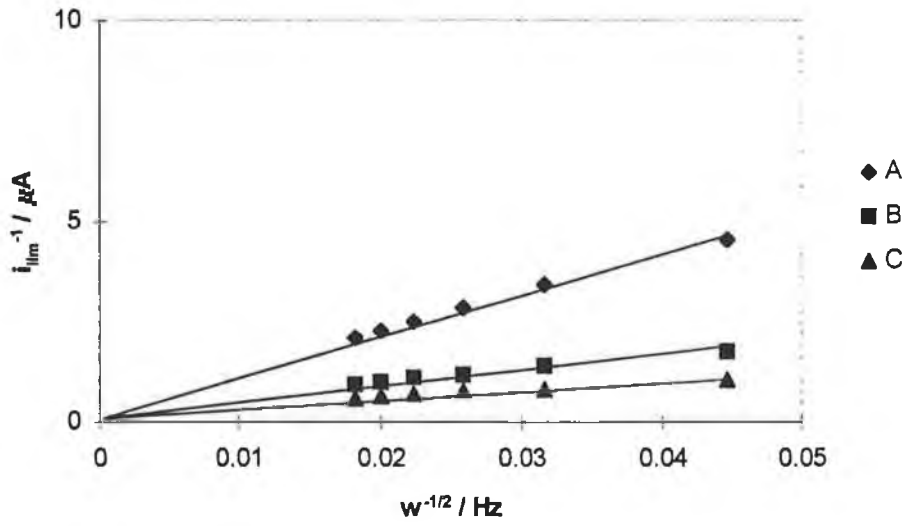


Figure 5.6 Koutecky-Levich plots for the reduction of 100 ppm HClO in 0.1 mol $dm^{-3}$ $KH_2PO_4/K_2HPO_4$ electrolyte at pH 6. A = 5 x $10^{-10}$mol $cm^{-2}$ $Os(bpy)_2(PVP)_{10}Cl]Cl$ modified electrode; B = 1 x $10^{-9}$ mol $cm^{-2}$ $[Os(bpy)_2(PVP)_{10}Cl]Cl$ modified electrode; and C = 2 x $10^{-9}$ mol $cm^{-2}$ $[Os(bpy)_2(PVP)_{10}Cl]Cl$ modified electrode

The second order rate constant, k" , for this reaction can be determined using the relationship $k'_{ME} = nk"b_o$. Table 5.1 shows the values found for $k'_{ME}$ and k" for this modified electrode at both pH 1 and pH 6. As expected, the rate constant was found to be higher at a higher pH. It should be remembered that the Levich plots showed

that currents obtained from this redox polymer also increased with increasing pH.

| pH | $k'_{ME}$ x $10^{-4}$ cm $s^{-1}$ | k" x 10-4 $dm^3$ $mol^{-1}$ cm $s^{-1}$ |
|---|---|---|
| 1 | 0.58 ±0.02 | 4.14 ±0.2 |
| 6 | 1.20 ±0.06 | 8.57 ±0.5 |

Table 5.1 Comparison of the modified rate constant and the second order rate constant for the reduction of HClO at a $[Os(bpy)_2(PVP)_{10}Cl]Cl$ modified electrode in 0.1 mol $dm^{-3}$ phosphate electrolyte at pH 1 and 6.

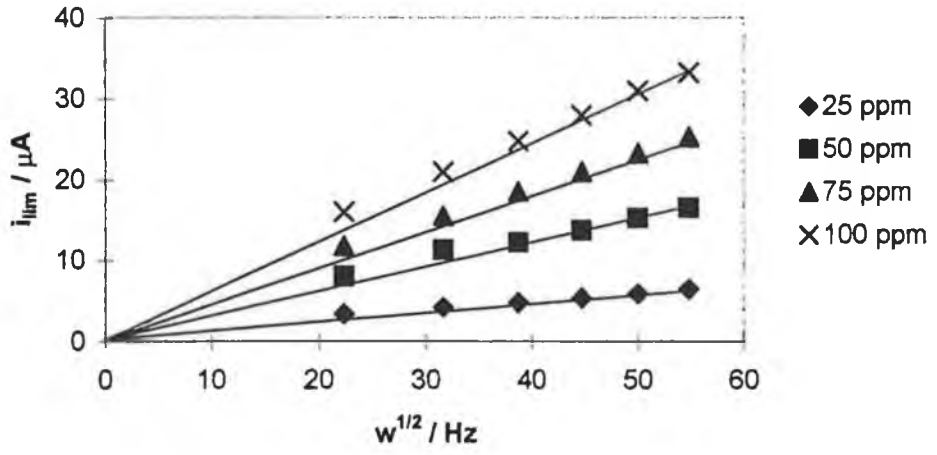


Figure 5.7 Levich plots for the reduction of several different concentrations of HClO at a 1 x $10^{-9}$ mol $cm^{-2}$ $[Os(bpy)_2(PVP)_{10}Cl]Cl$ modified electrode in 0.1 mol $dm^{-3}$ $KH_2PO_4/K_2HPO_4$ electrolyte at pH 6.

## 5.4 Sensor Development

The modified electrode investigated in the previous section on a macroelectrochemical level was then used as the working electrode in a flow injection analysis system and its characteristics as a thin film sensor were examined.

### 5.4.1 Effect of pH

The hydrogen ion concentration of the carrier electrolyte was adjusted and the consequent effect on the response of the modified electrode's response was examined. When injections of 100 ppm of the free chlorine solution were made at pH 1, a response current of 1 mA was obtained. The equivalent response at pH 6 was 3 mA. No response at pH 10 was obtained. Thus the response increased as the pH was increased until the carrier was adjusted to alkaline conditions at which point response ceased. This reflects what had previously been found when the osmium redox polymer was examined using a macroelectrochemical cell. That is, that the current obtained has a linear relationship with the pH of the electrolyte in acidic and neutral environments.

At both pH 1 and pH 6 the electrode gave easily measurable FIA peaks. But because the response was more sensitive at pH 6, it was possible to obtain a significantly enhanced response at the higher pH compared to the lower pH. At pH 1 the limit of detection was found to be 0.7 ppm (S/N = 2) but this limit was lowered by an approximate factor of 10 to 0.05 ppm when the electrolyte pH was increased to pH 6. Consequently, the carrier electrolyte used had a pH of 6 for all future experiments.

### 5.4.2 Effect of Applied Potential

The hydrodynamic voltammogram shown in Figure 5.8 shows the effect of applied potential on the electrochemical sensor's response over the range 0 to 0.5 V vs. SCE. As the voltage is decreased the response to the analyte is seen to increase. This decrease in voltage corresponds to an increase in the formation of Os (II) sites within the modifying film. At higher potentials the Osmium is present as Os (III) which has no catalytic effect on the free chlorine species. As the potential is decreased, the reduction of the Os (III) sites in the layer takes place and Os (II) is formed. The Os (II) then is free to exert its catalytic role. At approximately 0.25 V vs. SCE (the $E^{\frac{1}{2}}$ of the Os (II/III) redox couple) both Os (II) and Os (III) are present in equimolar amounts. Once the potential is lowered beyond this point, the majority of the

osmium present is now in the form of Os (II). This corresponds to a rapid rise in the current response of the sensor to the analyte. After this initial rise there is a smoothing out of the voltammogram until a plateau is reached beyond which a further decrease in voltage causes no comparative increase in current. This corresponds to a limit in the kinetic reaction of the Os (II) with the free chlorine. The maximum number of Os (II) sites is catalytically reacting with the analyte.

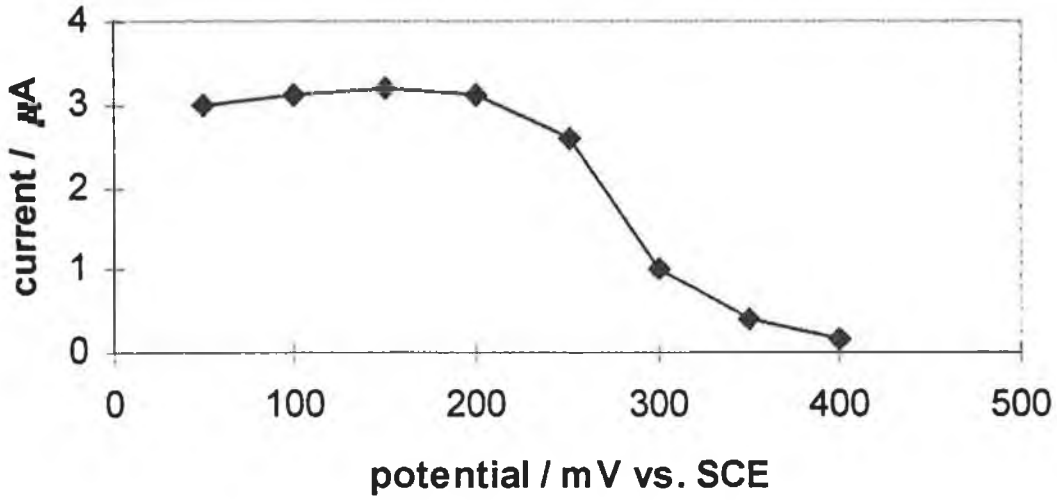


Figure 5.8 Hydrodynamic voltammogram for HClO reduction at a 1 x $10^{-9}$ mol $cm^{-2}$ $[Os(bpy)_2(PVP)_{10}Cl]Cl$ modified electrode in the thin layer electrochemical cell. The buffer was 0.1 mol $dm^{-3}$ phosphate at 1.0 $cm^3$ $min^{-1}$ electrolyte at pH 6. Analyte concentration was 100 ppm.

From the voltammogram a potential of 0.1 V vs. SCE was chosen as the optimum to use in future experiments due to the low number of species which can interfere at this voltage.

### 5.4.3 Effect of Flow Rate

The effect of the carrier flow rate was also examined and measurements were taken between 0.5 and 2 $cm^3$ $min^{-1}$. The relationship between the response (peak height) of the modified electrode and the reaction time, the residence time of the sample zone in

the flow system, was examined and is shown in Figure 5.9. The reaction time was changed by using different flow rates of the carrier stream. It was found that as the flow rate was increased peak currents also increased but the slope of the response peaks decreased.

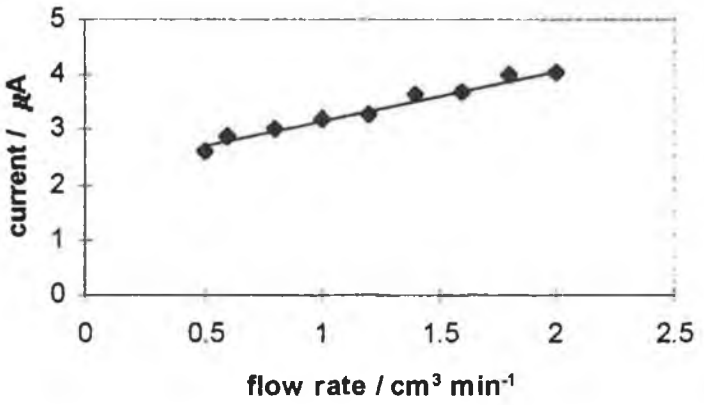


Figure 5.9 Electrolyte flow rate for HClO reduction at a 1 x $10^{-9}$ mol $cm^{-2}$ $[Os(bpy)_2(PVP)_{10}Cl]Cl$ modified electrode in the thin layer electrochemical cell. The buffer was 0.1 mol $dm^{-3}$ phosphate electrolyte at pH 6. Analyte concentration was 100 ppm. Flow rate was 1 $cm^3$ $min^{-1}$.

An optimum flow rate of 1 $cm^3$ $min^{-1}$ was used as this combined a good response with a useful peak shape. The sampling rate was approximately 75 $h^{-1}$ for this procedure using these standard conditions. The dispersing effect of the column was measured where dispersion is the amount that the chemical signal is reduced by injecting a sample plug onto the FIA system. The diffusion, D, of the analyte in this FIA system at 1.0 $cm^3$ $min^{-1}$ was examined by comparing the response obtained to an injection of 10 ppm free chlorine with the response when a similar concentration of analyte was present in the buffer.

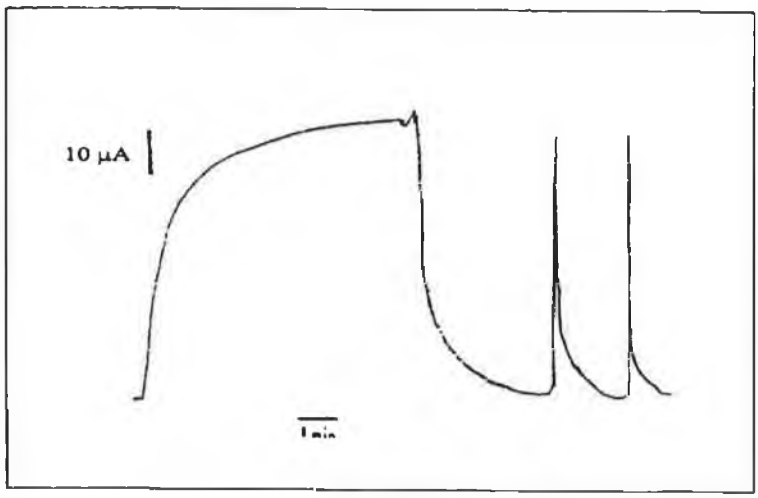


Figure 5.10 Diffusion in FIA system measured using 10 ppm HClO at a 1 x $10^{-9}$ mol $cm^{-2}$ $[Os(bpy)_2(PVP)_{10}Cl]Cl$ modified electrode in the thin layer electrochemical cell. The buffer was 0.1 mol $dm^{-3}$ phosphate at 1.0 $cm^3$ $min^{-1}$ electrolyte at pH 6. Flow rate was 1 $cm^3$ $min^{-1}$. A = response at a steady state and B= response at an FIA peak.

The response in this experiment was derived by measuring the generated currents. It was found that D was 1.03 which shows that very little diffusion was occurring within the flow injection manifold and this gives an indication of the efficiency of the flow injection system. A similar, but slightly smaller value was found in the analysis of iron on a flow injection system as described in Chapter 2.

### 5.4.4 Calibration

The linear range of the electrode's response to the analyte was measured. A linear range was calibrated between 0.1 and 50 ppm free chlorine with a previously described limit of detection of 0.05 ppm (S/N = 2). The modified electrode's reproducibility was found to have an R.S.D. of 0.5 % for 7 repeat injections. The concentration of residual chlorine in city water is usually in the range 0.1 to 0.5 ppm. Therefore, potable water samples will be within the observable range of this sensor.

### 5.4.5 Stability

The stability of this sensor was measured by running the FIA continuously with periodic injections of 100 ppm of the free chlorine. The initial response of the sensor to this injection measured 3 mA. This response remained constant (constant indicates that the variation in peak height between these injections did not exceed 3 % of peak height) for a period of 24 hours but after that time a gradual but rapid deterioration in the response peak was observed. A drop in peak height to half the initial height ($t^{\frac{1}{2}}$) was observed after 30 hours. This compares unfavorably with a similar sensor used for ascorbic acid detection (see chapter 6) which displayed a constant response for at least 60 hours. Generally such cross-linked modified electrodes do not display a decline in response until the severe hydrodynamic conditions present in FIA systems have caused physical wear and tear on the modified layer. It appears that the free chlorine under examination in this chapter is causing a decline in the integrity of the modifying layer sooner than would otherwise be expected. This analyte has been noted for causing surface changes in other electrochemical sensors [20,23]. It is possible that the surface wearing ability of the free chlorine species in conjunction with the hydrodynamic conditions present in the flow system combined to cause the shortening in the lifetime of the modifying surface.

### 5.4.6 Interferences

The effect of a number of ions which may be present in potable water was measured by mixing a solution of 100 ppm of the analyte with 1000 ppm of the possibly interfering species. Ionic species such as Ca(II), Mg(II), Na(I) and K(I) had no effect on the sensor's response to the free chlorine, even when present in concentrations much greater than the analyte's. The anionic ions Sulphate, $SO_4^{2-}$, and nitrate, $NO_3^-$, were also found not to interfere.

### 5.4.7 Application to Real Samples

Samples of water from the standard city water supply system were collected and injected onto the FIA. Table 5.2 shows the results obtained for a number of such experiments and also the equivalent amounts of residual chlorine found in these samples when analysed using the standard titration procedure. Good agreement was found between the two different methods.

| Water Sample | Modified Sensor ppm HClO | Standard Titration ppm HClO |
|---|---|---|
| 1 | 0.32 | 0.30 |
| 2 | 0.45 | 0.49 |
| 3 | 0.32 | 0.33 |

Table 5.2 Results of the comparative determination of the free chlorine concentration of a number of potable water samples using the modified electrode sensor and the standard iodometric titration procedure.

## 5.5 Conclusion

The $[Os(bpy)_2(PVP)_{10}Cl]Cl$ modified electrode was found to be an efficient and effective electrocatalyst for the reduction of free chlorine at acidic and neutral pH values. Its kinetic regime was found to be a surface type, Sk", and this did not change with changes in pH. Since the formal potential for the chlorine species' reduction is so much higher than the potential at which the electrocatalyst successfully mediated it, the free energy difference ($\Delta G$) between these species and the osmium electrocatalyst is negative and so is expected to occur spontaneously. However, mediation was not found to occur in highly alkaline pH environments (> pH 10).

The facile nature of the electrocatalytic reduction process allowed application of the osmium-modified electrode as a reasonably stable and reproducible electrochemical

sensor for free chlorine detection. Its linear range, low limit of detection, rapid response time and high sample throughput are of considerable advantage in the development of a sensor.

The technique proposed here offers many improvements over the standard manual methods. First, it is faster with the ability to process up to 75 samples per hour compared with 20-40 min per sample for the batch method. Second, it is simpler, as flow injection analysis eliminates the need for any air-exclusion step such as is necessary in the batch method due to use of a hexane layer. The limit of detection of 0.05 ppm is similar to other research using flow injection teamed with amperometric detection which was measured at 0.06 ppm [21]. Finally, the sensitivity of this method compares with the standard method.

## 5.6 References


1. S. W. Kubala, D. C. Tilotta, M. A. Busch, K. W. Busch, Anal. Chem., 61 (1989) 2785
2. D. B. Easty, J. E. Johnson, A. A. Webb, Pap-Puu, 68 (1986) 415
3. E. P. Achterberg, C. M. G. van den Berg, Anal. Chim. Acta, 291 (1994) 213
4. E. Pip, Urban Drinking Water Quality: A Survey of Selected Literature, Institute of Urban Studies, Winnepeg, Manitoba, 1993, p.43 - 46
5. P. de Witt, J. J. Kelly, J. Electroanal. Chem., 336 (1992) 125
6. A. E. Greenberg, R. R. Trussell, L. S. Clesceri, Standard Methods for the Examination of Water and Wastewater, American Public Health Association, Washington, DC, Sixteenth Edition, 1985, p. 286 - 327
7. M. Hahn, A. Liebau, H. H. Ruttinger, R. Thamm, Anal. Chim. Acta, 289 (1994) 35

8. M. Khan, M. Kasha, Proc. Natl. Acad. Sci. USA, 91 (1994) 12362

9. R. Clark, S. Summers, Strategies and Technologies for Meeting SDWA Requirements, Technomic Publishing Co. Ltd., Lancaster, Pennsylvania, 1993, p. 190-194

10. C. Anderson, Nature, 354 (1991) 255

11. D. L. Swerdlow, E. D. Mintz, M. Rodriguez, E. Tejada, C. Ocampo, L. Espejo, K. D.Greene, W. Saldana, L. Seminario, R. V. Tauxe, J. G. Wells, N. H. Bean, A. A. Ries, M. Pollack, B. Veritz, P. A. Blake, The Lancet, 340 (1992) 28

12. N. Ishibashi, T. Imato, H. Ohura, S. Yamasaki, Anal. Chim. Acta, 214 (1988) 349

13. F. Quentel, C. Elleouet, C. Madec, Anal. Chim. Acta, 295 (1994) 85

14. D. G. Themelis, D. W. Wood, G. Gordon, Anal. Chim. Acta, 225 (1989) 437

15. G. P. Irons, G. M. Greenway, Anal. Proc., 31 (1994) 91

16. D. Gonzalez-Robledo, M. Silva, D. Perez-Bendito, Anal. Chim. Acta, 228 (1990) 123

17. T. Nakagama, M. Yamada, T. Hobo, Anal. Chim. Acta, 231 (1990) 7

18. T. Nakagama, M. Yamada, T. Hobo, Analyst, 114 (1989) 1275

19. G. P. Irons, G. M. Greenway, Analyst, 120 (1995) 477

20. A. N. Tsaousis, C. O. Huber, Anal. Chim. Acta, 178 (1985) 319

21. A. Y. Chamsi, A. G. Fogg, Analyst, 111 (1986) 879

22. A. Ivaska, P. Forsberg, R. Heikka, Anal. Chim. Acta, 238 (1990) 223

23. A. G. Fogg, A. Y. Chamsi, A. A. Barros, J. O. Cabral, Analyst, 109 (1984) 901

24. J. A. Chesney, J. R. Mahoney, J. W. Eaton, Anal. Biochem., 196 (1991) 262

25. Y. Xie, C. O. Huber, Anal. Chem., 63 (1991) 208

26. S. Motomizu, T. Yoden, Anal. Chim. Acta, 261 (1992) 461

27. T-F. Tang, G. Gordon, Anal. Chem., 52 (1980) 1430

28. L. C. Adam, G. Gordon, Anal. Chem., 67 (1995) 535

29. C. Piraud, E. Mwarania, G. Wylangowski, J. Wilkinson, K. O'Dwyer, D. J. Schiffrin, Anal. Chem., 64 (1992) 651

30. S. Dennison, D. M. Bonnick, Anal. Proc., 32 (1995) 13

31. A. H. J. Paterson, R. J. Kerekes, J. Assoc. Off. Anal. Chem., 67 (1984) 132

32. T. Pal, A. Ganguly, D. S. Maity, Chem. Anal., 33 (1988) 703

33. B. Chiswell, K. R. O'Halloran, Anal. Chim. Acta, 249 (1991) 519

34. B. Chiswell, K. R. O'Halloran, Analyst, 116 (1991) 657

35. I. J. Fletcher, P. Hemmings, Analyst, 110 (1985) 695

36. J. F. Coetzee, C. Gunaratna, Anal. Chem., 58 (1986) 650

37. G. E. Pacey, D. A. Hollowell, K. G. Miller, M. R. Straka, G. Gordon, Anal. Chim. Acta, 179 (1986) 259

38. L. C. Adam, I. Fabian, K. Suzuki, G. Gordon, Inorg Chem., 31 (1992) 3534

39. D. A. Skoog, D. M. West, F. J. Holler, Fundamentals of Analytical Chemistry, 5th ed., Saunders College Publishing, New York, 1988

# Chapter 6

## Development of an Electrochemical Sensor for the Detection of Ascorbic Acid

## 6.1 Introduction

### 6.1.1 Biological Importance of Ascorbic Acid

Ascorbic acid's role in the prevention of scurvy is well known and there are many historical accounts of sea voyages which were subject to a mysterious disease which caused hemorrhaging, bleeding gums, loss of teeth, anemia, weakness and eventually death. The role of fresh fruits and vegetables in preventing this disease was not formally acknowledged until James Lind, a Scottish surgeon, published a treatise on the subject in which he suggested that oranges and lemons were the best remedy for this affliction.

However, it was not until the twentieth century that the efficacious substance in fruit and vegetables was isolated and identified. Szent-Gyorgyi won the Nobel Prize for Medicine in 1937 for "his discoveries concerning the biological oxidation processes with special reference to vitamin C". In the same year Norman Haworth received the Nobel Prize for Chemistry for his work on " the structure of carbohydrates and vitamin C". As such, vitamin C, or ascorbic acid, was one of the earliest vitamins to have its structure determined and its chemistry has been studied for sixty years. Even so, new aspects of this apparently simple compound are being revealed each year and any perusal of a chemical journal would show a number of recent papers whose theme was a newly discovered aspect of this molecule's chemistry.

The metabolism of ascorbic acid has not yet been completely characterized and its physiological role, though it has been pursued by many researchers, has not yet been satisfactorily explained. The requirement for ascorbic acid by all plants and animals, i.e. all eucaryote organisms, is acknowledged but the significance of such a universal presence is unknown. Equally interesting is the absence of ascorbic acid from procaryote organisms This again points to some unknown yet essential difference between these two forms of living organisms in which the function of ascorbic acid has yet to be clarified.

Ascorbic acid is a chiral compound and only the L-enantiomer is biologically active [1]. The oxidation of L-ascorbic acid to dehydro-L-ascorbic acid occurs under very facile

conditions followed by further oxidation to produce degradation products. L-ascorbic acid is commonly known as vitamin C. Vitamin C has also been described as the sum of L-ascorbic acid and dehydroascorbic acid present in biological samples. This is because dehydroascorbic acid has a similar, but reduced, biological effect as ascorbic acid. Both reduced (ascorbic acid) and oxidised (dehydroascorbic acid) vitamin C are present in biological systems. Dehydroascorbic acid diffuses through cell membranes more efficiently than ascorbic acid.

Ascorbic acid is classified as a carbohydrate and it has the chemical structure 1-keto-1-threo-hexono-g-lactone-2,3-enediol. It is the enediol group which is responsible for the acidic and reducing properties of the molecule. Vitamin C is a cofactor for protocollagen hydroxylase which is responsible for the posttranslational modification of proline and lysine residues in connective tissue peptides. As a result, deficient levels of this vitamin manifest as the aforementioned scurvy. With symptoms including swollen tender joints, bleeding gums cutaneous bleeding, pinpoint hemorrhages and bruises. Scurvy is now an uncommon illness, especially in the western world. A number of groups within society do, however, remain vulnerable to a deficiency of vitamin C. These include the elderly who might not eat a balanced diet, and smokers, as smoking causes the rapid deterioration in physiological levels of this vitamin. Vitamin C also acts as an organic reducing compound and consequently takes part in antioxidant activity. As an allied function it increases iron absorption by reducing dietary ferric iron.

The usefulness large doses of vitamin C has, however, become a source of controversy. The necessity of ingesting a daily amount to prevent the onset of scurvy is not disputed. What is contentious is the level required for optimum health (the "Recommended Daily Amount") and the appropriateness of taking large amounts (megadoses) of the compound, especially by those suffering from cancer. The most famous advocate for this treatment was the late Nobel-winning chemist Linus Pauling. He believed that daily doses of 10g of vitamin C could retard the growth of tumors in cancer patients and generally improve the longevity and quality of their lives. However, his thesis has caused much acrimonious dispute with accusations of badly designed studies and failure to assess novel treatments. [2-4]

It has been postulated that a danger with taking such large doses of vitamin C is the effect on the body when such doses are stopped suddenly, the so called 'rebound effect'. If a person suddenly stops taking daily megadoses , the level of vitamin C circulating in their body drops far below normal. This is because the body is used to catabolising it at an increased rate and metabolic adjustment to lower levels may take some weeks, meanwhile the physiological level of ascorbic acid has drastically fallen. However, recent reports have suggested that there may be more serious effects of ingesting large quantities of ascorbic acid on a daily basis.

It is theorized that the beneficial effects of ascorbic acid are as a result of its antioxidative properties [5]. Oxygen is essential for all aerobic life. However, it forms free radicals in the body and evidence suggests the action of such electrophillic species may cause physiological phenomena such as aging, carcinogenesis, drug toxicity and inflammation. It has a toxic effect when present in high concentrations and it has been shown to cause growth abnormalities in plants and to inhibit chloroplast development. The reduction of oxygen to the superoxide free radical and hydrogen peroxide and the formation of singlet oxygen are believed to be the source of this toxic effect found in plants. Ascorbic acid is present in chloroplasts in millimolar concentrations and it is now believed that it acts to protect the chloroplast against toxic oxygen derived species by acting as a scavenger of superoxide, hydroxyl radicals and singlet oxygen. Dehydroascorbic acid is considered to be the form of the vitamin which crosses the cell membranes. When ascorbic acid is oxidised to dehydroascorbic acid, it is believed that vitamin E is kept in a reduced state. Thereby stabilising the presence in the body of another antioxidative species.

The addition of ascorbic acid to plant cells exposed to ozone exhibited an alleviation of its respiratory inhibiting effects [6]. Work suggested that plants may protect themselves from the harmful effects of ozone by concentrating ascorbic acid in their cell walls. By reacting with ozone in the cell wall, the ascorbic acid prevents the ozone from penetrating further into the more vulnerable parts of the cell. This effect could prove very useful due to the increasing problem of air pollution which has been associated with crop loss and forest depletion.

The formation of oxygen radicals and lipid peroxidation are also believed to play a major role in carcinogenic and mutagenic mechanisms by contributing heavily to DNA damage in animals. Ascorbic acid has been shown to have an antioxidant effect and almost completely checks peroxidation [7] Its role as a redox buffer in reducing oxidised tocopherol radicals in biological membranes in order to maintain vitamin E levels in tissues has also been documented [7,8] It has demonstrated an anticarcinogenic effect in laboratory animals exposed to ultraviolet radiation, benzo[a]pyrene and nitrite, which forms nitroso carcinogenic compounds. Low levels of ascorbic acid have also been linked to human uterine cervical dysplasia. Ascorbic acid has been linked with male fertility as ascorbic acid is about eight times more concentrated in seminal fluid than in blood plasma. It has been found to protect DNA in sperm and also appears to protect biomolecules such as lipids which are associated with sperm motility [9].

The use of ascorbate as an antiatheroslerotic drug has been recently postulated [10]. It is believed that antioxidants trap radicals which cause oxidative modification of low density lipoproteins which may be involved in the development of atheroslerotic lesions. Removal of the radicals therefore may lessen the risk of developing ischemic heart disease.

An anti-cancer compound based on ascorbic acid has been documented based on the molecule cis-diamminedichloroplatinum II [11]. Previously this molecule has anti-cancer properties itself but also displays severe side effects [12]. Kidney failure was caused by the platinum component of this drug. A complex in which this molecule is attached to ascorbic acid has shown efficacy when used to treat mouse tumors. The vitamin C-*cis*-diamminedichloroplatinum II complex contains a Platinum-Carbon bond rather than a Platinum-Oxygen bond and as such is the first example of a carbon bound analogue of *cis*-diamineplatinum II to display good anti-tumor activity *in vivo*.

### 6.1.2 Applications of Ascorbic Acid

Interactions of ascorbic acid with metal ions, especially transition metals has been a rich source of study [13-15] Ascorbic acid is a common ingredient in pharmaceutical

preparations, particularly multivitamin supplements and cold remedies [16]. It has also been found to have beneficial effects on germination and root growth. Most animals can synthesize ascorbic acid. Among the exceptions are guinea pigs, insects, fish and humans. Ascorbic acid is added to food to replace the loss of the vitamin due to processing. It is also added due to its preservative effect and to prevent oxidation. Ascorbic acid can be oxidised in both basic and acidic environments and is used as an antioxidising agent in the food industry. It is also commonly used in the baking industry due to its use as a flour improver. How the vitamin acts in the bread mixture is not fully understood but the L-ascorbic acid improves the texture of bread when it is added to the dough.

The manufacture of ascorbic acid is now a profitable industry due to its popular uses as an additive in the aforementioned foods and beverages and as a vitamin supplement. The world-wide market for L-ascorbic acid is worth approximately $400 million. Consequently, new methods of producing large amounts of this substance cheaply are being investigated. One of the more novel methods recently described is that of the application of recombinant DNA technology to this process. The construction of a recombinant metabolically engineered bacterial strain, Erwinia herbicola, that is able to synthesise 2-keto-L-gulonic acid, a key intermediate in the production of ascorbic acid, has been reported. The bacterial approach to production of this vitamin has the advantage of automatically preventing racemisation. Ascorbic acid is a chiral compound with only one version actually being useful and this bacterial manufacturing process only produces the enzymatically useful version of the vitamin [17]

L-ascorbic acid has many other applications. Ascorbate has been used as an electron donor in the investigation of electron transfer properties of novel compounds such as buckminsterfullerene. [18] Ascorbic acid has also been examined for its potential in metallic reductions, coating technology, electroplating processes and control of oxidation. The chemically modifying effect of ascorbic acid on graphite furnace atomic absorption signals has been well documented [19, 20].

The presence of ascorbic acid in food can also give rise to unwanted side effects. It has been demonstrated that oxidative degradation of ascorbic acid to dehydroascorbic acid and its further reaction with other compounds such as sugars leads to non-enzymatic browning in citrus juices. This is a major factor in the deterioration of such foodstuffs [21]. Greater concern is caused by recent work which demonstrates that hydroxyl radicals, which can be formed as previously demonstrated by the metal catalysed reduction of oxygen and peroxide by ascorbic acid, can react with benzoic acid to produce benzene [22]. Sodium benzoate is a common food preserving agent with its antimicrobial activity effective at low pH. As such, the conditions in which it could react with ascorbic acid, especially acidic beverages, are prevalent.

### 6.1.3 Analysis of Ascorbic Acid

Analytical techniques for the assay of ascorbic acid are many and varied. Certain properties of ascorbic acid must be considered before a technique is considered as the optimum. In aqueous solution, ascorbic acid can be oxidised due to atmospheric oxygen, therefore analysis must take place under an inert atmosphere or the analysis must take place with minimum delay. This decomposition can be accelerated by a number of factors which are heat, light, alkalis, oxidative enzymes and the presence of trace amounts of iron or copper. This oxidation can be slowed by using an acidic medium or by reducing the experimental temperature. Instability can also be caused by microbial metabolism. [23]

A number of techniques have been reported for the determination of ascorbic acid. Titration with 2,6-dichlorophenolindophenol to its reduced form is commonly used [24]. This dye has also been used in spectrophotometric determinations. However this reagent is unstable and cannot always be applied to coloured samples. It requires correction factors for co-oxidisable species present in the sample matrix. Spectrophotometric methods can be direct or indirect, and often have complex and time consuming designs [25, 26]. Factors such as the timescale, temperature and pH have to be carefully controlled. The fluorometric and liquid chromatographic techniques can be very sensitive, however the equipment used can be expensive and not easily available. A

method for the catalytic, kinetic determination of ascorbic acid with single-sweep oscillopolarography has been reported [27] but the procedure is long and inconvenient. Use of the oxidoreductase enzyme ascorbate oxidase as a selective oxidative catalyst for ascorbate has received some attention. This enzyme catalyzes the oxidation of ascorbate in the presence of oxygen. However background levels of reductants must be separately analysed.

The determination of ascorbate and dehydroascorbate has been demonstrated in leaf tissue by the technique of reduction of Fe(III) to Fe(II) by ascorbate and then spectrophotometrically measuring the Fe(II) complexed with 2,2'-dipyridyl. Measurement of dehydroascorbate is effected by a difference calculation after its reduction to ascorbate by preincubation with dithiothreitol [28].

The technique of ESR has also been applied to the determination of ascorbate. One study reported its use in determining ascorbate radicals in fresh cows milk and investigated its reported antimicrobial activity in the milk. [29] The study found evidence to suggest that ascorbate plays a role in preventing peroxidation of milk lipids which cause rancidity.

Ion-pairing high-performance liquid chromatography with electrochemical detection is a common method for use in the determination of electroactive substances and has been applied to the analysis of ascorbic acid. It is especially useful in the analysis of its transformation products and has been used in determining the main catabolic pathways of ascorbic acid in mammalian tissue [30]

In biological samples, spectroscopic analysis is a common means of determination. HPLC allied to UV-Vis detection is commonly used [31, 32]. These electroanalytic methods can be cumbersome and time-consuming and inaccurate due to interferences from other substances present in biological samples. The addition of HPLC to these methods of detection is a common method of overcoming these limitations [33, 34]. However, these methods can often involve complex manifolds such that sample pretreatment requires relatively large sample volumes with a long analysis time. Due to the highly unstable nature of ascorbic acid, it is desirable that the analysis takes as short a

time as possible. Many of these techniques can only be applied to one type of sample matrix [35].

2nd and 3rd order derivative spectrophotometric techniques have been used for the analysis of ascorbic acid in soft drinks. [36] This technique can be subjected to interference from additives and colouring agents in the drinks and therefore must be compared with a sample blank in which all the ascorbic acid has been destroyed. This can be a time-consuming process involving the addition of a metal catalyst and the thermostatic control of the samples.

A chemiluminescent assay for ascorbic acid in juices has been developed. This method involved stopped flow analysis with the addition of hydrogen peroxide, luminol and peroxidase to induce chemiluminescence. [37]

A recently published paper compared methods used by a number of different laboratories to determine ascorbic acid levels in foodstuffs using their routine methods [38]. The differences between the laboratories were found to be rather high with RSDs of 15% to 23%. HPLC with fluorescent detection was commonly used. This required oxidation of ascorbic acid to dehydroascorbic acid and subsequent reaction with o-phenylenediamine to form a fluorescent quinoxaline. Other methods used included the enzymatic oxidation of the ascorbic acid and oxidation of ascorbic acid with activated carbon. Other laboratories used methods such as HPLC with applied UV detection which measures only the ascorbic acid content. The classical dichlorophenolindophenol titration was also used to determine ascorbic acid. The endpoint is described as sluggish and is hard to discern. This indicator cannot be used with highly coloured samples and is reduced by iron(II) species which are commonly present in multivitamin supplements [39, 40]

Electrochemical methods of ascorbic acid detection have also received widespread examination and a number of reviews of such techniques have appeared recently [41-43]. Ascorbic acid has a low potential value, $E_o$ = 54 mV, but it experiences high overpotentials when undergoing electrochemical oxidation at metal and carbon-based electrodes. And consequently it experiences interference by other oxidisable substances

present in real biological solutions. The bare electrode surface also undergoes fouling after a relatively short time resulting in a progressive deterioration in sensing ability. Pretreatment processes on carbon electrodes have been found to suffer less from surface fouling [44], but sluggish electron transfer kinetics remain. Attempts to overcome this include the use of thick film graphite electrodes and of optical pyrolytic graphite disk electrodes. [45] These electrodes were found to be less sensitive at higher concentrations of ascorbic acid, perhaps due to the electrode surface undergoing fouling.

More common methods of determining ascorbic acid electrochemically involve modifying the surfaces of these electrodes with electrocatalytic compounds so that the electrochemical oxidation of ascorbic acid can be persuaded to proceed at a lower potential. A number of electrocatalysts have been examined for their suitability for such a role as chemical modifiers. These modified electrodes have then been applied to the development of analytical assays for ascorbic acid determination in fruit juices [46]. The microdisk electrodes used in that study were affected by other redox compounds present in the samples. Compounds such as p-tetracyanoquinodimethane, ferrocene, 1,1'-dimethylferrocene and tetrathiafulvalene have been used to modify graphite electrodes [47]. This modified electrode was stable and could detect ascorbic acid in juices in the millimolar range. An organic conducting salt electrode based on tetrathiafulvalene-*p*-tetracyanoquinodimethane was used to determine the concentration of ascorbate in aqueous samples [48]. The modifier allowed low operating potentials to be used which removed interference effects from other reductants present in the sample. However, this electrode was found to be strongly dependent on pH and it was necessary to use the electrode between pH 7.5 and 9.0. Buffer concentration was also found to have an effect on the electrode's response.

The electrocatalysis of ascorbic acid oxidation has also been undertaken using polymeric layers coated on electrode surfaces. A study described a polypyrrole coated electrode used for such a purpose. [49] Oxidised polypyrrole films contain within them cationic sites which minimise the electrostatic repulsion between the ascorbate anion and the polymer surface. In this study the polypyrrole was doped with chloride ion and dodecylbenzene sulphonate ion. However, experimental conditions necessitated that the

electrode potential was high, 500 mV, so as to hold the polymer in its electronically conducting form.

Electrooxidation of ascorbic acid at a bis(4-pyridyl)disulfide modified gold electrode was studied [50]. It was shown that the oxidation process was pH dependent with diffusion controlled oxidation at pH < 5.5. It was necessary to carry out deoxygenation of the analyte-containing solutions before analysis.

Other electrodes studied have been modified by prussian blue [51], polypyrrole-9-dodecyl sulphate [52] and 7,7,7,7-tetracyanoquinodimethane [53]. Initial work on these modified electrodes indicates that they may be applied to the determination of ascorbic acid in more complex matrices but problems such as lack of specificity have first to be overcome.

Other electrochemical techniques have been used such as ion-selective electrodes [54] and enzyme modified electrodes [55]. The ion-selective electrode method involved the direct potentiometric titration of ascorbic acid with copper sulphate using a copper (II) Ion Selective Electrode to monitor the reaction. Due to the slowness of the titration it was necessary to titrate in an inert atmosphere in order to prevent atmospheric oxidation of the ascorbic acid. The enzyme based sensor was prone to instability and experimental conditions had to be closely controlled.

A method now receiving widespread application is that of Flow Injection Analysis (FIA). The advantages of flow injection analysis techniques include simplicity of design and concept and ease of automation. The FIA system allows a reproducible response to be monitored. However the use of FIA techniques in food analysis has not yet received wide application due to the complexity of the sample matrices [56]. Because there is no separation step involved in the design of the manifold, the detection must be selective and not prone to fouling.

An FIA technique has exploited the use of cerium (IV) as a titrant of ascorbic acid by monitoring the decrease in its absorbance spectrophotometrically. [57] The cerium (IV)

oxidises the ascorbic acid to dehydroascorbic acid in the presence of sulphuric acid Ascorbic acid has also been found to react with potassium iodate in the presence of hydrochloric acid to produce a coloured product which on extraction with carbon tetrachloride can be determined spectrophotometrically [58] A polarographic method has been proposed based on the anodic polarographic waves produced in Walpole acetate buffer at acidic pH [59].

As demonstrated above, a variety of analytical procedures are available for the detection of ascorbic acid. However, no one technique is completely satisfactory due to the numerous interfering species contained in sample matrices. This in turn emphasizes the lack of specificity of most techniques. The foregoing description of the many techniques currently being employed for the determination of ascorbic acid in various media demonstrate a number of advantages and disadvantages. Colorimetric and spectroscopic methods are reproducible and stable but are subject to interference from coloured samples. In addition, the detection equipment is often complex and expensive. Electrochemical techniques suffer from the sluggish kinetics associated with ascorbic acid and also from the fouling of the electrode surface due to accumulation of oxidative products. Enzymatic methods, though sensitive, are prone to interference. A method of determination is required which is stable and not subject to fouling or contamination; is free from a wide range of interfering species; is sensitive to ascorbic acid over a large concentration range; and is reproducible in its response. The sensor which will be described in this chapter is based on a redox electropolymer modified electrode used as the working electrode in a flow injection manifold. This sensor will be shown to demonstrate stability, sensitivity and selectivity towards ascorbic acid in real samples whilst delivering a reproducible response.

## 6.2 Experimental

### 6.2.1 Synthesis

The synthesis of the redox materials $[Os(bpy)_2(PVP)_{10}Cl]Cl$ and $[Ru(bpy)_2(PVP)_{10}Cl]Cl$ was described in chapter 2 of this thesis.

### 6.2.2 Reagents

In the flow injection experiments, the electrolyte was prepared from analytical reagent grade $K_2HPO_4$ and $KH_2PO_4$ (Aldrich) to produce 0.1 mol $dm^{-3}$ phosphate buffer, the pH of which was adjusted to 7.0 with 1M KOH. In the cyclic voltammetric experiments 0.1 mol $dm^{-3}$ $Na_2SO_4$ was used. The ascorbic acid solutions were prepared immediately prior to use. All the solutions used throughout were prepared freshly from MilliQ water and protected from light.

### 6.2.3 Apparatus

Cyclic voltammetry and RDE voltammetry were carried out using a conventional three electrode assembly. The potentiostat used was the EG&G Princeton Applied Research Model 362. The rotating disc assembly was the Metrohm Model 629-10 RDE. Voltammograms were recorded on a Linseis X-Y recorder. The working electrodes were 3 mm diameter glassy carbon discs encased in Teflon and supplied by Metrohm. The electrodes were polished 5 mm alumina prior to addition of the modifying layer. Modification was by a drop coating technique using a solution that was 1% w/v of the redox polymer in methanol. This layer was then cross-linked by the addition of a methanolic solution of 1,10-dibromodecane. Surface coverages were determined by integration of the charge (Q) under a sweep rate cyclic voltammogram of 1 mV/s where Q = nFT and T is the number of active sites, n = number of electrons and F is Faraday's constant. The counter electrode was 1$cm^2$ platinum gauze placed in proximity to the working electrode. The reference electrode was saturated KCl calomel electrode (SCE). All potentials are quoted with respect to SCE. All measurements took place at room temperature.

The flow injection apparatus consisted of an EG&G Princeton Applied Research Model 400 electrochemical detector fitted with a thin-layer flow cell, a Gilson Minipuls 3 peristaltic pump, a six-port Rheodyne injection valve with a 20 µl fixed-volume sample loop and a Philips PM 8252 X-t recorder. The working electrodes were 3 mm glassy carbon shrouded in Teflon (EG&G) and were modified as described above. The

Ag/AgCl electrode acted as the reference while the stainless-steel body cell body acted as the counter electrode. Potentials are quoted after conversion to the SCE scale. Silicone rubber tubing was used at the pump and Teflon 1/16 in od x 1/32 in id tubing for the rest of the system. Sample injections were made using a 2 $cm^3$ glass syringe fitted with a Rheodyne square-tipped injection needle.

### 6.2.4 Standard Method of Analysis

A standard method of analysis described by Petersson was used for comparing the analytical results obtained by the sensor under investigation [60]. The standard method involved a colorimetric titration with 2,6-indodiphenol as the colour-changing reagent. The reagent contained 0.025g of the phenol compound made up to 100 $cm^3$ with 0.021 g $NaHCO_3$. A solution of 0.1 g ascorbic acid was made up to 100 ml in 3% m-phosphoric acid and 20 mg EDTA. A 1/10 dilution of this solution was titrated with the reagent and used as a reference to allow the calculation of the number of cubic centimeters of reagent was equivalent to 1 mg of ascorbic acid.

## 6.3 Results and Discussion

### 6.3.1 Kinetics and Mechanism

In Figure 6.1(a,b) cyclic voltammograms of the redox polymers $[Os(bpy)_2(PVP)_{10}Cl]Cl$ and $[Ru(bpy)_2(PVP)_{10}Cl]Cl$ are shown. The surface coverage is 1.0 x $10^{-9}$ mol $cm^{-3}$ and the electrolyte is 0.1 mol $dm^{-3}$ $Na_2SO_4$. The CV shows a single reversible oxidation/reduction process corresponding to (a) the Os (II/III) redox couple and (b) the Ru (II/III) couple. The half wave potential of the Os couple is 250 mV vs. SCE and for the corresponding Ru couple the half wave potential is 750 mV vs. SCE. A number of general comments can be made regarding their redox characteristics. The peak-to-peak separation is essentially zero and the peak width at half height is approximately 90 mV. The anodic peak currents, $i_{pa}$, were found to increase linearly as a function of potential

sweep rate up to a scan rate of 100 mV $s^{-1}$, thereby demonstrating finite diffusion behavior. These results closely mimic the ideal behavior expected of a surface immobilised redox species in thermodynamic equilibrium with the electrode potential. [61]

Previous work has characterised the formal potentials for ascorbic acid oxidation at various pH values [62]. Therefore, any study of the mechanism of the ascorbic acid reaction in aqueous solution will be influenced by the effect of pH on the nature of the reactants. Changing the pH will not only affect the protonation of both the polymer layer and the ascorbic acid species, but also the driving force of the mediated reaction. At pH 7.0, the $E_o$ is -0.187 V vs. SCE and at pH 5.0, $E_o$ is -0.105 V vs. SCE. Therefore the formal potential for ascorbic acid oxidation is cathodic of the formal potentials of both the electropolymers being examined. Consequently, mediation of the oxidation of ascorbic acid is thermodynamically feasible by the redox polymer under consideration.

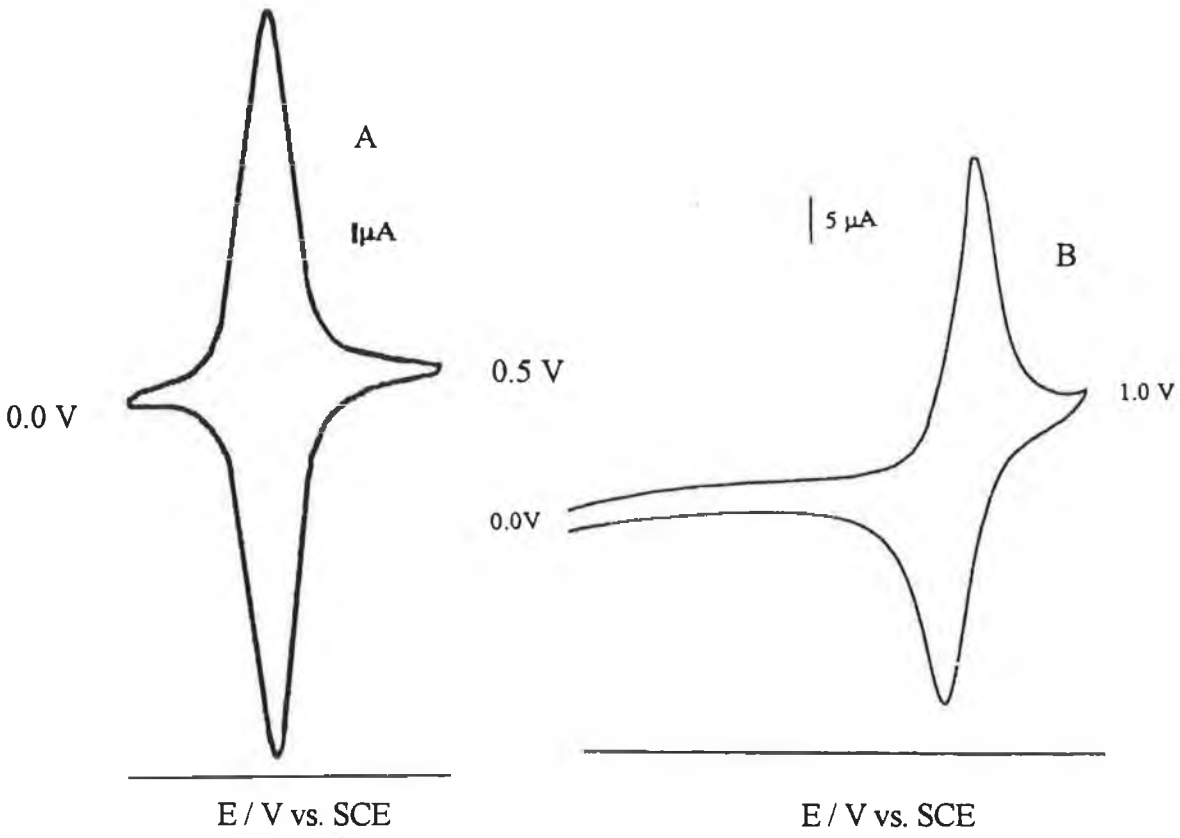


Figure 6.1 (A) CV of a 1.0 x $10^{-9}$ mol $cm^{-3}$ $[Os(bpy)_2(PVP)_{10}Cl]Cl$ modified electrode in 0.1 mol $dm^{-3}$ $Na_2SO_4$ electrolyte at 100 mV $s^{-1}$. (B) CV of a 1.0 x $10^{-9}$ mol $cm^{-3}$ $[Ru(bpy)_2(PVP)_{10}Cl]Cl$ modified electrode in 0.1 mol $dm^{-3}$ $Na_2SO_4$ electrolyte at 100 mV $s^{-1}$.

At a bare glassy carbon electrode, shown in Figure 6.2A, the oxidation of ascorbic acid is observed but the ill-defined nature of the voltammogram's signal indicates that the electrode kinetics are sluggish as expected. The oxidation reaction commences at approximately 450 mV vs. SCE and its half-wave potential is ill-defined. In comparison, the oxidation of ascorbic acid at the modified electrode is also shown. For the Os redox polymer, the on-set of the ascorbic acid oxidation reaction occurs at 150 mV vs. SCE with a maximum response being reached close to the polymer's redox potential at 270 mV vs. SCE. The significance of the half wave potential corresponding closely to the redox potential is that this indicates that the oxidation occurs under the influence of the redox couple's potential region where mediation by an outer sphere electrocatalytic process. The effect of pH on the oxidation reaction at the redox couple is demonstrated by comparing voltammograms obtained at low and high pH levels as is illustrated in the Figure 6.2B.

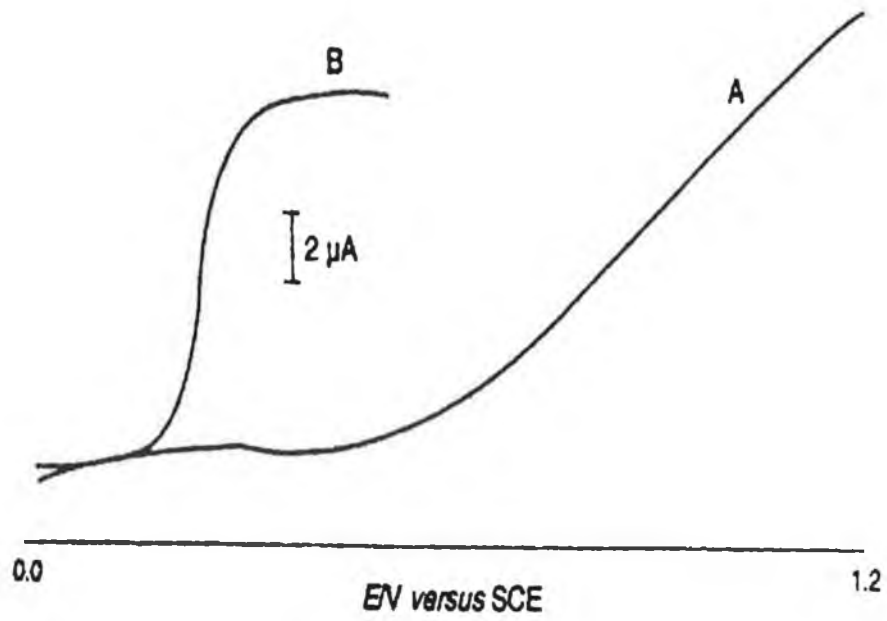


Figure 6.2A (A) RDE voltammogram of 2.0 x $10^{-4}$ mol $dm^{-3}$ ascorbic acid at a polished glassy carbon electrode in 0.1 mol $dm^{-3}$ $Na_2SO_4$ at pH 7. The potential sweep rate was 10mV $s^{-1}$. (B) RDE voltammograms of 2.0 x $10^{-4}$ mol $dm^{-3}$ ascorbic acid at a 1.0 x $10^{-9}$ mol $cm^{-3}$ $[Os(bpy)_2(PVP)_{10}Cl]Cl$ modified electrode in 0.1 mol $dm^{-3}$ $Na_2SO_4$ electrolyte at pH 7.

In media with less acidic pH, a single well-defined wave centred at the half-wave potential of the redox couple is observed which is characteristic of an outer sphere electrocatalytic process. However, in acidic media with a pH 1.0, a more complex voltammogram is obtained in which two waves are evident as shown in Figure 6.3. The first wave is as before centred on the half wave potential of the redox couple, the second occurs at a higher potential, approximately 450 mV vs. SCE. As the Os redox polymer is electroinactive in this region, the process which results in this wave is most likely unconnected with any mediation by the redox polymer. This unmediated process implies that the ascorbic acid is being oxidised at the underlying electrode. In that case the morphology of the modifying layer must provide facile transport of ascorbic acid through the electropolymer to the underlying electrode. Literature does in fact suggest that poly-4-vinylpyridine is permeable to ascorbic acid at low pH [63].

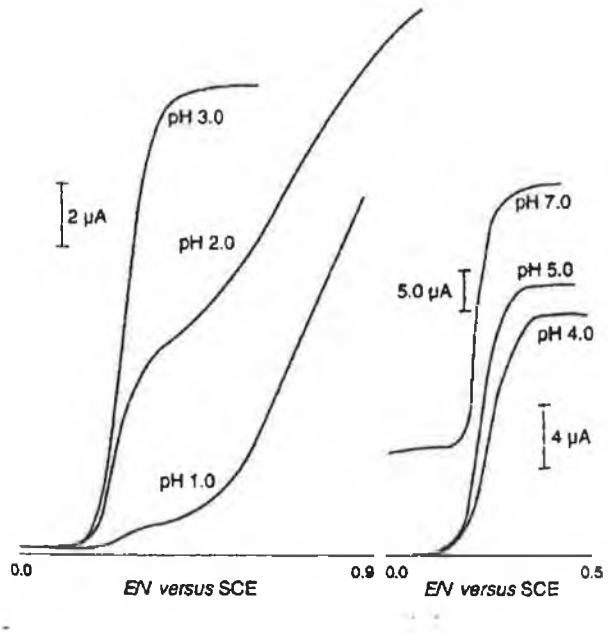


Figure 6.2B RDE voltammograms of $2.0 \times 10^{-4}$ mol $dm^{-3}$ ascorbic acid at a $1.0 \times 10^{-9}$ mol $cm^{-3}$ $[Os(bpy)_2(PVP)_{10}Cl]Cl$ modified electrode in 0.1 mol $dm^{-3}$ $Na_2SO_4$ electrolyte at pH 1 - 7.

The $pK_a$ of PVP is approximately 3.3 and is therefore protonated at low pH. The $pK_1$ of the following reaction is 4.25 [64].

$$H_2A \Leftrightarrow H^+ + HA^- \qquad \text{(Eq. 6.1)}$$

Whilst the $pK_2$ of the further reaction of this species is 11.79.

$$HA^- \Leftrightarrow H^+ + A^{2-} \qquad \text{(Eq. 6.2)}$$

Therefore at pH 1, the polymer is fully protonated and swollen to give a polycationic chain network. The ascorbic acid is a weak acid in aqueous solution with $pK_1 = 4.25$ and $pK_2 = 11.79$. Neutral ascorbic acid is the major form of this species at pH 1. This through-layer penetration may also be promoted by the swollen nature of the polymer layer which aids the diffusion of the ascorbic acid. Therefore at pH < 3, the ascorbic acid diffuses through the modifying layer and at lower potentials is oxidised at the electrocatalytic sites whilst at higher potentials oxidation occurs at both these sites and at the underlying electrode.

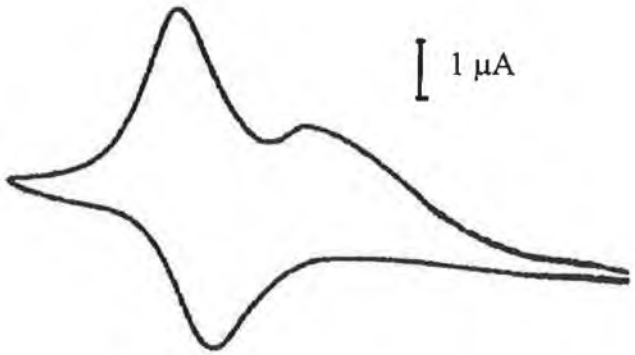


Fig. 6.3 CV voltammogram of $5.0 \times 10^{-4}$ mol $dm^{-3}$ ascorbic acid at a $1.0 \times 10^{-9}$ mol $cm^{-3}$ $[Os(bpy)_2(PVP)_{10}Cl]Cl$ modified electrode in 0.1 mol $dm^{-3}$ $Na_2SO_4$ electrolyte at pH 1.

As pH is increased, the PVP film appears to effectively exclude the negative ascorbate ions. In the phosphate buffer, pH 7, the PVP is deprotonated and no longer swollen. From the pKa value, the ascorbic acid at this pH is mainly present as the anionic form $HA^-$. The exclusion of the dissociated ascorbic acid is also likely to be influenced by the

now compact nature of the polymer backbone. A network of polycationic chains is no longer present at the higher pH and the anionic ascorbic moieities are excluded from the layer. This species no longer partitions into the polymer layer effectively and the cross-exchange reaction occurs at the layer/electrolyte interface. To summarize, at higher pH values ($\geq 3$), the polymer film is no longer permeable to the ascorbic acid. Since it can no longer penetrate to the underlying glassy carbon electrode the oxidation occurs only at the surface-immobilised redox centres.

Since it appears that the site of the ascorbic acid oxidation changes with changes in pH, it follows that the kinetics of the electrocatalytic reactions must also be altered. The kinetic case can be identified by investigating the site of the electrocatalysis at the redox polymer modified electrode. At $pH \leq 3.0$ it has been established that the ascorbic acid analyte can permeate the modifying layer completely and is found to react at both the electrocatalytic sites within the layer and at the underlying electrode. This indicates that a through-layer reaction is occurring (the $L_k$ case as described in chapter 1). This is illustrated further in Figure 6.3 which shows a cyclic voltammogram of ascorbic acid at pH 1.

The Levich plots of the oxidation of ascorbic acid at pH 7 are linear and the intercepts pass through the same point, the origin and the corresponding Koutecky-Levich plots are also linear (see Figure 6.4). These observations would not be evident if the ascorbic acid had to permeate through the polymer layer before reacting. This implies that the steady state current response appears to be independent of layer thickness. This in turn implies that the ascorbate is oxidised at the polymer layer-solution interface.

A surface reaction is more likely than one within the modifying layer. If then the reaction is occurring in a thin zone near the polymer/solution interface, the rate constant of this reaction will reflect a rate determining diffusion of the ascorbic acid. The slope of these plots does not change significantly with changing layer thickness. This would not be the case if the ascorbic acid had to diffuse through the polymer layer to react. Instead it appears that the ascorbate reacts at the polymer/solution interface and not within the polymer matrix.

The theory of Albery and Hillman was applied to investigating this kinetic reaction in order to allow its more detailed analysis of the reaction sites (Note: This theory was first discussed in Chapter 1). The Levich constant $C_{Lev}$ is defined as: $C_{Lev} = 1.554\ D^{2/3}\ v^{-1/6}$ where D is the diffusion coefficient and v is the kinematic viscosity of the electrolyte. From the Levich plots a value of $7.4 \pm 0.2 \times 10^{-4}$ cm $s^{-1/2}$ was obtained for $C_{Lev}$. This value is identical with the inverse slope of the Koutecky -Levich slope for the modified electrode (See Table 6.1).

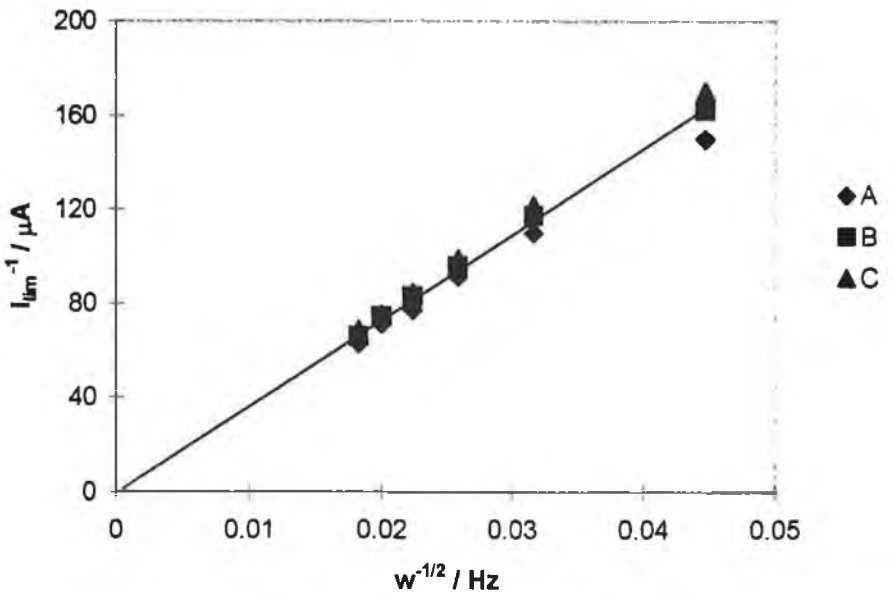


Figure 6.4 Koutecky-Levich plots for the oxidation of 1.0 (A), 2.0 (B) and 5.0 (C) x $10^{-4}$ mol $dm^{-3}$ ascorbic acid at a 1.0 x $10^{-9}$ mol $cm^{-3}$ $[Os(bpy)_2(PVP)_{10}Cl]Cl$ modified electrode in 0.1 mol $dm^{-3}$ $Na_2SO_4$ electrolyte at pH 7.

When compared with the bare glassy carbon electrode's experimentally determined value of $6.2 \pm 0.2 \times 10^{-4}$ cm $s^{-1/2}$, it can be seen that though the bare electrode's smaller slope mirrors the more sluggish electron transfer kinetics that were observed, this variation represents only a decrease of 16 % which can be considered insignificant experimentally. This result allows the elimination of the $LRZt_et_y$ kinetic regime where mediation would take place in a narrow reaction zone somewhere within the layer. As observed before, increasing the polymer surface coverage did not lead to an alteration in the value of the

intercepts of the Koutecky-Levich plots which in turn means that the modified electrode rate constant, $k'_{me}$, also did not change with changes in polymer surface coverage. Therefore, the reaction order with respect to layer thickness was zero which eliminates the through layer, $L_k$, and the reaction layer close to the electrode, LEty, as possible kinetic cases. This leaves the possible kinetic regimes of Sk", a surface reaction at the layer/electrolyte interface, and $LS_k$, a reaction layer close to the layer/electrolyte interface. These two possible regimes may be distinguished by determining what the reaction order of the modified electrode rate constant is with respect to the concentration of electrocatalytic sites within the polymer film, $b_o$. This concentration can be varied by altering the electrode potential as the immobilised redox sites are in thermodynamic equilibrium with the this potential.

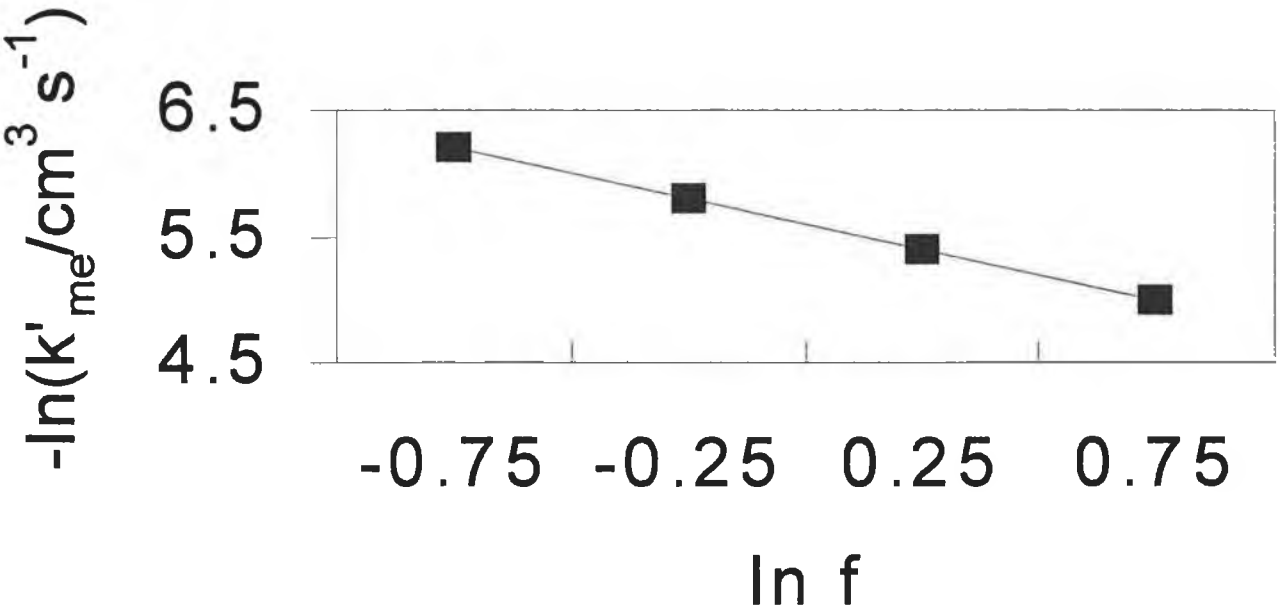


Figure 6.5 Plot of In $k'_{ME}$ vs. In f for the oxidation of 1.0 x $10^{-4}$ mol $dm^{-3}$ ascorbic acid at a 1.0 x $10^{-9}$ mol $cm^{-3}$ $[Os(bpy)_2(PVP)_{10}Cl]Cl$ modified electrode in 0.1 mol $dm^{-3}$ $Na_2SO_4$ electrolyte at pH.7.

A plot of In $k'_{me}$ vs. In f, the fraction of the redox centres in the catalytic Os (III) state, is shown in Figure 6.5. The plot is linear with a slope of 0.9 ± 0.1. This linear relationship allows the elimination of the LSk kinetic case and further implies that the correct kinetic

regime is Sk". For this kinetic case, the rates of cross-exchange and electron diffusion are large but the ascorbic acid diffusion rate through the polymer layer is small, in fact it can only diffuse through the polymer film with difficulty.

The mediation process is occurring in the outer boundary of the film. The cross-exchange reaction is occurring between the ascorbic acid in the electrolyte and the osmium redox sites situated at the polymer/electrolyte interface. The rate of this reaction is sufficiently high to allow all the ascorbic acid arriving at the interface to be oxidised at these sites, thus resulting in currents controlled by diffusion of the ascorbic acid in the electrolytic solution. This conclusion corresponds with the observation made that the Levich plots were linear with zero intercepts, which also implies diffusionally controlled kinetics. The calculations therefore reveal that a surface reaction occurs between the ascorbate analyte and the immobilised osmium centres. This is not the ideal kinetic case for a modified electrode. It cannot act as a three dimensional mediator instead the ascorbic acid is excluded from the bulk of the modifying layer. This two dimensional mode of action it possesses is not efficient, only a small percentage of the available redox centres are employed in reacting with the analyte and consequently a weaker response is obtained. This mode of action can also be an advantage, however, in that mediation occurs only at the surface, the thickness of the modifying layer is no longer crucial and therefore, modifying layers with similar characteristics are more easily obtained.

| **pH** | **$k'_{ME}$** **x $10^{-4}$ cm $s^{-1}$** | **k"** **x $10^{-4}$ $dm^3$ $mol^{-1}$ cm $s^{-1}$** | **Inverse Slope** **x $10^{-4}$ cm $s^{-1/2}$** |
|---|---|---|---|
| 1 | 0.8 +/- 0.08 | 6.0 +/- 0.6 | - |
| 4.5 | 1.1 +/- 0.05 | 7.8 +/- 0.4 | 7.4 +/- 0.2 |
| 7 | 1.3 +/- 0.08 | 9.1 +/- 0.6 | 7.4 +/- 0.3 |

Table 6.1 A comparison of $k'_{ME}$ and k" at a number of different pH values using a modified layer thickness of 1.0 x $10^{-9}$ mol $cm^{-3}$ $[Os(bpy)_2(PVP)_{10}Cl]Cl$ in 0.1 mol $dm^{-3}$ $Na_2SO_4$.

The second order rate constant, k", for the surface reaction can be calculated from the modified rate constant using the relationship $k'_{me} = n\ k''\ bo$, where n = 2. Table 6.1 illustrates the values for $k'_{me}$ and k" found for this redox polymer at a number of low and high pH values. This shows that, as expected, the rate constant increases with increasing pH. Figure 6.2 shows how the redox modified electrode responds to similar concentrations of ascorbic acid at different pH values. Increasing the pH of the electrolyte results in higher currents. Table 6.1 compares the modified rate constant at various pH values and shows a similar result. As shown, the reaction order with respect to hydrogen ion concentration is -1 (Figure 6.6 and the order with respect to ascorbate concentration is 1 (Figure 6.7).

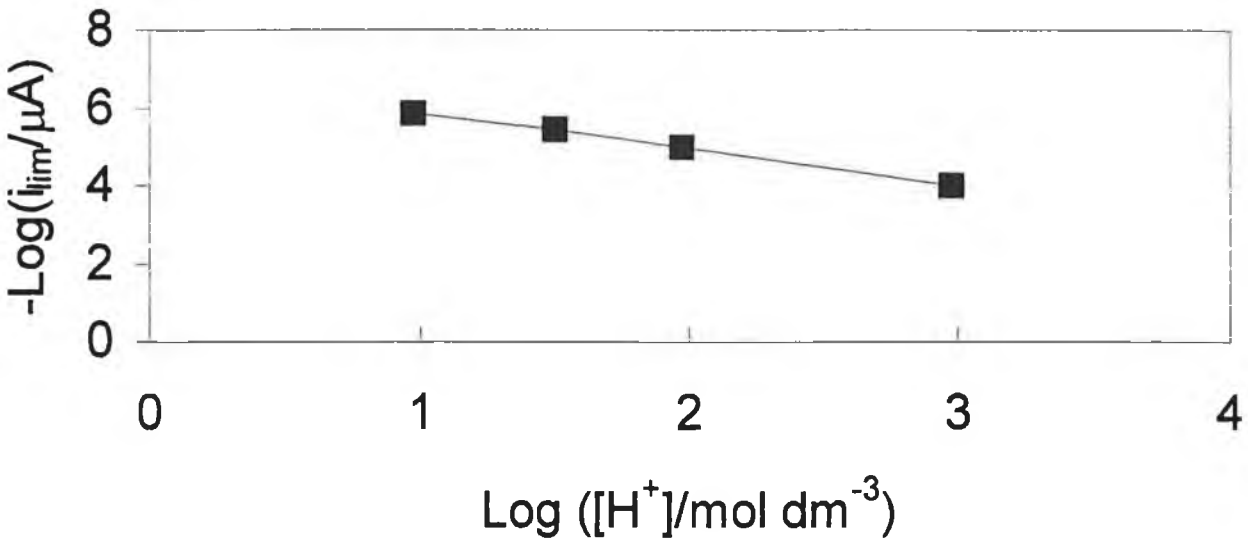


Figure 6.6 Reaction order plot of $[H^+]$ for the oxidation of 1.0 x $10^{-4}$ mol $dm^{-3}$ ascorbic acid at a 1.0 x $10^{-9}$ mol $cm^{-3}$ $[Os(bpy)_2(PVP)_{10}Cl]Cl$ modified electrode in 0.1 mol $dm^{-3}$ $Na_2SO_4$ electrolyte at pH 7.

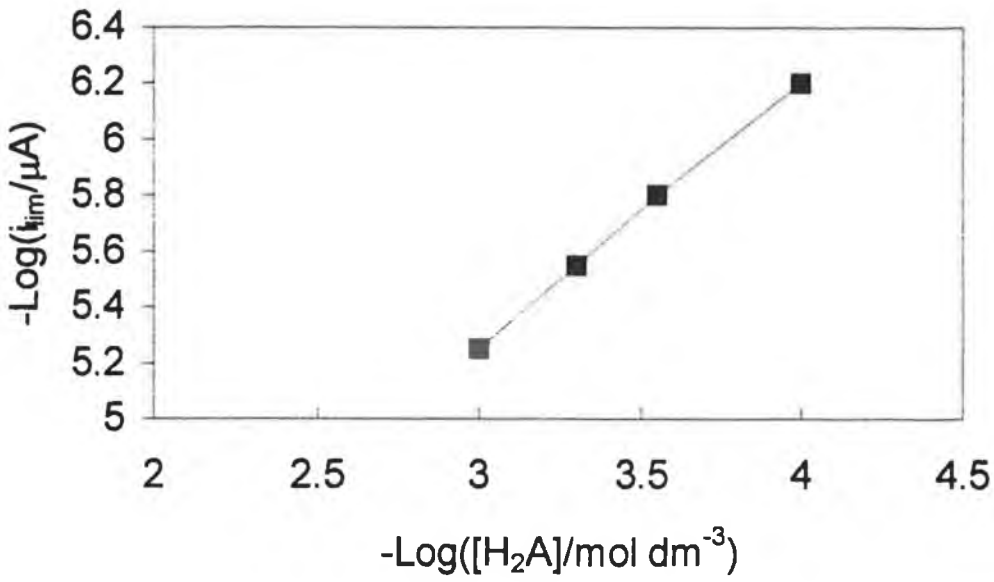


Figure. 6.7 Reaction order plot of $[H_2A]$ oxidation at a 1.0 x $10^{-9}$ mol $cm^{-3}$ $[Os(bpy)_2(PVP)_{10}Cl]Cl$ modified electrode in 0.1 mol $dm^{-3}$ $Na_2SO_4$ electrolyte at pH 7.

Furthermore, if we consider that the mediation reaction, at pH $\geq$ 3.0, takes place only at the electrocatalytic sites on the modified electrode's surface, the following reaction sequence for the oxidation of ascorbic acid can be postulated :

$$AH_2 \Leftrightarrow AH^- + H^+ \qquad \text{(Eq. 6.3)}$$

$$AH^- \Leftrightarrow A^{\cdot-} + H^+ + e^- \qquad \text{(Eq. 6.4)}$$

$$A^{\cdot-} \Leftrightarrow A + e^- \qquad \text{(Eq. 6.5)}$$

$$A + H_2O \Leftrightarrow A(H_2O) \qquad \text{(Eq. 6.6)}$$

Where $AH_2$ denotes ascorbic acid and $A^{\cdot-}$ denotes the radical anion intermediate and A denotes dehydroascorbic acid. This two electron process, with the first electron transfer

resulting in the formation of the ascorbate radical intermediate, is well known and has been proposed as the mechanism for a number of other modified electrodes. [65]. The formation of the radical anion is the rate determining step.

The role of the transition metal redox modified electrode in the catalysis of this redox reaction of ascorbic acid involves a step in which the Os (III) ion is first reduced. After the ascorbic acid molecule forms the ascorbate anion in the aqueous electrolyte, it diffuses to the modified electrode where it encounters the surface catalytic Os (III) sites and is completely electrolytically consumed with the reaction products being the radical intermediate and the non-catalytic Os (II). The second order rate constant, k", for this reaction increases with increasing pH, as shown in Table 6.1.

Similar observations were reported for the oxidation of ascorbic acid on graphite [44], mercury [66] and gold [67] electrodes. This pH effect indicates that the anionic form [$HA^-$], not the neutral form [$H_2A$] is the electrochemically active species that is directly involved in the electron transfer.

$$AH^- + Os\ (III) \Leftrightarrow A^{\cdot -} + H^+ + Os\ (II) \qquad \text{(Eq. 6.7)}$$

This radical anion further reacts at other Os (III) sites where it is oxidised to produce dehydroascorbic acid and more Os (II).

$$A^{\cdot -} + Os\ (III) \Leftrightarrow A + Os\ (II) \qquad \text{(Eq. 6.8)}$$

Finally, the reduced Os (II) sites within the polymer film undergo re-oxidation due to the fast self-exchange rates between the Os (II/III) couples within the mediating layer.

$$2Os\ (II) + 2e\text{-} \Leftrightarrow 2Os\ (III) \qquad \text{(Eq. 6.9)}$$

This reaction mechanism shares similar characteristics with other mechanisms proposed for the oxidation of ascorbic acid by transition metal ions and complexes in that the first oxidation step invariably results in the formation of an ascorbate radical. The further

reaction of that radical with another metal ion is then proposed [1]. The radical ion, monodehydroascorbic acid, is present in tissue as a relatively stable free radical. This stability allied with its ability to disproportionate into dehydroascorbic acid and ascorbic acid is believed to be the reason why ascorbic acid is so successful in its role as an antioxidant [16].

No corresponding reduction current was found when the modified electrode was scanned in the negative direction after the positive sweep. This indicates that the oxidation product of the ascorbic acid, dehydroascorbic acid, does not undergo reduction at the electrode. This appears to be because dehydroascorbic acid undergoes rapid hydration in aqueous solution. Consequently, the oxidation of ascorbic acid at this modified electrode is irreversible.

### 6.3.2 Change in Redox Couple

The kinetics of this reaction at a ruthenium-modified electrode were investigated to examine if the reaction process would change with the metallic centre. The $E_{\frac{1}{2}}$ of the ruthenium polymer is 0.75 V vs. SCE, its $E_{\frac{1}{2}}$ is more positive that the formal potential of ascorbic acid and therefore it should also be capable of the electrocatalytic oxidation of this species. As the ascorbic acid's formal potential is more negative of the ruthenium couple's redox potential (0.75 V vs SCE) in comparison to the osmium couple's (0.25 V vs SCE), it might be expected that the corresponding higher driving force would result in an enhanced response to the oxidation of the ascorbic acid due to the presence of a larger driving force. It was found that as the pH, of the medium was increased, the Ru-modified electrode's response to the ascorbic acid was shifted to lower potentials.

The plots, shown in Figure 6.8, representing the response of different surface coverages of the ruthenium polymer modified electrode to ascorbic acid at pH 7 have similar slopes and indicate a surface reaction.

The results also suggest that the kinetic action of these electropolymers is heavily influenced by the structure of the polymer backbone. The impermeability of the PVP polymer to ascorbic acid at higher pH allows for only a surface reaction of the electroactive centres with the ascorbate. Further work involving alteration of the backbone might result in an alteration of the kinetics of this reaction. Previous work, which also utilised cross-linked polymer modified electrodes, demonstrated that such electrodes could control the partitioning of electroactive species in the modifying layer. Two species could be measured simultaneously because the partitioning effect of the cross-linked layer resulted in their speciation [68].

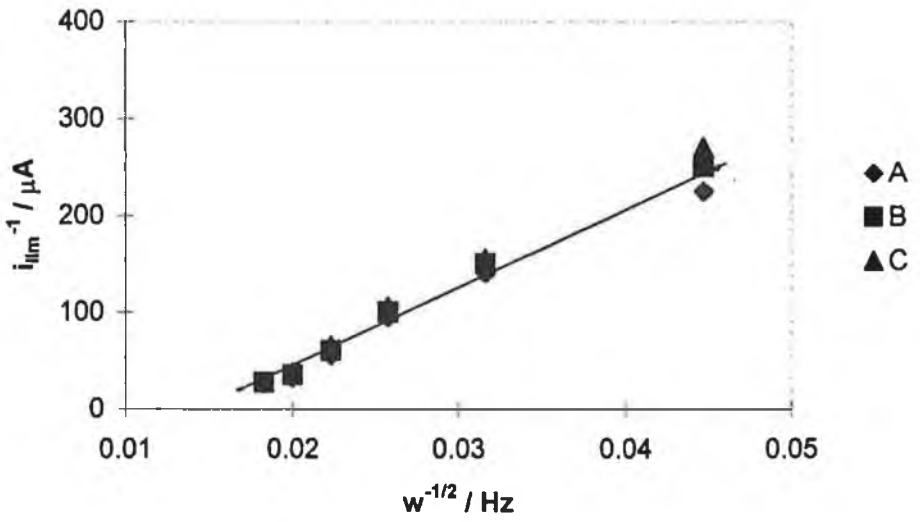


Figure 6.8 Koutecky-Levich plots for the oxidation of 1.0 (A), 2.0 (B) and 5.0 (C) x $10^{-4}$ mol $dm^{-3}$ ascorbic acid at a 1.0 x $10^{-9}$ mol $cm^{-3}$ $[Ru(bpy)_2(PVP)_{10}Cl]Cl$ modified electrode in 0.1 mol $dm^{-3}$ $Na_2SO_4$ electrolyte at pH 7.

## 6.4 Sensor Development

The rapid charge transfer of the near steady state voltammograms previously demonstrated for the macroelectrochemical cell indicate that the osmium redox polymer should behave similarly when used to modify a thin layer flow cell, as has previously been shown for other analytes [69].

It was necessary to choose between the two polymers when deciding on the best modifying layer for the sensor. A number of points must be weighed when considering which is the optimum electropolymer to use in the development of an ascorbic acid sensor. The most important properties of a sensor when used in analytical applications are stability, reproducibility, sensitivity and selectivity. The ruthenium electropolymer was found to be sensitive but demonstrated only a short-term reproducible response and no long-term stability due to its photoreactivity and its higher working potential would result in a reduced selectivity. Considering these factors, it was decide that the ruthenium electropolymer's sensitive response to ascorbic acid did not outweigh the other drawbacks of using this sensor. The Os modified layer was of comparable sensitivity and displayed better stability. Also, the Ru polymer could not be shown to have any advantages over the Os polymer as regards the kinetics of the sensor's response, as they were shown to be identical, the Ru polymer could not be shown to demonstrate a sufficient advantage over the Os polymer for it be used in the development of the sensor.

### 6.4.1 pH effect

As the pH is increased, so too does the electrode's response increase. At pH 7 the response is shown to be sensitive to the presence of the ascorbate analyte as well as exhibiting a well-shaped and easily measurable FIA peak. The response to an injection of 10 ppm ascorbic acid at this pH is equivalent to the response obtained for a solution containing 500 ppm of ascorbic acid in the presence of the electrolyte at pH 1. In other words, the response is significantly enhanced by increasing the pH. The limit of detection of the electrode decreases as the pH increases. This clearly demonstrates how a chemically modified electrode's response can depend on close attention being paid to the

optimisation of all the experimental conditions used in the determination of an analyte. Consequently, the analytical behavior of the redox modified electrode was characterised for ascorbic acid detection. This work was carried out in a flow injection system with the modified electrode situated in a thin layer flow cell with a phosphate carrier buffered to pH 7.0 since the fluctuations of the pH could have serious repercussions on the reproducibility of the sensor's response. Fruit juices, e.g., are fairly acidic and their injection onto an unbuffered FIA system could cause localised decreases in pH at the site of the working electrode which in turn could result in a reduced response.

### 6.4.2 Optimum Potential

A hydrodynamic voltammogram shows the effect of applied potential on the electrochemical sensor's response. Figure 6.9 shows such a voltammogram for the sensor under investigation over the range 0 to 0.5 V vs. SCE.

A dramatic increase in the response to ascorbic acid can be observed as the working potential is increased. This corresponds to an increase in the formation of active Os (III) layers within the modifying layer. At lower potentials the osmium is present mostly in the reduced pre-catalytic Os (II) form. As the potential is increased, the Os (II) becomes oxidised to form Os (III). At 0.25 V both Os (II) and Os (III) are present in equal amounts.

Increasing the potential beyond 0.25 V results in Os (III) becoming the major form of osmium present. The response of the sensor to a solution of ascorbic acid is shown to be at an optimum at approximately 0.25 V vs. SCE. This corresponds to the $E_{1/2}$ of the Os redox couple present in the modifying layer of the sensor. It can be seen that as more Os (III) is formed there is not a corresponding rise in the response to the ascorbic acid, i.e. the further increase of catalytic Os (III) species does not encourage increased oxidation of the analyte. This confirms that the postulated kinetic mechanism of the oxidation of ascorbic acid at this modifying surface at pH 7 is correct.

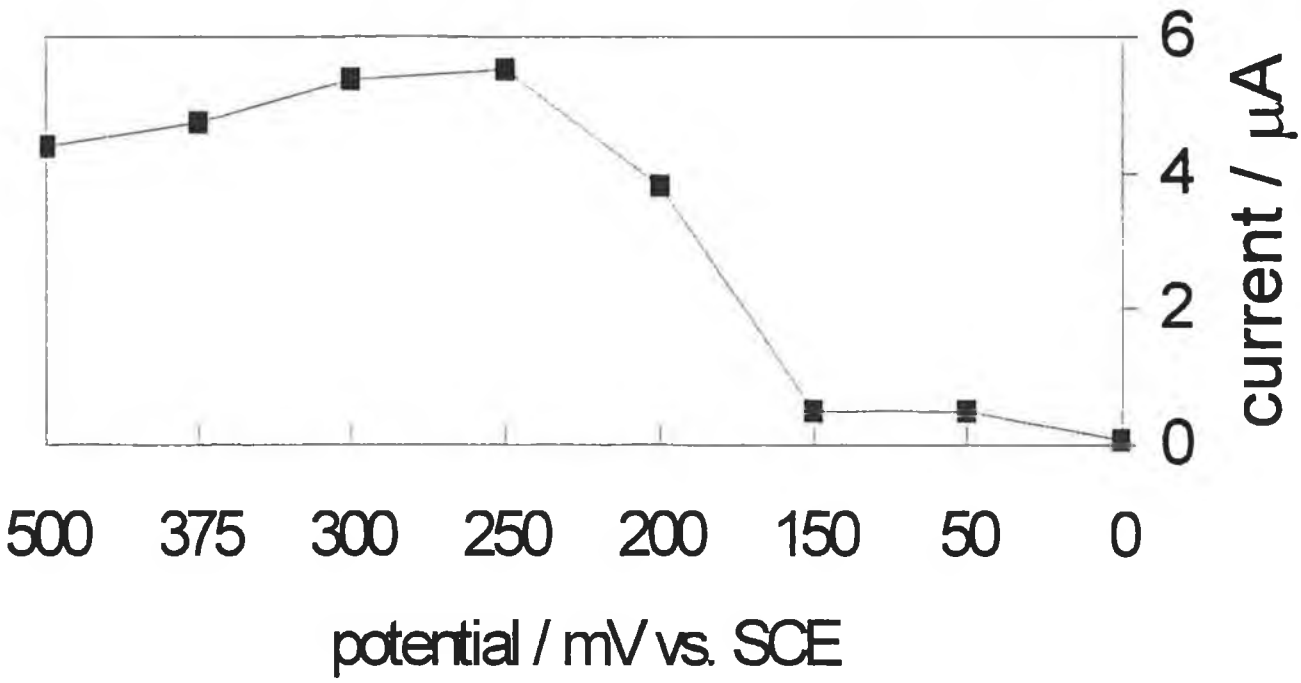


Figure 6.9 Hydrodynamic Voltammogram of the oxidation of $5.0 \times 10^{-4}$ mol $dm^{-3}$ ascorbic acid in 0.1 mol $dm^{-3}$ $K_2HPO_4$ / $KH_2PO_4$electrolyte at pH 7. Carrier flow rate is 1.0 $cm^3$ $min^{-1}$. Surface coverage of the modified electrode is $1.0 \times 10^{-9}$ mol $cm^{-3}$ $[Os(bpy)_2(PVP)_{10}Cl]Cl$.

The presence of more Os(III) species does not affect the reaction because the reaction is occurring at the surface. The ascorbic acid has no access to the increased number of catalytic sites and is not affected by them. This working potential is far lower than the typical undesirable high potentials used for oxidation of ascorbic acid at carbon and metallic electrodes, > 0.5 V vs. SCE. [70,71]

### 6.4.3 Carrier Flow Rate

The effect of the carrier flow rate was also measured between 0.2 and 2.0 $cm^3$ $min^{-1}$. A hyperbolic shaped curve was obtained as shown in Figure 6.10. Lower flow rates caused the area of the FIA peak to increase.

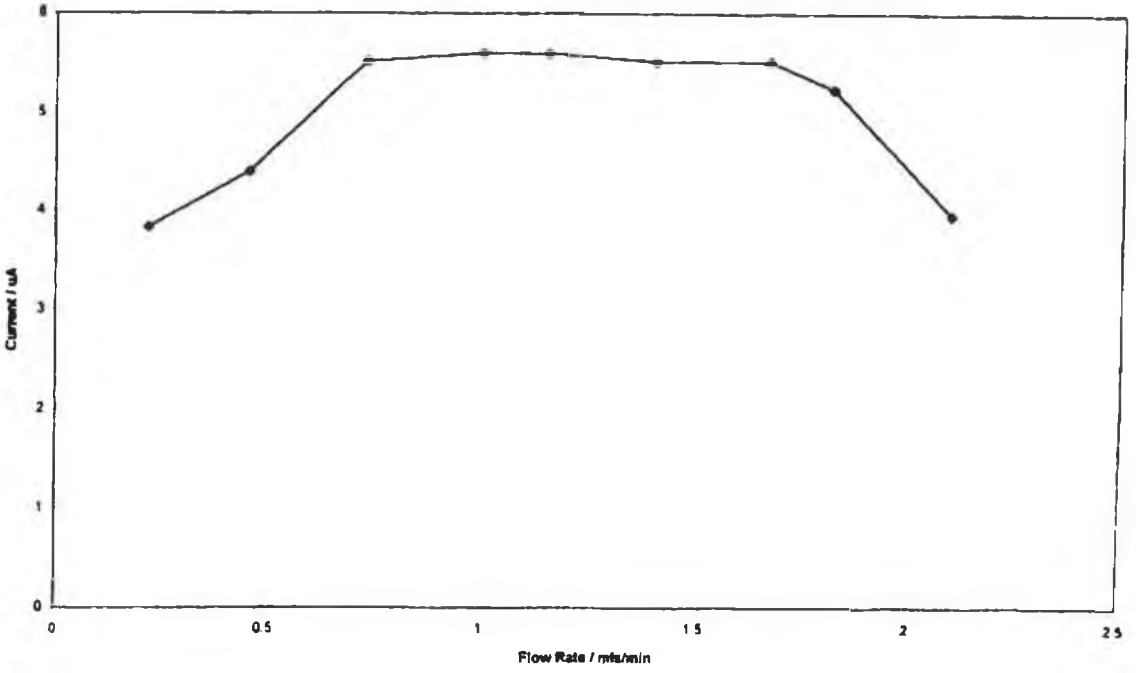


Figure 6.10 Effect of carrier flow rate on the sensor's response to the oxidation of 5.0 x $10^{-4}$ mol $dm^{-3}$ ascorbic acid in 0.1 mol $dm^{-3}$ $K_2HPO_4$ / $KH_2PO_4$electrolyte at pH 7. A potential of 0.25 V vs. SCE was used. . Surface coverage of the modified electrode is 1.0 x $10^{-9}$ mol $cm^{-3}$ $[Os(bpy)_2(PVP)_{10}Cl]Cl$.

A similar shaped curve was found when investigating an osmium containing redox polymer used in the development of a flow through glucose oxidise modified microelectrode for the detection of glucose. [72] This broadening decreased as flow rate increased. At higher flow rates the peak height and thus the sensitivity if the response also decreased. A flow rate of 1.0 $cm^3$ $min^{-1}$ was chosen as it combined a sensitive response, easily measurable FIA peak shapes and good sample through-put.

### 6.4.4 Linear Range and Limit of Detection

The linear range of the electrode's response to the analyte was measured. Initially, a linear range was calibrated between 0.1 and 1.0 mM ascorbic acid with a slope of 7.3 μA $dm^3$ $mM^{-1}$ and an intercept of -1.32 μA, r = 0.998. This calibration graph is similar to the one found for another chemically modified ascorbic acid electrochemical sensor [73] though not quite as good as that found when measuring ascorbic acid using a graphite-epoxy composite electrode chemically modified with cobalt phthalocyanine [74]. The detection limit, defined as a signal to noise ratio of 2:1, was found to be 1 x $10^{-3}$ mM. (Note: At pH 1, the LOD is 1 x $10^{-3}$ mol $dm^{-3}$ (S/N = 2) but is 1 x $10^{-6}$ mol $dm^{-3}$ at pH 7.) The modified electrode's reproducibility was found to have an R.S.D. value of 0.4 % for 11 repeat injections.

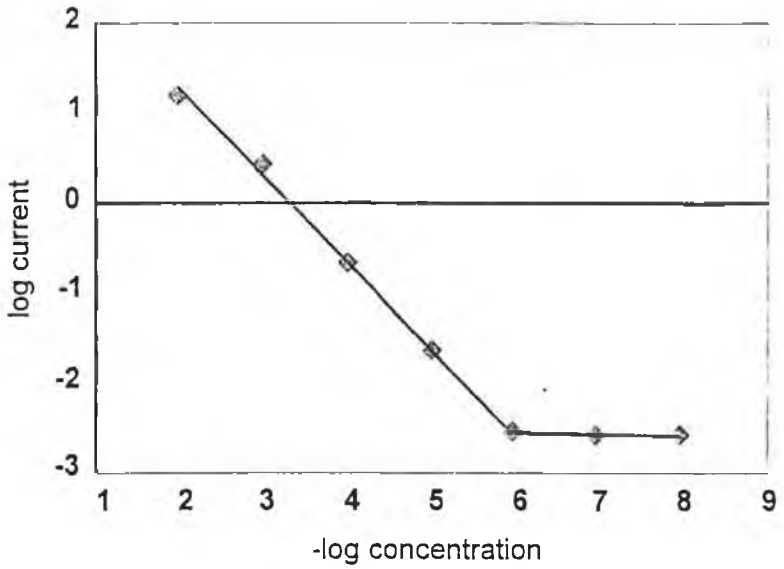


Figure 6.11 Linear range of ascorbic acid at a 1 x $10^{-9}$ mol $cm^{-2}$ $[Os(bpy)_2(PVP)_{10}Cl]Cl$ modified electrode in 0.1 mol $dm^{-3}$ $KH_2PO_4/K_2HPO_4$ electrolyte at pH 7. Carrier flow rate is 1 $cm^3$ $min^{-1}$.

It was then decided to try and improve this linear range. The highly unstable nature of the ascorbic acid was considered to be the limiting factor in the extending of this range. The clear tubing used throughout the FIA system rendered the ascorbic acid vulnerable to the photo-degradation. Comparison with a standard method indicated that only a percentage of the injected ascorbate was surviving in the system to react at the modified surface and that this percentage decreased as the carrier flow rate decreased. After the flow injection tubing and the injection syringe were covered with aluminium foil, further tests showed that essentially all the injected ascorbic acid could be detected. Another linear range was then calculated and it was shown that linearity extended over 4 orders of magnitude whilst the limit of detection remained unchanged at $1 \times 10^{-6}$ mol $dm^{-3}$ (see Figure 6.11). Thus by exercising more caution with regard to the particular nature of the ascorbic acid substrate, it was possible to extend the linearity of the sensor.

### 6.4.5 Stability

Bare electrode surfaces undergo fouling after a short time when used for amperometric measurements resulting in a deterioration in sensing capability. A stability study of the modifying layer was carried out by keeping the FIA working continuously over 75 hours with periodic injections of a solution containing $2.4 \times 10^{-4}$ mol $dm^{-3}$ ascorbic acid. The modifying layer's response to the ascorbic acid remained steady for the first 60 hours with an average measured current signal of 5.6 μA but thereafter experienced a drop-off in height to 2.9 μA resulting in a close to 50 % decrease in the signal's response after 75 hours.

### 6.4.6 Interferences

Ascorbic acid is prone to various modes of degradation. These include temperature, salt and sugar concentration, pH, oxygen, enzymes and metal catalysts. Therefore, to obtain an accurate reflection of the actual concentration of a ascorbic acid in a sample, it is necessary to use a sensing method which avoids extremes and which can be carried out in the minimum amount of time.

The lower overpotential of this redox modified electrode compared to non-modified electrodes means that it is inherently more selective and thus would be expected to suffer less from other oxidizable compounds existing in real biological solutions.

A reducing agent was also examined for its interfering effect, m-phosphoric acid is commonly added to samples containing ascorbic acid due to its preservative nature. The acid itself produced no response on the sensor, but when present with ascorbic acid had an effect on the appearance of the analytical peak. The peak area remained the same but the peak height was much reduced. Resulting in a very broad response peak.

Citric acid is often found in samples containing ascorbic acid e.g. fruit juices. It is generally present in amounts significantly larger than ascorbate and as such could cause a serious interfering effect if it produced a response from the sensor. A sample containing 1 mol $dm^{-3}$ citric acid was found to produce a response equivalent to a solution containing 5 x $10^{-5}$ mol $dm^{-3}$ ascorbic acid. This small sensor response would be insufficient to cause a significant interfering effect.

Since a number of real samples were to be measured using this sensor, species present in fruit juices and pharmaceutical formulations were examined for their interfering effect on the FIA system. Sodium citrate was found to have little or no interfering effect. A solution containing molar amounts of the citrate obtained a response from the sensor equivalent to a solution containing 0.1 ppm ascorbic acid. Organic compounds such as paracetomal and glucose elicited no response from the sensor.

Salts of Ca(II), Mg(II), Na(I) and K(I) made up to molar concentrations, similarly gained no response from the sensor. Metal ions such as copper or iron could cause interference and for this reason, EDTA was added to the electrolyte. EDTA does not cause an interfering response and aids in the removal of any metal ions which may be present in samples which could cause an interfering response at the modified electrode or which could cause degradation to the ascorbic acid.

An advantage of using a modified electrode is that as a low potential is used as the working potential, many of the species which could cause an interfering effect are effectively screened out. Since as the working potential is increased, the number of possible interfering species increases exponentially.

### 6.4.7 Analysis of Real Samples

A number of real samples were used to demonstrate the utility of the sensor. Sample preparation was minimal. In the case of the pharmaceutical formulation the powder was dissolved in electrolyte. The fruit juices were injected straight onto the FIA. Further preparation involved only the dilution of the samples so that they fell within the linear range of the sensor.

| Sample | Concentration Found Using Various Methods | | | |
|---|---|---|---|---|
| | Titrimetric Method / ppm | Linear Range / ppm | Standard Addition / ppm | Recovery Results % |
| Blackcurrant Juice | - | 265 | 267 | 98 |
| Orange Juice | 636 | 659 | 646 | 95 |
| Cold remedy | 1,640 | 1,480 | 1,400 | 105 |

Table 6.3 Determination of the level of ascorbic acid in a number of real samples using a standard method of analysis and the ascorbic acid sensor under investigation including the results of a recovery test.

Table 6.2 compares the results obtained by the FIA to those obtained using a standard titration method. The titration involves use of the indicator 2,6-indodiphenol to monitor a colour reaction. This reaction is the basis for the official ascorbic acid determination. A drawback of this method is its impracticality for use with coloured samples. The colorimetric techniques for ascorbic acid measurement all suffer from this interfering effect and as a result many sophisticated techniques have been proposed for analysis of real samples. Consequently, each sample type has a different method of detection which is associated with it and there is no one technique which can be used with accuracy.

The validity of the method was also established by the addition of standard ascorbate concentrations to various fruit juices and comparing the obtained response with the theoretical response. Essentially, complete recovery of the ascorbate was obtained in all cases (See also Table 6.2) which demonstrates that the sensor was unaffected by the many other species present in these complex matrices.

## 6.5 Conclusion

Electrodes modified with osmium and ruthenium-containing redox polymers were used for the oxidation of ascorbic acid was examined. The kinetics of the mediated reaction was found to alter depending on pH. At pH $\leq$ 3.0 a through film reaction occurs with both reaction at the underlying glassy carbon electrode and mediated catalysis being observed. On increasing the pH, a changeover in the kinetic regime to a surface reaction occurs. Altering the redox catalyst did not affect the kinetics or the site of the reaction. The nature of the polymer backbone, poly(4-vinylpyridine) played a more important role in determining the site of this reaction. This was because of the polymer's response to variations in pH. At lower pH values it allowed transport of the ascorbate substrate through the modifying layer where it could react at the underlying glassy carbon electrode as well as at all the redox sites in the film covering the electrode. By increasing the pH, the polymer was rendered impermeable to the ascorbate which now could react only at the modifying surface.

This proved advantageous from a sensing point of view because, by the reaction being a surface limiting case, the modifying layer was no longer dependent on its thickness. In a through-layer kinetic case, it would be necessary to closely control the size of the layer as an increase in the film size would lead to a corresponding increase in its response to the substrate. Therefore, from a practicable point of view, the surface kinetic case enables modified electrodes to be prepared more readily and quickly. For example, producing a screen-printed version of this modified electrode could be carried out with ease.

From a sensing point of view, this ascorbic acid sensor also showed to have qualities which are not present in many current analytical techniques. The most important properties of a sensor when used in analytical applications are stability, reproducibility, sensitivity and selectivity. The sensor was shown to have a sensitivity comparable to spectrophotometric techniques accompanied by a specificity conferred on it by the redox qualities of its modifier. The spectrophotometric method requires 20-30 min for each assay and has a detection limit of 10 μM and can be affected by the presence of many compounds which also give a spectroscopic response. Specificity can generally only be obtained by adding a chromatographic column which adds considerably to the time and expense involved in the analysis. Many electrochemical techniques also suffer from this same lack of specificity and they too use techniques such as HPLC to offset this problem [41]. Other drawbacks include electrode fouling, slow kinetics, interference from other redox compounds or expensive instrumentation [40].

The ascorbic acid sensor under investigation is free from many interferences commonly found in sample matrices containing ascorbic acid because of the low working potential it can utilise, 0.25 V vs. SCE. The electrooxidation of ascorbic acid at conventional working electrodes generally requires high working potentials, typically greater than 0.5 V, and the higher the working potential, the greater the number of potential interferents. That is, the electrocatalyst present in the sensor can overcome this over-potential.

The sensor showed, through the recovery tests, that it did not suffer from any of the interferents present in the samples studied. This in turn meant that a pre-sensor separating column was unnecessary. The modified surface showed reasonable stability

and was not prone to fouling. Its characteristics suggest that future work could be carried out on the analysis of ascorbic acid in other complex matrices of interest such as milk and blood.

It must be emphasized that the sensor described in this chapter is an ascorbic acid sensor and not a vitamin C sensor. This is because vitamin C can be classified as both ascorbic acid and dehydroascorbic acid. This sensor could be further developed to detect dehydroascorbic acid but sample pretreatment would be necessary to detect the dehydroascorbic acid. This would involve adding an agent to the sample under investigation to reduce the dehydroascorbic acid to ascorbate and then total vitamin C could be measured. A difference value between this response and the response obtained for the untreated sample would allow measurement of the individual species.

## 6.6 References


1. M. B. Davies., J. Austin., D. A. Partridge, Vitamin C: Its Chemistry and Biochemistry, Royal Society of Chemistry, Cambridge, 1991
2. E. Richards, New Scientist, v109, n1497 (1986) 46
3. O. Sattaur, New Scientist, v107, n1464 (1985) 23
4. I. Anderson, New Scientist, v105, n1440 (1985) 22
5. M. Baringa, Science, 254 (1991) 374
6. W. L. Chameides, Environ. Sci. Tech., 23 (1989) 595
7. V. W. Bowry, R. J. Stocker, Am. Chem. Soc., 115 (1993) 6029
8. (a) B. M. Kwon, C. S. Foote, S. I. Khan, J. Am. Chem. Soc., 111 (1989) 1854 (b) ) B. M. Kwon, C. S. Foote, J. Am. Chem. Soc., 110 (1988) 6582
9. Bradley, New Scientist, 133 (1992) 20

10. K. U. Ingold, V. W. Bowry, R. Stocker, C. Walling, Proc. Natl. Acad. Sci. USA, 90 (1993) 45

11. L. S. Hollis, A. R. Amundsen, E. W. Stern, J. Am. Chem. Soc., 107 (1985) 274

12. J. Burgess, Trans. Metal Chem., 18 (1993) 439

13. F. Walmsley, J. Chem. Ed., 69 (1992) 936

14. J. M. Leal, P. L. Domingo, B. Garcia, S. Ibeas, J. Chem. Soc. Faraday Trans., 89 (1993) 3571

15. J. L. Cole, D. P. Ballou, E. I., Solomon, J. Am. Chem. Soc., 113 (1991) 8544

16. P. A. Seib, B. M. Tolbert, Ascorbic Acid, ACS, New York, 1982

17. S. Anderson, C. B. Marks, R. Lazarus, Science, 230 (1985) 144

18. K. C. Hwang, D. Mauzerall, J. Am. Chem. Soc., 114 (1992) 9705

19. J. P. Byrne, C. L. Chakrabarti, G. F. R. Gilchrist, M. M. Lamoureux, P. Bertels, Anal. Chem., 65 (1993) 1267

20. A. B. Volynsky, S. V. Tikhomirov, V. G. Senin, A. N. Kashin, Anal. Chim. Acta, 284 (1993) 367

21. M. Sawamura, S. Takemoto, Z. F. Li, J. Ag. Food Chem., 39 (1991) 1735

22. L. K. Gardner, G. D. Lawrence, J. Ag. Food Chem., 41 (1993) 693

23. T. L. Helser, J. Chem. Ed., 72 (1995) A10

24. T. S. Rao, R. B. Dabke, B. S. Biradar, J. Chem. Ed., 71 (1994) 438

25. A. Safavi., L. Fotouhi, Talanta, 41 (1994) 1225

26. M. Blanco , J. Coello, H. Iturriaga, S. Maspoch, C. Delapezuela, Talanta, 40 (1993) 1671

27. Z. L. Jiang, A. H. Liang, Anal. Chim. Acta, 278 (1993) 53

28. K. Kampfenkel, M. Vanmontagu, D. Inze, Anal. Biochem., 225 (1995) 165

29. M. Nakamura, J. Biochem., 116 (1994) 621

30. E. Kimoto, H. Tanaka, T. Ohmoto, M. Choami, Anal. Biochem., 214 (1993) 38

31. W. A. Pryor, J. A. Cornicelli, L. J. Devall, B. Tait, B. K. Trivedi, D. T. Witiak, M. D. Wu, J. Org. Chem., 58 (1993) 3521

32. K. Robards, M. Antolovich, Analyst, 120 (1995) 1

33. T. Moeslinger, M. Brunner, P. G. Spieckermann, Anal. Biochem., 221 (1994) 290

34. G. Lazzarino, D. DiPierro, B. Tavazzi, L. Cerroni, B. Giardina, Anal. Biochem., 197 (1991) 191

35. G. Barja de Quiroga, M. Lopex-Torres, R. Perez-Campo, C. Rojas, Anal. Biochem., 199 (1991) 81

36. F. G. Montelongo, M. J. Sanchez, J. C. G. Castro, A. Hardisson, Anal. Lett., 24 (1991) 1875

37. J. M. Kim, Y. Huang, R. D. Schmid, Anal. Lett., 23 (1990) 2273

38. J. M. Lopez-Fernandez, A. Rios, M. Valcarel, Analyst, 120 (1995) 2393

39. P. C. H. Hollman, J. H. Slangen, P. J. Wagstaffe, U. Faure, D. A. T. Southgate, F. M. Finglas, Analyst, 118 (1993) 481

40. V. Kumar, P. Courie, S. Haley, J. Chem. Ed., 69 (1992) A213

41. P. M. Bersier, J. Bersier, Electroanalysis, 6 (1994) 171

42. S. Mannino, J. Wang, Electroanalysis, 4 (1992) 835

43. D. J. Anderson, F. Van Lente, F. S. Apple, S. C. Kazmierczak, J. A. Lott, M. K. Gupta, N. McBride, W. E. Katzin, R. E. Scott, J. Taffaletti, C. J. Menendez-Botet, M. K. Schwartz, W. J. Castellani, Anal. Chem., 63 (1991) 165R

44. G. N. Kamau, J. F. Rusling, Electroanalysis, 6 (1994) 445

45. X. K. Xing, T. C. Tan, M. Shao, C. C. Liu, Electroanalysis, 4 (1992) 191

46. A. M. Farrington, N. Jagota, J. M. Slater, Analyst, 119 (1994) 233

47. J. Kulys, A. Drungiliene, Electroanalysis, 3 (1991) 209

48. U. Korell, R. B. Lennox, Anal. Chem., 64 (1992) 147

49. M. E. G. Lyons, W. Breen, J. Cassidy, J. Chem. Soc. Faraday Trans., 87 (1991) 115

50. Y. W. Xie, S. J. Dong, Electroanalysis, 6 (1994) 119

51. S. J. Dong, G. L. Che, J. Electroanal. Chem., 315 (1991) 191

52. Z. Q. Gao, A. Ivaska, Anal. Chim. Acta, 284 (1993) 393

53. A. S. N. Murthy, Biosens. Bioelec., 9 (1994) 439

54. A. Campiglio, Analyst, 118 (1993) 545

55. S. Uchiyama, Y. Hasebe, S. Suzuki, Electroanalysis, 5 (1993) 653

56. S. M. Sultan, A. M, Addennabi, F. E. O. Suliman, Talanta, 41 (1994) 125

57. S. M. Sultan, Talanta, 40 (1993) 593

58. S. Z. Qureshi, A. Saeed, S. Haque, M. A. Khan, Talanta, 38 (1991) 637

59. F. Belal, Electroanalysis, 4 (1992) 589

60. M. Petersson, Anal. Chim. Acta, 187 (1986) 333

61. A. R. Hillman in Electrochemical Science and Technology of Polymers, V. 1, (R. G. Linford, ed.) Elsevier, Amsterdam, 1987, pp. 102, 241

62. F. C. Anson, Y-M. Tsou, J. M. Saveant, J. Electroanal. Chem., 178 (1984) 113

63. M. Koppenhagen, M. Majda, J. Electroanal. Chem., 189 (1985) 379

64. P. Ferrutti, R. Barbucci, Adv. Polm. Sci., 58 (1984) 55

65. M. E. G. Lyons, Analyst, 119 (1994) 805

66. J. J., Ruiz, A. Aldaz, M. Dominguez, Can. J. Chem., 56 (1978) 1533

67. M. Rueda, A. Aldaz, F. Sanchez-Burgos, Electrochim. Acta, 23 (1978) 419

68. A. P. Doherty, J. G. Vos, Anal. Chem., 65 (1993) 3424

69. A. P. Doherty, M. A. Stanley, C. E. Koning, R. H. G. Brinkhuis, J. G. Vos, Electroanalysis, 7 (1995)

70. M. A. Kutnik, J. H. Skula, H. E. Sunkerlich, S. T. Omage, J. Chromatogr., 8 (1985) 31

71. N. Cenas, J. Rozgaite, A. Pocius, J. Kulys, Electroanal. Chem., 154 (1983) 121

72. E. Rohde, E. Dempsey, M. R. Smyth, J. G. Vos, H. Emons, Anal. Chim. Acta, 278 (1993) 5

73. J. Kulys, E. J. D'Costa, Anal. Chim. Acta, 243 (1991) 173

74. S. A Wring, J. P. Hart, B. J. Birch, Anal. Chim. Acta, 229 (1990) 63

# Chapter 7

## Concluding Comments

For the detection of analytes, such as the oxidation of ascorbic acid, which are mediated throughout the redox polymer layer, the thickness of the polymer film has to be carefully controlled in order to generate reproducible results as the presence of a greater number of mediating sites leads to a proportionally greater response by the polymer film. This stringent requirement can have disadvantages in the application of such polymer modifying films to routine analytical applications. For those analytes which display only surface mediation such as the reduction of free chlorine this is not a difficulty since the analyte does not enter the film and only those redox sites at the polymer-solution interface are involved in the mediation. However, the use of only the surface sites means that the advantages of a three-dimensional polymer mediating film are ignored and the optimum catalytic properties of the film are not realised. Also, for routine analytical applications, it has not been possible to match the stability found in sensors based on electrochemical techniques such as potentiometric electrodes.

However, the field of biosensors appears to be now examining in detail the properties of metallo-polymers, including $[Os(bpy)_2(PVP)_{10}Cl]Cl$. Rather than voltammetric chemical sensors, it appears that biosensors offer the best opportunities for future research on the applications of redox polymers. These polymer modified amperometric biosensors are receiving a wider examination because of the ease of immobilising enzymes within the hydrophobic polymer matrix. The three-dimensional nature of the redox polymer and the ability to vary its thickness means that enzyme loading can be increased and the rapid electron self-exchange rates between the catalytic redox sites within the film ensure that there is efficient mediation between the enzyme and the underlying electrode. These polymer films are far more stable compared to the typical monolayer films previously used for immobilising enzymes at electrode surfaces. The resistance of polymer films to surface fouling and passivation and their permselective qualities have major advantages in the application of such sensors to biological samples. The range and scope of applications of electroactive polymers in bioelectrochemistry is expanding rapidly. A number of papers describing the application of $[Os(bpy)_2(PVP)_{10}Cl]Cl$ for such use is described in section 1.10 of chapter 1.

In the previous chapters, the use of osmium, and to a lesser extent ruthenium, poly(pyridyl) redox polymers in the preparation of electroactive surfaces for the detection of a number of different analytes has been discussed. Post-modification of these redox polymers by partial cross-linking has been shown to improve the stability of the modified surfaces without adversely affecting its surface behaviour or the polymer's charge transport characteristics.

The polymer $[Os(bpy)_2(PVP)_{10}Cl]Cl$ has been shown to be capable of the detection of a number of analytes. For example, it was shown to electrocatalyse the reduction of nitrite and by adapting a flow injection system with a cadmium reduction column, a nitrate sensor was developed. The utility of such a sensor was further developed by adaptation of an off-line absorption technique for $NO_2$ to form a $NO_x$ sensor. The sensor characteristics found compared well with the standard method of analysis for $NO_x$. The reduction of Fe(III) and free chlorine and the oxidation of ascorbic acid have also been demonstrated and this ability has been translated into the development of sensors for these analytes by the modification of thin layer flow cells and their use as detectors in flow injection analysis.

The behaviour of cross-linked $[Os(bpy)_2(PVP)_{10}Cl]Cl$ in conventional three electrode cell systems has been analysed with respect to its surface behaviour and charge transport characteristics using cyclic voltammetry and rotating disc electrode voltammetry and the results of this analysis have been compared with similar investigations in the thin layer flow cell under hydrodynamic flow conditions. Certain differences in the amperometric surface behaviour between the two cell types was found. This appeared to be due to the non-steady state response found in the flow cell compared with the conventional cell.

The behaviour of $[Ru(bpy)_2(PVP)_{10}Cl]Cl$ has also been examined and its amperometric surface characteristics and charge transport properties have been compared favourably with those of $[Os(bpy)_2(PVP)_{10}Cl]Cl$. However, its use in the development of sensors is severely limited due to its unstable nature as discussed in chapter 2.

# Appendix

## Published Papers

ELSEVIER

Analytica Chimica Acta 299 (1994) 81–90

ANALYTICA CHIMICA ACTA

# Comparison of the analytical capabilities of an amperometric and an optical sensor for the determination of nitrate in river and well water

Margaret A. Stanley [a], Joe Maxwell [b], Mairead Forrestal [a], Andrew P. Doherty [a], Brian D. MacCraith [b,*], Dermot Diamond [a], Johannes G. Vos [a,*]

[a] *School of Chemical Sciences, Dublin City University, Dublin 9, Ireland*

[b] *School of Physical Sciences, Dublin City University, Dublin 9, Ireland*

Received 18 February 1994; revised manuscript received 20 July 1994

**Abstract**

The analysis of nitrate in water has been studied using novel amperometric and optical sensors. A flow-injection analysis system with amperometric detection has been developed in which nitrate is determined as nitrite after reduction in a cadmium column. The working electrode is glassy carbon modified with a crosslinked redox polymer. The linear range is 0.1 to 190 mg/l $NO_3$-N ($r > 0.999$) and the limit of detection (LOD) is 50 $\mu$g/l $NO_3$-N. A fibre optic sensor based on a dual wavelength absorption approach has also been developed. A signal at 210 nm where nitrate absorbs was referenced against a signal at 275 nm where nitrate does not absorb. Its linear range is from 0.4 to 30 mg/l $NO_3$-N and its LOD is 400 $\mu$g/l $NO_3$-N. These diverse methods have been applied to the analysis of the same river water samples and good correlations have been observed between the two measurement techniques and a standard ion chromatography method.

*Keywords*: Amperometry; Flow Injection; Sensors; Nitrate; Waters

## 1. Introduction

Nitrate enters natural waters from many sources and over the past few decades, its concentration has increased progressively in the environment [1]. The dominant factor in this trend has been the increased usage of nitrate-based fertilisers in agriculture and the consequential leaching of nitrate into freshwater supplies [2–4]. The nitrate anion is quite mobile because of its solubility in water and the predominantly negative charge on soil particles, and so it is readily leached if not utilised by plants. The solubility aspect means that agriculture is a major contributor to nitrate loading in freshwater supplies and consequently in drinking water [3].

Nitrate represents a potential hazard because of its participation in reactions similar to those found in the human stomach which give rise to *N*-nitroso compounds, some of which are carcinogenic [5,6]. It has been suggested that gastric cancer is associated with nitrate intake through this mechanism [7]. Furthermore, certain species of bacteria in humans can enzymatically reduce nitrate to nitrite [8]. The toxic effects of nitrite, vasodilation, lowering of blood pressure and formation of methaemoglobin, are well known [9].

* Corresponding authors.


*SSDI* 0003-2670(94)00328-9

The European Community Directive on the quality of water intended for human consumption came into effect in August 1985 with a limit of 11 mg/l $NO_3$-N (nitrate as nitrogen) as the maximum admissible level for nitrate [10].

The standard method for nitrate measurement involves reduction of nitrate to nitrite using a copper activated cadmium catalyst and determination of the nitrite concentration by reaction with sulphanilamide and *N*-1-naphthylethylenediamine in HCl to produce a purple/red azo dye. The absorbance of this dye at 543 nm is measured using a spectrophotometer and this is related to the sample nitrate concentration by means of a calibration curve derived from reference nitrate standards [11].

In view of the increase in interest in the quality of drinking water, sensitive, selective and simple methods for the determination of nitrate are desirable. One approach to this problem is the development of a modified electrode sensor which can be incorporated into a bench-top flow-injection analysis system (FIA) [12]. A second is the development of a fibre optic sensor which has shown itself capable of in situ monitoring [13]. In this contribution both of these types of sensor are investigated in detail. An ion chromatographic system was used to provide a reference method against which these more novel methods of detection could be compared.

Due to the selective detection of the amperometric and the optical sensors described in this paper, the analysis of nitrate can be carried out without the added requirement of mixing the sample with numerous reagents or the expense of chromatographic columns. This allows an added flexibility in the design of these sensors without compromising their sensitivity.

## 2. Experimental

### 2.1. Electrolytes and solutions

The electrolyte used was 0.1 mol $dm^{-3}$ $H_2SO_4$. Nitrite solutions were prepared freshly each day from $NaNO_2$. $NaNO_3$ was used to prepare the nitrate solutions. The carrier solution used with the cadmium column was composed of 0.1 mol $dm^{-3}$ NaCl and 2.5 g/l EDTA. A 2% w/v solution of $CuSO_4 \cdot 5H_2O$ was used to copperise the cadmium. All chemicals described in the text were of A.R. grade and were prepared with Milli-Q water.

### 2.2. Preparation of $[Os(bipy)_2(PVP)_{10}Cl]Cl$

This material was synthesised according to the procedure described by Forster and Vos [14] except that 2-methoxyethanol was used as the solvent instead of ethanol. A metal loading of one osmium centre per ten vinyl pyridine units was chosen as this loading has been shown to display optimum charge transfer characteristics [15]. PVP (poly-4-vinyl pyridine) of molecular weight 600,000 a.m.u. was used, and bipy = bipyridine.

### 2.3. Preparation of modified electrode

Modified electrodes were prepared by polishing glassy carbon electrodes with 5 $\mu$M alumina as an aqueous slurry on a felt cloth followed by a thorough rinsing with distilled water and methanol. The freshly prepared electrode surfaces were modified by drop coating using a 1% w/v methanolic solution of the polymer. Cross-linking of this polymer was achieved by adding an appropriate volume of 1,10-dibromodecane dissolved in methanol to the polymer deposited on the electrode [16]. These two solutions were then mixed gently and allowed to dry slowly overnight in a methanolic atmosphere.

### 2.4. Flow injection apparatus

The flow injection apparatus consisted of a Gilson Minipuls 3 peristaltic pump, a six port Rheodyne injector valve (No. 9125) fitted with a 20-$\mu$l fixed volume sample loop, a Rheodyne switching valve (No. 0792), an EG and G Princeton Applied Research Model 400 electrochemical detector and a Kipp and Zonen *X–t* recorder. Silicone rubber tubing was used at the peristaltic pump and PTFE 1/16″ o.d. × 1/32″ i.d. tubing for the rest of the system. For the reduction column a 3 mm bore, 50 mm length glass column was used. This was filled with cadmium granules (40–60 mesh) which had been washed in a 2% solution of copper sulphate. The column thus obtained was found to give a stable response over a two week period. A schematic diagram of the FIA apparatus can be seen in Fig. 1. Sample injections were made using a 2 $cm^3$ glass syringe fitted

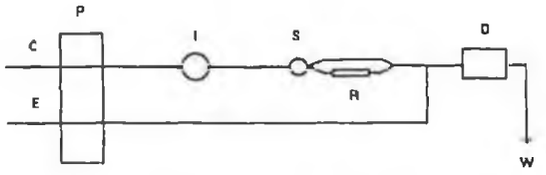


Fig. 1. Manifold of flow injection analysis system. P = Peristaltic pump, I = injection valve, S = switching valve, R = Cu/Cd reduction column, D = electrochemical detector, W = waste. $C = 0.1$ mol dm$^{-3}$ NaCl + $2.5 \times 10^{-3}$ kg/dm$^{-3}$ EDTA. $E = 0.1$ mol dm$^{-3}$ $H_2SO_4$.

with a Rheodyne injection needle. In the standard EG and G flow cell, an Ag/AgCl electrode acted as the reference and the auxiliary electrode was the stainless steel cell body.

### 2.5. Fibre optic sensor

*Optical system design*

Light from a 30-W Hamamatsu L2196 deuterium lamp was coupled to the optical fibre through two rotating filters. The lamp output beam was collimated by a system of fused silica lenses before passing through a custom-made filter wheel to another lens which focused the UV light into the optical fibre. The optical fibre took light to the absorption cell while another fibre transmitted light from the cell to the photomultiplier and amplifier. The optical fibre used was Fibreguide Industries Superguide G SFS600/660B UV–visible optical fibre with a 600 $\mu$m core diameter, a minimum bend radius of 50 mm and a numerical aperture of 0.22. The attenuation at 210 nm was approximately 1.5 dB per metre. The absorption cell shown in Fig. 2 was made at the university. The absorption path length is adjustable but in the work reported here a path length of 1 mm was used.

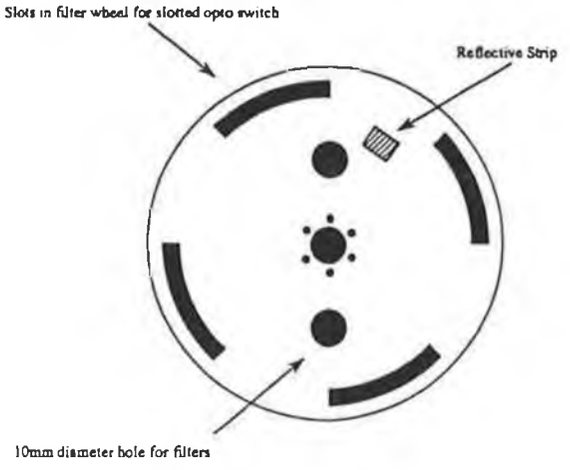


Fig. 3. Filter wheel for fibre optic sensor.

*Electronic system*

The Hamamatsu R269 photomultiplier tube was mounted directly onto the Hamamatsu C1556 amplifier module to prevent noise pickup from long leads. The amplifier was connected to a 12 bit analogue to digital converter (ADC) via a sample-and-hold circuit (SHA). The AD585 SHA device held the analogue voltage level constant while the AD574 ADC performed a conversion. The ADC was configured to accept a 0–10 V full scale input signal to directly match the output of the amplifier. Spectral selection was accomplished by a custom made filter wheel (see Fig. 3) which was mounted on a Scitec optical chopper which provided a variable speed motor to turn the wheel together with a slotted opto-switch to provide timing pulses. The two interference filters were located diametrically opposite on the wheel. Slots cut along the outer edge of the wheel were used to initiate a "hold" of the optical signal followed by a data conversion on the ADC. Two other slots over opaque areas of the filter wheel enabled subtraction of background light. A small

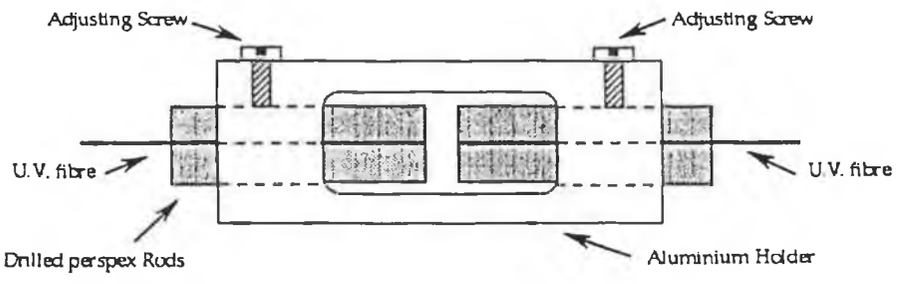


Fig. 2. Absorption cell of the fibre optic sensor. Water is free to move through the hollow inner space.

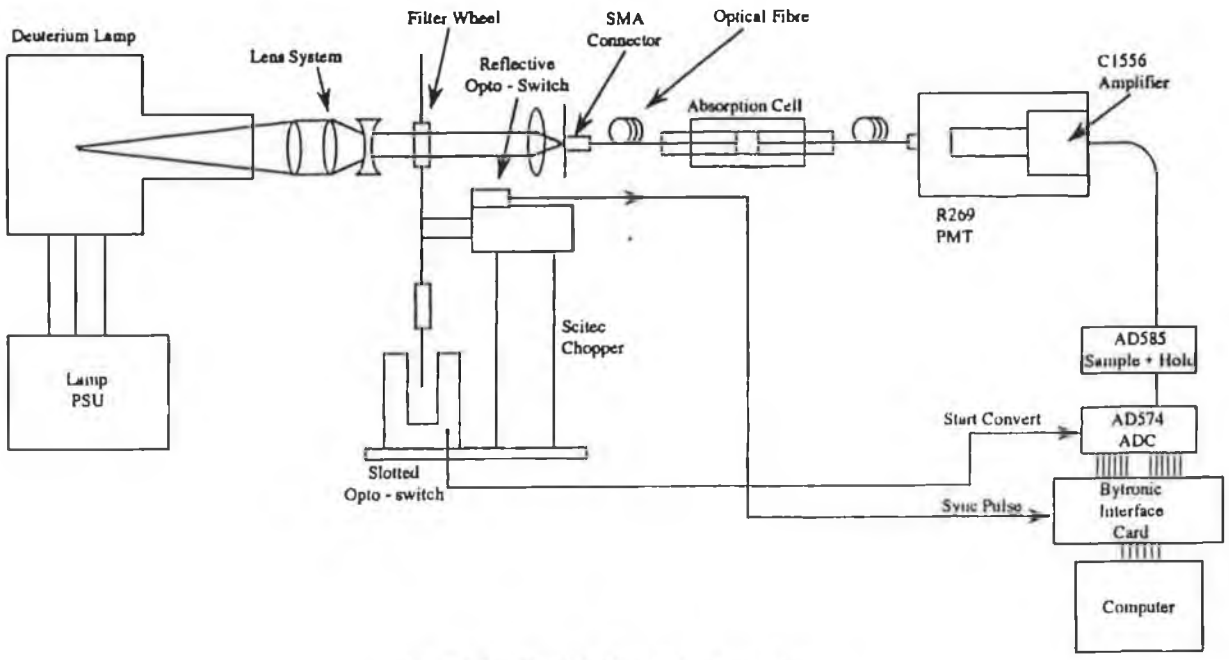


Fig. 4. Manifold of the fibre optic nitrate sensor.

reflective strip placed on the wheel was used to trigger a reflective opto-switch. This provided a synchronisation pulse so that data was collected in the correct sequence on every rotation of the filter wheel.

*Nitrate sensor design*

A schematic diagram of the prototype optical fibre sensor is shown in Fig. 4. This figure details the layout of the optical and electrical systems in relation to each other. Two narrow band filters were centered on 210 nm and 275 nm in a rotating filter wheel placed between the lamp and the launch fibre. The 210 nm interference filter had a full width at half maximum of 16 nm and a peak transmission of 18% while the 275 nm filter had a full width at half maximum of 9.5 nm and a peak transmission of 19%.

The analogue detection system consisted of a R269 UV-sensitive photomultiplier tube and low noise preamplifier. The output from the preamplifier was fed to an analogue to digital converter via a 'sample and hold' amplifier (SHA) which is synchronised to the rotating filter wheel. The SHA circuit effectively holds the signal at a constant value while an analogue to digital conversion was carried out. Signals corresponding to light levels at 210 nm and 275 nm were stored by a computer. The average of 250 points was then used to provide absorbance factor values for the nitrate solution placed in the absorption cell.

### 2.6. Sample treatment

All samples were collected in polyethylene containers, which had been washed with Milli-Q water to ensure they were free from contamination. Before filling, the bottles were rinsed three times with the water to be collected. River water samples were collected manually, by dipping the container into the river, a short distance from the riverbank. The samples from the

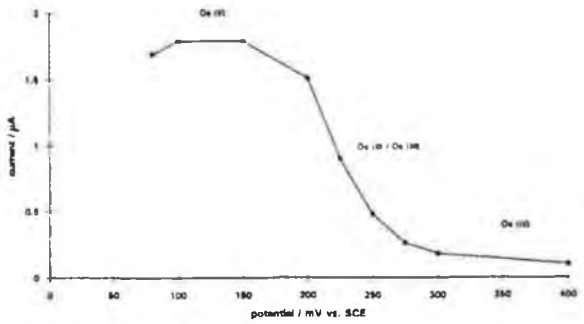

Fig. 5. Hydrodynamic voltammogram for the measurement of 15 mg/l $NO_3$-N at the modified electrode in the thin layer electrochemical flow cell. Flow rate is 0.5 $cm^3$ $min^{-1}$. Other conditions are as described in the text.

wells were collected by means of a pump. These were obtained only after the well was pumped sufficiently to ensure that the sample represented the groundwater source. On collection all samples were sealed, labelled and dated. Samples were refrigerated at 4°C and analysed within 48 h. Repeat measurements were made after several weeks and no loss of nitrate was found to have occurred.

## 3. Results and discussion

### 3.1. Modified electrode sensor

*Effect of applied potential*

An electrode modified with the $[Os(bipy)_2(PVP)_{10}Cl]Cl$ was used to detect nitrate anions after reduction to nitrite by a copperised cadmium column. Fig. 1 shows the layout of the FIA system. It can be used to detect both nitrite and nitrate ions depending on whether the reducing column is bypassed or not.

A hydrodynamic voltammogram of the system's response to nitrate is shown in Fig. 5. At a potential of 0.40 V vs. SCE no response to the reduced nitrate was observed. At this potential, the electrocatalytic sites were in the Os(III) state and therefore could not mediate the reduction of the nitrite. Decreasing the applied potential below 0.4 V vs. SCE resulted in the generation of catalytic Os(II) sites within the polymer and the onset of mediated reduction of nitrite was evident. From these results the optimum potential for detection was found to be 0.120 V vs. SCE and this potential was used for all subsequent measurements.

*Sensor response characteristics*

A high pH was required for reduction of nitrate by the cadmium column. So the carrier solution was adjusted to pH 9 with sodium hydroxide. However, detection of the reduced nitrate at the redox polymer had previously been found to be dependent on the hydrogen ion concentration [17]. Therefore a low pH was required for optimum detection sensitivity. It was found that at pH 4 the response to a solution containing 14 mg/l $NO_3$-N was 0.07 $\mu$A while at pH 1 the response to the same solution was 2 $\mu$A. This demonstrates how altering the pH of the electrolyte at the detector significantly affects the sensor's response. Consequently the flow of carrier from the column was merged with the sulphuric acid electrolyte before reaching the detector.

The peaks obtained using this FIA system were well defined and useful analytically. The precision of the response was found to be excellent with a relative standard deviation of 0.91% ($n = 10$). The sample throughput was calculated to be 100 samples/hour from basewidth measurement. At bare electrodes this reaction has been found to cause surface passivation [18]. This passivation was not observed at the modified electrode. No deterioration in the electrode's response was found even after hundreds of determinations. This stability was obtained by crosslinking the metallopolymer with 1,10-dibromodecane. Crosslinking the polymer bestowed greater stability on the electrode without compromising its sensitivity or selectivity. The effect of two weeks of constant electrolyte flow on the sensor's performance was monitored. The peak current of a standard solution of nitrate containing 1.0 mg/l $NO_3$-N was found to have decreased from 0.135 $\mu$A to 0.117 $\mu$A over this period, a reduction in signal of only 13%. The precision of this signal slightly decreased to a relative standard deviation of 0.75% for $n = 10$. This showed a remarkable improvement in stability compared with the uncrosslinked polymer which was found to have a half-life of only 46 h [17].

At a surface coverage of $1 \times 10^{-9}$ mol cm$^{-2}$ the sensitivity of the modified electrode in this flow cell was found to be 0.05 $\mu$A mg$^{-1}$ cm$^3$. The linear range extends from 0.1 to 190 mg/l $NO_3$-N with correlation coefficients typically $> 0.999$. The linear range encompassed both the normal nitrate levels and the occasionally excessive levels found in environmental water samples without the need for dilution. The limit of detection, defined as twice the height of the noise ($S/N = 2$), was found to be 50 $\mu$g/l $NO_3$-N.

*Selectivity*

Millimolar concentrations of the cationic species K(I), Na(I), Li(I), Mg(II), Al(III) produced no interfering response at the sensor. The anions $Cl^-$, $SO_4^{2-}$, $PO_4^{3-}$ similarly did not interfere. Ascorbic acid, though it is a common interferent in colorimetric procedures, was found to have no interfering effect at the osmium polymer.

A possible interferent is Fe(III) which has previously been shown to be capable of mediation by the osmium polymer [19]. The formal potential of the Fe(II)/Fe(III) couple is 0.46 V vs. SCE therefore the

reduction of Fe(III) can be mediated by the osmium couple (whose $E_{1/2} = 0.25$ V vs. SCE). However, formation of the EDTA complex of iron results in a shift in the formal potential to a region negative of the formal potential of the osmium electrocatalyst. The $[Fe(EDTA)]^+$ formal potential being $-0.13$ V vs. SCE, which eliminates the interference.

Nitrite will of course interfere in the analysis. This can be overcome by comparing the sample's response directly at the sensor and then via the column. Any difference being due to the presence of nitrate.

### 3.2. Fibre optic sensor

*Sensor operation*

The principle of operation of the fibre optic sensor was based on the known ultraviolet absorption of the nitrate ion in the 200 nm spectral region. The strong absorbance of nitrate in the 210 nm region was measured relative to the absorbance in a region where nitrate does not absorb. The wavelength 275 nm was chosen for this purpose because nitrate does not absorb at this wavelength and it can be used to compensate for mainly organic interferents when these are present in significant concentrations. This dual wavelength approach was achieved by using two narrow band filters centered on 210 nm and 275 nm in a rotating filter wheel placed between the lamp and the launch fibre. This approach also compensated for spectrally neutral drifts within the system such as ageing of the light source and detector.

The detected signals are processed to yield an absorbance factor A which is defined as

$$A = \log_{10}\left(\frac{I_o}{I}\right) \quad (1)$$

The detected signal at 210 nm was represented by $I$ and the signal at 275 nm represented by $I_o$. The spectral response of the system at 210 nm was very different to that at 275 nm. Consequently, when $A$ was calculated using Eq. 1 the result was not a true absorbance expressible in absolute absorbance units, i.e. when no nitrates were present the calculated value of $A$ was non-zero due to the fibre itself absorbing more at 210 nm compared to 275 nm. For this reason the calculated result was referred to as an absorbance factor.

*Sensor response characteristics*

In order to be viable as a groundwater nitrate monitor the sensor must be capable of detecting nitrates at considerable distances from the optical detector and signal processing electronics. With this in mind the sensor was tested using a total length of 40 m of optical fibre, i.e. 20 m between the source and the absorption cell and 20 m between the absorption cell and the detector. A calibration curve obtained with nitrate concentration given in units of mg/l $NO_3$-N is shown in Fig. 6a. This curve showed a marked levelling off of the slope for concentrations greater than 30 mg/l $NO_3$-N and hence a great reduction in sensitivity in this region. Consequently the range of this sensor over a total distance of 40 m was limited from 0.4 to 30 mg/l $NO_3$-N. Experiments carried out on the sensor using only 2 m of optical fibre showed a less marked levelling off of the calibration curve (see Fig. 6b) and the absorbance factor values were much lower than in the case of the 40 m length of fibre. This is a result of the greater total attenuation experienced at 210 nm compared to 275 nm. When the signals at these two wavelengths were

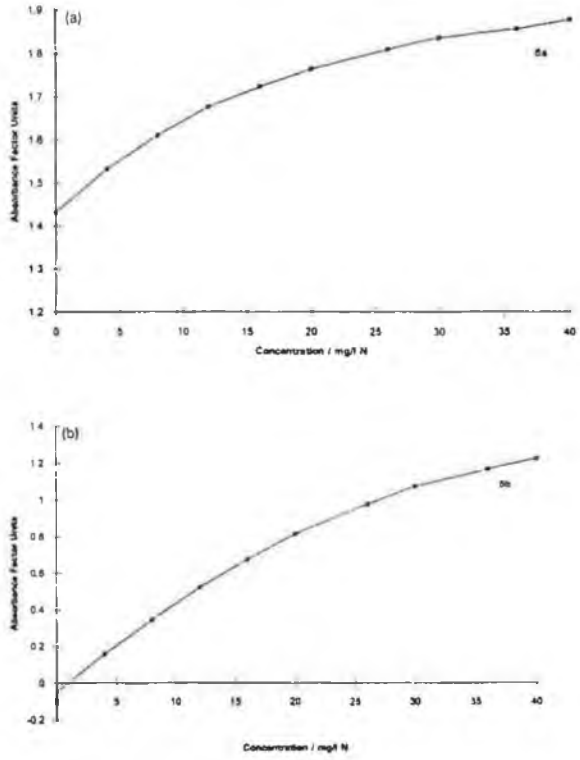


Fig. 6. Calibration curves of the fibre optic sensor. (a) Total fibre length was 40 m; (b) total fibre length was 2 m.

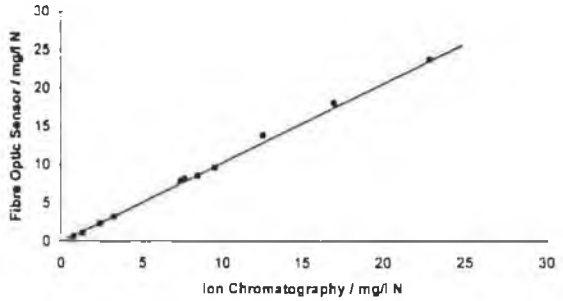


Fig. 7. Comparison of the fibre optic sensor with the standard ion chromatographic method.

ratioed the lower transmission at 210 nm resulted in a larger absorbance factor value. The fibre attenuation was 1.5 dB per metre which means 50% of the light was lost every two metres.

This non-linearity at higher concentrations can also be accounted for by the fact that the Beer-Lambert law is successful in describing the behaviour of dilute solutions only. At high concentrations the refractive index and absorptivity of the solution are not constant but may deviate considerably from their values at low concentrations.

Because the calibration curve for this sensor was not linear over the complete range tested it is not possible to quote an overall sensitivity value. However the sensitivity was approximately 0.04 AFU per mg/l $NO_3$-N (AFU = absorption factor unit) below 9 mg/l $NO_3$-N. At higher concentrations the slope gradually decreased and as a result the sensitivity also decreased to approximately 0.02 AFU per mg/l $NO_3$-N. The resolution of the sensor at lower concentrations was found to be 0.25 mg/l $NO_3$-N but this rose to 0.55 mg/l $NO_3$-N in the non-linear region. The repeatability found in consecutive measurements was found to be 1.7% well within the 2.5% specification set down by the UK Water Industry [20].

*Selectivity*

Although many inorganic anions absorb ultraviolet radiation at wavelengths in the 200 nm region, the majority of the more commonly occurring anions in water such as sulphate and phosphate only show appreciable absorption at shorter wavelengths [21]. Chloride is however expected to interfere and the sensor can therefore only be used for fresh water determinations. A degree of detection selectivity therefore exists for the sensor and this allows nitrate analysis in the presence of relatively high and variable background levels of inorganic ions. This coupled with the fact that direct UV detection is particularly suited to the nitrate ion in view of its relatively high molar absorptivity [22] ensures that the fibre optic sensor is very selective for nitrate determinations in water.

A number of chemical species other than nitrate do absorb in the 210 nm region. These include nitrites, iron(III) species, carbonates and humic acids. Interference from nitrite would be unlikely as nitrite levels in natural waters are extremely low, less than 0.01 mg/l $NO_3$-N, and any nitrate results due to unusually high concentrations of nitrite would be useful as a pollution indicator.

The effect of carbonates was investigated by using a solution containing 4 mg/l $NO_3$-N and 300 mg/l carbonate. It was found that the presence of carbonate resulted in a positive 4.5% error. A 4 mg/l iron(III) solution was found to have a maximum absorbance value of only 0.03 AFU. So unless it was present in high concentrations it would not have a large interfering effect. The presence of 40 mg/l of humic acid in a solution of 4 mg/l $NO_3$-N produced a 10% positive error. However this concentration is much greater than would be expected in most waters and considerably more than that found in groundwater where organic material is negligible.

One way of eliminating these interferents is to prevent them entering the absorption cell. Thompson and Blankley [23] used a conventional dialysis membrane as a filter to prevent iron and large molecules such as humic acids from entering the absorption cell. This technique could be readily applied to the fibre optic sensor's absorption cell. The effect of other interferents such as carbonates depends upon their concentration and this in turn depends upon the geographical location

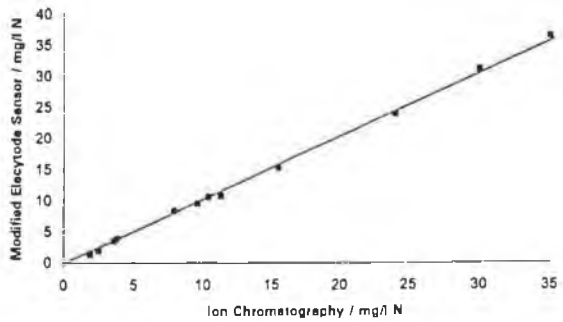


Fig. 8. Comparison of the modified electrode sensor with the standard ion chromatographic method.

of the water source. The interfering effect of nitrite can be discounted as it occurs in extremely small concentrations and any excessive amounts are a clear indication of serious pollution.

### 3.3. Validation of methods

These two experimental methods of nitrate detection, the modified electrode sensor and the fibre optic sensor, were then compared with an ion chromatographic procedure based on the Dionex Method AU131. The regression graphs (see Figs. 7 and 8) were plotted using the data obtained for both the experimental methods and the standard method. Each point on the graphs represents a single sample analysed by both methods in comparison with the ion chromatographic system. The graphs show only a slight deviation from the ideal with a correlation coefficient of 0.998 for the fibre optic sensor and a coefficient of 0.994 for the modified electrode sensor. This shows that minimum systematic errors occur in the fibre optic sensor and the modified electrode sensor.

*Sample analysis*

Having established the methods were accurate and precise for the determination of nitrate a number of real samples were collected from rivers in various locations. No sample preparation of any kind was performed on these samples before analysis by any of the systems. The results are shown in Table 1. The matrix concentrations and nature of the different samples are given in Tables 2 and 3 [24]. Good correlation between all three methods can be observed. Interestingly, although the chloride ion is expected to interfere in the fibre optic method the different concentrations of this ion present in the samples (see Table 2) do not adversely affect the results obtained from this sensor.

Use of the ion chromatographic procedure allowed the analysis of the water samples for the presence of other anions apart from nitrate. In the ion chromatographic method, due to the chromatographic process, nitrate is separated from any other anions present thus removing any interferences. Once separation has occurred results depend only on the performance of the

Table 2
Concentrations of a number of anions found in the water samples using ion chromatography (data taken from Ref. [24])

| Sample | Concentration of species (mg/l) | | | |
|---|---|---|---|---|
| | Chloride | Bromide | Phosphate | Sulphate |
| Arvagh | 23.75 | < 1 | < 1 | 18.56 |
| Boyne | 21.85 | < 1 | < 1 | 66.49 |
| Hillcrest | 16.3 | < 1 | < 1 | 10.65 |
| Kells | 29.79 | < 1 | < 1 | 39.33 |
| Kill (1) | 14.73 | < 1 | < 1 | 18.78 |
| Kill (2) | 13.86 | 1.24 | < 1 | 17.71 |
| Knockmoylan | 50.59 | 1.22 | < 1 | 32.77 |
| Mattock | 24.68 | < 1 | < 1 | 14.38 |
| Monasterevin | 16.48 | < 1 | 1.28 | 20.05 |
| Stradbally | 16.76 | 1.22 | < 1 | 10.84 |
| Tinnock | 62.87 | 1.21 | < 1 | 19.62 |
| Ward | 45.57 | 1.14 | 2.19 | 11.63 |

Table 1
Concentration of nitrate in the river and well water samples (NA = not analysed)

| Sample | Concentration (mg/l N) | | |
|---|---|---|---|
| | Ion chromatographic method | Fibre optic sensor method | Modified electrode method |
| Arvagh | 2.32 | 2.45 | NA |
| Boyne | 0.84 | 0.73 | 0.89 |
| Hillcrest | 2.43 | 2.37 | 2.48 |
| Kells | 18.47 | 17.34 | 19.83 |
| Kill (1) | < 0.1 | < 0.5 | < 0.05 |
| Kill (2) | < 0.1 | < 0.5 | < 0.05 |
| Knockmoylan | 2.52 | 2.71 | 2.61 |
| Mattock | 2.1 | 2.02 | 2.41 |
| Monasterevin | 3.45 | 3.29 | NA |
| Stradbally | 3.67 | NA | 3.61 |
| Tinnock | 13.12 | 13.99 | 13.74 |
| Ward | 1.97 | 2.24 | 1.99 |

Table 3
Location of water sampling sites (data taken from Ref. [24])

| Sample | Source | County | Well depth (feet) | Additional information |
|---|---|---|---|---|
| Arvagh | Well | Cavan | 25 | Agricultural area |
| Boyne | River | Louth | – | Agricultural area |
| Kells | Well | Meath | 22 | Tillage area |
| Kill (1) | Well | Kildare | 85 | Limestone area |
| Kill (2) | Well | Kildare | 70 | Limestone area |
| Mattock | River | Louth | – | Agricultural area |
| Hillcr est | Well | Laois | 70 | Tillage area |
| Stradbally | Well | Laois | 35 | Tillage area |
| Knockmoylan | Well | Kilkenny | 80 | Devonian |
| Monast erevin | River | Kildare | – | Limestone area |
| Tinnock | Well | Wexford | 80 | Tillage area |
| Ward | River | Dublin | – | Agricultural area |

conductivity detector and calibration procedures. The fibre optic and modified electrode sensors, however, measure the nitrate in the presence of these ions whose concentrations vary from sample to sample. Despite this these sensors showed good selectivity for nitrate.

## 4. Conclusions

Two sensors suitable for the detection of nitrate in water samples have been described. A prototype optical fibre sensor for groundwater monitoring has been designed, constructed and tested. At this stage in its development the sensor is semi-portable and further work is being carried out on it to allow it to become a more compact, portable instrument. For example the use of a CCD array instead of the photomultiplier tube would allow the capture of complete spectra thus eliminating filters from the design, with the added bonus of being able to compensate for turbidity. Furthermore this approach would facilitate the development of multiwavelength algorithms which would impart greater selectivity

The electrochemical sensor has been designed for the laboratory environment. It provides a stable detection method housed in an easy to construct manifold. Its main advantages are twofold; first of all no sample pre-treatment is needed and fast sample throughput is possible. Secondly, with this measurement technique the effect of interferences is enormously reduced since with these polymer modified electrodes only species with an appropriate redox potential are detected. This selectivity can be controlled by the choice of the redox potential of the coating. Of all species normally occurring in river and well water, only nitrite and iron could possibly interfere in the reduction process, these can however be dealt with by adapting the measuring technique. Other species present will not interfere at levels up to at least 100 mM. Also the electrodes show a long linear range, fouling of the electrode surface is not observed and the modified electrodes are stable over a long period.

Both sensors approach the problem of nitrate detection but from vastly different approaches. Though not as flexible as the ion chromatography system, which can analyse for the presence of any ion, both sensors are simple to use with short analysis times. Both are reliable methods of detection which show good correlation between each other and with another standardised method. Neither use the costly reagents associated with typical nitrate analyses [11].

## Acknowledgements

We thank EOLAS (the Irish Science and Technology Agency) for financial assistance for this work.

## References

[1] P. Brimblecombe and D.H. Stedman, Nature, 298 (1982) 460.
[2] D. Forman, S. Al-Dabbagh and R. Doll, Nature, 313 (1972) 620.

[3] H. Moller J. Landt, E. Pedersen, P. Jensen, H. Autrup and O. Moller Jensen, Cancer Res., 49 (1989) 3117.
[4] P.J. Flanagan, Parameters of Water Quality: Interpretation and Standards, Environmental Research Unit, Dublin, 1990,
[5] R. Armijo, A. Gonzalez, M. Orellana, A. H, Coulson, J.W. Sayre and R. Detels, Int. J. Epidemiol., 10 (1981) 57.
[6] C. Cuello, P. Correa, W. Haenszel, G. Gordillo, C. Brown, M. Archer and S. Tannenbaum, J. Natl. Cancer Inst., 57 (1976).
[7] P. Correa, Cancer Surv., 2 (1983) 437.
[8] Assembly of Life Sciences (U.S.). Committee on Diet, Nutrition, and Cancer, Diet, Nutrition, and Cancer, National Academy Press, Washington, DC, 1982.
[9] W. Lijinsky and S. Epstein, Nature, 225 (1970) 21.
[10] D.J. Briggs, The State of the Environment in the European Community 1986, Office for Official Publications of the European Communities, Luxembourg, 1987.
[11] A.E. Greenberg, R.R. Trussel and L.S. Clesceri, Standard Methods for the Examination of Water and Waste Water, American Public Health Association, 1985.
[12] M.D. Imisides, G.G. Wallace and E.A. Wilke, Trends Anal. Chem., 7 (1988) 143.
[13] L.A. Saari, Trends Anal. Chem., 6 (1987) 85.
[14] R.J. Forster, J.G. Vos, Macromolecules, 23 (1990) 4372.
[15] R.J. Forster, J.G. Vos and M.E.G. Lyons, J. Chem. Soc., Faraday Trans., 87 (1991) 3761.
[16] A.P. Doherty and J.G. Vos, Electroanalysis, in press.
[17] A.P. Doherty and J.G. Vos, J. Chem. Soc., Faraday Trans., 88 (1992) 2903.
[18] G. Mengoli and M.M. Musiani, J. Electroanal. Chem., 199 (1989) 99.
[19] A.P. Doherty, R.J. Forster, M.R. Smyth and J.G. Vos, Anal. Chem., 64 (1992) 572.
[20] F. Campbell, Nitrate Measuring Instruments, UK Water Industry Specifications, Information and Guidance Notes, No. 7-11-00, Issue 1, July 1991.
[21] P.R. Haddad and P.E. Jackson, Ion Chromatography – Principles and Applications, Journal of Chromatography Library, Vol. 46, Elsevier, Amsterdam, 1990.
[22] H. Avsec, L. Kosta and I. Janzekovic, Vestn. Slov. Kem. Drus., 33 (1986) 413.
[23] K.C. Thompson and M. Blankley, Analyst, 109 (1984) 1053.
[24] M. Forrestal, M.Sc. Thesis, Dublin City University, 1993.

# The Effect of the Nature of the Polymer Backbone on the Stability and the Analytical Response of Polymer-Modified Electrodes

*A.P. Doherty,*[+] *M.A. Stanley,*[+] *G. Arana,*[+] *C.E. Koning,*[++] *R.H.G. Brinkhuis,*[++] and *J.G. Vos**[+]

[+] School of Chemical Sciences, Dublin City University, Dublin 9, Ireland
[++] Laboratory of Polymer Chemistry, State University Groningen, 9747 AG Groningen, The Netherlands

Received: February 21, 1994
Final version: May 2, 1994

**Abstract**
The synthesis, characterization, and sensor application of the novel redox polymer $[Os(bipy)_2(PS)_{7.5}(DMAP)_{2.5}Cl]Cl$, where bipy = 2,2′-bipyridyl, PS = polystyrene, and DMAP = poly[4-(*N*-methyl-*N*-*p*-vinylbenzylamino) pyridine], are described. The charge transport properties of electrodes modified with the redox material are investigated using cyclic voltammetry and chronoamperometry. The modified electrode behaves as an efficient electrocatalyst for the outer-sphere reduction of $Fe^{III}$, with the cross-exchange reaction occurring at the surface of the polymer (*Sk″*) at concentrations less than $1.0 \times 10^{-3}$ mol dm$^{-3}$ $Fe^{III}$, with a change over to the $St_e$ kinetic regime at higher substrate concentrations. Direct agreement was observed between the kinetic behavior at rotating disk electrodes and in thin-layer flow cells. Application of the modified electrodes for the determination of iron in pharmaceutical formulations and the long term stability of the electrodes are investigated. The results obtained are compared with those reported for the analogous metallopolymer $[Os(bipy)_2(PVP)_{10}Cl]Cl$, where PVP is poly-4-vinylpyridine.

**Keywords:** Modified electrode, Redox polymer, Sensor, Flow injection analysis, Iron

## 1. Introduction

Modified electrodes have been the subject of active investigation over the last two decades because of the many potential applications which can be envisaged for these devices, e.g., solar energy conversion [1], heterogeneous electrocatalysis [2], sensor development [3], and electrochromics [4]. Many novel materials have been developed for the modification of electrode surfaces; however, much criticism has been voiced concerning the stability of the modifying layers under operational conditions [5, 6]. The introduction of polymeric materials for electrode modification with greatly enhanced stability resulted in rapid developments in this area of research [6]. However, for optimum analytical performance the redox polymer should interact strongly with the contacting electrolyte, a condition which tends to reduce the physical stability. As a result, polymeric modifiers can also be subject to serious stability problems. Several approaches have been adopted to enhance the physical stability of these redox polymer films. The redox polymer $[Ru(bipy)_2(PVP)_5Cl]Cl$ was found to have a half-life ($t_{\frac{1}{2}}$) of 8 h under the hydrodynamic conditions of flow-injection analysis [7]. Overlaying this polymer with electropolymerized poly(3-methylthiophene) or poly(*N*-ethyltyramine) resulted in electrodes with $t_{\frac{1}{2}}$ greater than 48 h. However, reduced electrode responses due to mass transport restrictions were evident. The incorporation of styrene residues via copolymerization with vinylpyridine to form styrene copolymers of poly(vinylpyridine) (PVP) has been found to greatly increase the physical stability of the ruthenium polymer, without significantly affecting the electrocatalytic behavior of the material towards the oxidation of substrates such as nitrite [8, 9]. Responses from these modified electrodes were found to remain constant for up to 14 days under severe hydrodynamic conditions. Cross-linking PVP films on electrode surfaces with dibromoalkanes was also found to increase the stability of electrostatically incorporated redox sites within the polymer film. Cross-linking was found to inhibit leaching of the electrostatically incorporated redox sites [10].

The use of polymer-bound catalysts for thermal reactions is well-established due to the advantages associated with such systems [11]. In particular, application of the engineering polymer poly[styrene-*co*-4-(*N*-methyl-*N*-*p*-vinylbenzylamino) pyridine] has been well-documented. This material and its monomeric analog compound 4-[(*N*,*N*-dimethylamino)pyridine have been exploited for the catalysis of many reactions, and is of particular importance due to its physical stability [12]. In this article, the synthesis and characterization of the redox polymer $[Os(bipy)_2(PS)_{7.5}(DMAP)_{2.5}Cl]Cl$ from $((PS)_{7.5}(DMAP)_{2.5})$ via the coordinative immobilization of osmium redox sites is described. The electrochemical and analytical performance of electrodes modified with this material and their long-term stability are discussed in relation to the model compound $[Os(bipy)_2(PVP)_{10}Cl]Cl$ [13]. The sensor is applied to the analysis of iron in tablet formulations.

## 2. Experimental

### 2.1. Materials and Reagents

The polymeric material poly[styrene-*co*-4-(*N*-methyl-*N*-*p*-vinylbenzylamino) pyridine] was synthesized as previously described [14]. The redox polymer $[Os(bipy)_2(PS)_{7.5}(DMAP)_{2.5}Cl]Cl$ was prepared as follows: 100 mg of the $((PS)_{7.5}(DMAP)_{2.5})$ material was dissolved in 40.0 cm$^3$ 2-methoxyethanol. $[Os(bipy)_2Cl_2]$ (55.1 mg) was dissolved in a separate 40 cm$^3$ aliquot of 2-methoxyethanol. The two solutions were then mixed in a 150 cm$^3$ round-bottomed flask. The mixture was then held under reflux for 48 h at 125°C. The reaction was monitored by UV/visible spectroscopy and cyclic voltammetry (CV). The disappearance of the redox wave at 0.0 V vs. the saturated calomel electrode (SCE) due to $[Os(bipy)_2Cl_2]$, and the formation of a redox wave at 0.250 V vs. SCE due to the species $[Os(N)_5Cl]$ indicated the formation of the polymer-bound redox material. After completion of the reaction, the resulting redox polymer was precipitated twice from 2-methoxyethanol in diethylether. The precipitate was dried in vacuo at 80°C for 24 h. 136 mg of product was recovered, which corresponds to 88% yield.

All electrolytes were prepared from water obtained from the Milli-Q water purification system. Reagent grade $H_2SO_4$,

  *1040-0397/95/0404-333 $ 5.00+.25/0*

$Na_2SO_4$, $HClO_4$, $NaClO_4$, and toluene-*p*-sulfonic acid (TpSA) were used without further purification. Fresh $Fe^{II}$ and $Fe^{III}$ solutions were prepared from $[(HN_4)_2Fe(SO_4)_2] \cdot 6H_2O$ and $[(NH_4)Fe(SO_4)_2] \cdot 12H_2O$, respectively, in 0.1 mol dm$^{-3}$ $H_2SO_4$.

### 2.2. Procedures

*2.2.1. UV/Visible and Luminescence Spectroscopy*

UV/visible spectroscopy was carried out using a Shimadzu UV 240 scanning spectrophotometer. Matched 1.0 cm quartz cells were used for all measurements. The scan rate was 10 nm s$^{-1}$ with a slit width of 2 nm. The polymeric material was dissolved in a 1:1 mixture of methanol:acetonitrile. Spectra were recorded on four polymer solutions over the redox center concentration range of $1.48 \times 10^{-5}$ mol dm$^{-3}$ to $1.48 \times 10^{-4}$ mol dm$^{-3}$. The solutions were prepared by serial dilution, and the methanol:acetonitrile solvent system was used as the reference. The wavelengths of absorption $\lambda_{max}$ were estimated from the recorded spectra, while the molar extinction coefficient, $\epsilon$, was estimated from the slope of the plot of absorbance vs. concentration.

Luminescence spectroscopy was carried out using the Perkin Elmer LS50 luminescence spectrophotometer. Room temperature luminescence was carried out using a 1.0 cm quartz luminescence cell, while at −196°C a quartz tube was used. The excitation and emission slit widths were 10 nm for all experiments.

*2.2.2. Electrochemical Measurements*

Cyclic voltammetry (CV) and rotating disk electrode (RDE) voltammetry were carried out using a conventional three-electrode assembly and a EG&G Princeton Applied Research Model 362 potentiostat. The RDE assembly was the Metrohm (Herisau, Switzerland) Model 629-10. Voltammograms were recorded on a Linseis Model LY17100 $X-Y$ recorder. The working electrodes were 3 mm glassy carbon electrodes shrouded in Teflon (Metrohm). The counter electrode was $\approx 1$ cm$^2$ platinum gauze placed parallel to the working electrode. A saturated calomel electrode (SCE) was used as the reference electrode. All potentials are quoted without regard to the liquid junction potential. Coulometry was carried out using the EG&G Princeton Applied Research Model 379 digital coulometer placed in series between the working electrode and the potentiostat return. The charge due to the oxidation of $Os^{II}$ to $Os^{III}$ within the polymer film was measured during slow sweep rate CV (1.0 mV s$^{-1}$) from 0.0 V to 0.6 V vs. SCE. Sample current voltammetry was carried out using an EG&G Princeton Applied Research Model 273 potentiostat interfaced to a BBC microcomputer for data acquisition. A pulse width of 200 ms followed by a 10 s interval between successive pulses was employed. Sampling times of 1, 2, 4, and 10 ms after the application of the pulse, where the current is under semiinfinite diffusional control, was used. Chronoamperometry was carried out using a Philips 3311 digital storage oscilloscope interfaced to the BBC microcomputer. Five potential steps were used per measurement and averaged. Capacitive currents were corrected for by linear extrapolation of the currents generated at small potential steps prior to the redox wave due to $Os^{II}$ oxidation. All measurements, unless otherwise stated, were carried out at room temperature.

Glassy carbon electrodes were prepared by polishing with 5 $\mu$m alumina followed by treatment with chlorosulfonic acid. Modified electrodes were prepared by droplet evaporation using a 1.0% w/v solution of the redox polymer in methanol:acetonitrile (1:1). The electrodes were allowed to dry slowly and were cured overnight in vacuo before use.

*2.2.3. Flow-Injection Analysis*

The flow injection system consisted of a Gilson Minipuls 3 peristaltic pump, and a Rheodyne 9125 injection port fitted with a 20 $\mu$L fixed volume sample loop. The detection system was a Hewlett Packard 1049A electrochemical detector. The working electrodes were 3 mm glassy carbon electrodes shrouded in Teflon. The reference electrode was the Ag/AgCl electrode. All potentials are quoted following numerical conversion to the SCE scale. The auxiliary electrode was the stainless steel cell body. Sensor responses were recorded on a Philips PM 8252 $X-t$ chart recorder. The carrier electrolyte was 0.1 mol dm$^{-3}$ $H_2SO_4$.

*2.2.4. Sample Preparation*

Iron tablets (Fersaday from Duncan, Flockhart & Co. Ltd.) were dissolved in 0.1 mol dm$^{-3}$ $H_2SO_4$. Aliquots of this sample were transferred to 100 cm$^3$ volumetric flasks and 1.0 cm$^3$ of 35% $H_2O_2$ was added. This oxidizes the $Fe^{II}$ to $Fe^{III}$, it does not in itself interfere with the measurement and can therefore be added in excess. The solutions were then made up to the mark with 0.1 mol dm$^{-3}$ $H_2SO_4$. These solutions were then used, following dilution, for the flow-injection analysis of $Fe^{III}$ using the modified electrode. For comparison purposes, a standard spectrophotometric method for the determination of $Fe^{III}$ was also carried out [15]. This involved the determination of $Fe^{III}$ colorimetrically at 480 nm following complexation with thiocyanate.

## 3. Results and Discussion

The formation of the redox polymer is based on the lability of the chloride ligand of the $[Os(bipy)_2Cl_2]$ complex. The reaction proceeds according to the following sequence

$$Os(bipy)_2Cl_2 + S \rightarrow [Os(bipy)_2(S)Cl]^+Cl^- \quad (1)$$

$$[Os(bipy)_2(S)Cl]^+Cl^- + Pol_n \rightarrow [Os(bipy)_2(Pol)_nCl]^+Cl^- + S \quad (2)$$

where S is 2-methyoxyethanol, Pol is the polymer, and $n$ is the number of monomer units/metal center. Substitution of the second chloride ligand is difficult and is not observed under the conditions used here. The structure of the resulting redox polymer, which has one osmium center per 10 monomer units, is shown in Figure 1. This synthetic approach is advantageous, as the metal loading of the polymer backbone can be controlled precisely by varying the PVP:$[Os(bipy)_2Cl_2]$ ratio in the reaction mixture.

### 3.1. Spectroscopic Characterization of $[Os(bipy)_2(PS)_{7.5}(DMAP)_{2.5}Cl]Cl$

Electronic spectroscopy has proven useful in the characterization of redox polymers containing coordinated osmium and ruthenium centers [13]. In the visible region, three electronic transitions are evident. These occur at 740 nm ($\log \epsilon = 3.18$), 510 nm ($\log \epsilon = 3.75$), and 360 nm ($\log \epsilon = 3.93$). A shoulder at 430 nm ($\log \epsilon = 3.77$) can also be identified. These transitions can be assigned to metal-to-ligand charge transfer (MLCT)

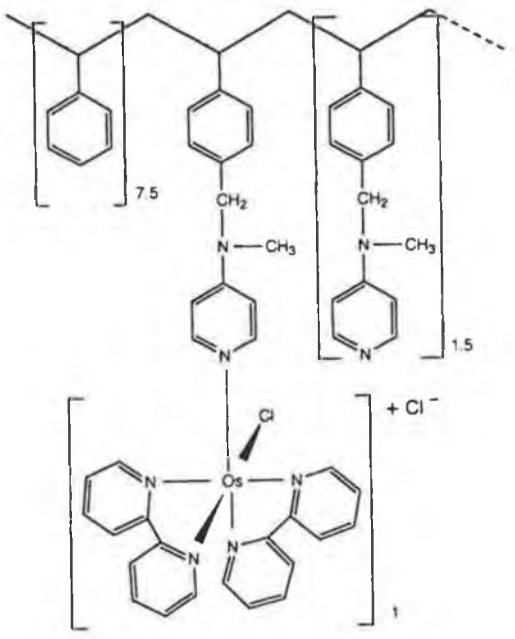


g. 1. Structure of $[Os(bipy)_2(PS)_{7.5}(DMAP)_{2.5}Cl]Cl$.

ocesses, i.e., from the metal d orbital to the $\pi^*$ bipyridyl bitals. These wavelengths of transition and molar extinction efficients are in close agreement with the model compound $[Os(bipy)_2(PVP)_{10}Cl]Cl$, with transitions occurring at 730 nm $(\log \epsilon = 3.45)$, 486 nm $(\log \epsilon = 4.05)$, 431 nm $(\log \epsilon = 4.08)$, and 4 nm $(\log \epsilon = 4.05)$. Slight differences in $\lambda$ and $\epsilon$ may be tributed to factors such as solvent effects and different degrees hydration of the redox polymer. The proposed structure of e product is furthermore confirmed by the absence of any ission both at room temperature and at −196°C [13].

## 2. Electrochemistry of $[Os(bipy)_2(PS)_{7.5}(DMAP)_{2.5}Cl]Cl$

CV has been used extensively for the characterization of dox polymers, as this technique yields both qualitative and antitative information concerning the electrochemical havior of the electroactive material. Certain criteria for the eal CV behavior of surface immobilized electroactive species ve been established and are useful in the analysis of the charge nsport properties of electroactive films [16, 17]. In Figure 2a, typical CV of the metallo-polymer coated on a glassy carbon ctrode in an aqueous electrolyte can be seen. The wave shape characterized by considerable diffusional tailing and a nsiderable peak-to-peak separation ($\Delta E$); features which

ble 1. The effect of electrolyte on charge transport parameters, surface havior, and half-wave potential for an $Os(bipy)_2(PS)_{7.5}(DMAP)_{2.5}Cl]Cl$-odified electrode.

| ectrolyte [a] | $E_{\frac{1}{2}}$ [mV] [b] | $\Delta E_p$ [mV] | $i_{pa}/i_{pc}$ | $D_{ct}$ [$10^{-12}$ $cm^2$ $s^{-1}$] |
|---|---|---|---|---|
| $SO_4$ | 250 ± 5 | 115 ± 5 | 0.87 ± 0.01 | 0.45 ± 0.2 [c] |
| $_2SO_4$ | 250 ± 5 | 105 ± 5 | 0.87 ± 0.01 | 0.31 ± 0.2 |
| $ClO_4$ | 167 ± 5 | 115 ± 5 | 1.03 ± 0.01 | 1.50 ± 0.3 |
| $aClO_4$ | 180 ± 5 | 145 ± 5 | 0.88 ± 0.01 | 0.76 ± 0.3 |
| )SA [d] | 200 ± 5 | 100 ± 5 | 0.87 ± 0.01 | 4.4 ± 0.2 |
| $_4SO_4$ | 250 ± 5 | 105 ± 5 | 0.86 ± 0.01 | 0.63 ± 0.3 |
| % ethanol | | | | |

All electrolytes are 0.1 mol $dm^{-3}$. [b] Potentials quoted with respect to CE. [c] $D_{ct}$ estimated by CV on at least three different films. [d] TpSA is luene-*p*-sulfonic acid.

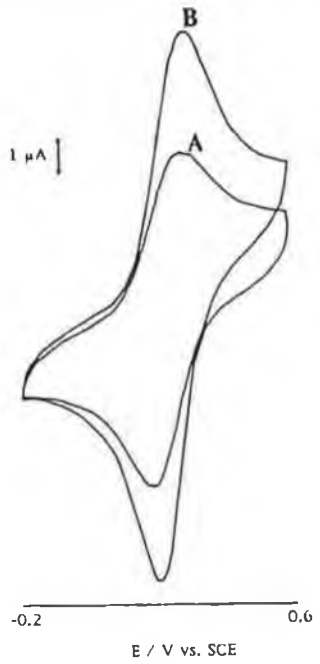


Fig. 2. Cyclic voltammograms of $Os(bipy)_2(PS)_{7.5}(DMAP)_{2.5}Cl]Cl$ in A) 0.1 mol $dm^{-3}$ $H_2SO_4$ and B) 10% v/v ethanol in 0.1 mol $dm^{-3}$ $H_2SO_4$, sweep rate: 0.10 V $s^{-1}$.

are indicative of slow charge transport rates. The values for $\Delta E$, the half-wave potential ($E_{\frac{1}{2}}$), and the ratio of the anodic-to-cathodic peak currents ($i_{pa}/i_{pc}$) are given in Table 1. The $E_{\frac{1}{2}}$ in sulfate-based electrolytes is 0.250 V vs. SCE, while in perchlorate the values are 0.170 V vs. SCE and 0.180 V vs. SCE for the acid and sodium forms, respectively. In TpSA the $E_{\frac{1}{2}}$ is 0.200 V vs. SCE. These values are in agreement with the PVP-based polymer and indicate that the redox site microenvironment is not affecting the redox potential of the polymer-bound redox moiety. However, contrary to the $[Os(bipy)_2(PVP)_{10}Cl]Cl$ polymer, a considerable peak-to-peak separation is observed in all electrolytes, typically greater than 0.100 V, along with a peak current ratio less than 1.0, both of which indicate nonideal behavior. A plot of $i_{pa}$ vs. the square root of potential sweep rate ($\nu$) can be seen in Figure 3; the plot is linear from 1.0 mV $s^{-1}$ up to 200 mV $s^{-1}$ with an intercept at zero. This demonstrates infinite linear diffusion behavior and suggests that the redox material does not exhibit finite diffusional behavior even at very slow sweep rates, again indicating slow, diffusionally controlled homogeneous electron transport. It is interesting to note that in

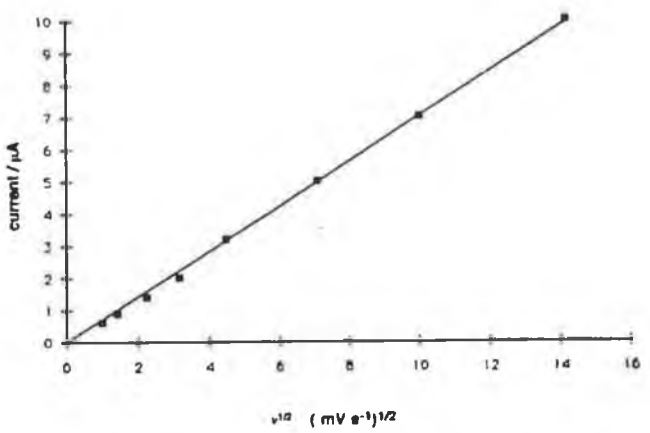


Fig. 3. The variation of peak current with potential sweep rate $\nu$. (The slope of this line is 1.66 μA/(mV $s^{-1}$)$^{\frac{1}{2}}$ with an intercept of 0.11 μA and a correlation coefficient of 0.9998.)

Table 2. Activation parameters for charge transport through $Os(bipy)_2(PS)_{7.5}(DMAP)_{2.5}Cl]Cl$ in $HClO_4$ and TpSA.

| *Activation parameter* | *$HClO_4$ [0.1 mol dm$^{-3}$]* | *TpSA [a] [0.1 mol dm$^{-3}$]* |
|---|---|---|
| $E_a$ [kJ mol$^{-1}$] | 71.2 ± 8 [b] | 47.4 ± 4 [b] |
| $\Delta S^{\ddagger}$ [J mol$^{-1}$ K$^{-1}$] | −5.7 ± 8 | −76.6 ± 3 |
| $\Delta G^{\ddagger}$ [kJ mol$^{-1}$] | 70.4 ± 6 | 67.8 ± 4 |
| $\Delta H^{\ddagger}$ [kJ mol$^{-1}$] | 68.7 ± 7 | 45.0 ± 4 |

[a] TpSA is toluene-*p*-sulfonic acid. [b] Errors are calculated from the standard deviation of the slope and intercept of the least squares fit for each line.

the presence of 10% v/v ethanol in 0.1 mol dm$^{-3}$ $H_2SO_4$, the CV wave increases in magnitude (Fig. 2b), while the characteristic parameters listed in Table 1 are largely unaffected. This appears to indicate that more redox centers become electroactive in the presence of ethanol, possibly due to plasticization or solvation of the polymer backbone, while the charge transport controlling process is maintained. This may be a result of inhomogeneity in the polymer film on the electrode surface, with redox sites being 'shielded' in insulating domains in the aqueous electrolyte, which are subsequently released for redox processes in the presence of organic solvent in the electrolyte. Domain formation has been observed previously for other redox polymers [18]. This view is supported by coulometry results which show that for surface coverages greater than approximately $1 \times 10^{-8}$ mol cm$^{-2}$ the entire film is not electroactive over time scales up to 30 min, and is typically less than 50% electroactive at 1.0 mV s$^{-1}$. Estimation of the heterogeneous charge transfer rate constant ($k^0$) by sample current voltammetry in 0.1 mol dm$^{-3}$ $H_2SO_4$ yields a value of $2.1 \pm 1.5 \times 10^{-6}$ cm s$^{-1}$. This value is 1–2 orders of magnitude smaller than those of the PVP- and PS/PVP-based redox polymers [19]. This observation may reflect nonconducting regions of redox polymer blocking surface sites for heterogeneous electron transfer [20] or counter-ion transport limitations [19].

The generally accepted mechanism of charge transport through redox polymers is by a process of electron self-exchange ('electron hopping') between fixed redox sites [21]. The rate of charge transport may be limited by (a) the intrinsic barrier to self-exchange, (b) counter-ion movement to maintain electroneutrality, or (c) polymer segmental motion required for redox site juxtapositioning. The rates of charge transport through the redox polymer in a number of electrolytes are listed in Table 1. These values have been estimated by CV, as this technique reveals information that is more representative of the bulk polymer structure. The rate of charge transport $D_{ct}$ varies from $3.1 \times 10^{-13}$ cm$^2$ s$^{-1}$ to $4.4 \times 10^{-12}$ cm$^2$ s$^{-1}$ in the range of electrolytes used. The presence of 10% v/v ethanol leads to an increase in the magnitude of $D_{ct}$ of about 50%, which again suggests the rate-determining process is most likely unaltered by the addition of the organic solvent. These values for $D_{ct}$ are 1–2 orders of magnitude smaller than for the PVP model compound [22], which is in agreement with the diffusional behavior observed for slow sweep rate CV. The use of activation data has been useful in assigning the rate-determining process for charge transport [23]. In Table 2 the activation parameters for charge transport through the redox polymer (as obtained using the method described by Daum et al. [23]) in TpSA and $HClO_4$ are shown. In the perchloric acid electrolyte, the activation energy ($E_a$) for charge transport is 71 kJ mol$^{-1}$, which is indicative of counter-ion motion controlling the process. However, the possibility that self exchange is rate-determining can not be ruled out completely. The entropy value ($\Delta S^{\ddagger}$) is −5.7 J mol$^{-1}$ K$^{-1}$; this indicates that no significant change in the ordering of the polymer occurs upon redox. For TpSA, a smaller activation energy of 47 kJ mol$^{-1}$ is observed, which again suggests that counter-ion motion is the rate-determining process for charge transport. For this electrolyte, a relatively large negative entropy value is obtained (−76.6 J mol$^{-1}$ K$^{-1}$), which suggests considerable ordering of the polymer film upon incorporation of this counter-ion. Measurement of $D_{ct}$ by chronoamperometry in 0.1 mol dm$^{-3}$ $H_2SO_4$ yields a value of $1.2 \times 10^{-10}$ cm$^2$ s$^{-1}$. This value is considerably larger than the CV values. Discrepancies between CV, potential step, and steady state measurements of $D_{ct}$ have been reported before; however, the origin of this behavior is uncertain. Possible explanations include: differences in film structure between the polymer/electrode and the polymer/electrolyte interface and the presence of different limiting processes over different time scales [24, 25].

### 3.3. Mediated Electrocatalytic Reduction of $Fe^{III}$

The electrochemical behavior of $Fe^{III}$ at glassy carbon electrodes is poor and it does not undergo redox chemistry in the potential region of the electrocatalyst studied here, although the formal potential for the reduction of $Fe^{III}$ is 0.46 V vs. SCE [26, 27]. As the $E_{\frac{1}{2}}$ of the $Os^{II}/Os^{III}$ redox couple is 0.250 V vs. SCE, the electrocatalytic reduction of $Fe^{III}$ is thermodynamically favorable at the modified electrode with a 0.210 V electrochemical driving force. The cross-exchange reaction occurs according to Reaction 3

$$Fe^{III} + Os^{II} \rightarrow Fe^{II} + Os^{III} \quad (3)$$

In Figure 4a a CV for the reduction of $Fe^{III}$ at a modified electrode can be seen. This CV, when compared to Figure 2b,

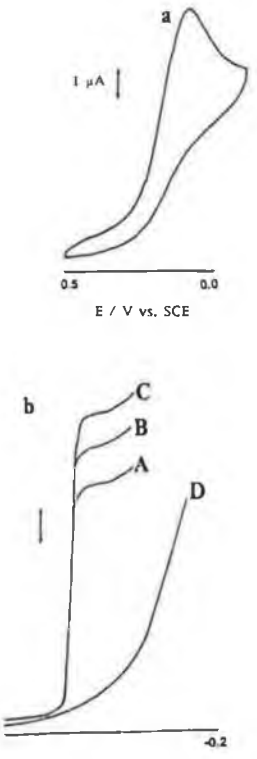


Fig. 4. CV of a) $1.0 \times 10^{-3}$ mol dm$^{-3}$ $Fe^{III}$ at an $Os(bipy)_2(PS)_{7.5}(DMAP)_{2.5}Cl]Cl$-modified electrode, and b) current–potential curves for $Fe^{III}$ reduction ($1.0 \times 10^{-3}$ mol dm$^{-3}$) at A) 500 rpm, B) 1000 rpm, and C) 2000 rpm. Curve D) is for $Fe^{III}$ reduction at glassy carbon at 5000 rpm. The electrolyte was 0.1 mol dm$^{-3}$ $H_2SO_4$.

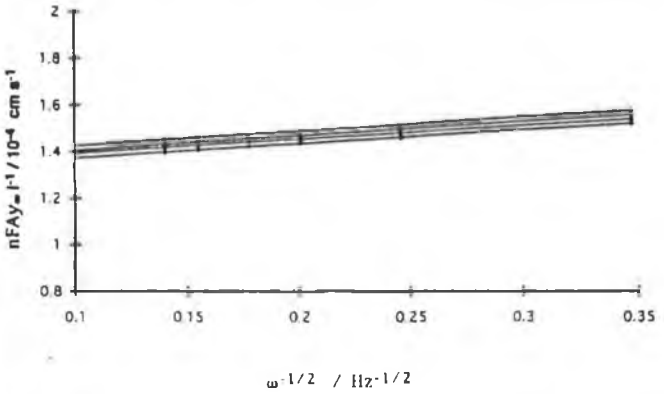


Fig. 5. Koutecky–Levich plots for the reduction of $8.0 \times 10^{-4}$ mol dm$^{-3}$ $Fe^{III}$ at modified electrodes with polymer surface coverages (from the top) of $3.3 \times 10^{-8}$, $4.2 \times 10^{-8}$, $1.7 \times 10^{-8}$, and $4.0 \times 10^{-9}$ mol cm$^{-2}$.

shows that the redox polymer mediates the reduction of $Fe^{III}$. It is also clear that a reverse wave is absent, suggesting that the mediated reaction is irreversible. This is expected considering the thermodynamics of the system. In Figure 4b RDE voltammograms for the reduction of $Fe^{III}$ at the modified electrode and at bare glassy carbon electrodes are shown. As the onset of mediation occurs at a potential of 0.35 V vs. SCE, which corresponds to the onset of $Os^{II}$ generation within the film, and as the reaction occurs at less negative potential compared to at the bare electrode, these traces again clearly demonstrated mediated electrocatalysis of $Fe^{III}$ reduction.

Several theoretical models have been proposed for the analysis of the kinetic behavior of redox polymer-modified electrodes [25, 28]. These models utilize RDE voltammetry as the mass transport of substrate to the electrode surface can be controlled precisely. The diagnostic scheme of Albery et al. [29] is used here to analyze the kinetics of the mediated reduction of $Fe^{III}$ at the modified electrode. In Figure 5 typical Koutecky–Levich plots for the reduction of $Fe^{III}$ are shown. At an $Fe^{III}$ concentration of $8.0 \times 10^{-4}$ mol dm$^{-3}$ the plots are linear and the electrode currents are proportional to the square root of the electrode rotation speed. These observations allow the elimination of the $St_e$, $LSt_e$, and $LEk$ kinetic regimes. The inverse of the slope of the Koutecky–Levich plot at this substrate concentration was found to be $1.0 \pm 0.8 \times 10^{-3}$ cm s$^{-1/2}$. This value has been estimated for a clean unmodified electrode in previous studies to be $1.01 \times 10^{-3}$ cm s$^{-1/2}$ [24, 29]. These values are in close agreement and allow elimination of the $LRZt_et_y$ kinetic case. With the exclusion of the above cases, the mechanism must lie within the $Sk''$, $LSk$, $Lk$, or $LEt_y$ kinetic zones. These can be distinguished by the dependency of $k'_{ME}$, the modified electrode rate constant, on the polymer layer thickness $L$, and the concentration of electroactive sites $b_0$ within the polymer film. From the Koutecky–Levich plots, it is evident that the intercepts ($k'_{ME}$) are independent of layer thickness. This allows the elimination of the $Lk$ and $LEt_y$ kinetic cases. In Figure 6 a plot of $\ln k'_{ME}$ vs. $\ln(1-f)$, where $f$ is the fraction of redox sites in the $Os^{III}$ state, is shown. The value of $f$ was calculated from the stepwise integration of the slow sweep rate CV. This plot is linear with a slope of $1.02 \pm 0.11$. This indicates a first-order relationship with respect to $b_0$ and suggests that the kinetic regime is $Sk''$. Under this kinetic case, electron transfer occurs from a region of molecular dimensions at the surface of the polymer to a solution phase $Fe^{III}$ species, and the rate constant for the electrocatalytic reaction controls the limiting currents. Consequently, $Fe^{III}$ does not permeate the polymer film. The analytical expression describing $k'_{ME}$ for the $Sk''$ kinetic case is of the form [29]

$$k'_{ME} = b_0 k'' \quad (4)$$

where $k''$ is the homogeneous second-order rate constant for the surface cross-exchange reaction. A value of $1.6 \pm 0.5 \times 10^{-4}$ cm s$^{-1}$ has been estimated for $k'_{ME}$, which gives a value of $2.3 \pm 0.7 \times 10^{-4}$ mol$^{-1}$ dm$^3$ cm s$^{-1}$ for $k''$ with $b_0 = 0.7 \times 10^{-3}$ mol cm$^{-3}$ ($b_0$ was calculated from the dry density of the polymer). This value is similar to that found for the reduction of $Fe^{III}$ at $[Os(bipy)_2(PVP)_{10}Cl]Cl$-modified electrodes under conditions where a surface reaction was taking place [26]. This confirms the surface nature of the mediated reaction and suggests that the rate of the cross-exchange reaction between the mediator and substrate for a surface reaction is independent of the polymer matrix.

At higher substrate concentrations, e.g., $1.4 \times 10^{-3}$ mol dm$^{-3}$, the electrode currents become independent of electrode rotation speed, as expected from the Albery and co-workers model; this corresponds to a change over to the $St_e$ kinetic regime from $Sk''$. Under these conditions, electron transport through the polymer film becomes the rate-limiting process. This is not surprising considering the slow rate of homogeneous electron transport through the polymer film. This type of behavior may have serious implications for the use of this type of sensor at high substrate concentrations.

### 3.3.1. *Analysis of Iron in Pharmaceutical Formulations by FIA*

The modified electrode was applied to the determination of $Fe^{III}$ by flow injection analysis (FIA). The optimum applied potential was $-0.050$ V vs. SCE, with a carrier flow rate of 1.0 cm$^3$ min$^{-1}$. This allowed an analytical throughput of 75 samples per hour (using a basewidth calculation). Typical detector traces can be seen in Figure 7. The sensor responses

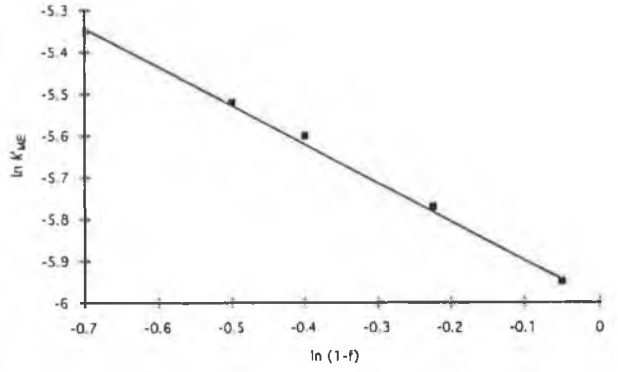


Fig. 6. Plot of $\ln k'_{ME}$ vs. $\ln(1-f)$ for the mediated reduction of $Fe^{III}$ at the modified electrode.

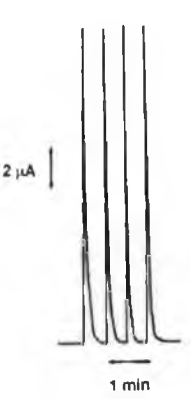


Fig. 7. Typical FIA traces for the detection of $1.0 \times 10^{-3}$ mol dm$^{-3}$ $Fe^{III}$ at the modified electrode.

were found to be linear over the concentration range $1.0 \times 10^{-5}$ mol dm$^{-3}$ to $1.0 \times 10^{-3}$ mol dm$^{-3}$ $Fe^{III}$ with correlation coefficients $r \geq 0.999$. The limit of detection was $3.0 \times 10^{-6}$ mol dm$^{-3}$ $Fe^{III}$ at a signal-to-noise ratio ($S/N$) of 3/1. The sensitivity of the sensor was $1.81 \pm 0.01$ $\mu$A mmol$^{-1}$ over the linear concentration range. At concentrations greater than $1.0 \times 10^{-3}$ mol dm$^{-3}$ $Fe^{III}$, the electrode responses in the thin-layer flow cell become independent of the $Fe^{III}$ concentration. The linear concentration range reflects the kinetically controlled currents generated under the $Sk''$ kinetic regime. At higher substrate concentrations, the change over to the $St_e$ kinetic cases is observed with electrode currents becoming independent of the substrate concentration. It is significant that the electrochemical behavior observed for the macroelectrochemical cell can be transferred to the environment of the thin-layer flow cell. This demonstrates the utility of the theoretical models in predicting electrode responses under operational conditions.

Iron tablets were analysed for Fe content (as $Fe^{III}$) using the electrochemical sensor and by a standard spectrophotometric method. The nominal concentration of iron is 100 mg/tablet. The concentration found using the modified electrode was $103 \pm 3$ mg/tablet, while for the spectrophotometric method a concentration of $101 \pm 1$ mg/tablet was found. These results indicate the applicability of the electrode for the analysis of iron in pharmaceutical formulations. The electrochemical method has a reasonable analytical throughput combined with experimental simplicity.

### 3.4. Stability of $[Os(bipy)_2(PS)_{7.5}(DMAP)_{2.5}Cl]Cl$

One of the main advantages of redox polymers with coordinated electroactive sites is the chemical stability of the attached redox center compared to electrostatically incorporated sites. Physical stability of the polymer film is, however, more difficult to attain, as preformed linear polymers tend to interact more strongly with the contacting electrolyte [30]. The adhesion of polymers to electrode surfaces is little understood, but appears to be a combination of nonspecific adsorption processes and insolubility in the contacting electrolyte. For the redox polymer studied here, the physical stability was found to be excellent compared to the model compound. Under the severe hydrodynamic conditions of the RDE and thin-layer flow cells with 0.1 mol dm$^{-3}$ $H_2SO_4$ as the electrolyte, the $[Os(bipy)_2(PS)_{7.5}(DMAP)_{2.5}Cl]Cl$ redox polymer was found to be completely stable for up to at least seven days. No evidence of polymer delamination was evident. In contrast, for RDE experiments, the $t_{\frac{1}{2}}$ (time required to remove 50% of original surface coverage) for the model compound $[Os(bipy)_2(PVP)_{10}Cl]Cl$ is approximately 24 h, while in thin-layer flow cells the $t_{\frac{1}{2}}$ is approximately 46 h. This considerably enhanced stability can be attributed to the insolubility of the polymer in the aqueous electrolytes and is of great importance in the development of these devices for commercial exploitation.

## 4. Conclusions

The results obtained in this study show the flexibility available in the design of modified electrodes when using redox polymers. Well-documented synthetic procedures exist which make it possible to prepare tailor-made electrode surfaces. In our present investigations we are particularly interested in the development of novel electrocatalytic layers that show improved physical stability, since stability is a primary concern for the application of modified electrodes as sensors. For the DMAP material reported here the physical stability under measurement conditions is considerably improved compared with the parent PVP-based redox polymer. At the same time the redox potential of the electroactive center is not affected by the change in the polymer backbone, so that from the thermodynamic point of view the mediating properties of the PVP material are maintained in the new DMAP polymers. However, the charge transport and the substrate partition in the layer are affected. Consequently, the mediation of $Fe^{III}$ reduction occurs at the polymer/electrolyte interface rather than throughout the whole layer, as observed for the PVP-based materials, and the linear range for the detection of $Fe^{III}$ is therefore reduced from that observed for the parent material ($1 \times 10^{-7}$ to $1 \times 10^{-2}$ mol dm$^{-3}$) [30]. This shows that the most sensitive sensor is obtained when through the layer, three-dimensional mediation is obtained, and that the price to pay here for the increased stability is a reduction in the linear range. However, despite its more limiting linear range, the DMAP-based redox polymer has considerable potential for application as a sensor material because of its excellent physical stability and because of the possibility that the charge transport properties might be improved by the addition of organic solvents. Furthermore, partitioning might be more favorable for other substrates; this is at present under investigation.

## 5. Acknowledgement

The authors thank EOLAS (the Irish Science and Technology Agency) for financial assistance.

## 6. References

[1] H.D. Abruna, A.J. Bard, *J. Am. Chem. Soc.* **1981**, *103*, 6898.
[2] F.C. Anson, *J. Phys. Chem.* **1980**, *84*, 3336.
[3] R.W. Murray, A.G. Ewing, R.A. Durst, *Anal. Chem.* **1987**, *59*, 379A.
[4] H. Akahoshi, S. Toshima, K. Itaya, *J. Phys. Chem.* **1982**, *86*, 818.
[5] S. Dong, Y. Wang, *Electroanalysis* **1989**, *1*, 99.
[6] R.W. Murray, *Acc. Chem. Res.* **1980**, *13*, 135.
[7] G.G. Wallace, M. Meaney, M.R. Smyth, J.G. Vos, *Electroanalysis* **1989**, *1*, 357.
[8] D.P. Leech, R.J. Forster, M.R. Smyth, J.G. Vos, *J. Mater. Chem.* **1991**, *1*, 629.
[9] D.P. Leech, *Ph.D. Thesis*, Dublin City University, Dublin **1991**.
[10] B. Lindholm, M. Sharp, *J. Electroanal. Chem.* **1986**, *198*, 37.
[11] J. Lieto, D. Milstein, R.L. Albright, J.V. Minkiewitz, B.C. Gates, *Chem. Tech.* **1983**, *13*, 46.
[12] G. Hoefle, W. Steglich, H. Vorbrueggen, *Angew. Chem. Int. Ed. Engl.* **1978**, *17*, 97.
[13] R.J. Forster, J.G. Vos, *Macromolecules* **1990**, *23*, 4372.
[14] C.E. Koning, T. Jongsma, R. Brinkhuis, G. Challa, *Reactive Polym.* **1988**, *8*, 255.
[15] *Vogels Textbook of Quantitative Inorganic Analysis*, 6th ed. (Eds. J. Bassette, R.C. Denny, G.H. Jeffery, J. Mendham), Longman, New York **1978**, p. 741.
[16] K. Aoki, K. Tokuda, H. Matsuda, *J. Electroanal. Chem.* **1983**, *146*, 417.
[17] K. Aoki, K. Tokuda, H. Matsuda, *J. Electroanal. Chem.* **1984**, *160*, 33.
[18] K. Sumi, F.C. Anson, *J. Phys. Chem.* **1986**, *90*, 3845.
[19] R.J. Forster, J.G. Vos, M.E.G. Lyons, *J. Chem. Soc., Faraday Trans.* **1991**, *87*, 3769.
[20] C. Amatore, J.M. Saveant, D. Tessier, *J. Electroanal. Chem.* **1983**, *146*, 37.
[21] F.B. Kaufman, H. Schroeder, E. Engler, S.R. Kramer, J.Q. Chambers, *J. Am. Chem. Soc.* **1980**, *102*, 483.
[22] R.J. Forster, A.J. Kelly, J.G. Vos, M.E.G. Lyons, *J. Electroanal. Chem.* **1989**, *270*, 365.

[23] P. Daum, J.R. Lenhard, D. Rolinson, R.W. Murray, *J. Am. Chem. Soc.* **1980**, *102*, 4649.
[24] R.J. Forster, J.G. Vos, M.E.G. Lyons, *J. Chem. Soc., Faraday Trans.* **1991**, *87*, 3761.
[25] W.J. Albery, A.R. Hillman, *Annu. Rep. Prog. Chem. Sect. C* **1981**, 377.
[26] R.J. Forster, J.G. Vos, *J. Chem. Soc., Faraday Trans.* **1991**, *87*, 1863.
[27] C.P. Andrieux, O. Haas, J.M. Saveant, *J. Am. Chem. Soc.* **1986**, *108*, 8175.
[28] C.P. Andrieux, J.M. Dumas-Bouchiat, J.M. Saveant, *J. Electroanal. Chem.* **1982**, *131*, 1.
[29] W.J. Albery, M.G. Boutelle, A.R. Hillman, *J. Electroanal. Chem.* **1985**, *182*, 99.
[30] A.P. Doherty, R.J. Forster, M.R. Smyth, J.G. Vos, *Anal. Chem.* **1992**, *64*, 572.

# Electrocatalytic Oxidation of Ascorbic Acid at [Osmium(2,2′-bipyridyl)$_2$-(poiy-4-vinylpyridine)$_{10}$Cl]Cl Modified Electrodes; Implications for the Development of Biosensors Based on Osmium-containing Redox Relays

**Andrew P. Doherty,*,† Margaret A. Stanley and Johannes G. Vos**
*School of Chemical Sciences, Dublin City University, Dublin 9, Ireland*

**The oxidation of ascorbic acid at electrodes modified with the redox polymer [Os(bipy)$_2$(PVP)$_{10}$Cl]Cl (where bipy = 2,2′-bipyridyl and PVP = poly-4-vinylpyridine) has been studied. The reaction proceeds electrocatalytically at 0.250 V *versus* SCE by mediation *via* the $Os^{II}/Os^{III}$ redox couple immobilized in the polymer film. The reaction is negative first order with respect to proton concentration and positive first order with respect to ascorbic acid concentration. At pH ≥ 3.0, limiting currents are diffusionally controlled and the kinetic regime may be classified as an $S_k$ mechanism. The second order rate constant for the surface electrocatalytic reaction $k''$ at pH 4.5 is $7.8 \pm 0.4 \times 10^{-4}$ dm$^3$ mol$^{-1}$ cm s$^{-1}$, while at pH 7.0 $k''$ is $9.1 \pm 0.6 \times 10^{-4}$ dm$^3$ mol$^{-1}$ cm s$^{-1}$. At pH ≤2.0 ascorbic acid permeates the polymer film and reacts at the mediator sites within the polymer film giving an $L_k$ mechanism, while at potentials >0.4 V *versus* SCE the reaction proceeds both at the underlying electrode and with the $Os^{III}$ mediator sites within the polymer film. The modified electrode has been characterized as an electrochemical sensor for ascorbic acid in flow injection systems.**

*Keywords: Redox polymer modified electrode; kinetics; sensor; ascorbic acid; flow injection*

## Introduction

Since their inception, the use of polymer-modified electrodes for sensor development has received considerable attention.[1–3] Such attention has been fuelled by the advantages of these devices over conventional electrode surfaces, *e.g.*, sensitivity, selectivity, efficient electrocatalysis and low limits of detection. In particular, the electrochemical oxidation of ascorbic acid ($H_2A$) has been studied extensively because of the significance of this compound in bioelectrochemistry, neurochemistry and clinical diagnostics applications. The electrochemical oxidation of ascorbic acid at conventional electrodes is well documented and is known to proceed *via* two consecutive one-electron transfer processes involving the participation of a radical anion intermediate to form dehydro-L-ascorbic acid (A).[4,5] This species subsequently undergoes a hydration reaction characteristic of carbonyl groups to form an electroinactive product. The over-all process is classified as an electrochemical (EC) process.

Recently, work describing the use of polypyridylosmium-containing redox polymers as 'molecular wires' for mediated electron transfer in enzyme electrodes such as the glucose and lactate oxidase enzyme electrodes have been described.[6–8] However, in these types of electrode, ascorbic acid acts as an important interferent because of the ubiquitous nature of ascorbic acid in biological matrices and also the general nature of outer-sphere electrocatalytic processes.[9] For application in clinical diagnostics, the current (or charge) signal due to the oxidation of the adventitious interferent must be considered and evaluated. This is normally achieved by measuring the signal at a separate electrode in the absence of the enzyme, giving a two-electrode differential measurement. Alternatively, permselective layers can be coated over the enzyme layer to hinder mass transport of interferents to the active electrocatalyst.[10] These approaches are, however, fraught with difficulties, such as poor permselectivity and slow mass transport properties. However, we have recently described an alternative approach for isolating the current signals due to individual co-existing electroactive species electrolytically consumed at redox polymer modified electrodes.[11] This approach is based on the control of reaction *loci* at the redox polymer modified electrode and allows isolation of the individual currents associated with the interferent and the target analyte. In order to isolate the individual currents, a detailed knowledge of the kinetics of the electrocatalytic reactions and mass transport dynamics within the redox polymer is necessary. In order to assess the problem of ascorbic acid oxidation in osmium-containing enzyme electrodes, the evaluation of the kinetic and transport parameters for the electrocatalytic oxidation of ascorbic acid at osmium-containing redox polymer modified electrodes is of considerable importance.

In this paper we therefore describe the kinetics of the electrocatalytic oxidation of ascorbic acid at the redox polymer [Os(bipy)$_2$(PVP)$_{10}$Cl]Cl (where bipy = 2,2′-bipyridyl and PVP = poly-4-vinylpyridine) modified electrode and analyse the results in terms of the Albery and Hillman theory.[12,13] Using the kinetic and mechanistic information, an amperometric ascorbic acid sensor is demonstrated for application in biological buffer at pH 7.0 using flow injection (FI). The optimization and characterization of the sensor is described. The implications of the observed behaviour for the design of enzymic biosensors based on the incorporation of osmium-based redox relays is also discussed.

## Experimental

### *Apparatus*

Cyclic voltammetry (CV) and rotating disk electrode (RDE) voltammetry were carried out using a conventional three-electrode assembly. The potentiostat used was the EG&G Princeton Applied Research Model 362. The rotating disc assembly was the Metrohm Model 629-10 RDE. Voltammograms were recorded on a Linseis *X*–*Y* recorder. The working

* To whom correspondence should be addressed.
† Present address: Department of Chemistry, Bedson Building, University of Newcastle upon Tyne, Newcastle upon Tyne, UK NE1 7RU.

electrodes were 3 mm diameter glassy carbon discs shrouded in Teflon (Metrohm). The electrodes were polished with 5 μm alumina prior to modification; they were then modified by the drop coating technique using a 1% m/v redox polymer solution in methanol. Polymer surface coverages were determined by integration of the charge ($Q$) under a slow sweep rate (2 mV $s^{-1}$) CV where $Q = n F \Gamma$ and $\Gamma$ is the polymer surface coverage, $n$ the number of electrons and $F$ the Faraday constant. The counter electrode was 1 $cm^2$ platinum gauze placed parallel to the working electrode at distance of ≈1 cm. The reference electrode was a saturated KCl calomel electrode (SCE). All potentials are quoted with respect to SCE without regard to liquid junction potentials. All measurements were carried out at room temperature.

The FI apparatus consisted of an EG&G Princeton Applied Research Model 400 electrochemical detector fitted with a thin-layer flow cell, a Gilson Minipuls 3 peristaltic pump, a six-port Rheodyne injection valve with a 20 μl fixed-volume sample loop and a Philips PM 8252 *X-t* recorder. The working electrodes were 3 mm glassy carbon shrouded in Teflon (EG&G) and were modified as described above. The Ag/AgCl electrode acted as the reference while the stainless-steel cell body acted as the counter electrode. Potentials are quoted after numerical conversion to the SCE scale. Silicone rubber tubing was used at the pump and Teflon 1/16 in od × 1/32 in id tubing for the rest of the system. Sample injections were made using a 2 $cm^3$ glass syringe fitted with a Rheodyne injection needle.

### *Reagents*

The synthesis of the osmium redox polymer is described elsewhere.[14] The structure of the osmium-containing redox polymer is shown in Fig. 1. For electrochemical studies, ascorbic acid (Aldrich) solutions were prepared, prior to use, in nitrogen-purged 0.1 mol $dm^{-3}$ $Na_2SO_4$. Where the pH was varied, this was achieved by the addition of dilute (0.1 mol $dm^{-3}$) $H_2SO_4$ to the standard solution, the effect of dilution on electrode currents being accounted for. In FI experiments, the electrolyte was prepared from analytical reagent grade $K_2HPO_4$ and $KH_2PO_4$ (Aldrich) to produce 0.1 mol $dm^{-3}$ phosphate buffer, the pH of which was adjusted to 7.0 with KOH. All solutions were prepared freshly and protected from light.

## Results and Discussion

### *Kinetics and Mechanism*

In Fig. 2 a CV of the redox polymer $[Os(bipy)_2(PVP)_{10}Cl]Cl$ with a surface coverage of $1.0 \times 10^{-9}$ mol $cm^{-2}$ in 0.1 mol $dm^{-3}$ $Na_2SO_4$ is shown. The CV shows a single, reversible oxidation/reduction process corresponding to the facile $Os^{II}/Os^{III}$ redox couple with a half-wave potential of 0.250 V *versus* SCE. It can be seen that the peak-to-peak separation is close to zero and the peak width at half height is approximately 90 mV. The anodic peak current $i_{pa}$ was found to increase linearly as a function of potential sweep rate up to 100 mV $s^{-1}$, demonstrating finite diffusion behaviour. Collectively, these features are indicative of a surface-immobilized redox species in thermodynamic equilibrium with the electrode potential. Results of detailed studies concerning the charge transport properties of the osmium-containing redox polymer are described elsewhere.[15–17]

The pH-dependent formal potential, $E^\circ$, for ascorbic acid oxidation has been reported as −0.187 V *versus* SCE at pH 7.0 and −0.105 V *versus* SCE at pH 5.0.[18] As the $E^\circ$ for the ascorbic acid oxidation reaction is cathodic compared with the formal potential of the $Os^{II}/Os^{III}$ couple at 0.250 V *versus* SCE, mediation of the oxidation reaction by the polymer-immobilized $Os^{II}/Os^{III}$ redox centres is thermodynamically possible. In Fig. 3, A an RDE voltammogram for the oxidation of $4.0 \times 10^{-4}$ mol $dm^{-3}$ ascorbic acid at a polished glassy carbon electrode is shown. It can be seen that the onset of the oxidation reaction occurs at 0.450 V *versus* SCE and the half-wave potential is ≈0.8 V *versus* SCE. The wave shape due to elongation along the potential axis and the significant anodic potentials compared with the formal potential is indicative of sluggish electrode kinetics at a glassy carbon electrode for ascorbic acid oxidation. In Fig. 3, B the oxidation of $1.0 \times 10^{-4}$ mol $dm^{-3}$ ascorbic acid at a redox polymer modified electrode with a surface coverage of $1.0 \times 10^{-9}$ mol $cm^{-2}$ can be seen. The onset of ascorbic acid oxidation at the modified electrode occurs at 0.150 V *versus* SCE and the half-wave potential is approximately 0.270 V *versus* SCE. Clearly, electrode modification with the redox polymer significantly lowers the discharge potential for ascorbic acid compared with bare glassy carbon. In addition,

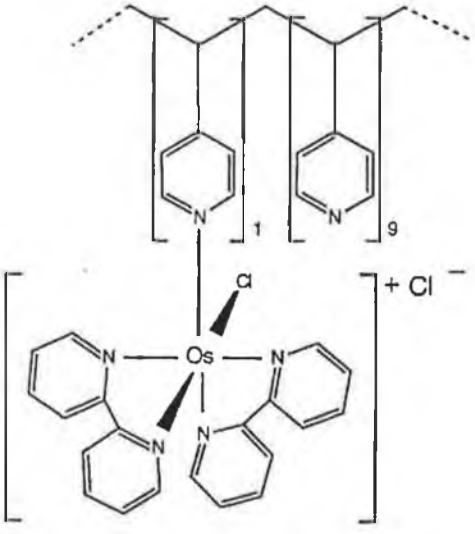


**Fig. 1** Structure of $[Os(bipy)_2(PVP)_{10}Cl]Cl$.

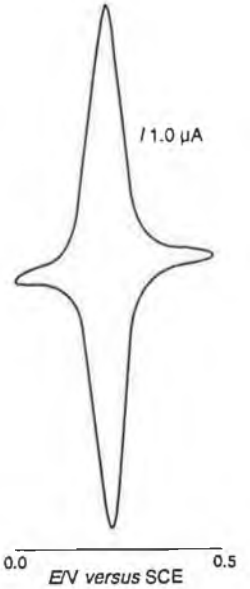


**Fig. 2** CV of a $1.0 \times 10^{-9}$ mol $cm^{-2}$ $[Os(bipy)_2(PVP)_{10}Cl]Cl$ modified electrode in 0.1 mol $dm^{-3}$ $Na_2SO_4$ electrolyte at 100 mV $s^{-1}$.

the reaction occurs in the potential region of the $Os^{II}/Os^{III}$ redox couple, indicating mediation by an outer-sphere electrocatalytic process. Considering the ascorbic acid concentrations in Fig. 3, A and B, the magnitude of the limiting current at the modified electrode suggests that the redox polymer is an efficient electrocatalyst for the oxidation of ascorbic acid.

In Fig. 4, a series of RDE voltammograms for the oxidation of $2.0 \times 10^{-4}$ mol $dm^{-3}$ ascorbic acid, at a modified electrode of surface coverage $1.0 \times 10^{-9}$ mol $cm^{-2}$ over the pH range 1.0–7.0, is shown. At pH $\geq$ 3.0 a single, well defined wave, centred at the half-wave potential of the $Os^{II}/Os^{III}$ redox couple, is evident, again indicative of an outer-sphere electrocatalytic process occurring. However, at pH $\leq$ 2.0 two waves are observed. The first wave is centred at the half-wave potential of the $Os^{II}/Os^{III}$ redox couple and again corresponds to electrocatalytic oxidation of ascorbic acid *via* $Os^{II}/Os^{III}$ mediation. The onset of the second wave occurs at 0.450 V *versus* SCE. Considering that mediation is already occurring at the $Os^{III}$ catalytic sites and that the redox polymer contains

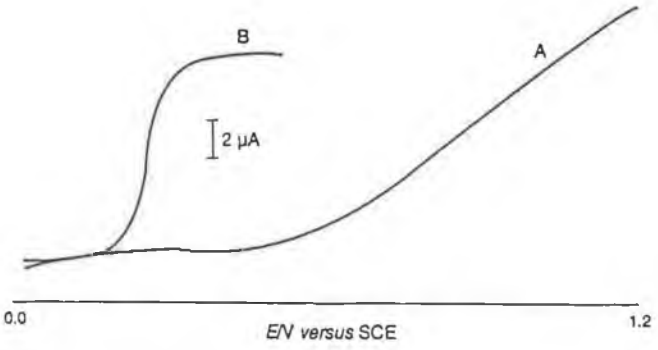


**Fig. 3** A, RDE voltammogram of $4.0 \times 10^{-4}$ mol $dm^{-3}$ ascorbic acid at a polished glassy carbon electrode in 0.1 mol $dm^{-3}$ $Na_2SO_4$ at pH 4.5. B, RDE voltammogram of $1.0 \times 10^{-4}$ mol $dm^{-3}$ ascorbic acid at a $1.0 \times 10^{-9}$ mol $cm^{-2}$ $[Os(bipy)_2(PVP)_{10}Cl]Cl$ modified electrode in 0.1 mol $dm^{-3}$ $Na_2SO_4$ at pH 4.5. The potential sweep rate was 2.0 mV $s^{-1}$ in both cases.

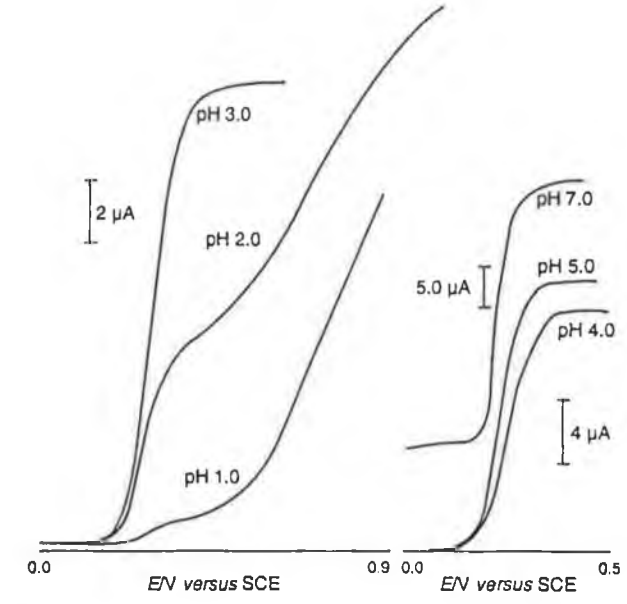


**Fig. 4** RDE voltammogram for the oxidation of $2.0 \times 10^{-4}$ mol $dm^{-3}$ ascorbic acid at a $1.0 \times 10^{-9}$ mol $cm^{-2}$ $[Os(bipy)_2(PVP)_{10}Cl]Cl$ modified electrode in 0.1 mol $dm^{-3}$ $Na_2SO_4$ at pH 1.0, 2.0, 3.0, 4.0, 5.0 and 7.0. The potential sweep rate was 2.0 mV $s^{-1}$ in all cases. Note the curve at pH 7.0 is offset for clarity.

no additional electroactive species in this potential region, this process is clearly unmediated by the redox polymer. The second wave can therefore be attributed to the oxidation of ascorbic acid at the underlying glassy carbon electrode. Therefore, at pH $\leq$ 2, ascorbic acid permeates the entire polymer film and is oxidized at the electrocatalytic sites throughout the polymer film at potentials <0.450 V *versus* SCE, resulting in an $L_k$ mechanism,[12,13] while oxidation occurs at both the catalytic sites and the underlying electrode at more positive potentials. However, at pH $\geq$ 3.0, the oxidation reaction occurs entirely at the $Os^{II}/Os^{III}$ redox centres immobilized in the redox polymer film.

There are eight possible polymer-controlled kinetic cases which may be identified with electrocatalysis at the redox polymer modified electrode at pH $\geq$ 3.0.[12,13] Elucidation of the kinetic regime pertaining at these type of modified electrodes can be achieved using the theory of Albery and Hillman.[12,13] In Fig. 5, Levich plots for the oxidation of 1.0, 2.0 and $4.0 \times 10^{-4}$ mol $dm^{-3}$ ascorbic acid at a $1.0 \times 10^{-9}$ mol $cm^{-2}$ modified electrode at pH 4.5 can be seen. These plots are linear and all pass through the origin. The observations suggest that the reaction flux is equivalent to the Levich flux, hence the modified electrode currents appear under diffusional mass transport control in solution under these conditions. Similar behaviour has been observed for ascorbic acid oxidation at Nafion- and polypyrrole-coated electrodes.[19,20] The Levich constant, $C_{Lev}$ (where $D$ is the ascorbic acid diffusion coefficient in solution and $\upsilon$ is the kinematic viscosity of the electrolyte is calculated from

$$C_{Lev} = 1.554\, D^{2/3}\, \upsilon^{-1/6} \qquad (1)$$

and is $7.4 \pm 0.2 \times 10^{-4}$ cm $s^{-1/2}$. The diffusion coefficient of $H_2A$ obtained from the Levich constants is $3.2 \times 10^{-6}$ $cm^2$ $s^{-1}$ under the conditions used. Koutecky–Levich plots for the oxidation of $2.0 \times 10^{-4}$ mol $dm^{-3}$ ascorbic acid at three polymer surface coverages ($4.0 \times 10^{-10}$, $1.0 \times 10^{-9}$ and $3.0 \times 10^{-9}$ mol $cm^{-2}$) are shown in Fig. 6. By using the theory of Albery and Hillman,[12,13] the exact kinetic regime can be elucidated. The Koutecky–Levich plots are linear and the limiting currents are dependent on the rotation speed of the electrode. This allows the elimination of the $S_{te}$, $LS_{te}$ and $LE_k$ kinetic cases. This is consistent with the rapid homogeneous charge transport rates associated with the redox polymer in sulfate electrolyte and the facile kinetics of the cross-exchange reaction.[15–17] The inverse slope of the Koutecky–Levich plots for the modified electrodes is found to be $7.4 \pm 0.2 \times 10^{-4}$ cm $s^{-1/2}$ (identical to the Levich constant above as expected), while at bare glassy carbon the experimentally determined inverse Koutecky–Levich slope is $6.2 \pm 0.3 \times 10^{-4}$ cm $s^{-1/2}$.

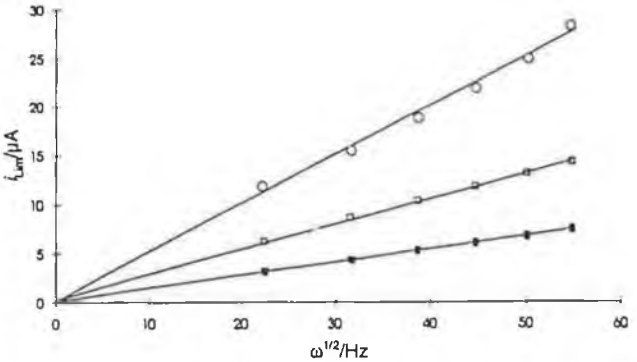


**Fig. 5** Levich plots for the oxidation of (■) $1.0 \times 10^{-4}$, (□) $2.0 \times 10^{-4}$ and (○) $4.0 \times 10^{-4}$ mol $dm^{-3}$ ascorbic acid at a $1.0 \times 10^{-9}$ mol $cm^{-2}$ $[Os(bipy)_2(PVP)_{10}Cl]Cl$ modified electrode in 0.1 mol $dm^{-3}$ $Na_2SO_4$ at pH 4.5.

The less steep slope may be a result of the sluggish electron transfer kinetics at the carbon electrode. These values, however, can be considered to be the same within experimental error, therefore the $LRZ_{tety}$ case can be eliminated. It can also be seen from Fig. 6 that increasing the polymer surface coverage ($\Gamma$) does not affect the modified electrode rate constant $k'_{ME}$ (where $k'_{ME}$ is the reciprocal of the intercept of Koutecky–Levich plot) at pH 4.5, therefore the reaction order with respect to layer thickness $L$ is zero. This observation allows the elimination of the $L_k$ and $LE_{ty}$ kinetic cases. This leaves the $S_k$- and $LS_k$ kinetic regimes. These cases can be distinguished by determining the reaction order of $k'_{ME}$ with respect to $b_0$ where $b_0$ is the concentration of electrocatalytic sites within the polymer film. The value of $b_0$ has been determined previously as $0.7 \times 10^{-3}$ mol cm$^{-3}$.[14] As the redox sites immobilized in the polymer film are in thermodynamic equilibrium with the electrode potential, they behave in a Nernstian fashion with an experimentally determined slope of 58 mV decade$^{-1}$; so, by varying the electrode potential, the concentration $b_0$ ($b_0 = [Os^{III}]$) can be varied easily and evaluated by using the Nernst equation. In Fig. 7, a plot of ln $k'_{ME}$ *versus* ln $f$, where $f$ is the fraction of the redox centres in the catalytic $Os^{III}$ redox state, is shown. The slope of this plot is $0.95 \pm 0.05$, which allows the elimination of the $LS_k$ kinetic case and indicates that the kinetic regime pertaining under these conditions is $S_k$-. In this situation, the cross-exchange reaction occurs between solution phase ascorbic acid and osmium redox sites at the polymer–solution interface, *i.e.*, substrate arriving at the modified electrode surface is entirely electrolytically consumed without penetration of the polymer film, thus resulting in currents controlled by substrate diffusion in solution. This mechanism is supported by the linearity and zero intercepts of the Levich plots found for ascorbic acid oxidation at modified electrodes at pH $\geqslant$ 3.0. The second-order rate constant $k''$ for the surface cross-exchange reaction can be determined from the modified electrode rate constant, $k'_{ME}$ by the relationship

$$k'_{ME} = n\,k''b_0 \qquad (2)$$

where $n = 2$. The value of $k'_{ME}$ was found to be $1.10 \pm 0.05 \times 10^{-4}$ cm s$^{-1}$. With $b_0$ of $0.7 \times 10^{-3}$ mol cm$^{-3}$ this yields a value for $k''$ of $7.8 \pm 0.4 \times 10^{-4}$ dm$^3$ mol$^{-1}$ cm s$^{-1}$. Analysis of the electrocatalytic behaviour at pH 7.0 yields identical solution mass transport behaviour and kinetic regime. The experimentally determined second-order rate constant at this pH is $9.1 \pm 0.6 \times 10^{-4}$ dm$^3$ mol$^{-1}$ cm s$^{-1}$. The higher value rate constant is expected at this pH due to the pH-dependent nature of ascorbic acid oxidation and consequently formal potential (*vide infra*). The $S_k$- kinetic case at physiological pH is particularly advantageous from the perspective of sensor development as the electrode responses are independent of polymer surface coverages and are not subjected to complicated mass transport or kinetic behaviour, hence the reproducibility of manufacturing processes is not critical for the production of reproducible electrode sensitivity.

Having established that the reaction is $L_k$ at low pH and $S_k$- at high pH, it is possible to offer some insight into the mechanism of the cross-exchange reaction. In Figs. 8 and 9, reaction order plots for $[H^+]$ and $[H_2A]$, respectively, are shown. The reaction order with respect to $[H^+]$ is negative first order with a slope of $-0.95 \pm 0.05$ and, for ascorbic acid, positive first order with a slope of $1.0 \pm 0.05$. Considering previously reported studies,[19,20] these observations indicate that the oxidation reaction at the $[Os(bipy)_2(PVP)_{10}Cl]Cl$ modified electrode proceeds *via* the well known two-electron process, with the first electron transfer process, resulting in the formation of the ascorbate radical anion, being the rate-determining process;[4,5] similar behaviour has been observed for the oxidation of ascorbic acid at other modified electrodes.[19,20] Considering that for ascorbic acid $pK_{a_1}$ is 4.04 and $pK_{a_2}$ is 11.34, this behaviour can be rationalized by the following reactions:

$$H_2A \longleftrightarrow HA^- + H^+ \qquad (3)$$

$$HA^- + Os^{III} \longleftrightarrow A^{\cdot -} + H^+ + Os^{II} \qquad (4)$$

$$A^{\cdot} + Os^{III} \longleftrightarrow A + Os^{II} \qquad (5)$$

$$2\,Os^{II} - 2e^- \longleftrightarrow 2\,Os^{III} \qquad (6)$$

Here, the ascorbate anion ($HA^-$) is initially oxidized by the surface polymer bound catalytic $Os^{III}$ sites to produce the

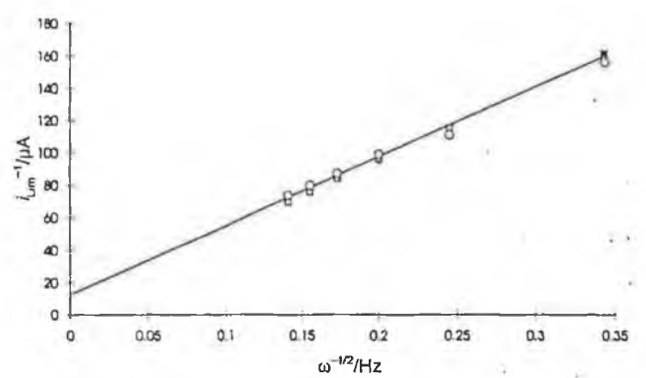


**Fig. 6** Koutecky–Levich plots for the oxidation of $2.0 \times 10^{-4}$ mol dm$^{-3}$ ascorbic acid at (■) $4.0 \times 10^{-10}$, (□) $1.0 \times 10^{-9}$ and (○) $3.0 \times 10^{-9}$ mol cm$^{-2}$ $[Os(bipy)_2(PVP)_{10}Cl]Cl$ modified electrodes in 0.1 mol dm$^{-3}$ $Na_2SO_4$ at pH 4.5.

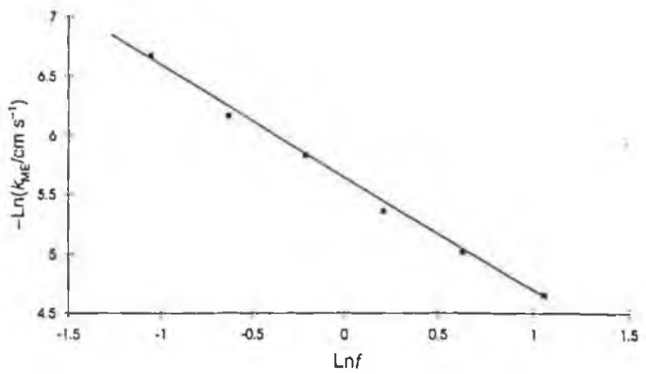


**Fig. 7** Plot of ln $k'_{ME}$ *versus* ln $f$ for the oxidation of $1.0 \times 10^{-3}$ mol dm$^{-3}$ ascorbic acid at a $1.0 \times 10^{-9}$ mol cm$^{-2}$ $[Os(bipy)_2(PVP)_{10}Cl]Cl$ modified electrode in 0.1 mol dm$^{-3}$ $Na_2SO_4$ at pH 4.5.

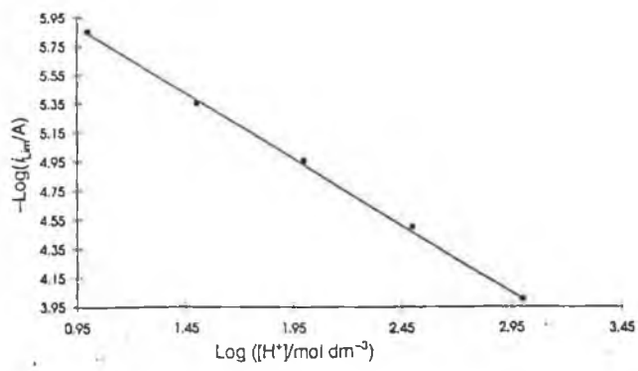


**Fig. 8** Reaction order plot of $[H^+]$ for the oxidation of $1.0 \times 10^{-3}$ mol dm$^{-3}$ $H_2A$ at a $1.0 \times 10^{-9}$ mol cm$^{-2}$ $[Os(bipy)_2(PVP)_{10}Cl]Cl$ modified electrode in 0.1 mol dm$^{-3}$ $Na_2SO_4$.

ascorbate radical anion ($A^{\bullet -}$) and $Os^{II}$. The radical anion is subsequently oxidized by $Os^{III}$ to produce dehydro-L-ascorbic acid (A) and $Os^{II}$. The reduced $Os^{II}$ sites at the polymer surface are re-oxidized rapidly by the electrode due to high homogeneous charge transport rates associated with the redox polymer and the fast self-exchange rates between the $Os^{II}/Os^{III}$ redox sites within the polymer film to complete the catalytic cycle.[15–17]

### *Sensor Development*

The rapid charge transfer rates and the near-ideal electrochemical behaviour associated with $[Os(bipy)_2(PVP)_{10}Cl]Cl$ modified electrodes[15–17] has previoulsy been shown to be transferable to the environment of thin-layer flow cells for use as electrochemical sensors.[21] As $[Os(bipy)_2(PVP)_{10}Cl]Cl$ modified electrodes are efficient electrocatalysts for ascorbic acid oxidation, the analytical responses of the redox polymer modified electrode were examined for ascorbic acid detection at physiological pH in FI. The effect of applied potential on modified electrode responses is shown with the hydrodynamic voltammogram in Fig. 10. An increase in the analytical response to ascorbic acid can be observed with increasing working electrode potential with the wave centres at ≈0.250 V *versus* SCE, which corresponds to the half-wave potential of the redox polymer. This behaviour represents the increasing potential-dependent concentration, $b_0$, of electrocatalytic $Os^{III}$ centres within the modifying layer, as expected from the Nernstian behaviour observed for the redox polymer in conventional electrochemical cells. The optimum applied potential is 0.29 V *versus* SCE and this was used for subsequent investigation. This working potential is significantly lower than those used for ascorbic acid detection at conventional carbon and metallic electrodes, which is typically >0.5 V *versus* SCE.[22,23] This is a considerable advantage since the number of interferences in electrochemical detection increase exponentially with increasing extremes of potential.

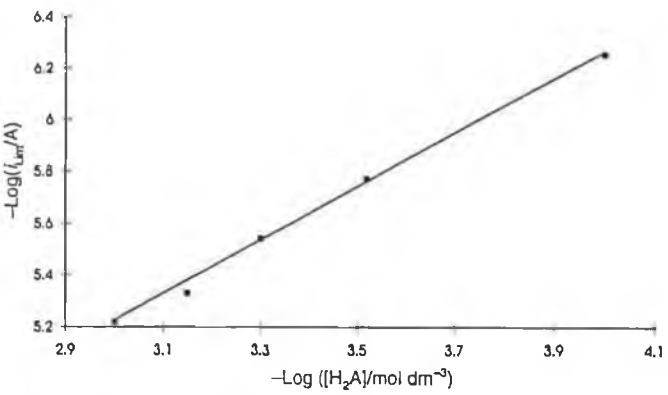


**Fig. 9** Reaction order plot of $[H_2A]$ oxidation at a $1.0 \times 10^{-9}$ mol cm$^{-2}$ $[Os(bipy)_2(PVP)_{10}Cl]Cl$ modified electrode in 0.1 mol dm$^{-3}$ $Na_2SO_4$ at a constant pH of 4.5.

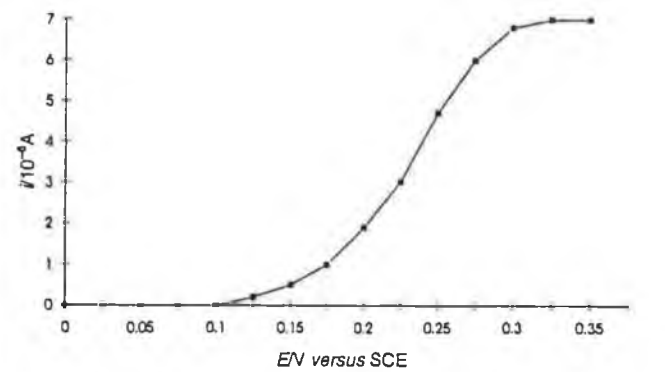


**Fig. 10** Hydrodynamic voltammogram for ascorbic acid oxidation at the $[Os(bipy)_2(PVP)_{10}Cl]Cl$ modified electrode in the thin-layer electrochemical cell. The carrier electrolyte was 0.1 mol dm$^{-3}$ phosphate buffer at 1.0 cm$^3$ min$^{-1}$. The concentration of ascorbic acid used was $2.4 \times 10^{-4}$ mol dm$^{-3}$.

The effect of the FI carrier flow rate on sensor responses was evaluated between 0.2 and 2.0 cm$^3$ min$^{-1}$. It was found that the sensor response increased with increasing electrolyte flow rate up to 0.7 cm$^3$ min$^{-1}$, where it remained constant to 1.7 cm$^3$ min$^{-1}$. Similar behaviour has been observed in the application of the redox polymer as 'molecular wires' in the development of flow-through glucose oxidase microelectrodes.[24] Because current is a time-dependent quantity, electrochemical sensors in a flow-through cell can be classified as mass-rate dependent detectors; the behaviour observed is consistent with the development of diffusion layer thicknesses dependent on carrier flow rate. A flow rate of 1.0 cm$^3$ min$^{-1}$ was used subsequently to give a rapid sample throughput with optimum sensitivity and was used to evaluate the sensor characteristics.

The linear range of the sensor was found to lie between $1.0 \times 10^{-4}$ and $1.0 \times 10^{-3}$ mol dm$^{-3}$ ascorbic acid with a sensitivity of 7.3 dm$^3$ mol$^{-1}$ and an intercept of $-1.32 \times 10^{-3}$ *A* with a correlation coefficient, *r*, of 0.998. The linear range is similar to that found for another electrochemical sensor for ascorbic acid.[25] The limit of detection (LOD), defined as a signal-to-noise ratio of 2:1, was found to be $1.0 \times 10^{-6}$ mol dm$^{-3}$. The precision of the sensor response was found to have a relative standard deviation of 0.1% for 11 repeat determinations. The response time, $\tau$, of the sensor, where $\tau$ is the time required to obtain 98% of the sensor response, was found to be ≈0.5 s with an ascorbic acid concentration of $1.0 \times 10^{-4}$ mol dm$^{-3}$. This rapid response time may be attributed to the highly efficient electrocatalysis of the oxidation reaction, resulting in the rapid development of a diffusion layer in the thin-layer electrochemical cell. The experimentally determined analytical throughput for the sensor was 50 samples min$^{-1}$ with baseline resolution. It is evident that the sensor exhibits a significant linear range, low LOD, high precision and rapid response time and sample throughput.

The long-term stability of electrochemical sensors is of considerable importance. Ascorbic acid detection at conventional electrode surfaces causes rapid and severe electrode passivation, resulting in a deterioration in electrode sensitivity. The response stability of the redox polymer modified electrode was examined with periodic injections of $2.4 \times 10^{-4}$ mol dm$^{-3}$ ascorbic acid over a 60 h period. The sensor response to the ascorbic acid remained relatively constant for 60 h at 5.6 mA, with a relative standard deviation of 6.5%. It is likely that this level of stability is due to the surface nature of the electrocatalytic reaction; slow removal of the redox polymer under the hydrodynamic conditions of the electrochemical flow cell should not result in a deterioration of electrode response as long as at least a monolayer of electrocatalyst remains. After 60 h a rapid decrease in sensor sensitivity was observed. We attribute this to the removal of redox polymer at sub-monolayer levels. However, crosslinking of the redox polymer film has been shown previously to be effective for the physical stabilizing of the polymer layer under severe hydrodynamic conditions without compromising charge transport dynamics and the kinetics of surface reactions;[26] consequently crosslinking of the redox polymer is likely to produce highly stable sensors with $S_k$- kinetics. The level of stability found is, however, considerable, which is an advantage in areas such as continuous monitoring application and where direct sensor calibration is difficult.

## Conclusions

The compound $[Os(bipy)_2(PVP)_{10}Cl]Cl$ is an efficient electrocatalyst for the oxidation of ascorbic acid at high pH values. The kinetic regime passes from a through-film $L_k$ mechanism to a surface $S_k$- mechanism with increasing pH. This is consistent with the pH-dependent nature of ascorbic acid oxidation. Essentially, as the formal potential for ascorbic acid oxidation shifts cathodically with increasing pH, the free energy difference ($\Delta G$) between the ascorbic acid and the electrocatalyst increases, resulting in increasingly efficient electrocatalysis, as expected from the linear free energy relation in Marcusian theory. This is reflected in the higher value for $k''$ at pH 7.0 compared with pH 4.5. At pH $\geq 3$, the electrocatalytic cross-exchange reaction is sufficiently facile to occur at the polymer–electrolyte interface under solution mass transport control. The facile nature of the electrocatalytic oxidation process at high pH allows application of the osmium–redox polymer modified electrode as a highly stable and reproducible electrochemical sensor for ascorbic acid detection. The wide linear range, low limit of detection, high precision, rapid response time, high sample throughput and stability of the sensor are of considerable advantage.

With a patent granted recently,[27] there is growing academic and commercial interest in osmium-containing redox polymers as 'molecular wires' in enzyme electrodes; this is primarily due to their low redox potentials and rapid charge transport characteristics, but also to their synthetic variablity and stability. It is clear from this study that the biologically ubiquitous ascorbic acid is an important source of interference for these types of electrodes in clinical applications. Modifying permselective layers have been used extensively to exclude such interferences: however, such layers are rarely totally excluding and frequently hinder analyte mass transport drastically, resulting in long response times.[28] From the results presented here, it is possible to postulate the future design of such enzyme electrodes for the elimination or isolation of interfering signals. The simple diffusion-controlled nature of the ascorbic acid reaction will easily allow the application of the two-electrode differential measurement approach to eliminate the interfering signal. The insensitivity of the reaction-to-polymer surface coverage is of particular importance in this regard.

We have suggested previously that the use of electrode arrays with modified electrodes of varying electrocatalytic and transport properties allows isolation of the signal for the target analyte and the interferent, thus allowing simultaneous quantification of both species.[11] Again, from the results presented here, this approach may also be applied to enzyme electrodes constructed from osmium-containing redox polymers. As the oxidation of ascorbic acid is independent of polymer layer thickness, the current signal for ascorbic acid oxidation will be constant for all reasonable polymer layer thicknesses (up to $\approx$2–4 μm), while varying the polymer layer thickness and/or enzyme loading increases the signal due to enzyme reaction, which allows measurement of the signal difference between the enzyme-catalysed reaction and ascorbic acid oxidation. This procedure is analogous to a differential kinetic measurement. Extrapolation to a zero enzyme loading and/or to an infinitely small surface coverage allows isolation of the individual currents and hence simultaneous measurements of both analyte and interferent.[11]

The authors would like to thank Forbairt, the Irish Science and Technology Agency, for funding for this work.

## References

1 Faulkner, L. R., *Chem. Eng. News*, 1984, **62**, 28.
2 Murray, R. W., Ewing, A. G., and Durst, R. A., *Anal. Chem.*, 1987, **59**, 379A.
3 Forster, R. J., and Vos, J. G., in *Comprehensive Analytical Chemistry*, ed. Smyth, M. R., and Vos, J. G., Elsevier, Amsterdam, 1992, vol. XXVII, ch. 7.
4 Falat, L., and Cheng, H. Y., *Anal. Chem.*, 1982, **54**, 3235.
5 Gondon, F. G., Fombariet, C. M., Buda, M. J., and Pujol, J. F., *Anal. Chem.*, 1981, **53**, 1386.
6 Ohara, T. J., Rajagopalan, R., and Heller, A., *Anal. Chem.*, 1994, **66**, 2451.
7 Gregg, B., and Heller, A., *J. Phys. Chem.*, 1991, **95**, 5970.
8 Ohara, T. J., Rajagopalan, R., and Heller, A., *Anal. Chem.*, 1993, **65**, 24.
9 Saveant, J. M., *Acc. Chem. Res.*, 1980, **13**, 323.
10 Turner, R. F. B., Harrison, D. J., Rajotte, R. V., and Baltes, H. P., *Sens. Actuators B*, 1990, **21**, 561.
11 Doherty, A. P., and Vos, J. G., *Anal. Chem.*, 1993, **65**, 3424.
12 Albery, W. J., and Hillman, A. R., *J. Electroanal. Chem.*, 1984, **170**, 27.
13 Albery, W. J., and Hillman, A. R., *Ann. Rep. Progr. Chem. C*, 1981, **78**, 377.
14 Forster, R. J., and Vos, J. G., *Macromolecules*, 1990, **23**, 4372.
15 Forster, R. J., Lyons, M. E. G., and Vos, J. G., *J. Chem. Soc., Faraday Trans.*, 1991, **87**, 3761.
16 Forster, R. J., Lyons, M. E. G., and Vos, J. G., *J. Chem. Soc., Faraday Trans.*, 1991, **87**, 3769.
17 Forster, R. J., Kelly, A. J., Vos, J. G., and Lyons, M. E. G., *J. Electroanal. Chem.*, 1989, **270**, 365.
18 Anson, F. C., Tsou, Y.-M., and Saveant, J. M., *J. Electroanal. Chem.*, 1984, **178**, 113.
19 Williams, N. H., and Yandell, J. K., *Aust. J. Chem.*, 1982, **35**, 1133.
20 Lyons, M. E. G., Breen, W., and Cassidy, J., *J. Chem. Soc., Faraday Trans.*, 1991, **87**, 115.
21 Doherty, A. P., Stanley, M. A., Koning, C. E., Brinkhuis, R. H. G., and Vos, J. G., *Electroanalysis*, 1995, **7**, 333.
22 Kutnik, M. A., Skula, J. H., Sunkerlich, H. E., and Omage, S. T., *J. Chromatogr.*, 1985, **8**, 3123.
23 Cenas, N., Rozgaite, J., Pocius, A., and Kulys, J., *Electroanal. Chem.*, 1983, **154**, 121.
24 Rohde, E., Dempsey, E., Smyth, M. R., Vos, J. G., and Emons, H., *Anal. Chim. Acta*, 1993, **278**, 5.
25 Kulys, J., and D'Costa, E. J., *Anal. Chim. Acta*, 1991, **243**, 173.
26 Doherty, A. P., Kelly, D., Buckley, T., and Vos, J. G., *Electroanalysis*, 1994, **6**, 553.
27 Spokane, R. B., *U.S. Pat.*, 5 298 144, Cl. 204–403; G01N27/3270, Mar. 29 1994, Appl. 944 963, September 15, 1992.
28 Wang, J., Golden, T., and Tuzhi, P., *Anal. Chem.*, 1987, **39**, 740.

*Paper 5/02829I*
*Received May 3, 1995*
*Accepted June 14, 1995*

ELSEVIER

Analytica Chimica Acta 319 (1996) 111–120

ANALYTICA CHIMICA ACTA

# Oxidative detection of nitrite at an electrocatalytic [Ru(bipy)$_2$poly-(4-vinylpyridine)$_{10}$Cl]Cl electrochemical sensor applied for the flow injection determination of nitrate using a Cu/Cd reductor column

Andrew P. Doherty [*,1], Margaret A. Stanley, Donal Leech [2], Johannes G. Vos

*School of Chemical Sciences, Dublin City University, Dublin 9, Ireland*

Received 29 June 1995; revised 7 September 1995; accepted 20 September 1995

**Abstract**

An electrochemical sensor developed from a redox polymer [Ru(bipy)$_2$(PVP)$_{10}$Cl]Cl (where bipy is 2,2′-bipyridyl and PVP is poly-(4-vinylpyridine)) modified electrode for nitrite detection is described. The modified electrode acts as an efficient electrocatalyst for nitrite oxidation with amplification of electrode current by at least a factor of 3 compared with unmodified electrodes. The electrocatalytic reaction occurs throughout the polymer film in a three dimensional reaction zone and may be classified as an $L_k$ mechanism. The second order rate constant for the cross exchange reaction is 3.02 ($\pm$0.20) $\times 10^1$ mol$^{-1}$ dm$^3$ s$^{-1}$. The sensor is applied to the determination of nitrate in a flow injection apparatus following the heterogeneous reduction of this species to nitrite at a copperised cadmium reductor column. The sensor exhibits a linear response range extending over three orders of magnitude from $1.0 \times 10^{-5}$ to $1.0 \times 10^{-2}$ mol dm$^{-3}$ nitrate with a limit of detection (signal-to-noise = 2) of $5.0 \times 10^{-6}$ mol dm$^{-3}$. The coefficient of variation for measurement of $1.0 \times 10^{-3}$ mol dm$^{-1}$ nitrite is 0.42% ($n$ = 20). No passivation of the electrode surface was evident after over 200 repeat determinations. The system was applied to the determination of nitrate in commercial fertiliser compound.

*Keywords:* Redox polymer; Sensors; Nitrate; Nitrite; Flow injection

## 1. Introduction

The determination of nitrate is one of the most frequent measurements in environmental analysis [1]. Nitrate is suspected to be toxic and is known to accelerate algae blooms and the eutrophication of lakes [2]. Traditionally nitrate has been determined by the Kjeldahl method for nitrogen [3]. This species has also been determined spectrophotometrically after nitration of chromotropic acid [4], phenol disulphonic acid [5], 2,6-xylenol [6] and 3,4-xylenol [7]. These procedures are slow, relatively insensitive, operator and reagent intensive and unreliable in many applications.

Several examples of the electrochemical determi-

* Corresponding author.

[1] Present address: Chemistry Department, Bedson Building, University of Newcastle, Newcastle upon Tyne, NE1 7RU, UK.

[2] Present address: Chemistry Department, University of Montreal, Montreal, H3C 3J7, PQ, Canada.

Elsevier Science B.V.
*SSDI* 0003-2670(95)00475-0

nation of nitrate have been proposed. Catalytic polarography in the presence of multicharged cations such as La(III), Yb(III) and Ce(III) has been investigated [8]. Although the detailed chemistry of these procedures is little understood, it appears that the lower oxidation state of the cation reduces nitrate and the cation is regenerated at the electrode surface in a catalytic cycle. Davenport and Johnson [9,10] used a rotating cadmium electrode for nitrate determination in the concentration region of ca. $10^{-4}$ mol $dm^{-3}$. Coating the cadmium electrode with metallic copper was found to improve the analytical performance of the electrode [11]. Albery et al. [12,13] used this theme with packed-bed wall-jet copper electrodes, but after several determinations severe poisoning of the electrode surface was evident.

Reductive electrochemical techniques require highly acidic conditions for the reduction reaction to proceed and therefore are not useful for routine analysis. In addition, reductive techniques require cathodic potential extremes where many sources of interference may be a problem, e.g., hydrogen evolution, oxygen reduction and the discharge of adventitious metal cations.

The most used methods for the determination of nitrate involve prior reduction to nitrite, followed by determination of the nitrite [14]. The reduction to nitrite can be accomplished with the use of highly efficient heterogeneous reductors prepared from zinc, cadmium, cadmium amalgams, or copperised cadmium [15]. Copperised cadmium appears to be the reductant of choice with the metallic copper deposit catalysing the reduction reaction. The nitrite generated is normally detected using conventional spectrophotometry following a diazotisation reaction [16]. Although popular, spectrophotometric techniques for nitrite suffer from a number of disadvantages including limited linear ranges, poor limits of detection (LOD), complicated experimental protocols and relatively low analytical through-put. In addition, many of the procedures often involve long reaction times and unstable colorimetric reactions and products and also may not be applicable to highly coloured samples. The direct detection of nitrite in such analytical protocols for nitrate may be advantageous by eliminating the uncertainty associated with the derivatisation unit process.

It is known that nitrite can be oxidised at conventional electrodes at moderate anodic potentials (ca. 1.0 V vs. SCE), however surface passivation of the electrode limits the usefulness of this approach [17]. In this paper we describe the kinetics of nitrite oxidation at $[Ru(bipy)_2(PVP)_{10}Cl]Cl$ modified electrodes (bipy = 2,2′-bipyridyl, PVP = poly-(4-vinylpyridine)) and demonstrate the use of such electrodes as electrochemical sensors for nitrite following the heterogeneous reduction of nitrate to nitrite using a copperised cadmium column with a flow injection analysis (FIA) protocol. The system is applied to the determination of nitrate in a commercial fertiliser mixture. The analytical parameters of the modified electrode sensor are compared to the commonly employed spectrometric systems.

## 2. Experimental

### 2.1. Electrochemical and flow injection apparatus

Cyclic voltammetry (CV) and rotating disk electrode (RDE) voltammetry was carried out using a conventional three electrode cell with an EG&G (Princeton Applied Research) Model 374 potentiostat and a Linseis X–Y recorder. The rotating disc assembly was the Metrohm Model 629-10 RDE. The working electrodes were 3 mm diameter glassy carbon shrouded in PTFE (Metrohm). The counter electrode was 1 $cm^2$ platinum gauze, while the reference electrode was the saturated calomel electrode (SCE).

A schematic diagram of the FIA system is shown in Fig. 1. The apparatus consisted of a Gilson Minipuls 3 peristaltic pump, a six port Rheodyne injector valve fitted with a 50 $\mu$l fixed volume

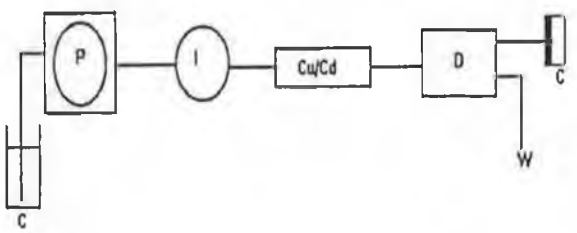


Fig. 1. Schematic diagram of the flow injection apparatus, C is the carrier electrolyte, P is the peristaltic pump, I is the injector, Cu/Cd is the copperised cadmium reductor column, D is the detector, C is the X–t recorder and W is waste.

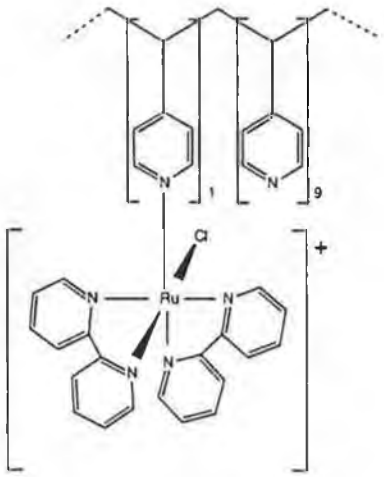


Fig. 2. Structure of $[Ru(bipy)_2(PVP)_{10}Cl]Cl$.

sample loop, a copperised cadmium chip reductor column, a EG&G Model 400 electrochemical detector connected with PTFE HPLC tubing and a Philips X–t chart recorder.

In the thin-layer flow-cell, a Ag/AgCl electrode acted as the reference electrode while the stainless steel cell body acted as the counter electrode. All potentials are quoted after numerical conversion to the SCE scale. The working electrodes were 3 mm diameter glassy carbon shrouded in a PTFE block (EG&G). Modified electrodes were prepared by polishing the glassy carbon electrodes with 5 $\mu$m alumina as an aqueous slurry. The polished electrodes were rinsed with distilled water and methanol and dried before modification. The electrodes were modified by drop coating using a 1% (w/v) methanolic solution of the redox polymer. The synthesis of the redox polymer is described elsewhere [18]; the polymer structure is shown in Fig. 2. Polymer surface coverages were estimated by integration of the charge ($Q$) under slow sweep rate CV (1.0 mV $s^{-1}$) using the relation $Q = nF\Gamma$, where $\Gamma$ is the surface coverage in mol $cm^{-2}$, $F$ is the Faraday constant and $n$ is the number of electrons. Sample injections were made using a 2.0 $cm^3$ glass syringe fitted with a Rheodyne injection needle.

The reductor columns were constructed from 0.2 cm i.d. silicone tubing packed with cadmium chips. The length of the reductor column was 1.2 cm. The cadmium chips were prepared from high purity (0.1 cm diameter, 99.9%, Goodfellows) cadmium wire. Various copperisation protocols were examined but the optimum procedure involved passing a solution containing 0.1 mol $dm^{-3}$ NaCl, 10 g $dm^{-3}$ ethylendiaminetetraacetic acid (EDTA) and 0.413 g $dm^{-3}$ $CuSO_4 \cdot 5H_2O$ continuously over cadmium chips prewashed in nitric acid (0.1 mol $dm^{-3}$) for 1 h. This resulted in the development of a pristine metallic copper layer on the cadmium chips. Problems with the rapid deactivation of the reductor column led to the copperisation solution being used as the carrier stream for the FIA experiments. The presence of EDTA was found to prevent a build-up of $[Cd(OH)_2]$ precipitate in the reductor column by the formation of a Cd–EDTA chelate, and the presence of $Cu^{2+}$ ensured continuous in situ regeneration of the copperised surface. Together these resulted in stable reductor columns until the exhaustion of the cadmium through oxidation by nitrate.

### 2.2. Determination of nitrate in commercial fertiliser

Finely ground fertiliser samples was sonicated for 15 min with 0.1 mol $dm^{-3}$ NaCl. The resulting supernatant solutions were transferred quantitatively to volumetric flasks and diluted with 0.1 mol $dm^{-3}$ NaCl. Such solutions were used for subsequent analysis. Calibration solutions were prepare from sodium nitrate in the concentration range $1.0 \times 10^{-3}$ to $1.0 \times 10^{-2}$ mol $dm^{-3}$ $NO_3^-$. No difference in analytical response between $NaNO_3$, $KNO_3$ or $NH_4NO_3$ was evident. The responses from the calibration solutions and the sample solutions were recorded at an applied potential of 0.95 V vs. SCE at the modified electrode. Blank responses were also recorded by replacing the Cu/Cd reductor column with a glass wool-packed column. The carrier flow rate was 0.5 $cm^3$ $min^{-1}$ and the copperised cadmium column was 1.2 cm in length. For comparison purposes, the concentration of nitrate in the sample was also determined potentiometrically using the Orion Model 93-07 nitrate ion selective electrode in conjunction with the Universal PT I6 high impedance voltmeter. The Nernstian slope (0.058 V $decade^{-1}$) for the ion selective electrode was measured using a series of standard $NO_3^-$ solutions prepared as described above. The method of standard addition was used using

stock nitrate solutions. All analyses were carried out in triplicate.

## 3. Results and discussion

### 3.1. Electrocatalytic oxidation of nitrite

Fig. 3 shows a cyclic voltammogram of the $[Ru(bipy)_2(PVP)_{10}Cl]Cl$ redox polymer modified electrode in 0.1 mol $dm^{-3}$ NaCl electrolyte. A single one-electron reversible wave can be observed with a half-wave potential of ca. 0.75 V vs. SCE. This half-wave potential is consistent with a $[Ru(N)_5Cl]$ type complex with the reversible oxidation/reduction process corresponding to Ru(II)/Ru(III) redox couple immobilised within the polymer film. Nitrite can be oxidised to nitrate according to the following reaction;

$$NO_2^- + H_2O \rightarrow NO_3^- + 2H^+ + 2e \quad (1)$$

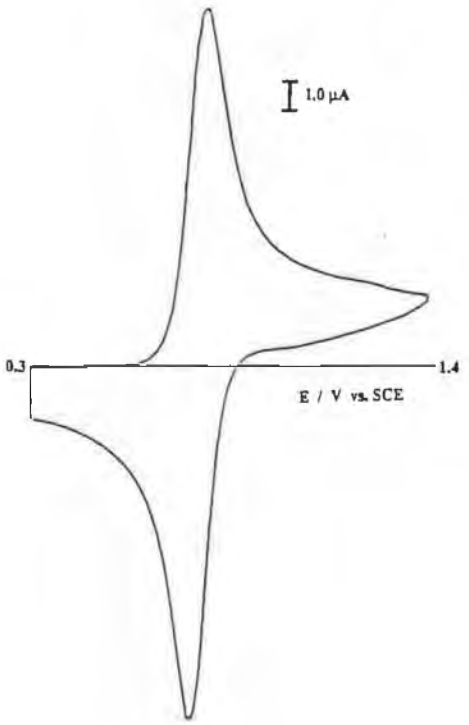


Fig. 3. Cyclic voltammogram of $[Ru(bipy)_2(PVP)_{10}Cl]Cl$-modified electrode, $\Gamma = 1.0 \times 10^{-8}$ mol $cm^{-2}$, in 0.1 mol $dm^{-3}$ NaCl at 100 mV $s^{-1}$.

with a formal potential $E^0$ of 0.59 V vs. SCE [19]. As the half-wave potential of Ru(II)/Ru(III) process is more positive than the formal potential for nitrite oxidation, the electrocatalytic oxidation of nitrite at the modified electrode is thermodynamically favourable with a 0.16 V electrochemical driving force. In Fig. 4A a RDE voltammogram of $2.5 \times 10^{-3}$ mol $dm^{-3}$ nitrite at a glassy carbon electrode can be seen. A single diffusion controlled oxidation process is evident with the onset of nitrite oxidation at ca. 0.8 V vs. SCE. In Fig. 4B a RDE voltammogram of $2.5 \times 10^{-3}$ mol $dm^{-3}$ nitrite at a redox polymer modified electrode with a surface coverage of $1.0 \times 10^{-8}$ mol $cm^{-2}$ is shown. For the modified electrode, the onset of nitrite oxidation occurs at a significantly lower potential of 0.64 V with the wave centred at 0.75 V which corresponds to the potential region of the polymer-immobilised electrocatalytic Ru(II)/Ru(III) redox couple. Comparing Fig. 4B with Fig. 4A, significant current enhancement is also evident at the modified electrode. Collectively, these observations may be attributed to the efficient electrocatalytic oxidation of nitrite by the polymer immobilised electrocatalytic Ru(III) sites within the polymer film along with the rapid oxidative regeneration of Ru(III) at the electrode according to the following mechanism:

$$NO_2^- + H_20 + 2Ru(III) \rightarrow NO_3^- + 2H^+ + 2Ru(II) \quad (2)$$

$$2Ru(II) \rightarrow 2Ru(III) + 2e \quad (3)$$

In order to investigate the kinetics and transport processes for this electrocatalytic process the RDE data were analysed using the theory of Albery and Hillman [20]. In Fig. 5 Koutecky-Levich plots for the oxidation of $2.5 \times 10^{-4}$ mol $dm^{-3}$ nitrite at various polymer surface coverages are shown. As all the plots are linear the $LE_k$ kinetic case can be eliminated. The average inverse slope of the Koutecky-Levich plots (yielding the Levich constant, $C_{Lev}$) is $3.7\ (\pm 0.4) \times 10^{-3}$ cm $s^{-1/2}$. Use of the relation;

$$C_{Lev} = 1.554 D^{2/3} \upsilon^{-1/6} \quad (4)$$

where $D$ is the diffusion coefficient of nitrite in solution and $\upsilon$ is the electrolyte kinematic viscosity ($8.9 \times 10^{-2}$ $cm^2$ $s^{-1}$), yields a value for $D$ of 3.7

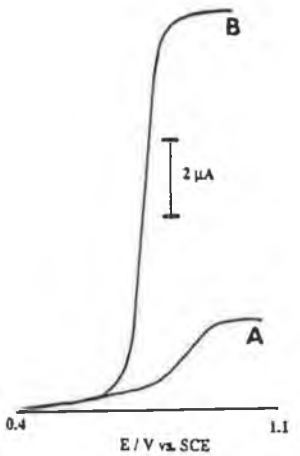


Fig. 4. RDE voltammograms of $2.5\times10^{-3}$ mol $dm^{-3}$ nitrite at (A) bare glassy carbon electrode and (B) $[Ru(bipy)_2(PVP)_{10}Cl]Cl$-modified electrode, $\Gamma = 1.0\times10^{-8}$ mol $cm^{-2}$, the potential sweep rate was 2.0 mV $s^{-1}$.

$(\pm0.16)\times10^{-5}$ $cm^2$ $s^{-1}$ which is consistent with the diffusion of small electrolyte particles. It is evident from the plots that the intercepts (modified electrode rate constant $k_{ME'}$) of the Koutecky-Levich plots decreased with increasing polymer surface coverage. This behaviour indicates that with increasing polymer layer thickness the electrocatalytic activity of the redox polymer increases. Using the theory of Albery and Hillman [20], such behaviour indicates that the electrocatalytic oxidation of nitrite occurs at redox centres throughout the polymer film and hence may be classified as an $L_k$ mechanism [20].

The fraction of electrocatalytic Ru(III) centres within the polymer film may be evaluated using the Nernst relation and a knowledge of the total polymer surface coverage. Plots of ln $k_{ME'}$ vs. ln $f$ where $f$ is the fraction of Ru(III) redox centres within the film were found to be linear with a slope of $1.1 \pm 0.2$. This indicates a first order relationship between the concentration of electroactive sites within the polymer film and the magnitude of the modified electrode rate constant $k_{ME'}$. Such behaviour is characteristic of an $L_k$ mechanism. For this mechanism, rapid penetration of the polymer film by nitrite is required. An estimate of the partition coefficient $K$ for nitrite may be obtained by using the analogous redox polymer $[Os(bipy)_2(PVP)_{10}Cl]Cl$ (where electrocatalytic oxidation of nitrite is thermodynamically impossible) as a surrogate film. Oxidationcurrents at glassy carbon electrodes and $[Os(bipy)_2(PVP)_{10}Cl]Cl$-modified electrodes were similar, suggesting similar interfacial concentrations of nitrite for both the modified and unmodified electrode. Hence, the partition coefficient for nitrite partition into the polymer film may be considered to be close to unity [21]. This is entirely consistent with the $L_k$ mechanism observed. Under these conditions, the second order rate constant, $k$, for the electrocat-

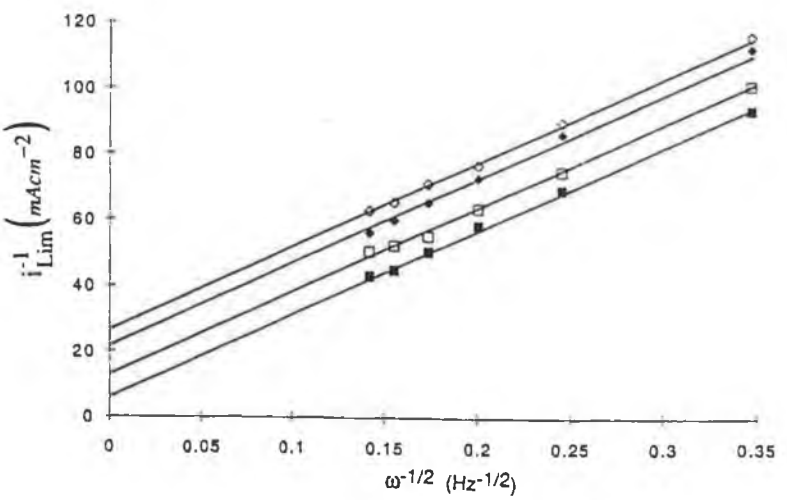


5. Koutecky-Levich plots for the electrocatalytic oxidation of $2.5\times10^{-4}$ mol $dm^{-3}$ nitrite at $[Ru(bipy)_2(PVP)_{10}Cl]Cl$-modified odes with surface coverages of (from top) $8.0\times10^{-10}$, $1.9\times10^{-9}$, $3.5\times10^{-9}$ and $1.25\times10^{-8}$ mol $cm^{-2}$.

alytic cross exchange reaction within the polymer film can be calculated from the relation [20];

$$k_{ME'} = nFAkK\Gamma y_s \quad (5)$$

where $A$ is the electrode surface area and $y_s$ is the nitrite concentration. Using the intercept values from Koutecky-Levich plots, a value of 3.02 ($\pm 0.20$) $\times$ $10^1$ mol$^{-1}$ dm$^3$ s$^{-1}$ for $k$, the second order rate constant is obtained. This value is consistent with rapid cross exchange kinetics in a three dimensional reaction zone.

### 3.2. Sensor development

From the results presented, it is evident that the redox polymer $[Ru(bipy)_2(PVP)_{10}Cl]Cl$ is an efficient electrocatalyst for nitrite oxidation. The enhancement of electrode kinetics achieved by through-film electrocatalysis results in a significant decrease in oxidation potential and increased electrode currents. Such features are advantageous for sensor development since the number of interferences increases exponentially with increasing operational potential, while enhanced electron transfer kinetics increases sensor sensitivity. In this section, therefore, the development of a nitrite sensor from $[Ru(bipy)_2(PVP)_{10}Cl]Cl$ modified electrodes and the application of this sensor for the detection of nitrate following its reduction to nitrite in a Cu/Cd reductor column will be discussed.

### 3.3. Sensor responses to nitrite in the FIA system

In Fig. 6 a hydrodynamic voltammogram is shown for the oxidation of $1.0 \times 10^{-3}$ mol dm$^{-3}$ nitrite at a $\Gamma = 1.0 \times 10^{-8}$ mol cm$^{-2}$ modified electrode in the FIA system at a carrier flow rate of 1.0 cm$^3$ min$^{-1}$. At potentials $\leq 0.640$ V no response to nitrite oxidation is evident. At this potential the electroactive sites are in the pre-catalytic Ru(II) state and thermodynamically cannot mediate the oxidation of nitrite. Increasing the applied potential results in the generation of catalytic Ru(III) sites within the polymer film, hence the onset of mediated oxidation of nitrite is evident. It can be seen from this plot that the greatest responses for electrocatalytic nitrite oxidation in the thin-layer flow-cell are obtained at an

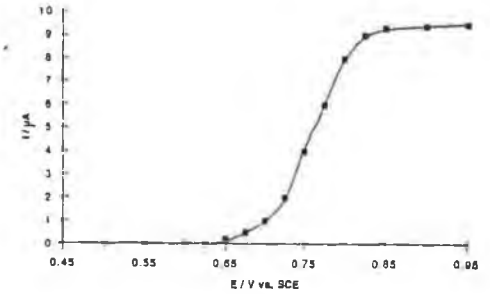


Fig. 6. Hydrodynamic voltammogram for the oxidation of $1.0 \times 10^{-3}$ mol dm$^{-3}$ nitrite at a $[Ru(bipy)_2(PVP)_{10}Cl]Cl$-modified electrode, $\Gamma = 1.0 \times 10^{-8}$ mol cm$^{-2}$ with a carrier flow rate of 1.0 cm$^3$ min$^{-1}$.

applied potential $> 0.85$ V. A potential of 0.95 V was used for all subsequent experiments.

Sensor responses over the concentration range $1.0 \times 10^{-6}$–$1.0 \times 10^{-2}$ mol dm$^{-3}$ nitrite were recorded at modified electrodes with a surface coverage of $1.0 \times 10^{-8}$ mol cm$^{-2}$ and compared to bare glassy carbon electrode responses. It was found that the responses at the modified electrode were greater by at least a factor of 3 compared to the unmodified electrode, e.g., at $1.0 \times 10^{-4}$ mol dm$^{-3}$ nitrite the response at the bare electrode was 1.26 $\mu$A while at the modified electrode it was 4.78 $\mu$A. Again, this is indicative of the efficient electrocatalysis of the oxidation of nitrite and agrees with the results obtained from the RDE experiments.

The linear range of the electrochemical sensor was found to extend over a concentration range of three orders of magnitude from $1.0 \times 10^{-6}$ to $1.0 \times 10^{-3}$ mol dm$^{-3}$ nitrite with a correlation coefficient of $r \geq 0.998$. The limit of detection (LOD) for nitrite (signal-to-noise = 2:1) was $5.0 \times 10^{-7}$ mol dm$^{-3}$. The baseline peak-width under these conditions was 5 s. This is indicative of the rapid response time of the modified electrode to nitrite detection due to the rapid penetration of the redox polymer film by nitrite and to the efficient electrocatalysis of the nitrite oxidation process. This allows an optimum analytical throughput of 720 h$^{-1}$. The precision of response was also found to be good; for 20 repeat injections of $1.0 \times 10^{-3}$ mol dm$^{-3}$ nitrite, a coefficient of variation of 0.42% was obtained. These results indi-

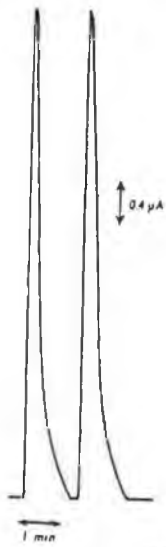


Fig. 7. Typical FIA responses to $1.0 \times 10^{-3}$ mol dm$^{-3}$ nitrate, at 0.5 cm$^3$ min$^{-1}$ carrier flow rate, 0.95 V vs. SCE at a [Ru(bipy)$_2$(PVP)$_{10}$Cl]Cl-modified electrode, $\Gamma = 1.0 \times 10^{-8}$ mol cm$^{-2}$.

cate that the modified electrode is an efficient electrochemical sensor for nitrite detection with low limits of detection, an extensive linear range and high sensitivity. Such features are attractive for the direct detection of nitrite following reduction of nitrate in catalytic Cu/Cd columns.

### 3.4. Sensor responses to nitrite generated from nitrate reduction at Cu / Cd

By introducing a Cu/Cd reductor column into the FIA system, nitrite generated from nitrate at the Cu/Cd catalyst may be directly detected electrochemically down-stream at an [Ru(bipy)$_2$(PVP)$_{10}$Cl]Cl modified electrode. In Fig. 7 typical modified electrode responses to nitrite generated by the reduction of nitrate (0.5 cm$^3$ min$^{-1}$, $1.0 \times 10^{-3}$ mol dm$^{-3}$ nitrate) in the FIA system can be seen. The sensor responses are well defined, nearly symmetrical and can be considered useful for analytical purposes. In Fig. 8 a plot of electrode response vs. carrier electrolyte flow rate with a nitrate concentration of $1.0 \times 10^{-3}$ mol dm$^{-3}$ can be seen. It is evident that increasing the flow rate of the electrolyte from 0.075 cm$^3$ min$^{-1}$ to 0.30 cm$^3$ min$^{-1}$ results in an exponential decrease in the response from the modified electrode. At flow rates $\geq 0.3$ cm$^3$ min$^{-1}$ the response levels off to a constant value. Injections of standard nitrite solution instead of nitrate results in an increase in electrode response with increasing flow rate which indicates the mass-rate behaviour of the electrochemical sensor as expected from the $i = nFdQ/dt$ relationship. The decrease in sensor response for the generated nitrite may be attributed to a decrease in efficiency of conversion of nitrate to nitrite by the Cu/Cd reductor column. Increasing the flow rate of the electrolyte decreases the residence time of the sample in the reduction column and therefore of the extent of nitrate reduction. Greatest responses are therefore obtained at low flow rates. In order to minimise sample dispersion and provide reasonable sample through-put rates, a flow rate of 0.5 cm$^3$ min$^{-1}$ was used throughout.

At an electrolyte flow rate of 0.5 cm$^3$ min$^{-1}$ the baseline peak-width is ca. 1.0 min. Such broad peaks are normal for the FIA spectrophotometric determination of nitrate due to reagent stream mixing prior to detection [22]. The broad nature and tailing of the peaks observed here may be attributed to the considerable dead volume in the reductor column and, to a lesser extent, the slow flow rate of the carrier electrolyte. Based on the peak-width under these operational conditions, an analytical through-put of 60

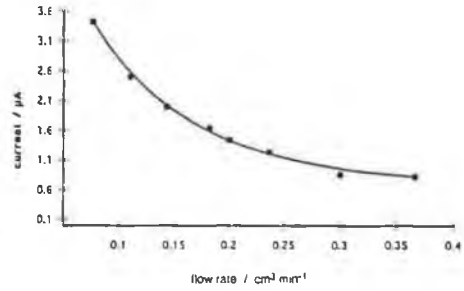


Fig. 8. Plot of sensor response vs. carrier flow rate for a nitrate concentration of $1.0 \times 10^{-3}$ mol dm$^{-3}$ at a [Ru(bipy)$_2$(PVP)$_{10}$Cl]Cl-modified electrode, $\Gamma = 1.0 \times 10^{-8}$ mol cm$^{-2}$, at 0.95 V vs. SCE.

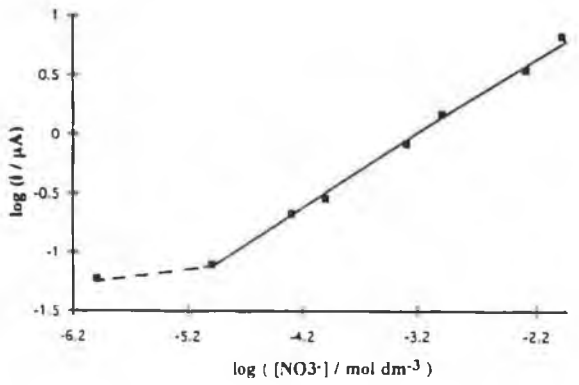


Fig. 9. Typical calibration graph for nitrate analysis, conditions as for Fig 7.

samples $h^{-1}$ can be achieved, which is comparable to spectrophotometric procedures [23]. This through-put rate is considerably less than in the absence of the Cu/Cd reductor column, however. Through-put rate may be improved by increased flow rates. In addition, optimisation of the Cu/Cd reductor column is likely to minimise dead volume and sample dispersion and therefore increase the sample through-put rate. The precision of response was assessed by repeat determinations of $5.0 \times 10^{-4}$ mol $dm^{-3}$ nitrate solutions. The coefficient of variation was found to be 2.0% for which injection is comparable to spectrophotometric procedures [23]. Considering the higher precision in the absence of the reductor column (0.42%), it is clear that the majority of the error for nitrate determination emanates from the conversion of nitrate to nitrite rather than from the electrochemical detector.

In Fig. 9 a typical calibration plot over the concentration range $1.0 \times 10^{-6}$ to $1.0 \times 10^{-2}$ mol $dm^{-3}$ nitrate can be seen. The linear range extends over a concentration range of three orders of magnitude from $1.0 \times 10^{-5}$ mol $dm^{-3}$ to $1.0 \times 10^{-2}$ mol $dm^{-3}$ with a correlation coefficients, of 0.999. This linear range is a significant improvement compared to those observed for spectrophotometric procedures which are normally linear over very narrow concentration ranges, typically $2.0 \times 10^{-5}$–$3.0 \times 10^{-4}$ mol $dm^{-3}$. The linear range also encompasses the normal nitrate levels found in environmental water samples, typically $\approx 2.0 \times 10^{-5}$–$6.0 \times 10^{-4}$ mol $dm^{-3}$ $NO_3^-$. For the spectrophotometric approach judicious dilution of samples with high levels of nitrate is required while for the electrochemical approach no dilution is necessary. The LOD (signal-to-noise = 2) was $5.0 \times 10^{-6}$ mol $dm^{-3}$ nitrate. Normally, special precautions such as experimental correction for light scattering are required to achieve a similarly low LOD using spectrophotometry [24]. The shift in linear range and higher limit of detection in the presence of the reductor column may be attributed to the significant sample dispersion due to the dead volume in the unoptimised reductor column.

### 3.5. Interferences and surface passivation

A common problem with conventional electrodes is surface passivation due to irreversible adsorption of electrolytic products and intermediates. This is known to limit the usefulness of glassy carbon electrodes for the oxidative detection of nitrite [17]. The electrocatalytic surface used here was found to be stable with no diminution in response over 200 repeat nitrite determinations. This indicates that the outer-sphere electrocatalytic reaction inhibits surface passivation frequently encountered at conventional electrodes [17]. However, it was established that the activity of the Cu/Cd reductor column diminished slowly with prolonged exposure to nitrate. We interpret this as a gradual reduction in active catalyst surface area due to Cd oxidation by nitrate. This may be circumvented by the use of high surface area copperised cadmium powder or cadmium sponge to ensure complete conversion of nitrate to nitrite.

A range of commonly encountered species were examined for possible interference effects on the electrochemical sensor response. These included thiocyanate, chloride, sulphate, phosphate, carbonate and ammonium. With the exception of thiocyanate, these species were found not to interfere with sensor response. The oxidation of thiocyanate, resulting in the formation of $(SCN)_2$, is characterised by a standard electrode potential of 0.525 V vs. SCE [19], therefore $SCN^-$ is oxidised efficiently at the $[Ru(bipy)_2(PVP)_{10}Cl]Cl$-modified electrode. However, the severe surface fouling encountered at conventional electrodes with $SCN^-$ oxidation does not occur at the modified electrode. By virtue of the differential measurement used for nitrate determination, i.e., analytical response = [(interferents re-

sponse + generated nitrite response) − interferents response], the effect of interferences can be eliminated.

### 3.6. Analysis of nitrate in commercial fertiliser

Having established appropriate experimental conditions, the nitrate concentration in a commercial fertiliser sample was determined by the electrochemical FIA method and by potentiometry for comparison. For the amperometric FIA method a calibration plot was constructed over the concentration range $1.0 \times 10^{-3}$ mol $dm^{-3}$ to $1.0 \times 10^{-2}$ mol $dm^{-3}$ nitrate. Test injections of 0.1 mol $dm^{-3}$ NaCl did not produce measurable responses. The average response for 3 determinations (comprising three replicate injections for each of the 3 samples) for the dissolved sample was $4.47 \pm 0.02$ mA. A blank response, obtained with a glass wool packed column, was found to be $0.29 \pm 0.01$ mA. The sample responses were adjusted for the blank response. The blank response is probably due to interferences such as nitrite in the fertiliser sample. These results yield a concentration of $46.1 \pm 0.5\%$ (w/w) $NO_3^-$ in the fertiliser sample. The potentiometric method utilising the standard addition method yielded $\Delta E$ values of $13.4 \pm 0.1$ mV ($n = 2$) for the addition of 2.0 $cm^3$ of 1.0 mol $dm^{-3}$ $NO_3^-$ to 40.0 $cm^3$ of the sample solution. The concentration of $NO_3^-$ in the sample solution was calculated and the original concentration in the fertiliser sample estimated to be $45.2 \pm 0.2\%$ (w/w) $NO_3^-$. The agreement between these results and the small error associated with the measurement indicate that the amperometric FIA procedure for the determination of nitrate is both accurate and precise.

## 4. Conclusions

There is currently a great need for improvements in the performance of methods for the determination of nitrate in environmental samples. This is especially important with respect to increasing the linear range and lowering the LOD. The electrochemical sensor approach demonstrated here addresses these problems by significantly lowering the LOD and extending the linear range to encompass the normal environmental nitrate levels. Optimisation of the Cu/Cd reductor column with respect to dead volume and sample dispersion is likely to decrease the LOD further. As nitrate analysis is one of the most frequent analyses, any improved methods must also be compatible with automation; FIA systems are widely used due to the ease of automation of these analytical protocols, with the system described here being no exception. These attributes confer considerable advantages to the electrochemical sensor approach compared to the conventional spectrophotometric methods.

## Acknowledgements

The authors would like to thank Fobairt (the Irish Science and Technology Agency) for financial assistance for this work.

## References

[1] A. Hulanicki, W. Matuszewski and M. Trojanowicz, Anal. Chim. Acta, 194 (1987) 119.
[2] M.A. Koupparis, K.M. Walczak and H.V. Malmstadt, Anal. Chim. Acta, 142 (1982) 119.
[3] J. Bassett, R.C. Denny, G.H. Jeffery and J. Mendham, Vogel's Textbook of Quantitative Inorganic Chemistry, 6th edn., Longman, 1978, pp 312–314.
[4] P.W. West and G.L. Lyles, Anal. Chim. Acta, 23 (1960) 227.
[5] F.B. Hora and P.J. Webber, Analyst, 85 (1960) 567.
[6] D.W.W. Andrews, Analyst, 89 (1964) 730.
[7] H. Barnes, Analyst, 75 (1950) 388.
[8] X. Xing and D.A. Scherson, Anal. Chem., 59 (1987) 962.
[9] R.J. Davenport and D.C. Johnson, Anal. Chem., 45 (1973) 1979.
[10] R.J. Davenport and D.C. Johnson, Anal. Chem., 46 (1974) 1971.
[11] G.A. Sherwood and D.C. Johnson, Anal. Chim. Acta, 129 (1981) 87.
[12] W.J. Albery, B.G.D. Haggett, C.P. Jones, M.J. Pritchard and L.R. Svanberg, J. Electroanal. Chem., 188 (1985) 257.
[13] W.J. Albery, P.N. Bartlett, A.E.G. Cass, D.H. Craston and B.G.D. Haggett, J. Chem. Soc., Faraday Trans., 82 (1986) 1033.
[14] D. Chen, M.D. Luque de Castro and M. Valcarcel, Analyst 39 (1991) 123
[15] A. Henriksen and A.R. Selmer-Olsen, Analyst, 95 (1970) 514.
[16] Standard Methods for the Examination of Water and Waste Water, 15th edn., American Public Health Association, New York, 1980.

[17] J.A. Cox and P.J. Kulesza, J. Electroanal. Chem., 175 (1984) 105.
[18] J.M. Clear, J.M. Kelly, C.M. O'Connell and J.G. Vos, J. Chem Res., (1981) 3037.
[19] Handbook of Chemistry and Physics, 66 edn., CRC Press, Boca Raton, FL, D153.
[20] W.J. Albery and A.R. Hillman, J. Electroanal. Chem., 170 (1984) 27.
[21] A.P. Doherty and J.G. Vos, J. Chem Soc., Faraday Trans., 88 (1992) 2903.
[22] R.B. Willis, Anal. Chem., 52 (1980) 1377.
[23] J.F. van Staden, Anal Chim. Acta, 138 (1982) 403.
[24] L. Anderson, Anal. Chim. Acta, 110 (1979) 123.